

# **Dithiafulvenyl Functional pi-Conjugated Oligomers and Polymers: Synthesis, Characterization, and Applications**

by

© **Mohammadreza Khademabolfazli**

A thesis submitted to the School of Graduate Studies

in partial fulfillment of the requirements for the degree of

Doctor of Philosophy

Department of Chemistry

Memorial University of Newfoundland

July 2017

# Abstract

This PhD thesis was aimed at design and synthesis of new functional organic polymers and macromolecules using 1,4-dithiafulvenes (DTFs) and tetrathiafulvalene vinylogues (TTFVs) as molecular building blocks. Despite enormous synthetic difficulties encountered at the initial stage of this work, reliable synthetic methodologies based on Suzuki coupling, phosphite-promoted olefination, and oxidative dithiafulvenyl dimerization reactions were successfully established, which led to the accomplishment of three research projects.

The first project investigated a series of bis(DTF)-end-capped fluorene derivatives which were prepared and subjected to a one-pot iodine-promoted oxidative polymerization to yield  $\pi$ -conjugated co-oligomers containing tetrathiafulvalene vinylogue and fluorene repeat units. The resulting  $\pi$ -oligomers were characterized to take either acyclic or cyclic molecular structures, depending on the  $\pi$ -conjugation length of the monomer used for the polymerization. Electronic and electrochemical redox properties were examined by UV-vis spectroscopic and cyclic voltammetric analyses, while the supramolecular interactions of the  $\pi$ -oligomers with single-walled carbon nanotubes were investigated by UV-vis-NIR and Raman spectroscopy. In the second project, DTF end groups were linked to the 1 and 8 positions of a pyrene core directly or via phenylene bridges to afford redox-active pyrene derivatives. Upon oxidation, the 1,8-bis(DTF)pyrene underwent stepwise electron transfers to form radical cation and dication species, whereas the phenylene-extended bis(DTF)pyrene derivative was cyclized into a macrocyclic trimer through sequential DTF oxidative coupling reactions in solution and in the solid state. The structural, electronic, and supramolecular properties of the pyrene-based macrocycle were investigated using various spectroscopic techniques and molecular modeling studies. In the third

and last project, redox-active DTF groups were attached to dendritic oligo(phenylene vinylene)s, which contain a non-planar, twisted anthraquinodimethane core. The ability of these  $\pi$ -electron rich molecules to bind with nitrobenzene and its derivatives was demonstrated, and their electrochemically generated polymer thin films were tested as efficient sensors for nitrobenzene.

# Acknowledgements

My first and sincere appreciation goes to my most amiable and supportive supervisor, Prof. Yuming Zhao. His genuine guidance during my time at Memorial University helped me fine-tune my research to its best. Brilliant with, passionate about, and enthusiastic for all things in chemistry, Prof. Zhao inspired me to be creative and critical at the same time, much suited to an aspiring organic chemist. As my main mentor along the way, he shared his vast and valuable knowledge unreservedly. For that, I am truly indebted to him.

I would like to acknowledge my supervisory committee members, Prof. Sunil Pansare and Prof. Christopher Rowley, for their encouragement and helpful suggestions during my research work.

I would like to thank Prof. Alex Adronov of McMaster University, as well as his PhD student Mr. Shuai Liang, who provided me assistance with the GPC analysis.

Sincere thanks to Prof. Rik Tykwinski and Dr. Frank Hampel of University of Erlangen-Nürnberg and Prof. Michael Katz of Memorial University for analyzing and solving single crystal structures.

I would also like to thank Dr. Karimulla Mulla for his training and invaluable insight. I also would like to extend my gratitude to all my labmates, especially master's student Ms. Kathleen Woolridge for her kind help and discussions.

I salute all the professors of the Organic Chemistry Department at Memorial University, including Prof. Graham Bodwell and his master's student Mr. Joshua Walsh, for their collaboration and dedication in my second project.

And to my beautiful lovely wife, Sajedah, without whose support and succor none of this would have been even possible, let alone successful. The PhD journey is a long, challenging, at

times frustrating, and yet at the end rewarding one. With her by my side and in my mind throughout the way, coupled with the charm and sweetness of my son Sadra, I felt warm at heart whenever I hit low, backed myself up, dusted myself down, and reignited afresh. For that, I am eternally grateful and happy.

I would also like to show my appreciation to all my past mentors, supervisors, and whoever aided me to be at this level of study and life.

Finally, my special gratitude goes to my parents and parents in law, for their unfailing love and charitable consolation all through life and I wish them all lifelong health and happiness.

# Contents

<b>Title.....</b>	<b>i</b>
<b>Abstract.....</b>	<b>ii</b>
<b>Acknowledgements.....</b>	<b>iv</b>
<b>Contents.....</b>	<b>vi</b>
<b>List of Figures.....</b>	<b>xi</b>
<b>List of Schemes.....</b>	<b>xxi</b>
<b>List of Tables.....</b>	<b>xxiv</b>
<b>List of Abbreviations.....</b>	<b>xxv</b>
<b>Chapter 1</b>	
<b>Introduction</b>	<b>1</b>
1.1 Tetrathiafulvalene and $\pi$ -Extended Tetrathiafulvalene Analogues.....	1
1.1.2 Synthetic Methods for TTF and TTF Derivatives.....	4
1.1.3 Applications of TTFs and Their Derivatives.....	9
1.1.3.1 TTF-based C-T Complexes as Organic Conductors.....	10
1.1.3.2 TTF-based Molecular Machines and Switches.....	11
1.1.3.3 TTF Derivatives as Chemosensors.....	15
1.1.3.4 TTF Derivatives in Metal Organic Frameworks (MOFs).....	21

1.1.3.5 TTF Derivatives in Covalent Organic Frameworks (COFs).....	24
1.2 Tetrathiafulvalene Vinylogues (TTFVs).....	26
1.2.1 Polymerized TTFVs and Their Applications.....	28
1.2.2 Synthetic Methods for Tetrathiafulvalene Vinylogues.....	40
1.3 Outline of This PhD Thesis.....	43
1.4 References .....	44
<b>Chapter 2</b>	
<b>Tetrathiafulvalene Vinylogue–Fluorene Co-oligomers: Synthesis, Properties, and Supramoleclar Interactions with Carbon Nanotubes</b>	<b>51</b>
2.1 Introduction.....	51
2.2 Result and discussion .....	56
2.2.1 Synthesis.....	56
2.2.2 Electronic and Redox Properties.....	59
2.2.3 Structural Elucidation of TTFV–Fluorene Co-oligomers.....	63
2.2.4 Mechanisms of Polymerization.....	69
2.2.5 Supramolecular Interactions of TTFV–Fluorene Co-oligomers with Single-Walled Carbon Nanotubes.....	70
2.2.6 Conclusions.....	75
2.3 Experimental Section.....	76

2.3.1 General Information.....	76
2.3.2 NMR Spectra for New Compounds.....	88
2.4 References .....	111
<b>Chapter 3</b>	
<b>A Macrocyclization of 1,8-Bis(dithiafulvenyl)pyrenes</b>	<b>117</b>
3.1 Introduction .....	117
3.2 Result and Discussion.....	119
3.2.1 Synthesis and Characterization of Precursors.....	119
3.2.2 Synthesis of the Macrocycle: Obstacles and Solutions .....	125
3.2.3 Binding Studies of the Macrocycle.....	129
3.2.4 Conclusions.....	130
3.3. Experimental.....	131
3.3.1 General.....	131
3.3.2 Synthesis.....	132
3.3.3 NMR Spectra for New Compounds.....	140
3.4 Density Functional Theory (DFT) Modeling of 73.....	154
3.5 UV-Vis Titration Data.....	163
3.6 Variable Temperature (VT) NMR Analysis of 77.....	167
3.7 References.....	168

## **Chapter 4**

### **Multivalent Dithiafulvenyl-functionalization of Dendritic Oligo(phenylene vinylene)s with an Anthraquinodimethane Core** **191**

4.1 Introduction .....	191
4.2 Result and Discussion.....	193
4.2.1 Synthesis and Characterization .....	193
4.2.2 Characterization of The Thin Film.....	202
4.2.3 Conclusions.....	203
4.3. Experimental .....	204
4.3.1 General.....	204
4.3.2 Synthesis.....	205
4.3.3 NMR Spectra for New Compounds.....	211
4.3.4 UV-Vis Titration Studies.....	221
4.3.5 Job Plot Analysis.....	223
4.4. Molecular Modeling Studies.....	225
4.5. SEM Imaging of Poly-[82].....	227
4.6 References.....	228

## **Chapter 5**

### **Synthesis of New DFT and TTFV Derivatives** **232**

5.1 Introduction .....	232
------------------------	-----

5.2. Results and Discussion.....	234
5.2.1 Direct Functionalization of Diphenyl-TTFV through Suzuki-Miyaura Cross Coupling.....	234
5.2.2 Direct Functionalization of Phenyl-DTF through Suzuki-Miyaura Cross Coupling.....	241
5.2.3 Functionalization of Phenylene Oligomers with DTF End Groups.....	243
5.2.4 Effects of Reaction Temperature on Phosphite-Promoted Olefination.....	245
5.2.5 Synthesis of TTFV-Phenylene Oligomers.....	247
5.2.6 Conclusions.....	252
5.3 Experimental .....	253
5.3.1 General.....	253
5.3.2 Synthesis.....	253
5.3.3 NMR Spectra for New Compounds.....	261
5.4 References.....	273

## Chapter 6

<b>Conclusions and Future Work</b>	<b>274</b>
------------------------------------	------------

# List of Figures

<b>Fig. 1.1</b> Selected examples of exTTFs <b>2-4</b> .....	3
<b>Fig. 1.2</b> Exemplar exTTFs with different molecular shapes and $\pi$ -topologies.....	4
<b>Fig. 1.3</b> Structure of $\alpha$ -(BEDT-TTF) <sub>4</sub> (Fe(Cp-CONHCH <sub>2</sub> SO <sub>3</sub> ) <sub>2</sub> ).4H <sub>2</sub> O ( <b>17</b> ).....	11
<b>Fig. 1.4</b> TTF-porphyrin based redox fluorescent switches.....	14
<b>Fig. 1.5</b> Rotaxane <b>24</b> as a redox-controlled molecular machine.....	15
<b>Fig. 1.6</b> Examples of crown-annulated or tethered TTFs as metal ion sensors.....	16
<b>Fig. 1.7</b> TTF-podand systems <b>31</b> and <b>32</b> as transition metal ion sensors.....	17
<b>Fig. 1.8</b> Bis(calixcrown)-TTF <b>33</b> as a Na <sup>+</sup> ion sensor.....	18
<b>Fig. 1.9</b> Anthraceny-TTF derivatives for sensing singlet oxygen.....	18
<b>Fig. 1.10</b> TTF-anthracene systems functionalized with phenylboronic acid groups as receptors for saccharides.....	20
<b>Fig. 1.11</b> Portions of crystal structure of MOF: (a) the infinite helical Zn-carboxylate chain (b) a side view of helical TTF stack with depiction of the shortest intermolecular S...S contact and (c) a view of benzoate-lined infinite pores down the <i>c</i> axis. Orange, yellow, red, and gray spheres represents Zn, S, O and C atoms respectively (adopted with permission from reference 67).....	23
<b>Fig. 1.12</b> a) Schematic representation of the synthesis of mesoporous TTF-Ph-COF and microporous TTF-Py-COF topological diagram. Slipped AA stacking structures of TTF-Ph-COF	

at a) top and b) side views and eclipsed stacking structures of TTF-Py-COF at c) top and d) side views (yellow: S, blue: N, grey: C; H was omitted for clarity. (Figure adopted from reference 77 with permission).....	26
<b>Fig. 1.13</b> Molecular structure of copolymer <b>41</b> (left) and the space-filling model optimized by molecular mechanics calculation (right).....	30
<b>Fig. 1.14</b> Bistable conformational changes of TTFV under redox and acid/base conditions. Reversible wrapping and unwrapping of SWNTs by a TTFV polymer.....	31
<b>Fig. 1.15</b> Conformation of a model hexamer of TTFV–fluorene copolymer: (a) side view, (b) front view. Two projections of the conformation of a model hexamer wrapping around a (10,0) SWNT: (c) side view, (d) front view. (Figure adopted from reference 88 with permission).....	32
<b>Fig. 1.16</b> (A) Copolymer <b>47</b> in a zig-zag conformation. (B) Front view, and (C) side view of <b>47</b> in a fully folded conformation. The geometries were optimized using the <i>MMFF</i> force field. To save computational cost, the OC <sub>14</sub> H <sub>29</sub> and SCH <sub>3</sub> groups in <b>47</b> were replaced by OCH <sub>3</sub> groups and H atoms, respectively. (Figure adopted from reference 89 with permission).....	34
<b>Fig. 1.17</b> TTFV-phenylacetylene based shape-persistent macrocycle <b>48</b> .....	35
<b>Fig. 1.18</b> Macrocycles <b>49</b> prepared <i>via</i> Cu-catalyzed alkyne-azide coupling (CuAAC).....	36
<b>Fig 1.19</b> optimized molecular structures for the 1:1 complexes of <b>55b</b> with C <sub>60</sub> (left), and <b>55b</b> with C <sub>70</sub> (right) fullerenes.....	39
<b>Figure 2.1</b> UV-vis spectra of TTFV-fluorene co-oligomers and related $\pi$ -precursors. All spectra were measured in CHCl <sub>3</sub> at room temperature.....	61

<b>Figure 2.2</b> Cyclic voltammograms of compounds <b>64a-c</b> , <b>65a-c</b> , <b>68</b> , and <b>69</b> measured in multiple scans. Electrolyte: Bu <sub>4</sub> NBF <sub>4</sub> (0.1 M); working electrode: glassy carbon; counter electrode: Pt wire; reference electrode: Ag/AgCl; scan rate: 100 mV s <sup>-1</sup> .....	62
<b>Figure 2.3</b> Partial <sup>1</sup> H NMR spectra of <b>65a-c</b> , <b>68</b> and <b>69</b> showing the aromatic and vinylic regions as well as relative integration values therein. The singlet at 7.24 ppm in each spectrum is due to residual CHCl <sub>3</sub> .....	65
<b>Figure 2.4</b> Space-filling model of macrocycle <b>69</b> ( <i>n=1</i> ) optimized using the MMFF force field: (A) side view, (B) top view. Long alkyl chains were replaced by CH <sub>3</sub> to save computational costs.....	67
<b>Figure 2.5</b> Illustration of different reaction pathways involved in the one-pot oxidative polymerization of bis(DTF)-fluorenes.....	70
<b>Figure 2.6</b> Optimized geometries of a TTFV-fluorene pentamer (A: front view; B: side view) and the oligomer wrapping around a (10,0) nanotube (C: front view; D: side view).....	71
<b>Figure 2.7</b> (A) UV-vis-NIR spectra of HiPCO SWNTs dispersed with co-oligomers <b>65a-c</b> in CHCl <sub>3</sub> . (B) UV-vis-NIR spectra of HiPCO SWNTs dispersed with co-oligomers <b>65a-c</b> in THF. (C) Raman spectra of SWNTs dispersed with co-oligomers <b>65a-c</b> . Inset: Expanded spectra showing the radical breathing mode (RBM) region.....	72
<b>Figure 2.8</b> Comparison of the Raman spectra of co-oligomer <b>65</b> , raw HiPCO SWNTs dispersed with <b>65</b> . Insets: Expanded spectra showing the radial breathing mode (RBM) region.....	75
<b>Fig. 2-9:</b> <sup>1</sup> H NMR (300 MHz, CDCl <sub>3</sub> ) spectrum of compound <b>62a</b> .....	88

<b>Fig. 2-10:</b> $^{13}\text{C}$ NMR (75 MHz, $\text{CDCl}_3$ ) spectrum of compound <b>62a</b> .....	89
<b>Fig. 2-11:</b> $^1\text{H}$ NMR (300 MHz, $\text{CDCl}_3$ ) spectrum of compound <b>62b</b> .....	90
<b>Fig. 2-12:</b> $^1\text{H}$ NMR (300 MHz, $\text{CDCl}_3$ ) spectrum of compound <b>62c</b> .....	91
<b>Fig. 2-13:</b> $^1\text{H}$ NMR (300 MHz, $\text{CDCl}_3$ ) spectrum of compound <b>64a</b> .....	92
<b>Fig. 2-14:</b> $^{13}\text{C}$ NMR (75 MHz, $\text{CDCl}_3$ ) spectrum of compound <b>64a</b> .....	93
<b>Fig. 2-15:</b> $^1\text{H}$ NMR (300 MHz, $\text{CDCl}_3$ ) spectrum of compound <b>64b</b> .....	94
<b>Fig. 2-16:</b> $^{13}\text{C}$ NMR (75 MHz, $\text{CDCl}_3$ ) spectrum of compound <b>64b</b> .....	95
<b>Fig. 2-17:</b> $^1\text{H}$ NMR (300 MHz, $\text{CDCl}_3$ ) spectrum of compound <b>64c</b> .....	96
<b>Fig. 2-18:</b> $^{13}\text{C}$ NMR (75 MHz, $\text{CDCl}_3$ ) spectrum of compound <b>64c</b> .....	97
<b>Fig. 2-19:</b> $^1\text{H}$ NMR (300 MHz, $\text{CDCl}_3$ ) spectrum of compound <b>65a</b> .....	98
<b>Fig. 2-20:</b> $^{13}\text{C}$ NMR (75 MHz, $\text{CDCl}_3$ ) spectrum of compound <b>65a</b> .....	99
<b>Fig. 2-21:</b> $^1\text{H}$ NMR (300 MHz, $\text{CDCl}_3$ ) spectrum of compound <b>65b</b> .....	100
<b>Fig. 2-22:</b> $^{13}\text{C}$ NMR (75 MHz, $\text{CDCl}_3$ ) spectrum of compound <b>65b</b> .....	101
<b>Fig. 2-23:</b> $^1\text{H}$ NMR (300 MHz, $\text{CDCl}_3$ ) spectrum of compound <b>65c</b> .....	102
<b>Fig. 2-24:</b> $^{13}\text{C}$ NMR (75 MHz, $\text{CDCl}_3$ ) spectrum of compound <b>65c</b> .....	103
<b>Fig. 2-25:</b> $^1\text{H}$ NMR (300 MHz, $\text{CDCl}_3$ ) spectrum of compound <b>66</b> .....	104
<b>Fig. 2-26:</b> $^{13}\text{C}$ NMR (75 MHz, $\text{CDCl}_3$ ) spectrum of compound <b>66</b> .....	105
<b>Fig. 2-27:</b> $^1\text{H}$ NMR (300 MHz, $\text{CDCl}_3$ ) spectrum of compound <b>67</b> .....	106
<b>Fig. 2-28:</b> $^{13}\text{C}$ NMR (75 MHz, $\text{CDCl}_3$ ) spectrum of compound <b>67</b> .....	107
<b>Fig. 2-29:</b> $^1\text{H}$ NMR (300 MHz, $\text{CDCl}_3$ ) spectrum of compound <b>68</b> .....	108
<b>Fig. 2-30:</b> $^{13}\text{C}$ NMR (75 MHz, $\text{CDCl}_3$ ) spectrum of compound <b>68</b> .....	109

<b>Fig. 2-31:</b> $^1\text{H}$ NMR (300 MHz, $\text{CDCl}_3$ ) spectrum of compound <b>69</b> .....	110
<b>Fig. 3.1</b> (A) ORTEP plot of compound <b>73</b> at 50% ellipsoid probability (CCDC#1450007). (B) Resonance structures for the singlet dication of <b>73</b> .....	121
<b>Fig. 3.2</b> Cyclic voltammograms of (A) bis(DTF)pyrene <b>73</b> , (B) bis(DTF)pyrene <b>75</b> , and (C) macrocycle <b>77</b> . Solvent: $\text{CH}_2\text{Cl}_2$ , electrolyte: $\text{Bu}_4\text{NBF}_4$ (0.1 M), working electrode: glassy carbon, reference electrode: $\text{Ag}/\text{AgCl}$ (3 M $\text{NaCl}$ ) counter electrode: Pt, scan rate: 0.3 V/s.....	123
<b>Fig. 3.3</b> Molecular structure of a 1:1 aggregate of <b>75</b> and <b>76</b> optimized at the semiempirical RM1 level (Spartan'10). (A) Top view of the capped-stick model. Space-filling models showing (B) top and (C) side view. Color scheme: blue = <b>75</b> , green = <b>76</b> . $\text{SC}_{10}\text{H}_{21}$ groups were replaced with hydrogen atoms and $\text{OC}_6\text{H}_{13}$ groups with $\text{OCH}_3$ groups to save computational expense.....	128
<b>Fig. 3.4</b> (A) Aromatic region of the $^1\text{H}$ NMR (500 MHz, $\text{CDCl}_3$ ) spectrum of <b>77</b> . (B) Top and (C) side views of the optimized geometry of <b>77</b> using the <i>MMFF</i> force field.....	130
<b>Fig. 3.5</b> $^1\text{H}$ NMR (300 MHz, $\text{CDCl}_3$ ) spectrum of compound <b>71</b> .....	140
<b>Fig. 3.6</b> $^{13}\text{C}$ NMR (75 MHz, $\text{CDCl}_3$ ) spectrum of compound <b>71</b> .....	141
<b>Fig. 3.7</b> $^1\text{H}$ NMR (300 MHz, $\text{CDCl}_3$ ) spectrum of compound <b>73</b> .....	142
<b>Fig. 3.8</b> $^{13}\text{C}$ NMR (75 MHz, $\text{CDCl}_3$ ) spectrum of compound <b>73</b> .....	143
<b>Fig. 3.9</b> $^1\text{H}$ NMR (300 MHz, $\text{CDCl}_3$ ) spectrum of compound <b>74</b> .....	144
<b>Fig. 3.10</b> $^{13}\text{C}$ NMR (75 MHz, $\text{CDCl}_3$ ) spectrum of compound <b>74</b> .....	145
<b>Fig. 3.11</b> $^1\text{H}$ NMR (300 MHz, $\text{CDCl}_3$ ) spectrum of compound <b>75</b> .....	146
<b>Fig. 3.12</b> $^{13}\text{C}$ NMR (75 MHz, $\text{CDCl}_3$ ) spectrum of compound <b>75</b> .....	147

<b>Fig. 3.13</b> $^1\text{H}$ NMR (300 MHz, $\text{CDCl}_3$ ) spectrum of compound <b>77</b> .....	148
<b>Fig. 3.14</b> $^{13}\text{C}$ NMR (75 MHz, $\text{CDCl}_3$ ) spectrum of compound <b>77</b> .....	149
<b>Fig. 3.15</b> $^1\text{H}$ NMR (300 MHz, $\text{CDCl}_3$ ) spectrum of compound <b>79</b> .....	150
<b>Fig. 3.16</b> $^{13}\text{C}$ NMR (75 MHz, $\text{CDCl}_3$ ) spectrum of compound <b>79</b> .....	151
<b>Fig. 3.17</b> $^1\text{H}$ NMR (300 MHz, $\text{CDCl}_3$ ) spectrum of compound <b>70</b> .....	152
<b>Fig. 3.18</b> $^{13}\text{C}$ NMR (75 MHz, $\text{CDCl}_3$ ) spectrum of compound <b>70</b> .....	153
<b>Fig. 3.19</b> Optimized geometry of compound <b>73</b> : (A) front view, (B) side view. MO plots: (C) LUMO (-1.90 eV, isovalue = 0.02), (D) HOMO (-4.75 eV, isovalue = 0.02).....	154
<b>Fig. 3.20</b> Optimized geometry of the radical cation of <b>73</b> : (A) front view, (B) side view. MO plots: (C) SOMO (-7.18 eV, isovalue = 0.02), (D) Spin density map (the blue color indicates the high spin density area).....	155
<b>Fig. 3.21</b> Optimized geometry of the singlet dication of <b>73</b> : (A) front view, (B) side view. MO plots: (C) LUMO (-10.04 eV, isovalue = 0.02), (D) HOMO (-10.66 eV, isovalue = 0.02).....	155
<b>Fig. 3.22</b> Optimized geometry of the triplet dication of <b>73</b> : (A) front view, (B) side view. MO plots: (C) SOMO 2 (-9.75 eV, isovalue = 0.02), (D) SOMO 1 (-10.43 eV, isovalue = 0.02).....	156
<b>Fig. 3.23</b> UV-Vis titration of macrocycle <b>77</b> ( $1.13 \times 10^{-5}$ M in $\text{CHCl}_3$ ) with nitrobenzene (0.0 to 16.4 molar equivalents) at room temperature. The arrows indicate the trend of spectral change with increasing titration.....	163

<b>Fig. 3.24</b> Oxidative UV-Vis titration of macrocycle <b>77</b> ( $2.27 \times 10^{-5}$ M in $\text{CHCl}_3$ ) with $\text{PhI}(\text{OAc})_2/\text{CF}_3\text{SO}_3\text{H}$ (1 : 4 molar ratio) at room temperature. The arrows indicate the trend of spectral change with increasing titration. The addition of oxidant goes as follows: 0, 0.11, 0.33, 0.55, 0.76 molar equivalents of $\text{PhI}(\text{OAc})_2$ .....	164
<b>Fig. 3.25</b> Oxidative UV-Vis titration of compound <b>75</b> ( $6.79 \times 10^{-5}$ M in $\text{CHCl}_3$ ) with $\text{PhI}(\text{OAc})_2/\text{CF}_3\text{SO}_3\text{H}$ (1 : 4 molar ratio) at room temperature. The arrows indicate the trend of spectral change with increasing titration. The addition of oxidant goes as follows: 0, 0.04, 0.11, 0.18 molar equivalents of $\text{PhI}(\text{OAc})_2$ .....	165
<b>Fig. 3.26</b> Oxidative UV-Vis titration of compound <b>73</b> ( $1.22 \times 10^{-4}$ M in $\text{CHCl}_3$ ) with $\text{PhI}(\text{OAc})_2/\text{CF}_3\text{SO}_3\text{H}$ (1 : 4 molar ratio) at room temperature. The arrows indicate the trend of spectral change with increasing titration. The addition of oxidant goes as follows: 0, 0.03, 0.08, 0.13, 0.18, 0.25, 0.35, 0.48, 0.62 molar equivalents of $\text{PhI}(\text{OAc})_2$ .....	165
<b>Fig. 3.27</b> Normalized UV-Vis absorption spectra of compounds <b>73</b> , <b>75</b> , and <b>77</b> .....	166
<b>Fig. 3.28</b> Expanded $^1\text{H}$ NMR (500 MHz, $\text{CD}_2\text{Cl}_2$ ) spectra of macrocycle <b>77</b> measured at different temperatures.....	167
<b>Fig. 4.1</b> Space-filling models of poly(DTF)-AQs (A) <b>82</b> and (B) <b>85</b> optimized at the PM6 level. (C) Frontier molecular orbitals of the 1:1 complex of <b>82</b> with nitrobenzene calculated at the B3LYP-6-31G(d)//PM6 level. The SC10H21 side-chains were replaced with hydrogen atoms to save computational time.....	196
<b>Fig. 4.2</b> (A) UV-Vis spectra of <b>82</b> (42.7 $\mu\text{M}$ ) titrated with nitrobenzene (0 to 3.18 molar equivalents) in $\text{CHCl}_3$ at room temperature. (B) UV-Vis spectra of <b>85</b> (20.4 $\mu\text{M}$ ) titrated with nitrobenzene (0 to 6.63 molar equivalents) in $\text{CHCl}_3$ at room temperature. (C) Normalized UV-	

Vis spectra of **82**, **85**, poly-[**82**], and poly-[**85**] measured in CHCl<sub>3</sub> at room temperature. (D) Partial <sup>1</sup>H NMR (500 MHz, CDCl<sub>3</sub>) spectra monitoring the oxidative polymerization of **82** at different reaction times. The signals due to the vinylic protons adjacent to the DTF groups are highlighted by asterisk mark.....198

**Fig. 4.3** Multi-cycle CV scans of (A) **82**, (B) poly-[**82**] thin film, (D) **85**, and (E) of poly-[**85**] thin film. DPV responses of the thin films of (C) poly-[**82**] and (F) poly-[**85**] upon titration with nitrobenzene from 0 to 0.52 mM in CH<sub>3</sub>CN. Experimental conditions: electrolyte: Bu<sub>4</sub>NBF<sub>4</sub> (0.1 M); working electrode: glassy carbon; reference: Ag/AgCl (3M NaCl); counter electrode: Pt wire; CV scan rate: 100 mV/s; DPV step: 4 ms, pulse width: 50 ms, pulse period: 200 ms, pulse amplitude 50 mV.....200

**Fig. 4.4** (A) Correlations of the concentration of NB with the DPV current intensity changes of poly-[**85**] during the titration. (B) Correlations of the concentration of NB with the oxidation potential changes of poly-[**85**] during the titration. (C) Schematic illustration of the two stages of interactions between NB molecules (red ovals) and the micropores in the thin film of poly-[**85**].....203

**Fig. 4.5** <sup>1</sup>H NMR (300 MHz, CD<sub>2</sub>Cl<sub>2</sub>) of compound **81**.....211

**Fig. 4.6** <sup>13</sup>C NMR (75 MHz, CD<sub>2</sub>Cl<sub>2</sub>) of compound **81**.....212

**Fig. 4.7** <sup>1</sup>H NMR (300 MHz, CDCl<sub>3</sub>) of compound **82**.....213

**Fig. 4.8** <sup>13</sup>C NMR (75 MHz, CDCl<sub>3</sub>) of compound **82**.....214

**Fig. 4.9** <sup>1</sup>H NMR (300 MHz, CD<sub>2</sub>Cl<sub>2</sub>) of compound **83**.....215

**Fig. 4.10** <sup>13</sup>C NMR (75 MHz, CD<sub>2</sub>Cl<sub>2</sub>) of compound **83**.....216

<b>Fig. 4.11</b> $^1\text{H}$ NMR (300 MHz, $\text{CD}_2\text{Cl}_2$ ) of compound <b>84</b> .....	217
<b>Fig. 4.12</b> $^{13}\text{C}$ NMR (75 MHz, $\text{CD}_2\text{Cl}_2$ ) of compound <b>84</b> .....	218
<b>Fig. 4.13</b> $^1\text{H}$ NMR (300 MHz, $\text{CD}_2\text{Cl}_2$ ) of compound <b>85</b> .....	219
<b>Fig. 4.14</b> $^{13}\text{C}$ NMR (75 MHz, $\text{CD}_2\text{Cl}_2$ ) of compound <b>85</b> .....	220
<b>Fig. 4.15</b> UV-Vis titration profiles of compound <b>82</b> (42.7 $\mu\text{M}$ in $\text{CHCl}_3$ , 298 K) with (A) nitrobenzene (0 to 3.18 molar equiv), (B) 2,4-dinitrotoluene (0 to 2.15 molar equiv), (C) 2,4,6-trinitrotoluene (0 to 0.34 molar equiv), (D) picric acid (0 to 0.34 molar equiv).....	221
<b>Fig. 4.16</b> UV-Vis titration profiles of compound <b>85</b> (20.4 $\mu\text{M}$ in $\text{CHCl}_3$ , 298 K) with (A) nitrobenzene (0 to 6.63 molar equiv), (B) 2,4-dinitrotoluene (0 to 4.48 molar equiv), (C) 2,4,6-trinitrotoluene (0 to 0.72 molar equiv), (D) picric acid (0 to 0.71 molar equiv).....	222
<b>Fig. 4.17</b> Job's plot for determination of the binding stoichiometry of octa(DTF)-AQ <b>85</b> with nitrobenzene (NB).....	224
<b>Fig. 4.18</b> Optimized structures and FMOs of compound <b>82</b> (left) and the 1:1 supramolecular complex of NB@ <b>82</b> (right). Structures optimized at the PM6 level and single-point calculations done at the B3LYP/6-31G(d) level of theory. FMO countours are plotted at an isovalue of 0.02.....	225
<b>Fig. 4.19</b> Molecular structure of the 1:1 complex of <b>82</b> and nitrobenzene (NB@ <b>82</b> ) optimized at the PM6 level. (A) Side view, (B) top view. The NB molecule is highlighted by the space-filling plot to better visualize the intermolecular interactions.....	226

<b>Fig. 4.20</b> Molecular structure of compound <b>85</b> optimized at the PM6 level. (A) Top view, (B) side view.....	226
<b>Fig. 4.21</b> SEM images of poly-[ <b>82</b> ] generated by oxidative coupling reactions.....	227
<b>Figure 5.1</b> Molecular structures of bis(DTF)-arenes <b>68</b> , <b>75</b> , and <b>103</b> .....	248
<b>Fig. 5.2:</b> <sup>1</sup> H NMR (300 MHz, CDCl <sub>3</sub> ) spectrum of compound <b>92</b> .....	261
<b>Fig. 5.3:</b> <sup>1</sup> H NMR (300 MHz, CDCl <sub>3</sub> ) spectrum of compound <b>93</b> .....	262
<b>Fig. 5.4:</b> <sup>1</sup> H NMR (300 MHz, CDCl <sub>3</sub> ) spectrum of compound <b>97</b> .....	263
<b>Fig. 5.5:</b> <sup>1</sup> H NMR (300 MHz, CDCl <sub>3</sub> ) spectrum of compound <b>98</b> .....	264
<b>Fig. 5.6:</b> <sup>1</sup> H NMR (300 MHz, CDCl <sub>3</sub> ) spectrum of compound <b>99</b> .....	265
<b>Fig. 5.7:</b> <sup>13</sup> C NMR (75 MHz, CDCl <sub>3</sub> ) spectrum of compound <b>99</b> .....	266
<b>Fig. 5.8:</b> <sup>1</sup> H NMR (300 MHz, CDCl <sub>3</sub> ) spectrum of compound <b>101</b> .....	267
<b>Fig. 5.9:</b> <sup>13</sup> C NMR (75 MHz, CDCl <sub>3</sub> ) spectrum of compound <b>101</b> .....	268
<b>Fig. 5.10:</b> <sup>1</sup> H NMR (300 MHz, CDCl <sub>3</sub> ) spectrum of compound <b>102</b> .....	269
<b>Fig. 5.11:</b> <sup>13</sup> C NMR (75 MHz, CDCl <sub>3</sub> ) spectrum of compound <b>102</b> .....	270
<b>Fig. 5.12:</b> <sup>1</sup> H NMR (300 MHz, CDCl <sub>3</sub> ) spectrum of compound <b>103</b> .....	271
<b>Fig. 5.13:</b> <sup>13</sup> C NMR (75 MHz, CDCl <sub>3</sub> ) spectrum of compound <b>103</b> .....	272
<b>Fig 6.1</b> Hexadeca-DTF functionalized $\pi$ -conjugated dendritic system <b>106</b> .....	277

# List of Schemes

<b>Scheme 1.1</b> Sequential single-electron transfers of TTF <b>1</b> that convert its two non-aromatic dithiole rings into aromatic ditholium units upon stepwise oxidation.....	2
<b>Scheme 1.2</b> Synthetic methods for preparation of TTF skeleton.....	5
<b>Scheme 1.3</b> Synthetic methods for (A) 1,3-dithiole-2-thiones and (b) ditholium salts.....	6
<b>Scheme 1.4</b> Synthetic methods for symmetrical TTF <b>9</b> , unsymmetrical TTF <b>12</b> and DTF <b>15</b> .....	7
<b>Scheme 1.5</b> Synthetic route for 1,3-dithiole-2-thione <b>16</b> involving the reduction of CS <sub>2</sub> with Na as the key step.....	8
<b>Scheme 1.6</b> Mechanism of the reduction and coupling of CS <sub>2</sub> with Na metal.....	9
<b>Scheme 1.7</b> BEDT-TTF-based organic charge transfer salt and the zwitterion of ferrocenesulfonate prepared by constant-current electrocrystallization method.....	11
<b>Scheme 1.8</b> Illustration of the three states of compound <b>20</b> after oxidation and reduction.....	12
<b>Scheme 1.9</b> Schematic illustration of the three states of <b>20</b> showing different dihedral angles after oxidation of TTF units (BN: binaphthalene unit).....	13
<b>Scheme 1.10</b> Possible mechanism for strong chemiluminescence (CL) of <b>34a</b> and <sup>1</sup> O <sub>2</sub> .....	19
<b>Scheme 1.11</b> Fluorescence detection mechanism of saccharides by TTF-anthracene based boronic acid sensors.....	21
<b>Scheme 1.12</b> Synthesis of <b>H<sub>4</sub>TTFTB</b> .....	22

<b>Scheme 1.13</b> Synthesis of two TTF-based COFs in which phenyl and pyrene were used as linkers.....	25
<b>Scheme 1.14</b> Redox-induced conformational switching of diphenyl TTFV <b>40</b> .....	27
<b>Scheme 1.15</b> Synthesis of TTFV-fluorene copolymer <b>44</b> .....	32
<b>Scheme 1.16</b> Synthesis of TTFV–pyrene-based copolymer <b>47</b> <i>via</i> Sonogashira coupling polymerization.....	34
<b>Scheme 1.17</b> proposed 1:1 binding mode sensor <b>50</b> with a saccharide molecule forming a stable chelate with the assistance of water.....	37
<b>Scheme 1.18</b> Synthesis of diathryl–TTFV molecular tweezers <b>52</b> <i>via</i> the CuAAC reaction.....	38
<b>Scheme 1.19</b> Synthesis of TTFV-arene tweezers <b>55a-c</b> <i>via</i> click reactions.....	39
<b>Scheme 1.20</b> Redox-regulated rotary motion of bis(9-triptycyl)-TTFV system.....	40
<b>Scheme 1.21</b> Retrosynthetic analysis of TTFVs.....	41
<b>Scheme 1.22</b> General synthetic approach to make TTFV.....	42
<b>Scheme 1.23</b> Mechanism of DTF oxidative dimerization reaction.....	42
<b>Scheme 2.1</b> General mechanism for the oxidative dimerization of phenyl-DTF.....	54
<b>Scheme 2.2</b> General polymerization route using DTF oxidative dimerization as the key step for polymer chain growth.....	55
<b>Scheme 2.3</b> Synthesis of fluorene-cored bis(DTF) derivatives <b>64a-c</b> and acyclic TTFV-fluorene oligomers <b>65a-c</b> .....	57

<b>Scheme 2.4</b> Synthesis of cyclic TTFV-fluorene oligomers <b>69</b> using bis(DTF)-oligomer <b>68</b> as precursor.....	59
<b>Scheme 3.1</b> General Mechanism for Oxidative DTF Coupling and Polymerization of Bis(DTF)-endcapped Arenes.....	118
<b>Scheme 3.2</b> Synthesis of Bis(DTF)pyrenes <b>73</b> and <b>75</b> .....	120
<b>Scheme 3.3</b> Oxidative Coupling Reactions of Bis(DTF)pyrene <b>75</b> under Different Conditions.....	127
<b>Scheme 4.1.</b> The general mechanism for the oxidative dimerization of an aryl-DTF.....	192
<b>Scheme 4.2.</b> (A) Synthesis of poly(DTF)-functionalized dendritic oligo(phenylene vinylene)s <b>82</b> and <b>85</b> . (B) ORTEP plots (50% ellipsoid probability, CCDC# 1518143) of the single crystal structure of compound <b>81</b> viewed from top and side.....	195
<b>Scheme 5.1</b> Retrosynthesis of TTFV derivatives through two Suzuki coupling approaches.....	235
<b>Scheme 5.2</b> Attempted Suzuki coupling between TTFV <b>86</b> and boronic acid <b>87</b> .....	235
<b>Scheme 5.3</b> Attempted Suzuki coupling reaction for TTFV <b>86</b> with boronic acid <b>88</b> under the catalysis of freshly prepared Pd(0) catalyst.....	237
<b>Scheme 5.4</b> Attempted Suzuki coupling reaction of TTFV <b>86</b> with boronate <b>89</b> under the catalysis of freshly prepared Pd(0) catalyst.....	238
<b>Scheme 5.5</b> Attempted conversion of dibromo-TTFV <b>86</b> into bis(boronate)-TTFV <b>89</b> under the catalysis of freshly prepared Pd(0) catalyst.....	239

<b>Scheme 5.6</b> Attempted conversion of dibromo-TTFV <b>86</b> into bis(boronate)-TTFV <b>89</b> under the catalysis of PdCl <sub>2</sub> (dppf).....	240
<b>Scheme 5.7</b> An alternative synthetic approach to bis(boronate)-TTFV <b>93</b> .....	241
<b>Scheme 5.8</b> Attempted Suzuki coupling reactions of boronate-DTF <b>92</b> with various aryl halides.....	242
<b>Scheme 5.9</b> Synthesis of oligo( <i>p</i> -phenylene)s <b>97</b> through Suzuki coupling.....	243
<b>Scheme 5.10</b> Synthesis of mono-DTF functionalized oligo( <i>p</i> -phenylene)s <b>98</b> .....	244
<b>Scheme 5.11</b> Phosphite-promoted olefination reaction of compound <b>62b</b> .....	244
<b>Scheme 5.12</b> Structure of compound <b>99</b> and proposed mechanism for the formation of the $\alpha$ -hydroxyphosphonate group in it.....	246
<b>Scheme 5.13</b> Synthesis of bis(DTF)-endcapped molecular tweezer <b>103</b> .....	249
<b>Scheme 5.14</b> Oxidative coupling of bis(DTF)-phenylene <b>103</b> .....	250
<b>Scheme 5.15</b> An isodesmic reaction for evaluation of the strain energy of TTFV-phenylene macrocycle <b>105</b> .....	252

## List of Tables

<b>Table 2.1</b> Summary of GPC Data for TTFV–fluorene Co-Oligomers and Their Calculated Degrees of Oligomerization ( <i>n</i> ).....	68
<b>Table 5.1</b> Optimization of the olefination reaction of dialdehyde <b>62b</b> .....	245

# List of Abbreviations

Å	Angstrom
AgNPs	Silver nanoparticles
APCI-MS	Atmospheric Pressure Chemical Ionization Mass Spectrometry
Aq	Aqueous
Ar	Aromatic
AuNPs	Gold nanoparticles
br.	Broad (in NMR)
Bu	Butyl
<i>t</i> -BuLi	<i>t</i> -butyllithium
B3LYP	Becke, 3-parameter, Lee-Yang-Parr
CuI	Copper Iodide
CT	Charge-transfer
CCl <sub>4</sub>	Carbon tetrachloride
COFs	Covalent organic frameworks
$\delta$	Chemical shift in ppm down-field from tetramethylsilane
DFT	Density functional theory

DMF	<i>N, N</i> -dimethylformamide
DMSO	Dimethyl sulfoxide
DNA	Deoxyribonucleic acid
HOMO	Highest occupied molecular orbital
Hz	Hertz
<i>J</i>	Coupling constant
<i>K<sub>assoc</sub></i>	Association constant
kJ	Kilojoule
Lit.	Literature
LUMO	Lowest unoccupied molecular orbital
MS	Mass spectroscopy
MMFF	Merck molecular force field
Me	Methyl
mp	Melting point
MOFs	Metal organic frameworks
min	minute(s)
MW	Microwave
NMR	Nuclear magnetic resonance

NR	No reaction
NBS	<i>N</i> -bromosuccinimide
<i>p</i>	Para-
Ph	Phenyl
ppm	parts per million
PET	Photoinduced electron transfer
PTI	Photon Technology International
PMT	photomultiplier tube
PCT	Photoinduced charge transfer
q	Quartet (in NMR)
rt	Room temperature
SAM	Self-assembled monolayer
SPR	Surface plasmon resonance
STM	Scanning Tunneling Microscopy
SEM	Scanning Electron Microscopy
s	Singlet (in NMR)
TMS	Tetramethylsilane (in NMR)
THF	Tetrahydrofuran

TLC	Thin-layer chromatography
<i>t</i>	Triplet (in NMR)
<i>tert</i>	Tertiary
UV-Vis	UV-visible spectroscopy

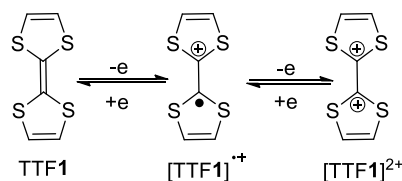
# Chapter 1

## Introduction

### 1.1. Tetrathiafulvalene and $\pi$ -Extended Tetrathiafulvalene Analogues

In the early 1970s Fred Wudl and co-workers reported the use of tetrathiafulvalene (TTF) as the active component to generate the first example of “organic semiconductors”.<sup>1,2</sup> Immediately after this seminal work, many researchers were attracted to this new type of sulfur-based heterocyclic compound, foreseeing their huge impact in the field of electronics. Active studies have been focused on the synthesis of new types of TTF derivatives, which resulted in the rapid development of modern TTF chemistry.<sup>3</sup>

TTF is a redox-active molecular building block and has been widely used in organic electronic materials and supramolecular assemblies. Owing to its electron-rich nature, TTF can readily form charge-transfer complexes when interacting with proper electron acceptors. Many of these complexes exhibit excellent metallic conductivity and semiconductivity.<sup>4-8</sup> The excellent electron-donating properties of TTF are mainly ascribed to its unique, aromaticity-stabilized cationic states after releasing one and/or two electrons (see Scheme 1.1).<sup>4-11</sup> There are also dramatic changes in molecular shape associated with the oxidation processes of TTF. For example, the TTF dication ((TTF1)<sup>2+</sup>, Scheme 1.1) prefers a geometry in which the two dithiolium moieties are perpendicular. Such changes also contribute to stabilizing the TTF dication by minimizing the disfavored charge repulsions within the molecule.



**Scheme 1.1** Sequential single-electron transfers of TTF **1** that convert its two non-aromatic dithiole rings into aromatic ditholium units upon stepwise oxidation.

Attachment of diverse  $\pi$ -conjugated functional groups to the parent structure of TTF has become a very efficient strategy for developing new  $\pi$ -extended TTF derivatives (exTTFs). Generally speaking, new TTF-based materials not only inherit the excellent electron-donating properties of pristine TTF, but also show varied oxidation potentials and electron-transfer mechanisms according to the  $\pi$ -extension and the substituents included in the molecular structures. For instance, many exTTFs show lowered oxidation potentials relative to that of unsubstituted TTF, primarily as a result of the stabilizing effect of extended  $\pi$ -frameworks on their cationic states. On the other hand, the conformational properties of exTTFs are considerably different from their parent TTF in the neutral and oxidized states. As such, exTTFs can be flexibly used as redox-controlled  $\pi$ -building blocks for the construction of advanced nanoscale devices featuring stimuli-responsiveness at the molecular and/or supramolecular levels. The most prominent examples of such research can be found in the well-known rotaxane and catenane-based molecular machines developed by Sir Fraser Stoddart, who was awarded the Nobel Prize in 2016 in Chemistry in recognition of his immense contributions to this area.

These unique properties and flexible tunability of exTTFs have for decades motivated material chemists to design functional organic electronic materials and molecular devices. So far, there is a vast array of exTTFs being reported, synthesized, and characterized in the literature.<sup>8,12,13</sup> The efforts to develop new TTF and exTTF materials are still growing in the current research.<sup>14,15</sup> Synthetically, the construction of  $\pi$ -extended TTF derivatives can be undertaken *via* two main approaches: (1) Attachment of  $\pi$ -conjugated moieties to the dithiole units (e.g., dibenzo-TTF **2** shown in Figure 1.1); (2) Insertion of a  $\pi$ -spacer between the two dithiole rings, such as the anthraquinoidal and vinyloungous exTTFs **3** and **4** illustrated in Figure 1.1. Most of the exTTFs are redox-active and have direct or potential application in the fields of materials science and nanotechnology.<sup>6,8,11,16</sup>

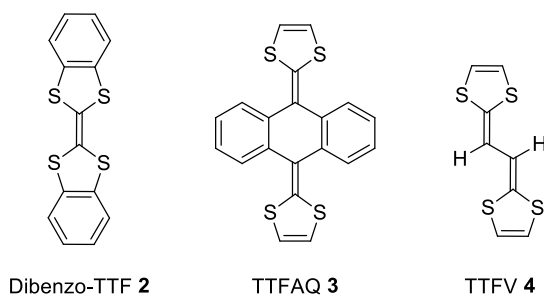


**Fig. 1.1** Selected examples of exTTFs **2-4**.

The spacer-insertion approach to derivatizing exTTFs can result in numerous molecular structures ranging from simple to rather complex scaffolds and topologies. Figure 1.2 illustrates a number of examples (exTTFs **5-7**) featuring linear (**5**), cruciform (**6**), and macrocyclic (**7**) molecular constructs. These molecules have been successfully

synthesized and characterized to show the applicability in polymer synthesis, molecular electronics, and chemical sensors.<sup>17-19</sup>

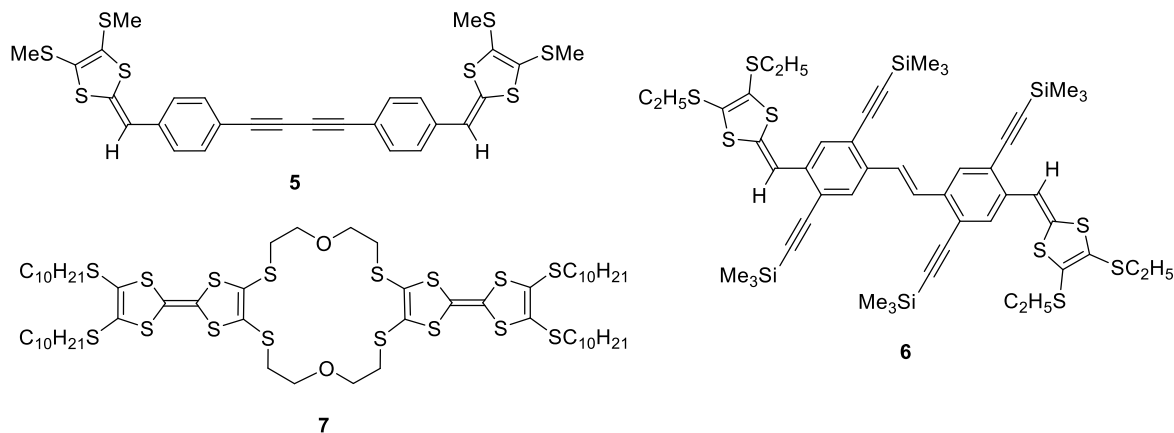
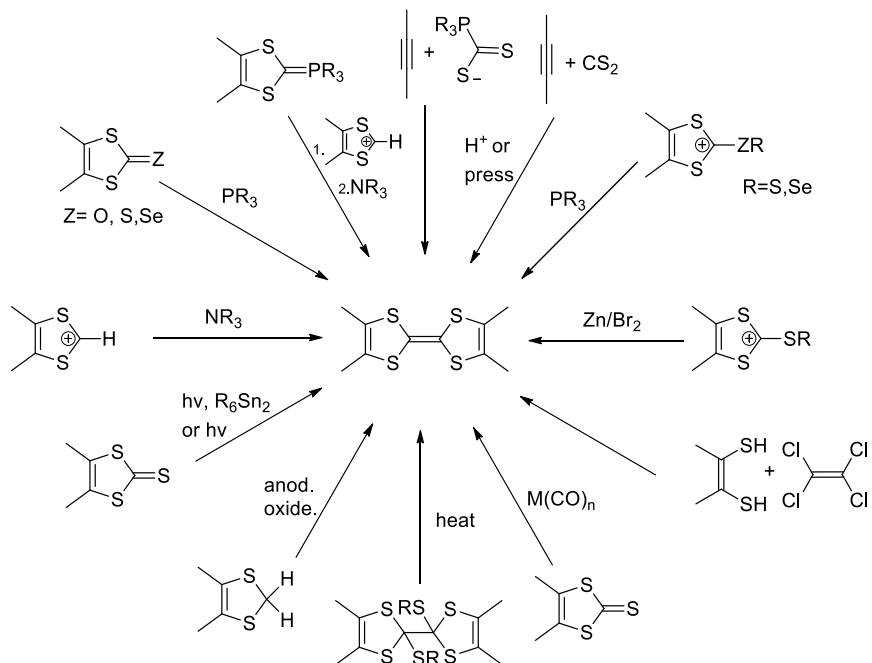


**Fig. 1.2** Exemplar exTTFs with different molecular shapes and  $\pi$ -topologies.

### 1.1.2 Synthetic Methods for TTF and TTF Derivatives

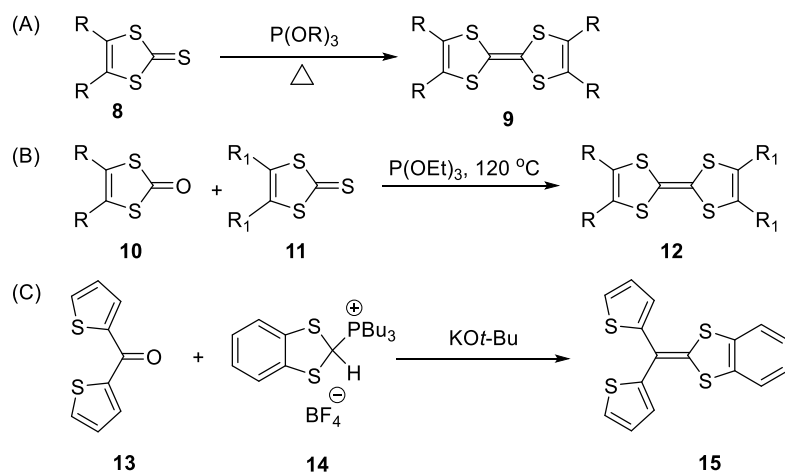
In general, the synthesis of TTFs can be categorized into two main classes: (1) the synthesis of simple TTFs and exTTFs with extension on the side chains of dithiole rings, and (2) the synthesis of exTTFs in which the two dithioles are connected by a  $\pi$ -conjugated spacer(s). The synthesis of TTFs requires an appropriate choice of precursor. The general synthetic routes to TTFs established in the current literature are presented in Scheme 1.2.<sup>20</sup> However, for the synthesis of many TTFs and TTF derivatives, the main precursors involve 1,3-dithiole-2-thione and dithiolium salt. Hence, the synthetic methods for them are described in Scheme 1.3.<sup>20</sup>



**Scheme 1.2** Synthetic methods for preparation of TTF skeleton.



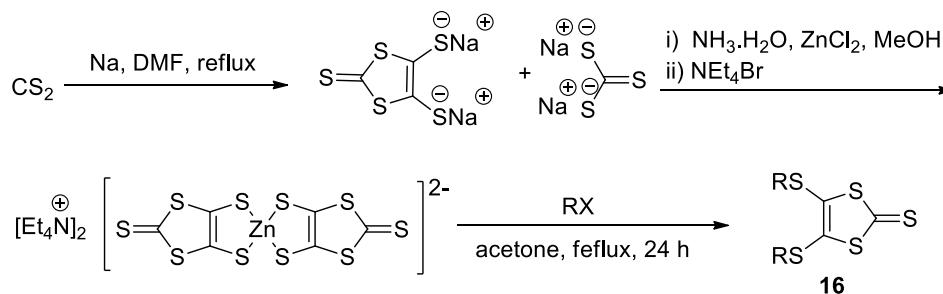
not just limited to the construction of symmetrically-substituted TTFs. Actually, unsymmetrically-substituted TTFs can also be prepared by reacting a 1,3-dithiole-2-thione with a 1,3-dithiole-2-one counterpart in the presence of a phosphite (e.g., Scheme 1.4B). For both of the phosphite-promoted synthesis, high reaction temperature is needed to achieve good reaction yields. Such harsh conditions make these methods inapplicable to the synthesis of TTF derivatives with limited thermal stability. An alternative methodology based on the Wittig olefination (e.g., the conversion of **13** to **15**, Scheme 1.4C) can be used to make TTFs and exTTFs to avert the heating problem. This method requires the preparation of a phosphonium or phosphonate ylide precursor at first (e.g., **14** in Scheme 1.4C). The ylide precursor then reacts with a carbonyl compound (ketone or aldehyde) in the presence of a strong base to install the dithiole unit to a suitable  $\pi$ -system via a C=C bridge.<sup>21,22</sup> This olefination approach can flexibly construct exTTFs and dithiafulvenyl (DTF) derivatives. Compared with the previous two approaches, it does not require high temperature and can thus be used to complement the other two methods.



**Scheme 1.4** Synthetic methods for symmetrical TTF **9**, unsymmetrical TTF **12** and DTF

**15.**

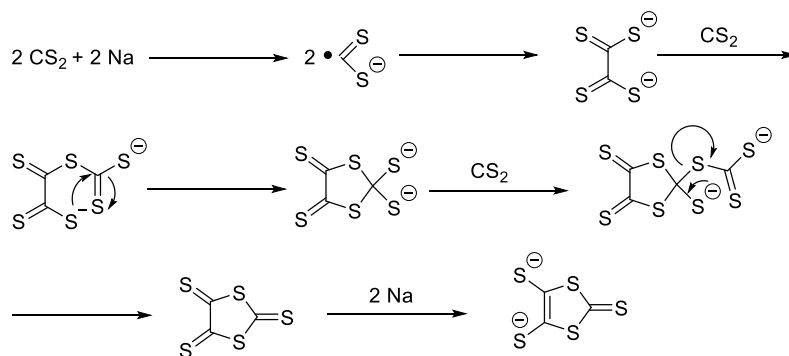
Since 1,3-dithiole-2-thione (e.g., **11**, Scheme 1.4) can be readily functionalized with a large variety of side groups (R), they have become a widely used starting material in the preparation of different types of DTFs and TTFs. The commonly used synthetic route to such thiones is illustrated in Scheme 1.5.



**Scheme 1.5** Synthetic route for 1,3-dithiole-2-thione **16** involving the reduction of  $\text{CS}_2$  with Na as the key step.

By this method, various 1,3-dithiole-2-thiones can be prepared on a large scale in a relatively low-cost manner. The method was originally developed by Hoyer's group in 1979.<sup>23</sup> The synthesis begins with the treatment of  $\text{CS}_2$  with an alkali metal (e.g., Na or K). Herein the alkali metal acts as a reducing agent to convert  $\text{CS}_2$  to 1,3-dithiole-2-thione-4,5-dithiolate. A multi-step mechanism for this transformation is proposed in Scheme 1.6.<sup>24</sup> When the reaction is complete, the dithiolate anion is then stabilized by an ammonium salt in which two dithiolate anions chelate with a zinc(II) cation. Depending

on the structure of 1,3-dithiole-2-thione desired, an appropriate electrophile is used to react with the zinc complex to yield the desired product **16**. The most common electrophiles for these reactions include propargyl halides, vinyl halides, alkyl halides, acyl chlorides, and so on.



**Scheme 1.6** Mechanism of the reduction and coupling of CS<sub>2</sub> with Na metal.

### 1.1.3 Applications of TTFs and Their Derivatives

The unique redox properties of TTF and exTTFs make them widely applicable in materials chemistry. As excellent  $\pi$ -electron donors, they can readily form C-T (charge transfer) complexes with electron-deficient molecules, yielding organic conductors, semiconductors, and even superconductors. The C-T and  $\pi$ - $\pi$  interactions between TTFs and other conjugated materials also facilitate their application in the realm of supermolecular chemistry and molecular machinery. In this section, a brief literature review on the application of TTFs and exTTFs is provided, with emphasis placed on examples representing the breakthroughs made over the many years of development in TTF-based materials chemistry.

### 1.1.3.1 TTF-based C-T Complexes as Organic Conductors

The seminal paper by Wudl<sup>25</sup> on the [TTF]<sup>+</sup>Cl<sup>-</sup> salt demonstrated the first organic conductor with an unprecedented metallic electric conductivity through molecular stacking. This study soon sparked interest in TTF-based C-T complexes with the aim of synthesis and characterization of new organic conductors. Shortly after the report of [TTF]<sup>+</sup>Cl<sup>-</sup> salt, an organic  $\pi$ -acceptor, tetracyanoquinodimethane (well-known as TCNQ) was paired with TTF, giving a C-T complex with even better metallic conductivity than Wudl's [TTF]<sup>+</sup>Cl<sup>-</sup> salt.<sup>26</sup> Delocalized electrons were generated through intermolecular charge transfer from electron rich TTF to electron-deficient TCNQ.<sup>27</sup> This C-T system was then used to fabricate thin film conductors, such as (BEDT-TTF)-TCNQ (herein BEDT stands for bis-(ethylenedithio)) by means of physical vapour deposition.<sup>14</sup> Ferrocene (Fc) exhibits versatile Fe(II)/Fe(III) redox chemistry and the ferrocenium ion can give rise to a variety of magnetic properties.<sup>28</sup> For this reason, the combination of TTF with Fc groups was investigated in order to obtain multifunctional materials with electrical conductivity and magnetism together. One of the best examples of this research is the first organic dianion containing the Fc derivative, namely  $\alpha$ -(BEDT-TTF)<sub>4</sub>(Fe(Cp-CONHCH<sub>2</sub>SO<sub>3</sub>)<sub>2</sub>).4H<sub>2</sub>O (**17**, Fig. 1.3). It was found to possess much better metallic properties than the individual functional component (TTF and Fc) separately.<sup>29</sup> Fc-TTF containing multifunctional materials were further developed by modification of the Fc moiety. For instance, a tetraphenylphosphonium salt of ferrocenesulfonate, (C<sub>5</sub>H<sub>5</sub>)Fe(C<sub>5</sub>H<sub>4</sub>-SO<sub>3</sub><sup>-</sup>) was devised as zwitter ion (see Scheme 1.7).<sup>2</sup>

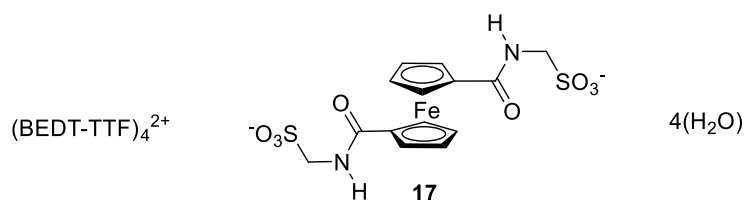
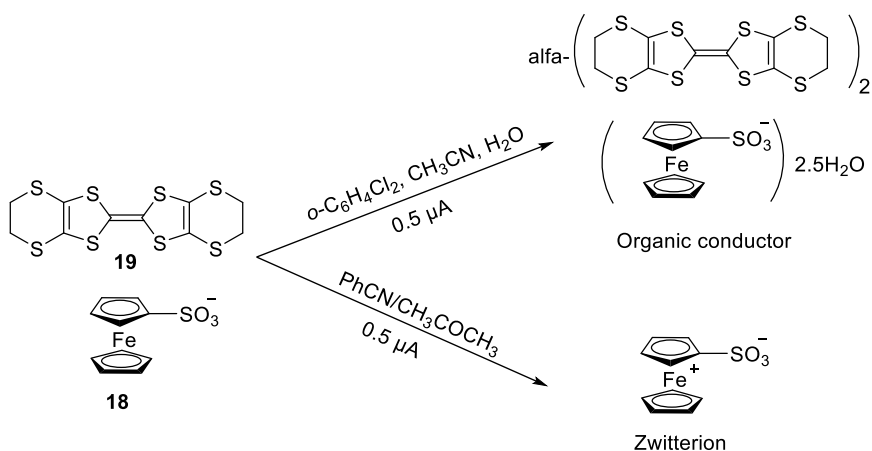


**Fig. 1.3** Structure of  $\alpha$ -(BEDT-TTF) $_4$ (Fe(Cp-CONHCH $_2$ SO $_3$ ) $_2$ ).4H $_2$ O (**17**)

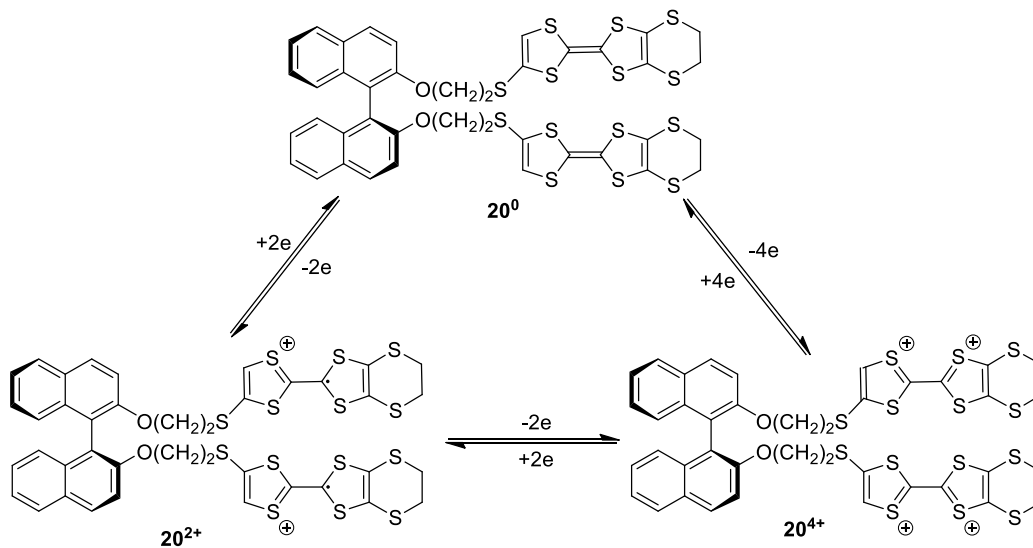


**Scheme 1.7** BEDT-TTF-based organic charge transfer salt and the zwitterion of ferrocenesulfonate prepared by constant-current electrocrystallization method.

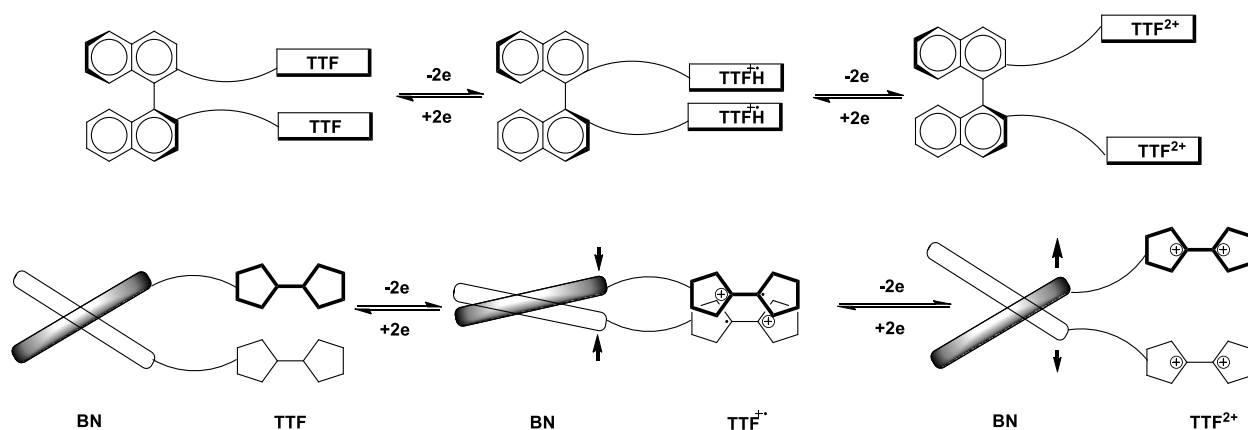
### 1.1.3.2 TTF-based Molecular Machines and Switches

TTFs show reversible redox behaviour and can be used as switchable units in advanced molecular devices. In the molecular design of functional molecular switches and machines, the redox properties of TTFs can be modified and finely tuned at the molecular level.<sup>8,30,31</sup> A simple and straightforward way to judge TTF oxidation is to observe its color change, which is usually very dramatic (e.g., from pale yellow to dark

green or deep blue). Application of this colorimetric property can be found from the work reported by Zhou *et al.*<sup>32</sup> in which chiroptical systems based on chiral binaphthyl units were covalently connected to two TTF groups. Binaphthalene molecules as axially chiral species often show strong circular dichroism (CD) signals that are readily detectable.<sup>33</sup> Changes in the oxidation states of TTFs lead to either repulsion or attraction between two TTFs and, as a result, the dihedral angle of the binaphthalene molecule is altered, giving rise to different CD signals accordingly (Scheme 1.8). A better comprehension of the dihedral angle changes in response to the oxidation and reduction processes can be made from the schematic representation in Scheme 1.9.



**Scheme 1.8** Illustration of the three states of compound **20** after oxidation and reduction.



**Scheme 1.9** Schematic illustration of the three states of **20** showing different dihedral angles after oxidation of TTF units (BN: binaphthalene unit).

Some other studies have been carried out on TTF-porphyrin based redox fluorescent switches, for example, compounds **21-23** (Figure 1.4).<sup>34</sup> The fluorescence of porphyrin can be quenched through electron transfer from TTF to porphyrin, but oxidation of TTF shuts down the electron transfer and hence enhances the fluorescence of the TTF-porphyrin compounds.<sup>34</sup>

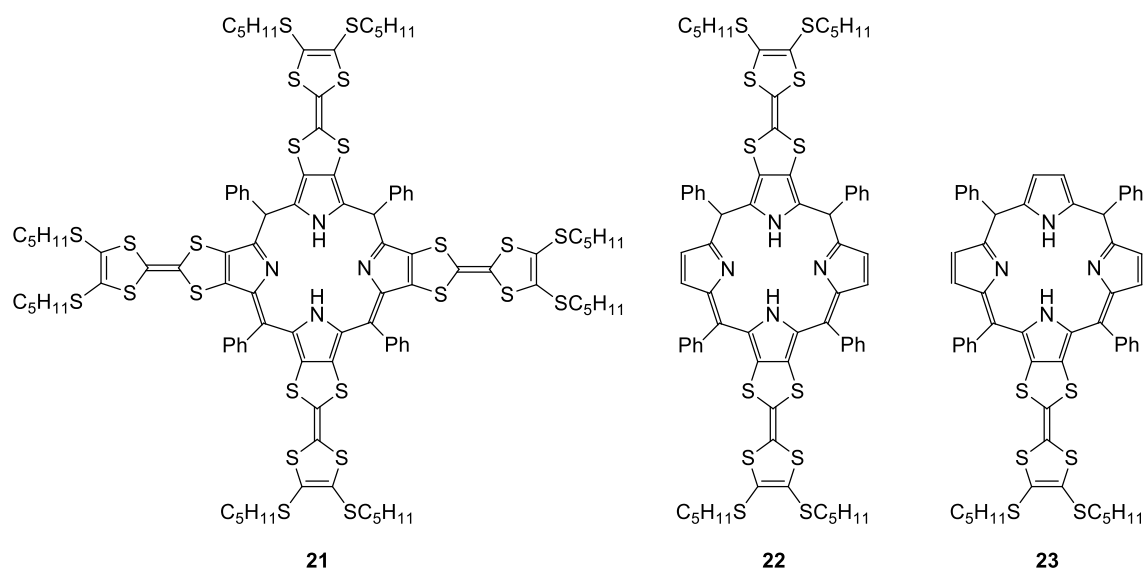


**Fig. 1.4** TTF-porphyrin based redox fluorescent switches.

Fabrication of a molecular machine based on TTF moieties (**24**, Fig. 1.5) was recently reported by the Stoddart group.<sup>35,36</sup> The bistable redox-controllable rotaxane undergoes controllable and reversible movement when TTFs are oxidized and reduced through chemical or electrical processes. The design idea of this rotaxane was based on the chemistry of guest-host recognition.<sup>37</sup> The positions of the CBPQT<sup>4+</sup> (cyclobis(paraquat-*p*-phenylene)) rings favor being around the two TTF stations R<sup>8+</sup>(rotaxane<sup>8+</sup>) as opposed to the two naphthalene (NP) stations. Chemical oxidation of the TTF leads to their dicationic form (TTF<sup>2+</sup>). The coulombic repulsion of similar charges then pushes the CBPQT<sup>4+</sup> rings to the NP stations. Overall, the main driving force for the movement comes from electrostatic charge-charge repulsion between the CBPQT<sup>4+</sup> rings and the TTF<sup>2+</sup> stations. Fig. 1.5 shows the interactions among CBPQT<sup>4+</sup>, neutral TTF and TTF<sup>+</sup> within the rotaxane molecule **24**.<sup>35</sup>

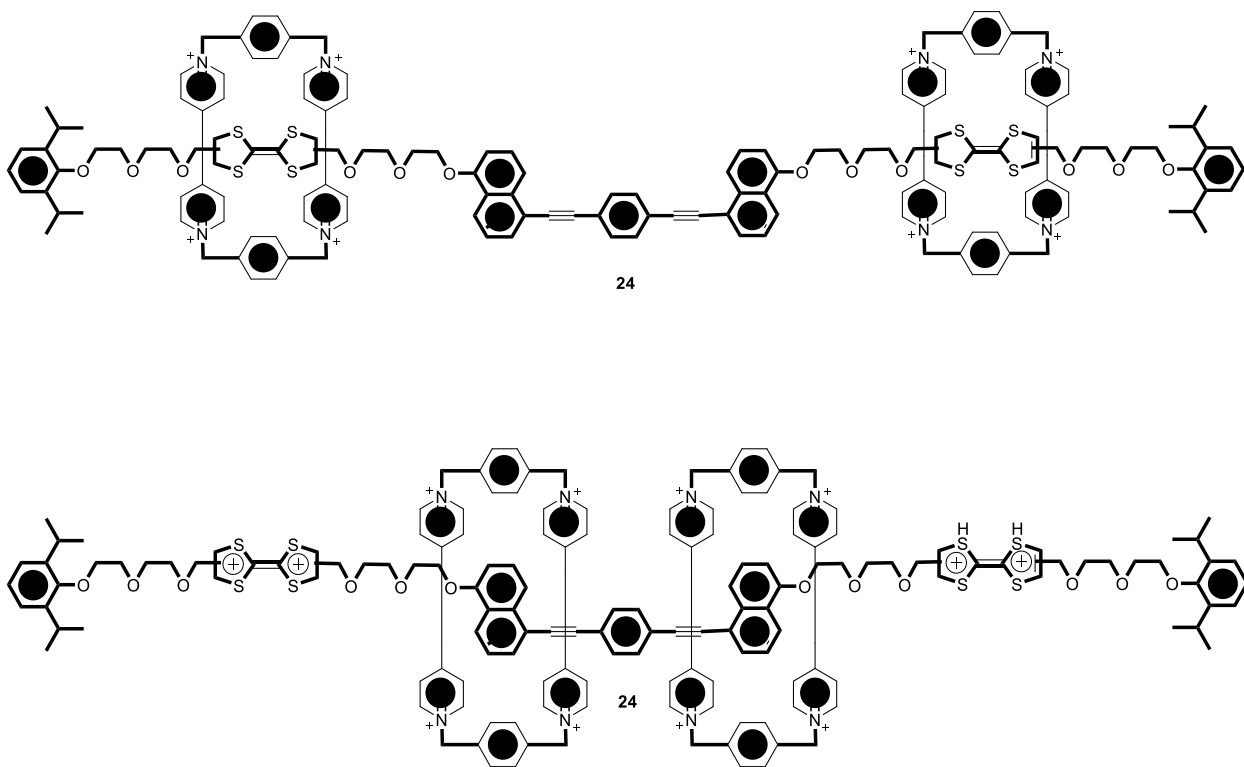


**Fig. 1.5** Rotaxane **24** as a redox-controlled molecular machine.

### 1.1.3.3 TTF Derivatives as Chemosensors

The redox switching properties of TTFs have found applications in molecular sensors, redox fluorescent switches, molecular clips and tweezers, redox-controlled gelation process.<sup>38-41</sup> Redox-active chemosensors utilizing TTF as the active component have been well developed for detection of various chemical species such as metal cations.<sup>42,43</sup> In a typical sensor system, a receptor group is linked to a TTF core which is usually designed as the reporter unit for certain binding events. For example, the crown ether-TTF hybrids **25-30** shown in Fig. 1.6 are electrochemical sensors for various metal cations. The crown ether groups here are selective metal ion receptors, to which various

metal cations can bind strongly. The metal binding enhances the inductive effects of the crown ether group, resulting in withdrawal of electron density away from the TTF core. As a result of this, the oxidation potential of the TTF unit is increased, and this can be readily monitored by voltammetric analyses. Pioneering in this area are Becker *et al.*<sup>44,45</sup> who synthesized crown ether annulated or tethered TTF derivatives **25-30** and tested them as cation sensors.

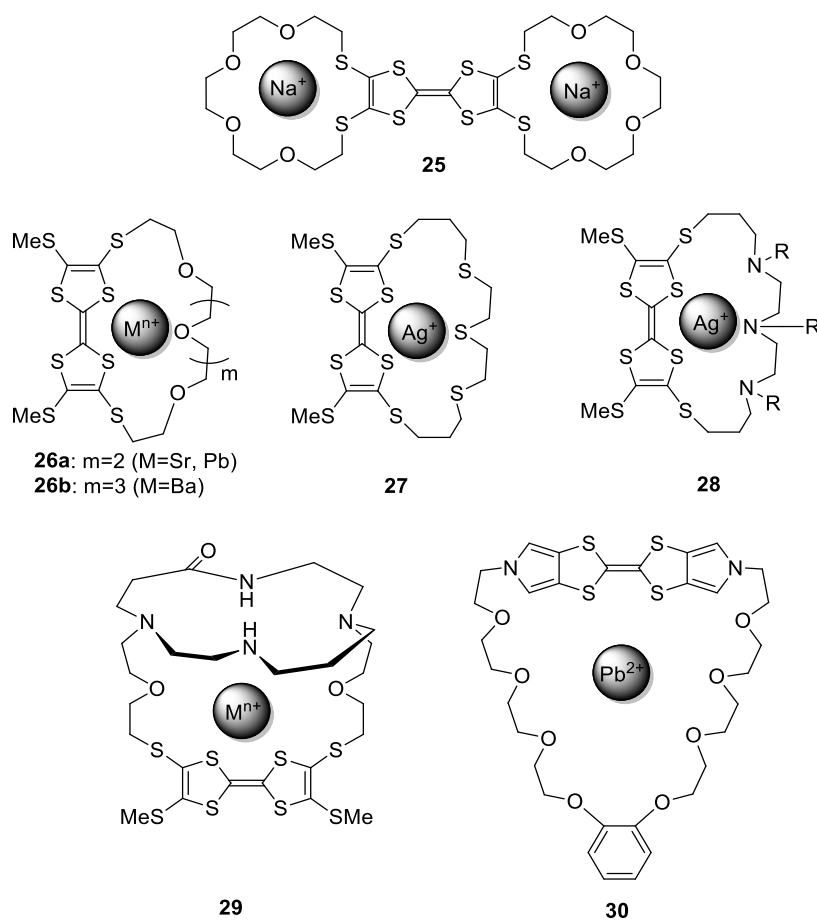


**Fig. 1.6** Examples of crown-annulated or tethered TTFs as metal ion sensors.

With a similar concept, Bryce and co-workers designed some TTF-podand systems (e.g., **31** and **32** in Fig. 1.7) in which the acyclic side chains serve as binding sites for certain transition metal ions.<sup>46,47,48</sup> Compared with the crown-TTF systems, these compounds can be more easily and efficiently synthesized, since the formation of crown ethers generally requires ultra-high dilution conditions to ensure satisfactory yields. Moreover, the construction of crown-TTF systems is much more tedious and often impeded by relatively low solubility due to less conformational flexibility. Nevertheless, the different binding properties of podand and crown ether ligands lead to different selectivity for metal ions as well as varied sensor performance, which were characterized by NMR and cyclic voltammetric analyses.

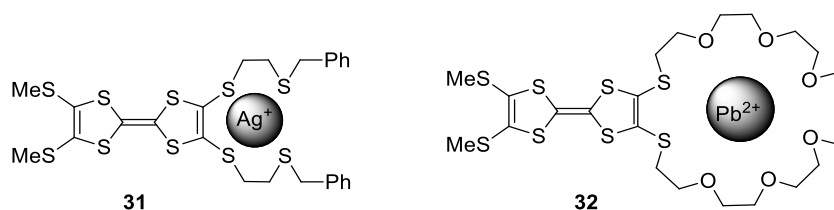


**Fig 1.7** TTF-podand systems **31** and **32** as transition metal ion sensors.

To obtain stronger metal ion binding ability, more rigid and pre-organized receptor units must be incorporated. This design strategy can be illustrated by a calix[4]arene-TTF system **33** (Fig. 1.8). The rigid calix[4]arene moieties in **33** create three-dimensional cavities that enhances the binding affinity and stoichiometry for metal ion guests such as sodium cation.<sup>49,50</sup>

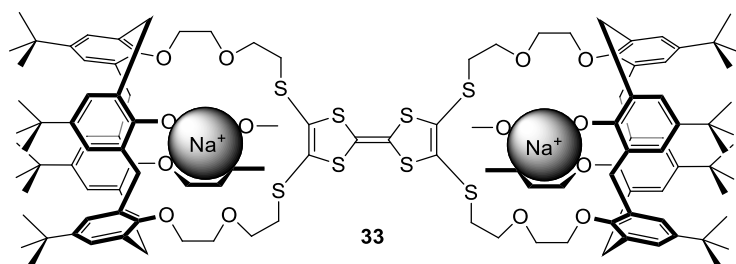
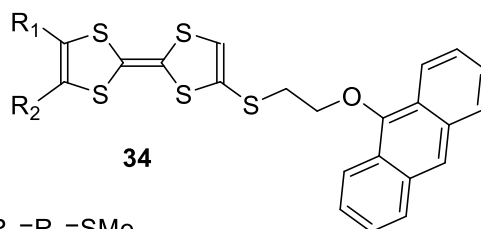


**Fig. 1.8** Bis(calixcrown)-TTF **33** as a Na<sup>+</sup> ion sensor.

Although a large portion TTF-based chemosensors was developed for cation sensing, TTF-based sensors for neutral and anionic chemical species have also been abundantly reported in the literature. For example, the detection of singlet oxygen as a cytotoxic chemical is very crucial in live cells,<sup>51,52</sup> and for this purpose anthracenyl-TTF derivatives **34a**<sup>53</sup> and **34b**<sup>54</sup> (Figure 1.9) were synthesized and applied as chemiluminescent traps to detect singlet oxygen.

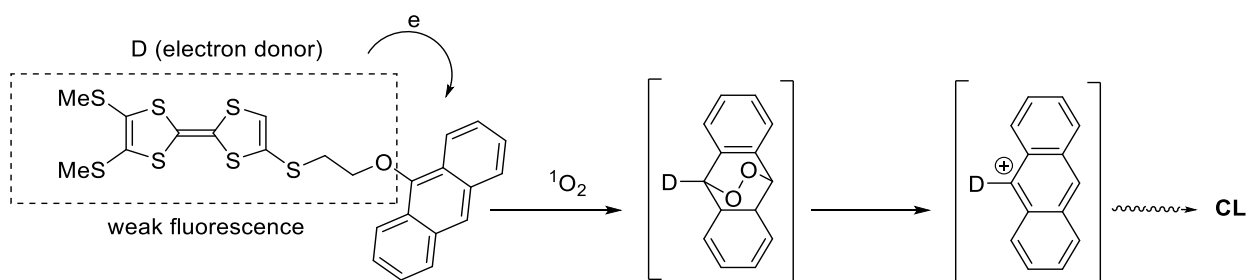


- 34a:** R<sub>1</sub>=R<sub>2</sub>=SMe  
**34b:** R<sub>1</sub>=SCH<sub>2</sub>CH<sub>2</sub>O-Anthryl; R<sub>2</sub>=H  
**34c:** R<sub>1</sub>=R<sub>2</sub>=S(SCH<sub>2</sub>CH<sub>2</sub>O)<sub>3</sub>CH<sub>2</sub>CH<sub>2</sub>OH

**Fig. 1.9** Anthracenyl-TTF derivatives for sensing singlet oxygen.

Anthracene itself is a reactive luminophore. Tethering strong electron donor such as TTF to it could result in trapping reactivity as well as photo-induced electron transfer (PET), as a result of which the fluorescence of anthracene is attenuated. The designed

systems **34a-b** showed high selectivity toward singlet oxygen ( $^1\text{O}_2$ ) with high chemiluminescence. The same magnitude of selectivity was not observed for other reactive oxygen species (ROS) such as  $\text{H}_2\text{O}_2$ ,  $\text{OCl}^-$ ,  $\text{O}_2^-$ . There are three steps involved in the proposed mechanism shown in Scheme 1.10. By mounting polar functional groups, the sensor molecule can be solubilized in water and surprisingly the same result was observed for compound **34c**.<sup>55</sup>



**Scheme 1.10** Possible mechanism for strong chemiluminescence (CL) of **34a** and  $^1\text{O}_2$ .

In a similar way, sensors for saccharides were designed based on TTF, anthracene and phenylboronic acid units. Compounds **35**<sup>56</sup> and **36**<sup>57</sup> (Fig. 1.10) are fluorescent sensors for saccharides, in which anthracene is included as a fluorophore and phenylboronic acid as the saccharide receptor. Without saccharide binding, the compounds are non-fluorescent due to the PET quenching effect of TTF. When these molecules are bound to saccharides, the PET process is disrupted and the fluorescence of anthracene is revived to give fluorescence turn-on sensing properties. Compound **35** shows a high selectivity towards D-fructose, whereas **36** is highly selective towards D-

glucose. The mechanism for the fluorescence sensing properties is schematically shown in Scheme 1.11.

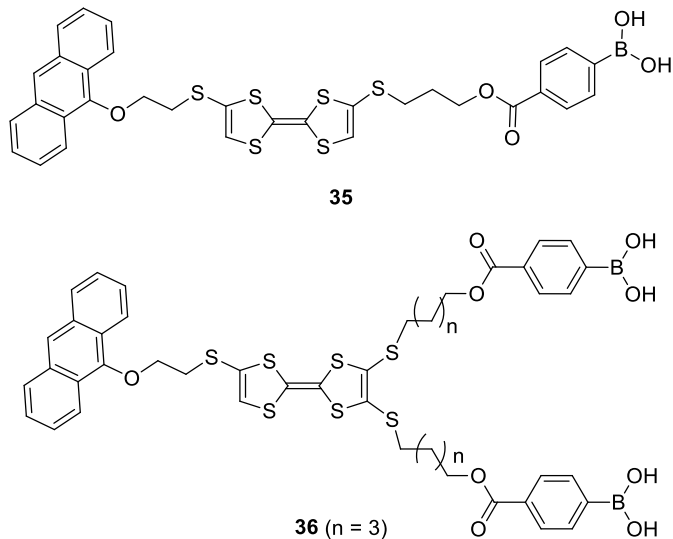
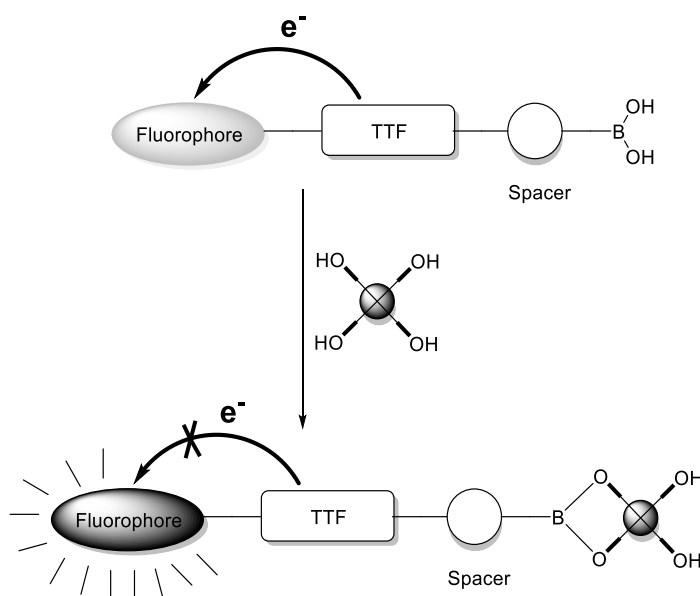


**Fig. 1.10** TTF-anthracene systems functionalized with phenylboronic acid groups as receptors for saccharides.

The simplified explanation for this phenomenon is the reverse process of PET. Basically, PET happens between TTF as electron donor and anthracene. When boronic acid is converted into boronate after binding with saccharides, it becomes a stronger Lewis acid (stronger electron acceptor) than free boronic acid. PET is then diverted from TTF to boronate instead of anthracene. This scenario allows the fluorescence of anthracene to increase, giving rise to fluorescence turn-on sensory performance upon saccharide binding.

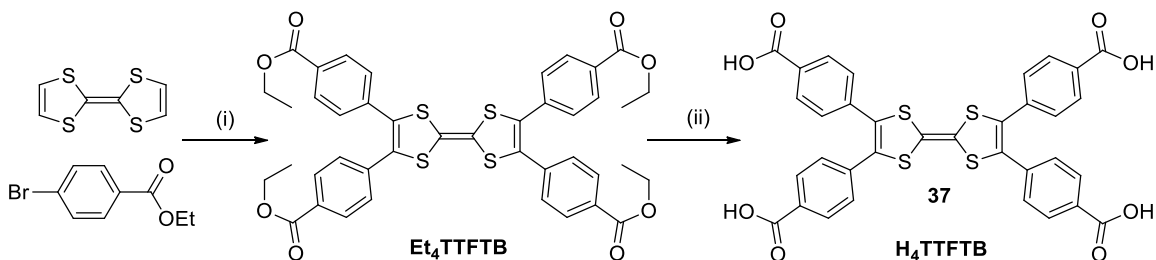


**Scheme 1.11** Fluorescence detection mechanism of saccharides by TTF-anthracene based boronic acid sensors.

#### 1.1.3.4 TTF Derivatives in Metal Organic Frameworks (MOFs)

Since the first study by Yaghi's group<sup>58</sup> in the late 1990s, MOFs have attracted huge attention as a new class of functional porous materials that are now a central research topic in the fields of materials science and engineering.<sup>59-64</sup> MOFs have been found useful in gas storage, separation, catalysis, chemical sensing, pharmaceutical and medicinal imaging. MOFs are crystalline, three-dimensional metal-organic structures that are formed by coordination reactions between metal ions and organic ligands. Metal ions such as zinc, copper, nickel, manganese, ruthenium and others are commonly used in preparation of MOFs. The organic ligands for MOFs are usually carboxylate or pyridine derivatives.<sup>58,65,66</sup> MOFs usually show low electrical conductivity. Thus for making more

conductive MOFs useful in solar cells, fuel cells, batteries and superconductors, the organic ligands need to be modified to enhance the conductivity behavior.<sup>67,68</sup> One of the organic ligands for fulfilling this goal is the carboxylated TTF derivative **H<sub>4</sub>TTFB** shown in Scheme 1.12.<sup>69,70</sup> This ligand can undergo coordination reaction with Zn(II) to form MOFs. The MOFs show both columnar stacking of TTF moieties and permanent pores lined up by benzoate linkers. Flash photolysis-time-resolved microwave conductivity (FP-TRMC) was used to measure the conductivity of the MOFs and the results showed charge mobility as good as some of the best conductive organic polymers.<sup>69</sup>



Conditions: (i) Cs<sub>2</sub>CO<sub>3</sub>, Pd(OAc)<sub>2</sub>, (HP-*t*-Bu<sub>3</sub>)(BF<sub>4</sub>) in THF, 18 h reflux; (ii) KOH in CH<sub>3</sub>OH, H<sub>2</sub>O, THF, 12 h reflux.

**Scheme 1.12** Synthesis of **H<sub>4</sub>TTFB**.

The single-crystal structure of the MOFs is shown in Fig. 1.11. The Dincă group<sup>70</sup> modified the electric conductivity of the MOFs by changing metal cations to Mn(II), Co(II) and Cd(II) instead of Zn(II).

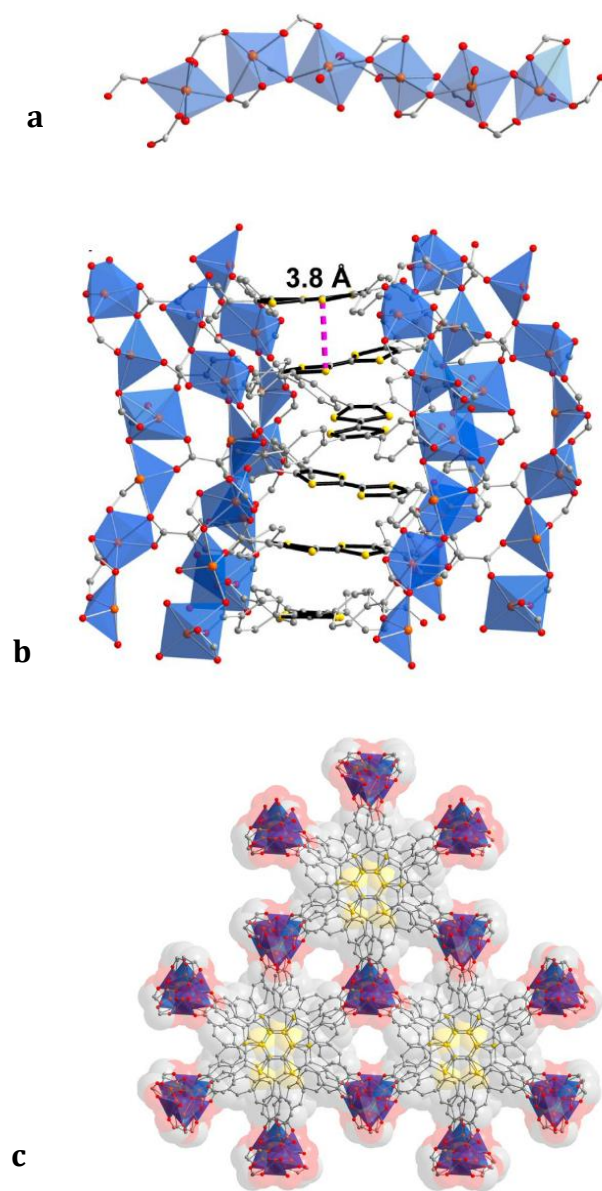


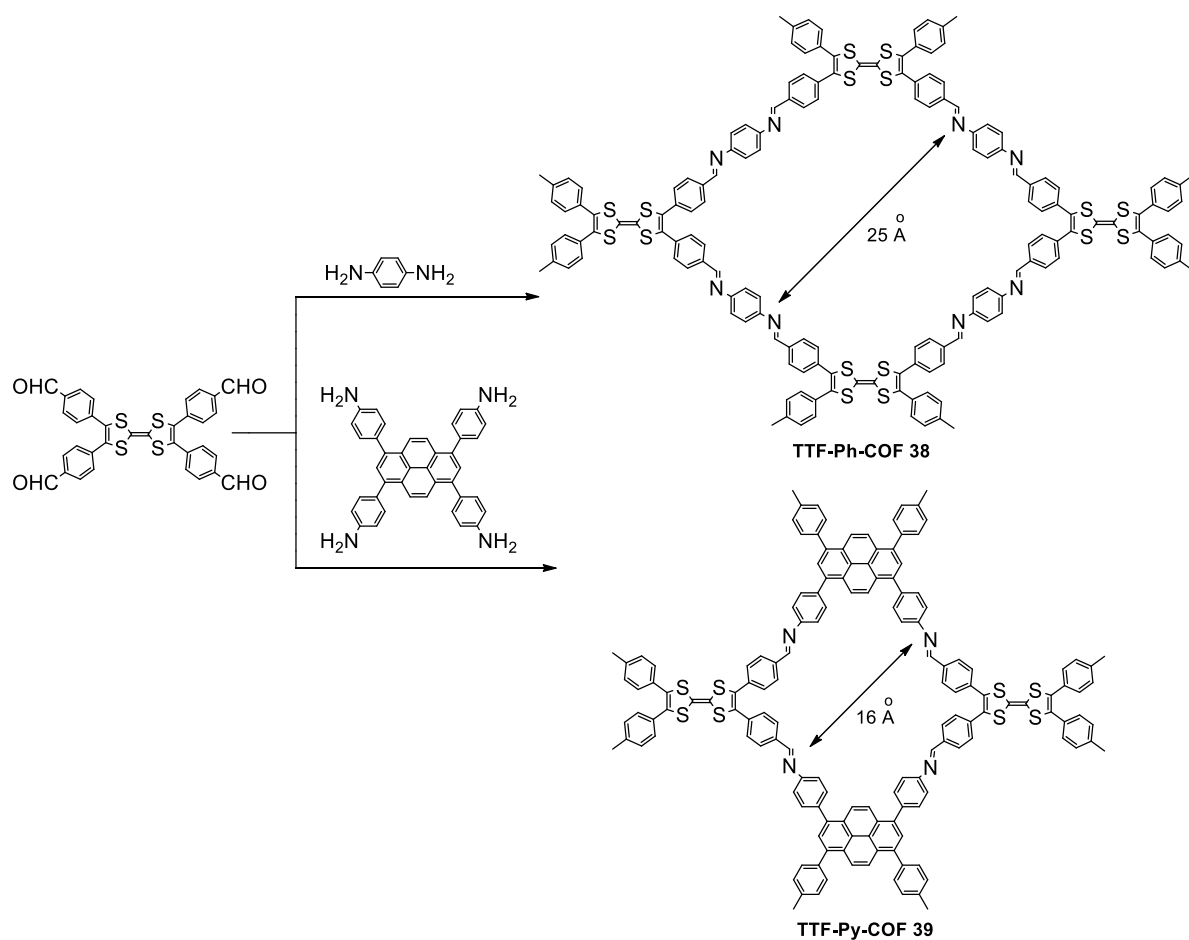
**Fig. 1.11** Portions of crystal structure of MOF: (a) the infinite helical Zn-carboxylate chain (b) a side view of helical TTF stack with depiction of the shortest intermolecular S...S contact and (c) a view of benzoate-lined infinite pores down the *c* axis. Orange,

yellow, red, and gray spheres represents Zn, S, O and C atoms respectively (adopted with permission from reference 67).

#### **1.1.3.5 TTF Derivatives in Covalent Organic Frameworks (COFs)**

Covalent organic frameworks (COFs) are another new type of porous crystalline materials, which emerged shortly after the discovery of metal organic frameworks but have ever since received considerable attention. Unlike MOFs, COFs are constructed by only organic building units using strong covalent bonds.<sup>71-73</sup> The enormous surface area, exceedingly high porosity, and relatively light weight of COFs make them appealing contenders to MOFs in many applications such as gas storage, adsorption, and catalysis. The seminal paper on COFs was published by Yaghi and co-workers in 2005,<sup>74</sup> in which self-condensation of benzenediboronic acid (BDBA) was used as the synthetic tool to give birth to the first example of a COF, namely COF-1. Later on, other co-condensation methodologies, such as triazine, boron, and imine based condensation reactions, have been investigated by different research groups.<sup>75</sup> Up to now, the number of scientific publications on COFs has been growing rapidly and many of the research objectives were focused on achieving excellent crystallinity, high surface area and porosity. Different building blocks can be used to construct COFs such as arenes, phthalocyanines, porphyrins, thiophenes, and diimides. These COFs exhibit significant light-emitting, semiconducting and/or photoconductive properties depending on the nature of the building blocks used.<sup>75-78</sup> To achieve efficient conductivity for COFs, the building blocks can be embedded with TTF moieties due to their electron donating properties and redox activity. Scheme 1.13 presents the synthesis of two recently reported TTF-based COFs in

which TTF building blocks are interconnected *via* phenyl and pyrene linkers. The important role of these linkers is to achieve layered lattice and assist in conductivity.<sup>79</sup> In the layered structure of this COF, TTF units stack in a columnar fashion that facilitates the charge mobility upon oxidation and results in enhancement in electric conductivity. Similar attempt was made to tune and optimize the conductivity properties of COFs by means of TTFs.<sup>80</sup> Fig. 1.12 provides the crystallographic views of the two COFs.



**Scheme 1.13** Synthesis of two TTF-based COFs in which phenyl and pyrene were used as linkers.

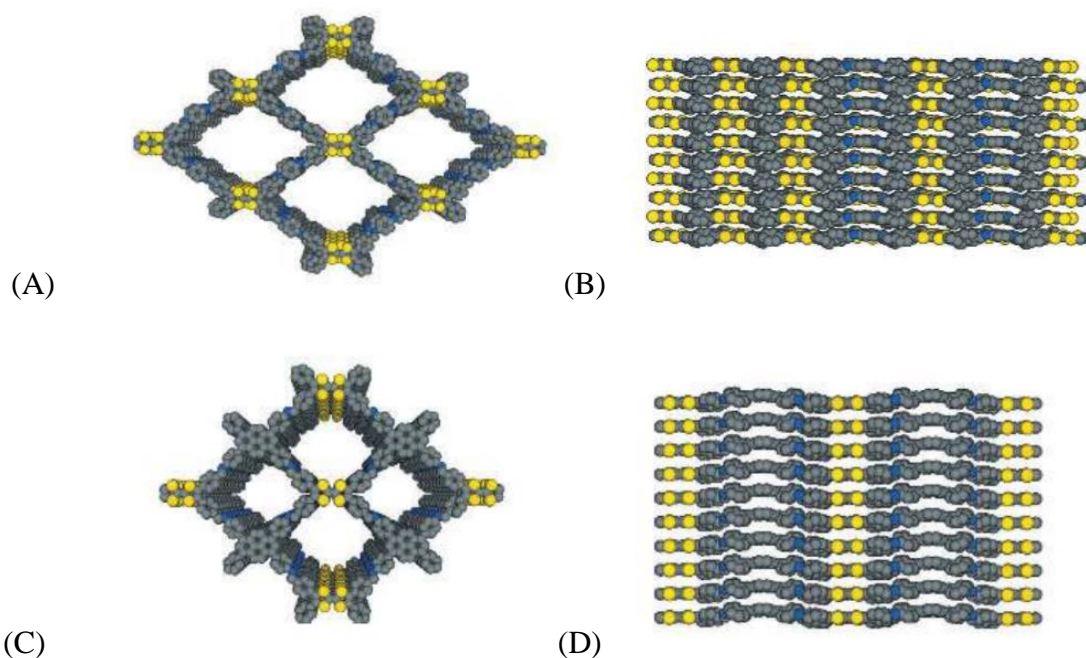
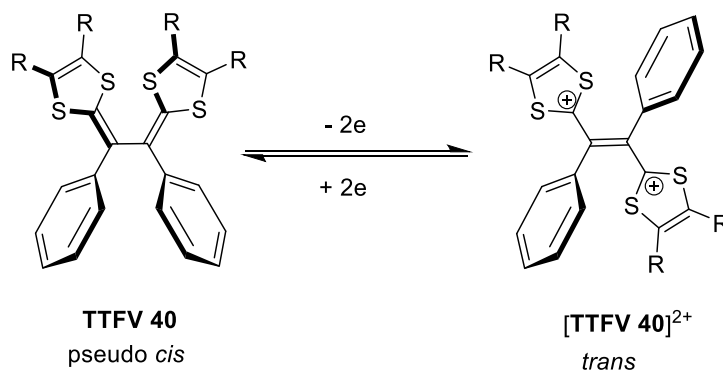


**Fig. 1.12** a) Schematic representation of the synthesis of mesoporous TTF-Ph-COF and microporous TTF-Py-COF topological diagram. Slipped AA stacking structures of TTF-Ph-COF at a) top and b) side views and eclipsed stacking structures of TTF-Py-COF at c) top and d) side views (yellow: S, blue: N, grey: C; H was omitted for clarity). (Figure adopted from reference 77 with permission).

## 1.2 Tetrathiafulvalene Vinylogues (TTFVs)

Tetrathiafulvalene vinylogues (TTFVs) are  $\pi$ -extended analogues of TTF bearing extended vinyl bridges between the two dithiol rings of TTF. Similar to the pristine TTF, TTFVs are also excellent electron donors and can undergo reversible electron transfer under mild redox conditions.<sup>81,82</sup> Aryl-substituted TTFVs can obtain different conformations in different oxidation states.<sup>12,83,84</sup> An example of this transformation is

shown in Scheme 1.14 in which the structure of diphenylated TTFV **40** can be transformed from pseudo *cis* to a complete *trans* conformation upon oxidation. The driving force for this redox-controlled conformational switching is the repulsion of positive charge on the two dithiolium moieties of TTFV dication versus steric interactions between dithiole and phenyl groups in the neutral molecule. In the neutral state of **40** the *cis*-like conformation encounters less steric interactions between the phenyl and dithiole ring and hence gives the most stable conformation. Oxidation of the TTFV to the corresponding dication produces two positive charges mainly populated on the two dithiolium units. The significant electrostatic repulsion hence supersedes the steric effects, driving the molecule to adopt a *trans* conformation.



**Scheme 1.14** Redox-induced conformational switching of diphenyl TTFV **40**.

Synthesis and application of TTFV-based  $\pi$ -conjugated materials have been actively investigated in recent years. The Zhao group is a major contributor to the development of this research topic. In this section, selected examples of TTFV derivatives are presented so as to cast an insight into the interesting fundamental aspects as well as the potential application of these molecules in nanomaterials and molecular devices. The remarkable

redox properties and controllable conformational switching behaviour of TTFVs are two key features taken advantage of in the design functional materials and devices containing TTFV building components. Especially, the supramolecular interactions between TTFVs and other molecules can be easily modulated and controlled by simply performing redox reactions on the TTFV units. By this way, intelligent nanomaterials and supramolecular systems have been developed, the performance of which are flexibly controlled under redox conditions.<sup>18,85,86</sup>

### 1.2.1 Polymerized TTFVs and Their Applications

In 2012, Zhao and Liang<sup>86</sup> reported the study of a conjugated phenylacetylene-TTFV copolymer **41** (Fig. 1.13) which shows similar redox activity of the TTFV monomer and dramatic conformational responsiveness to redox conditions. Furthermore, the TTFV units in this polymer were also found to be sensitive to pH change. Protonation of the polymer with a strong organic acid (TFA) could change the conformation of the TTFV copolymer from a coiled structure to a linear shape, as a result of the conformational change of each TTFV segment from pseudo *cis* to *trans*. The pH-dependant conformational switching behaviour of the TTFV copolymer was exploited to perform reversible dispersion and release of single-carbon nanotubes (SWNTs) in a controlled manner (illustrated in Fig 1.14). In the neutral state the copolymer favors a folded conformation, creating a hollow inner cavity suitable for encapsulation of guests with diameters of 1–2 nm (Fig. 1.13), such as an individual strand of SWNTs. Experimentally, it was found that polymer **41** would spontaneously wrap around SWNTs to form

supramolecular assemblies *via* favorable  $\pi$ - $\pi$  interactions. This effect led to efficient dispersion of SWNTs with **41** in common organic solvents, such as chloroform, with the aid of ultrasonication. Addition of TFA to the SWNT-**41** suspension caused protonation of copolymer **41**, which was accompanied by dramatic conformational changes to disrupt the polymer-SWNT interactions. As a result of this change, the SWNT-polymer assemblies were dissociated, leading to the precipitation of pristine SWNTs out of the solution phase. The protonated polymer, however, remained soluble in the organic solvent and could be recovered and reused in SWNT dispersion after neutralization with a base.

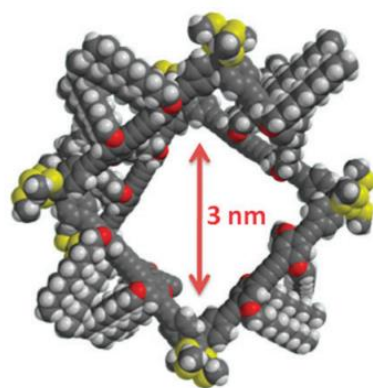
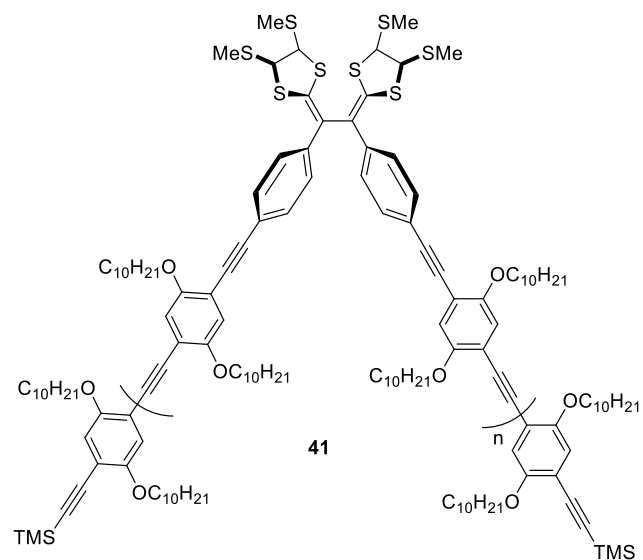


**Fig. 1.13** Molecular structure of copolymer **41** (top) and the space-filling model optimized by molecular mechanics calculation (bottom).

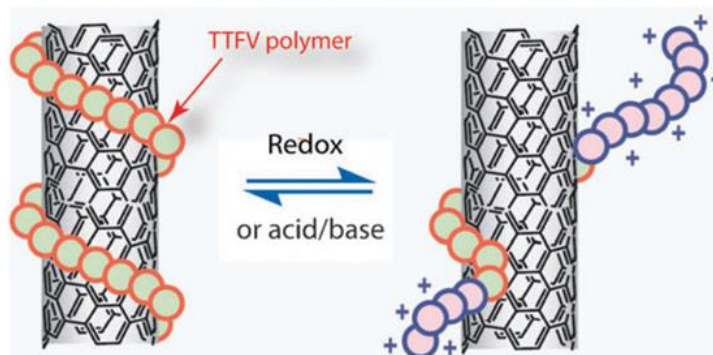
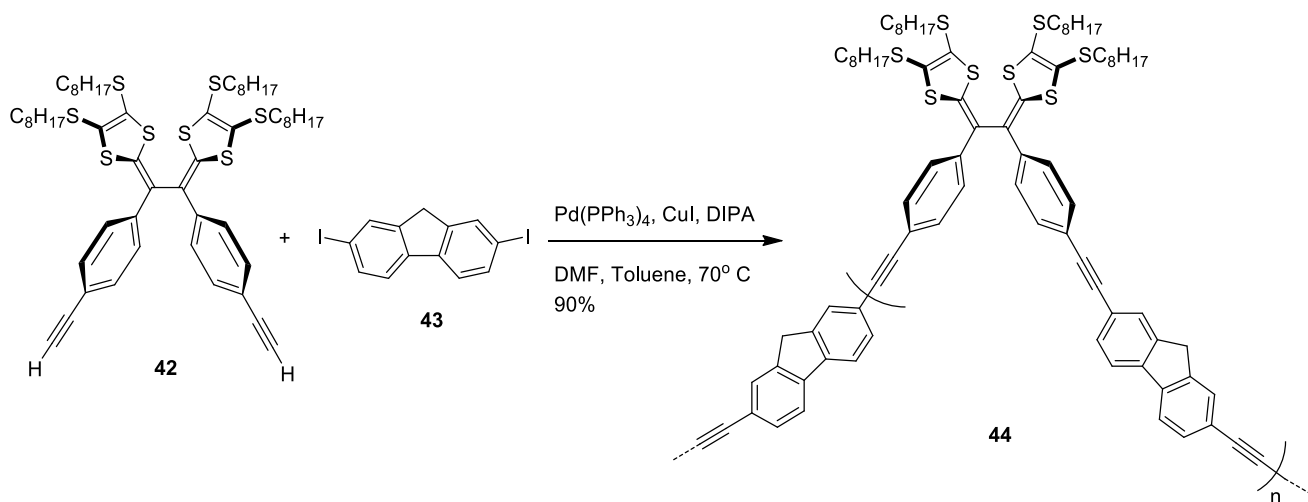


**Fig. 1.14** Bistable conformational changes of TTFV under redox and acid/base conditions. Reversible wrapping and unwrapping of SWNTs by a TTFV polymer.

In a similar study, which was carried collaboratively by Zhao and Adronov groups, a stimuli-responsive TTF-fluorene co-polymer **44** (Scheme 1.15) was designed and synthesized.<sup>85</sup> In the previous reports, the low molecular weights and poor solubility of TTFV-copolymers resulted in low SWNT concentrations dispersed in solution, and the copolymers did not show high selectivity for specific SWNT chiralities.<sup>86,87</sup> Introduction of highly  $\pi$ -conjugated aromatic units to the TTFV copolymer backbone was believed to improve the selectivity and dispersion efficiency, based on the consideration that fluorene-based polymers had been found to show excellent efficiency and selectivity in SWNT dispersion.<sup>88</sup> TTFV-fluorene copolymer **44** was synthesized through Sonogashira-Hagihara coupling in a good yield. Beside strong interactions with SWNTs, the copolymer is also capable of reversibly wrapping around and detaching from SWNTs under the control of pH. Spectroscopic analysis showed that **44** selectively disperse small-size semiconducting SWNTs in organic solvents. Computational studies (Fig. 1.15) suggested that the folding conformation of copolymer **44** in the neutral state allows

favoured  $\pi$ - $\pi$  stacking between the polymer backbone and SWNT, where the fluorene-SWNT interactions can be clearly identified as a major non-covalent force involved.



**Scheme 1.15** Synthesis of TTFV-fluorene copolymer **44**.

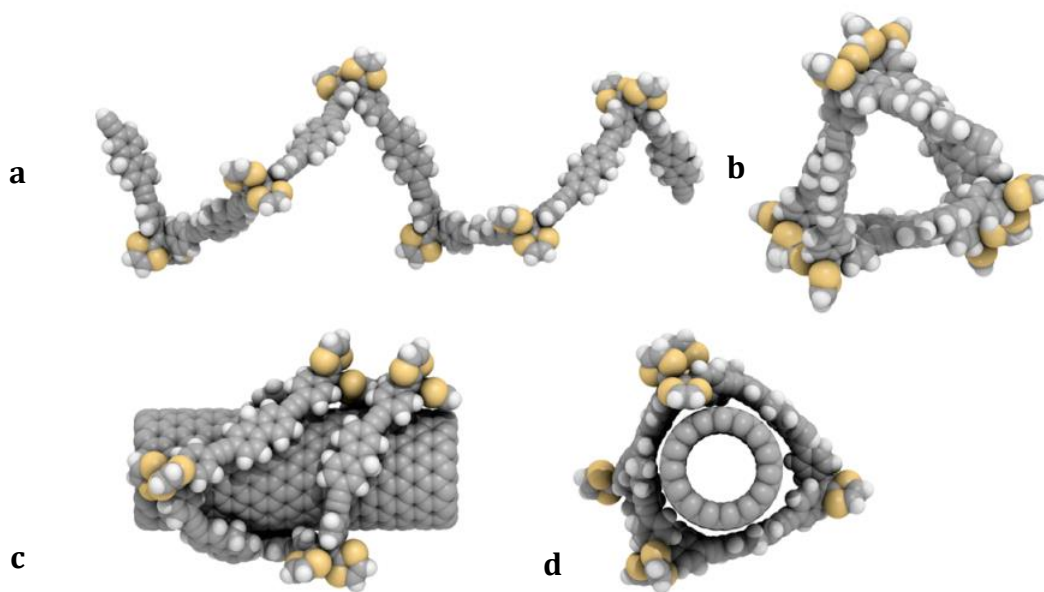


**Fig. 1.15** Conformation of a model hexamer of TTFV–fluorene copolymer: (a) side view, (b) front view. Two projections of the conformation of a model hexamer wrapping around a (10,0) SWNT: (c) side view, (d) front view. (Figure adopted from reference 88 with permission).

In 2015, Zhao and Bodwell collaboratively developed a TTFV-pyrene copolymer **47**, the synthesis of which is described in Scheme 1.16.<sup>89</sup> In this co-polymer, pyrene was adopted as one of the repeat units because of its remarkable photophysical properties of pyrene as well as its redox activity.<sup>90,91</sup> The combination of TTFV and pyrene groups in a  $\pi$ -conjugated polymer backbone delivered not only redox activity but intriguing solvent-dependent aggregation behaviour. Dynamic light scattering (DLS) measurements were performed to determine the size range of the polymer aggregates in different organic solvents. It was found that gradual addition of MeOH to the THF solution of copolymer **47** led to the formation of aggregates of varied sizes. The MeOH/THF ratio is a key factor dictating the size distribution ranging from ca. 620 nm to ca. 6.5  $\mu\text{m}$  in diameter. Modeling studies (Fig. 1.16) suggested that the conformation of the polymer backbone can vary from a zig-zag shape to self-aggregated foldamer, which plays an important role in the size change of the polymer aggregates.

In addition to pyrene–TTFV copolymers, TTFV-centered molecular tweezers containing pyrene endgroups were synthesized by Mulla and Zhao using click chemistry, and the compounds showed the performance of binding with  $\text{C}_{60}$  and  $\text{C}_{70}$  fullerenes and giving strong fluorescence turn-on responses.<sup>92</sup>



Other than conjugated polymers, macrocyclic compounds can also be generated when TTFV precursors were subjected to coupling reactions. The formation of acyclic or cyclic products is known to be dependent on several factors, including the pre-organization and concentration of the starting materials as well as the effects of “templating agents”. For example, Chen and Zhao reported the synthesis of TTFV-acetylene macrocycle **48** (Fig. 1.17)<sup>13,18</sup> through the Pd/Cu-catalyzed homocoupling reaction.<sup>93</sup> The reaction utilized an acetylenic-TTFV precursor and was carried out under dilute conditions (ca. 2.8 mM) in acetone under reflux for 2 days to afford a series of macrocyclic products ranging from trimer to pentamer as evidenced by MALDI-TOF MS analysis. After running column chromatographic separation, macrocycle **48** was obtained as the major product.

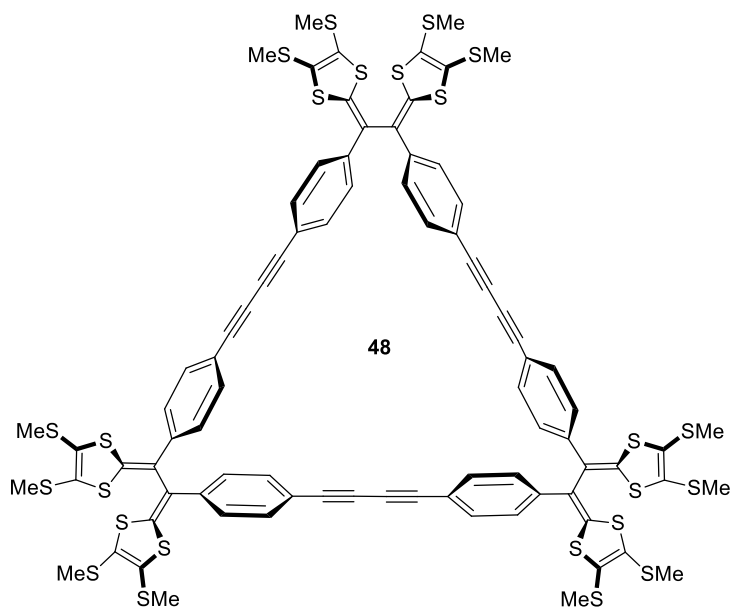


**Fig. 1.17** TTFV-phenylacetylene based shape-persistent macrocycle **48**.

The synthesis of a series of TTFV-arene macrocycles was subsequently reported by Mulla and Zhao.<sup>92</sup> Instead of the Pd/Cu-catalyzed alkynyl coupling, a more efficient Cu-catalyzed azide-alkyne coupling (CuAAC) reaction was used. As shown in Fig. 1.18, macrocycles **49** were successfully prepared *via* the CuAAC reaction between an acetylenic TTFV with various diazido-arenes.<sup>94,95</sup> The cyclization yields were very good due to the templating effect by the Cu(I) catalyst, since the triazole groups resulting from the CuAAC reaction can coordinate to Cu ions to form stable complexes.<sup>96</sup> This coordination effect can enhance the pre-organization of the reaction intermediates in favor of macrocyclization over other possible side reactions.

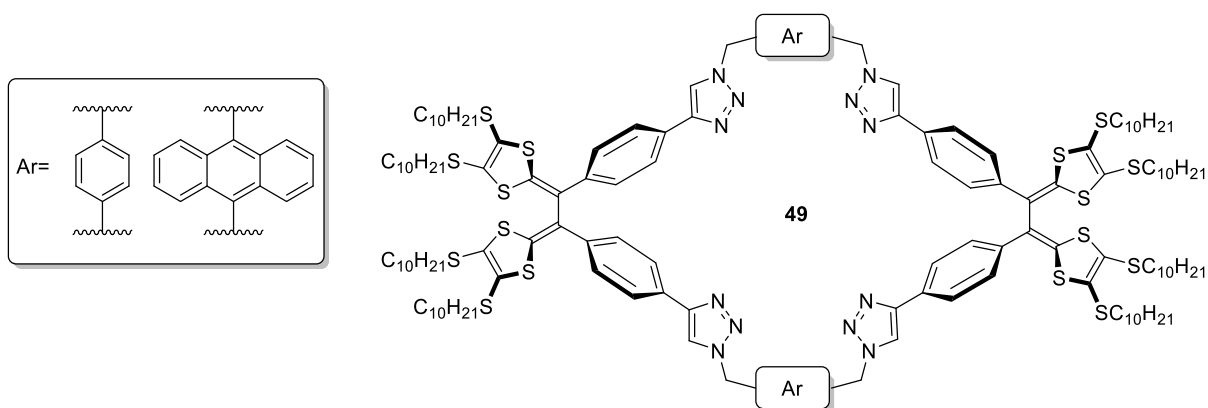
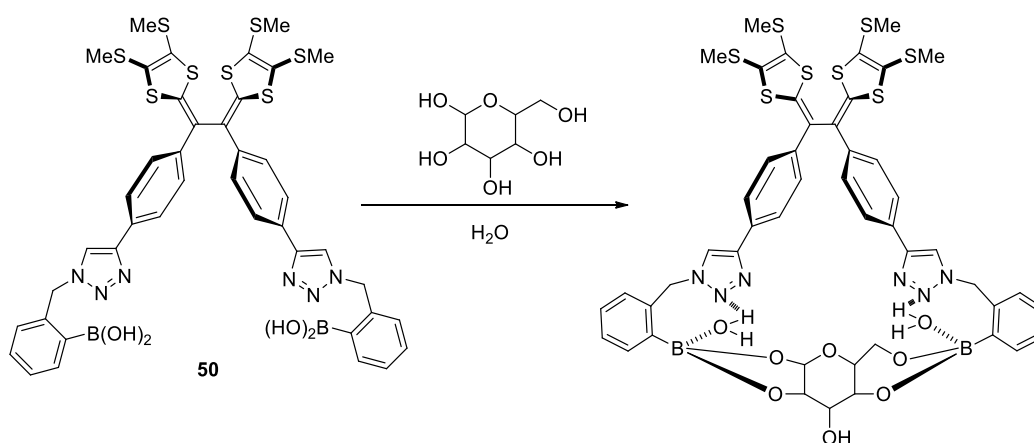


**Fig. 1.18** Macrocycles **49** prepared *via* Cu-catalyzed alkyne-azide coupling (CuAAC).

Other than TTFV-based polymers or macrocycles, tweezer-like TTFVs are interesting TTFV derivatives due to their ability to act as chemosensors for various species, such as sugars, transition metal ions, and fullerenes. TTFV-based molecular tweezers carrying phenylboronic groups (e.g., **50** in Scheme 1.17) was synthesized by the Zhao group using CuAAC reactions. It was found that the TTFV-boronic acid tweezers

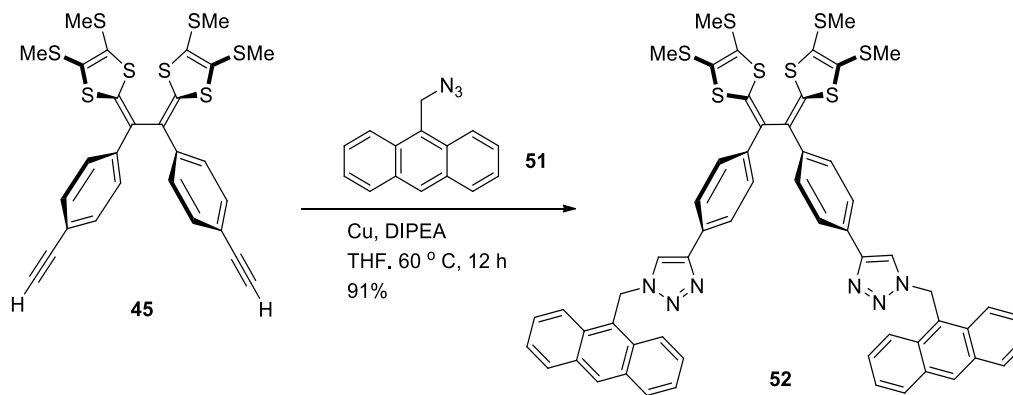
showed selective electrochemical sensing performance to different monosaccharides such as fructose, ribose, galactose and glucose in aqueous media under physiological conditions (pH 7.4).<sup>97</sup> Cooperative effects of the triazole and boronic acid groups enhanced the binding of **50** with saccharides, in which water molecules were proposed to participate actively.



**Scheme 1.17** Proposed 1:1 binding mode sensor **50** with a saccharide molecule forming a stable chelate with the assistance of water.

Another type of TTFV tweezers, dianthryl-TTFV **52**, was synthesized *via* the CuAAC strategy shown in Scheme 1.18.<sup>98</sup> TTFV **52** showed fluorescent turn-on sensing behaviour for  $\text{Cu}^{2+}$ ,  $\text{Fe}^{2+}$ , and  $\text{Cd}^{2+}$  ions in THF with low detection limit down to the sub-ppm level. Addition of metal ions was also observed to cause apparent color change in the solution of TTFV **52**, which can be deemed as colorimetric sensing. Nevertheless, the fluorescence turn-on properties are more advantageous than the color changes in terms of sensing efficiency. The reason for fluorescence enhancement (turn-on) comes from the

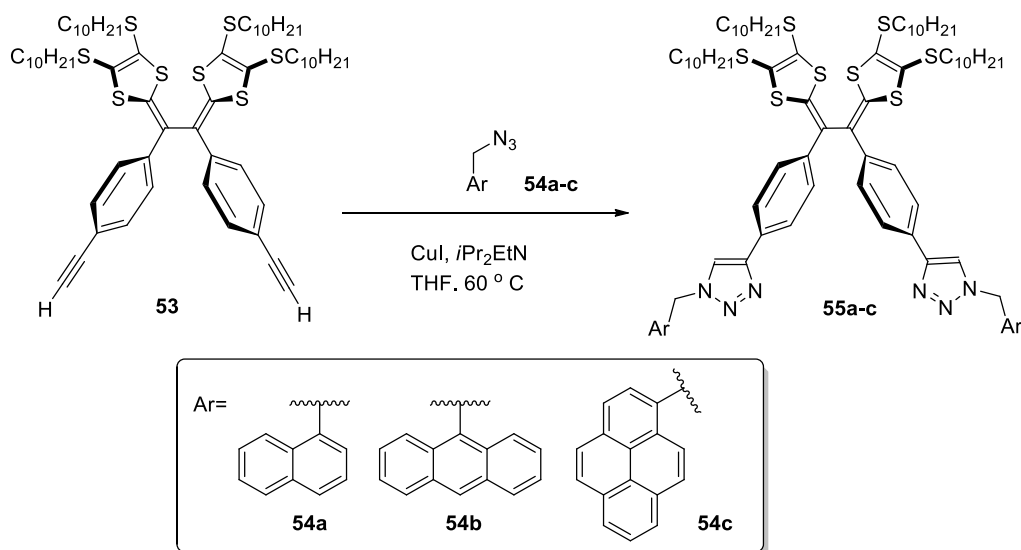
complexation of TTFV **52** with metal ions, which reduces the electron-donating ability of the TTFV unit. As a result, the PET quenching effect on the anthryl fluorophores by the TTFV unit is reduced or eliminated, leading to enhanced fluorescence of the sensor molecule.



**Scheme 1.18** Synthesis of diathryl-TTFV molecular tweezers **52** via the CuAAC reaction.

Due to fascinating properties and applications of fullerenes, development of effective methods for detection and separation of different fullerenes (e.g.,  $C_{60}$  and  $C_{70}$ ) has gained considerable attention.<sup>99</sup> Three TTFV-arene tweezers **55a-c** were synthesized and investigated as fullerene receptors/sensors (Scheme 1.19). Similar to the previous TTFV tweezers, **55a-c** were readily prepared through CuAAC reactions in good yields.<sup>92</sup> All these tweezers show fluorescence turn-on upon interacting with  $C_{60}$  and/or  $C_{70}$  fullerenes. The mechanism is similar to the metal sensing of dithranyl-TTFV **52**, while  $C_{60}/C_{70}$  fullerenes are electron-acceptors to disrupt the PET quenching effect. The selectivity of these tweezers towards fullerene  $C_{60}$  and  $C_{70}$  was determined by UV-Vis and

fluorescence spectroscopic titrations. Of great interest is TTFV **55b** which gives the best selectivity for C<sub>70</sub> over C<sub>60</sub> fullerene of 55a-c. Explanation for this outcome can be made by that C<sub>70</sub> is ellipsoidal in shape whereas C<sub>60</sub> is spherical. According to molecular modeling studies, C<sub>70</sub> better fits in the cavity of **55b** (Fig 1.19).



**Scheme 1.19** Synthesis of TTFV-arene tweezers **55a-c** via click reactions.

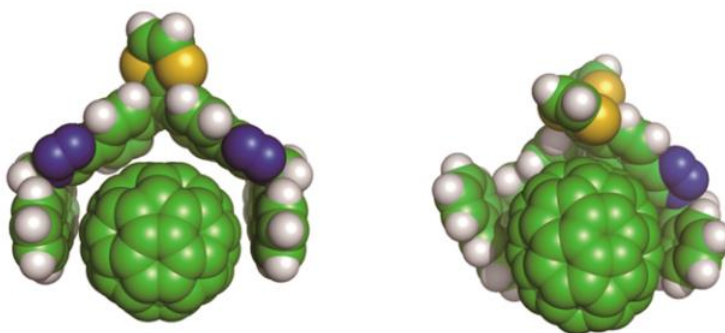
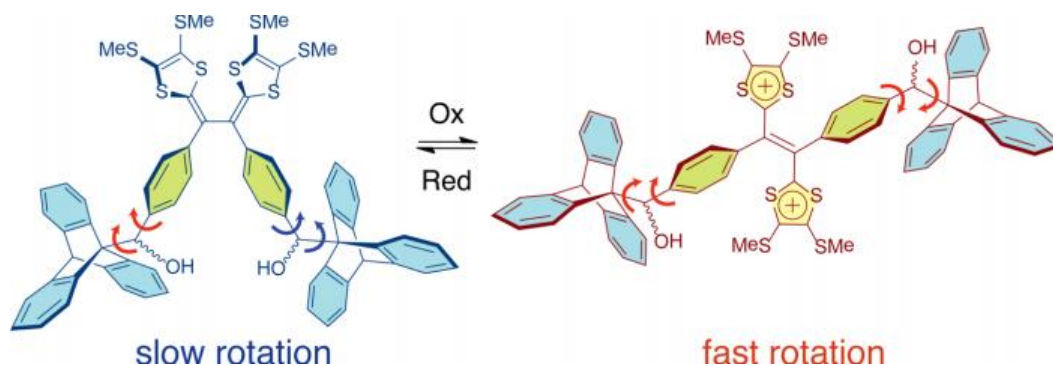


**Fig 1.19** Optimized molecular structures for the 1:1 complexes of **55b** with C<sub>60</sub> (left), and **55b** with C<sub>70</sub> (right) fullerenes.

As discussed in Section 1.1.3.2, TTF and derivatives can be used in fabrication of molecular machines. A very recent example worth mentioning here is the construction of a molecular rotor using TTFV as the control unit (Scheme 1.20).<sup>100</sup> This molecular rotor was obtained through multi-step synthesis using TTFV and triptycene as the essential building blocks. Dynamic NMR studies have shown that when the central TTFV is oxidized, the two triptycyl groups rotate at a faster rate than in the neutral state, which means that the redox state of the TTFV moiety exerts significant control over the rotational properties of two triptycyl units covalently bonded to it. This system represents the first example of synthetic rotors that are regulated by simple redox controls.

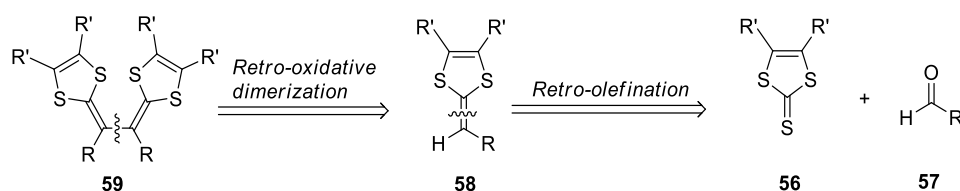


**Scheme 1.20** Redox-regulated rotary motion of bis(9-triptycyl)-TTFV system.

### 1.2.2 Synthetic Methods for Tetrathiafulvalene Vinylogues

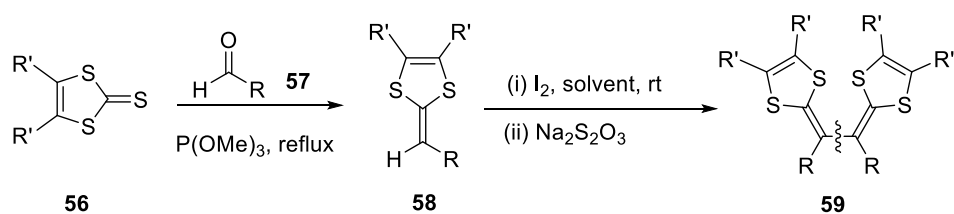
As TTFV-related compounds constitute an important part of this thesis work, it is imperative to provide an overview of the general synthetic methods for TTFVs and related structures. Scheme 1.21 illustrates the retrosynthetic analysis representing the most efficient approach for planning the synthesis of TTFVs. Herein, two sequential bond

disconnection steps result in two precursors, 1,3-dithiole-2-thione **56** and aldehyde **57**. Thione **56** can be easily prepared by the method described in Scheme 1.5, while aldehyde precursors are abundantly available in variety from commercial sources. As such, this synthetic strategy has become the most commonly used one in the preparation of TTFV derivatives so far.



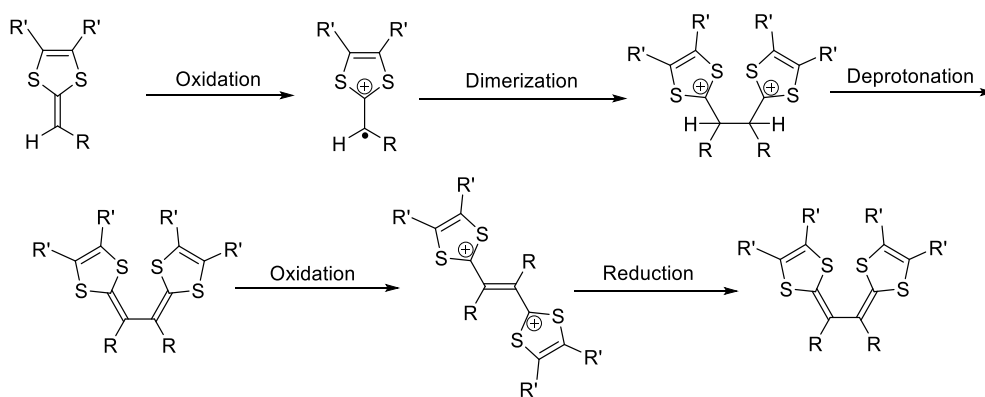
**Scheme 1.21** Retrosynthetic analysis of TTFVs.

Scheme 1.22 illustrates an exemplar synthesis of TTFV derivatives. The first step is to synthesize dithiafulvene (DTF) **58** by the reaction between 1,3-dithiole-2-thione **56** and an aldehyde **57** in the presence of a trialkyl phosphite (e.g., P(OMe)<sub>3</sub>, P(OEt)<sub>3</sub>).<sup>17,101</sup> Since the phosphite-promoted direct olefination typically requires relatively high temperature, the precursors must be thermally stable. This somehow limits the scope of this simple olefination methodology. The next step is to achieve TTFV through an oxidative dimerization. Usually, excess iodine is used as oxidant to convert DTF **58** into corresponding radical cation. The radical cation then undergoes a dimerization followed by deprotonation to afford TTFV **59**.<sup>102</sup> The TTFV once formed would be quickly oxidized into TTFV dication, hence a reductive workup is necessitated to produce neutral TTFV as the final product.



**Scheme 1.22** General synthetic approach to make TTFV.

The detailed mechanism of the DTF oxidative dimerization reaction is outlined in Scheme 1.23. It begins with a single electron transfer (SET) from DTF to the oxidant, forming the corresponding DTF radical cation. The DTF radical cation will then undergo dimerization to form a new carbon-carbon bond, and the acidic protons in the resulting dimer intermediate is then eliminated (deprotonation) to give the TTFV product, which is oxidized again under oxidative conditions to form a stable TTFV dication. When the oxidative dimerization is complete, a reducing agent such as sodium thiosulfate ( $\text{Na}_2\text{S}_2\text{O}_3$ ) is added to quench the excess oxidant and to re-generate the neutral TTFV.



**Scheme 1.23** Mechanism of DTF oxidative dimerization reaction.

### 1.3 Outline of This PhD Thesis

This PhD thesis has accomplished three major research projects on the synthesis and property characterization of functionalized  $\pi$ -conjugated oligomers, macrocycles and TTFV-based molecular materials. Suzuki coupling reaction, olefination and oxidative coupling have been utilized to a great extent in the synthetic portion, while advanced instrumental analytical techniques such as NMR, gel permeation chromatography (GPC), UV-Vis absorption spectroscopy, and cyclic voltammetry (CV), have been employed to understand the various properties of the new molecular materials developed. The detailed research results are outlined in Chapters 2 to 5.

Chapter 2 focuses on the synthesis and molecular properties of a new class of TTFV-fluorene co-oligomers and their supramolecular interactions with carbon nanotubes. Chapter 3 describes an investigation on different synthetic media for fabricating DTF-pyrene based macrocycle. Chapter 4 introduces the synthesis of a multivalent DTF-functionalization of dendritic oligo(phenylene vinylene)s with an anthraquinodimethane core and their application as electrochemical sensors for electron-deficient aromatics (e.g., nitrobenzene explosives). All these projects have met with success and the results are published in peer-reviewed scientific journals as three research articles in which the author of this thesis is the first author. So, the following chapters are organized with a paper-based structure.

Chapter 5 is the presentation of the initial pathways to accomplish the projects in Chapters 2-4. Since most of the reactions were ceased after getting disappointing results, the characterizations of compounds in this chapter are not comprehensive.

## 1.4 References

- (1) Wudl, F.; Smith, G. M.; Hufnagel, E. J. *J. Chem. Soc. D: Chem. Commun.* **1970**, 1453.
- (2) Akutsu, H.; Yamada, J.-i.; Nakatsuji, S. i.; Turner, S. S. *Dalton Trans.* **2013**, 42, 16351.
- (3) Rovira, C. *Chem. Rev.* **2004**, 104, 5289.
- (4) Raymo, F. M. *J. Am. Chem. Soc.* **2005**, 127, 9309.
- (5) Segura, J. L.; Martín, N. *Angew. Chem. Ed.* **2001**, 40, 1372.
- (6) Simonsen, K. B.; Becher, J. *Synlet* **1997**, 1997, 1211.
- (7) Nielsen, M. B.; Lomholt, C.; Becher, J. *Chem. Soc. Rev.* **2000**, 29, 153.
- (8) Canevet, D.; Salle, M.; Zhang, G.; Zhang, D.; Zhu, D. *Chem. Commun.* **2009**, 2245.
- (9) VandeVondele, J.; Lynden-Bell, R.; Meijer, E. J.; Sprik, M. *J. Phys. Chem. B* **2006**, 110, 3614.
- (10) Nielsen, M. B.; Sauer, S. P. A. *Chem. Phys. Lett.* **2008**, 453, 136.
- (11) Bendikov, M.; Wudl, F.; Perepichka, D. F. *Chem. Rev.* **2004**, 104, 4891.
- (12) Carlier, R.; Hapiot, P.; Lorcy, D.; Robert, A.; Tallec, A. *Electrochim. Acta* **2001**, 46, 3269.
- (13) Chen, G.; Mahmud, I.; Dawe, L. N.; Zhao, Y. *Org. Lett.* **2010**, 12, 704.
- (14) Solovyeva, V.; Keller, K.; Huth, M. *Thin Solid Films* **2009**, 517, 6671.
- (15) Massue, J.; Ghilane, J.; Bellec, N.; Lorcy, D.; Hapiot, P. *Electrochem. Commun.* **2007**, 9, 677.
- (16) Bryce, M. R. *J. Mater. Chem.* **1995**, 5, 1481.

- (17) Schou, S. S.; Parker, C. R.; Lincke, K.; Jennum, K.; Vibenholt, J.; Kadziola, A.; Nielsen, M. B. *Synlett* **2013**, *24*, 231.
- (18) Chen, G.; Mahmud, I.; Dawe, L. N.; Daniels, L. M.; Zhao, Y. *J. Org. Chem.* **2011**, *76*, 2701.
- (19) Akutagawa, T.; Kakiuchi, K.; Hasegawa, T.; Nakamura, T.; Christensen, C. A.; Becher, J. *Langmuir* **2004**, *20*, 4187.
- (20) Day, P.; Kurmoo, M. *J. Mater. Chem.* **1997**, *7*, 1291.
- (21) Blanchard, P.; Sallé, M.; Duguay, G.; Jubault, M.; Gorgues, A. *Tetrahedron Lett.* **1992**, *33*, 2685.
- (22) Märkl, G.; Bruns, D.; Dietl, H.; Kreitmeier, P. *Helv. Chim. Acta* **2001**, *84*, 2220.
- (23) Steimecke, G.; Sieler, H.-J.; Kirmse, R.; Hoyer, E. *Phosphorus and Sulfur and the Related Elements* **1979**, *7*, 49.
- (24) Parg, R. P.; Kilburn, J. D.; Ryan, T. G. *Synthesis* **1994**, *1994*, 195.
- (25) Wudl, F.; Wobschall, D.; Hufnagel, E. J. *J. Am. Chem. Soc.* **1972**, *94*, 670.
- (26) Jérôme, D. *Chem. Rev.* **2004**, *104*, 5565.
- (27) Bryce, M. R. *Adv. Mater.* **1999**, *11*, 11.
- (28) Miller, J. S.; Epstein, A. J.; Reiff, W. M. *Chem. Rev.* **1988**, *88*, 201.
- (29) Furuta, K.; Akutsu, H.; Yamada, J.; Nakatsuji, S. *Chem. Lett.* **2004**, *33*, 1214.
- (30) Zhang, Y.; Cai, L.-Z.; Wang, C.-Y.; Lai, G.-Q.; Shen, Y.-J. *New J. Chem.* **2008**, *32*, 1968.
- (31) Zhang, X.; Wang, C.; Lai, G.; Zhang, L.; Shen, Y. *New J. Chem.* **2010**, *34*, 318.
- (32) Zhou, Y.; Zhang, D.; Zhu, L.; Shuai, Z.; Zhu, D. *J. Org. Chem.* **2006**, *71*, 2123.

- (33) Setnička, V.; Urbanová, M.; Bouř, P.; Král, V.; Volka, K. *J. Phys. Chem. A* **2001**, *105*, 8931.
- (34) Nielsen, K. A.; Levillain, E.; Lynch, V. M.; Sessler, J. L.; Jeppesen, J. O. *Chem. Eur. J.* **2009**, *15*, 506.
- (35) Huang, T. J.; Brough, B.; Ho, C.-M.; Liu, Y.; Flood, A. H.; Bonvallet, P. A.; Tseng, H.-R.; Stoddart, J. F.; Baller, M.; Magonov, S. *Appl. Phys. Lett.* **2004**, *85*, 5391.
- (36) Nguyen, T. D.; Tseng, H.-R.; Celestre, P. C.; Flood, A. H.; Liu, Y.; Stoddart, J. F.; Zink, J. I. *Proc. Natl. Acad. Sci.* **2005**, *102*, 10029.
- (37) Tseng, H.-R.; Vignon, S. A.; Stoddart, J. F. *Angew. Chem. Ed.* **2003**, *42*, 1491.
- (38) Batail, P. *Chem. Rev.* **2004**, *104*, 4887.
- (39) Sarhan, A. E.-W. *A. O. Tetrahedron* **2005**, *61*, 3889.
- (40) Kitamura, T.; Nakaso, S.; Mizoshita, N.; Tochigi, Y.; Shimomura, T.; Moriyama, M.; Ito, K.; Kato, T. *J. Am. Chem. Soc.* **2005**, *127*, 14769.
- (41) Zheng, Y. B.; Yang, Y.-W.; Jensen, L.; Fang, L.; Juluri, B. K.; Flood, A. H.; Weiss, P. S.; Stoddart, J. F.; Huang, T. J. *Nano Lett.* **2009**, *9*, 819.
- (42) D. Beer, P.; A. Gale, P.; Z. Chen, G. *J. Chem. Soc., Dalton Trans.* **1999**, 1897.
- (43) Bernhardt, P. V.; Moore, E. G. *Austr. J. Chem.* **2003**, *56*, 239.
- (44) Hansen, T. K.; Joergensen, T.; Stein, P. C.; Becher, J. *J. Org. Chem.* **1992**, *57*, 6403.
- (45) Jorgensen, T.; Hansen, T. K.; Becher, J. *Chem. Soc. Rev.* **1994**, *23*, 41.
- (46) Johnston, B.; Goldenberg, L. M.; Bryce, M. R.; Katakya, R. *J. Chem. Soc., Perkin Trans. 2* **2000**, 189.

- (47) Lyskawa, J.; Le Derf, F.; Levillain, E.; Mazari, M.; Sallé, M.; Dubois, L.; Viel, P.; Bureau, C.; Palacin, S. *J. Am. Chem. Soc.* **2004**, *126*, 12194.
- (48) Lyskawa, J.; Le Derf, F.; Levillain, E.; Mazari, M.; Sallé, M. *Eur. J. Org. Chem.* **2006**, *2006*, 2322.
- (49) Zhao, B.-T.; Blesa, M.-J.; Mercier, N.; Le Derf, F.; Sallé, M. *J. Org. Chem.* **2005**, *70*, 6254.
- (50) Blesa, M.-J.; Zhao, B.-T.; Allain, M.; Le Derf, F.; Sallé, M. *Chem. Eur. J.* **2006**, *12*, 1906.
- (51) Sies, H. *Angew. Chem. Ed.* **1986**, *25*, 1058.
- (52) Devasagayam, T. P.; Kamat, J. P. *Indian J. Exp. Biol.* **2002**, *40*, 680.
- (53) Li, X.; Zhang, G.; Ma, H.; Zhang, D.; Li, J.; Zhu, D. *J. Am. Chem. Soc.* **2004**, *126*, 11543.
- (54) Zhang, G.; Li, X.; Ma, H.; Zhang, D.; Li, J.; Zhu, D. *Chem. Commun.* **2004**, 2072.
- (55) Zheng, X.; Sun, S.; Zhang, D.; Ma, H.; Zhu, D. *Anal. Chim. Acta* **2006**, *575*, 62.
- (56) Wang, Z.; Zhang, D.; Zhu, D. *J. Org. Chem.* **2005**, *70*, 5729.
- (57) Tan, W.; Wang, Z.; Zhang, D.; Zhu, D. *Sensors* **2006**, *6*, 954.
- (58) Li, H.; Eddaoudi, M.; Groy, T. L.; Yaghi, O. M. *J. Am. Chem. Soc.* **1998**, *120*, 8571.
- (59) Bétard, A.; Fischer, R. A. *Chem. Rev.* **2012**, *112*, 1055.
- (60) Cui, Y.; Yue, Y.; Qian, G.; Chen, B. *Chem. Rev.* **2012**, *112*, 1126.
- (61) Cook, T. R.; Zheng, Y.-R.; Stang, P. J. *Chem. Rev.* **2013**, *113*, 734.
- (62) Kreno, L. E.; Leong, K.; Farha, O. K.; Allendorf, M.; Van Duyne, R. P.; Hupp, J. T. *Chem. Rev.* **2012**, *112*, 1105.

- (63) Li, J.-R.; Sculley, J.; Zhou, H.-C. *Chem. Rev.* **2012**, *112*, 869.
- (64) Suh, M. P.; Park, H. J.; Prasad, T. K.; Lim, D.-W. *Chem. Rev.* **2012**, *112*, 782.
- (65) Yaghi, O. M.; Davis, C. E.; Li, G.; Li, H. *J. Am. Chem. Soc.* **1997**, *119*, 2861.
- (66) Cravillon, J.; Münzer, S.; Lohmeier, S.-J.; Feldhoff, A.; Huber, K.; Wiebcke, M. *Chem. Mater.* **2009**, *21*, 1410.
- (67) Hendon, C. H.; Tiana, D.; Walsh, A. *Phys. Chem. Chem. Phys.* **2012**, *14*, 13120.
- (68) Tiana, D.; Hendon, C. H.; Walsh, A.; Vaid, T. P. *Phys. Chem. Chem. Phys.* **2014**, *16*, 14463.
- (69) Narayan, T. C.; Miyakai, T.; Seki, S.; Dincă, M. *J. Am. Chem. Soc.* **2012**, *134*, 12932.
- (70) Park, S. S.; Hontz, E. R.; Sun, L.; Hendon, C. H.; Walsh, A.; Van Voorhis, T.; Dincă, M. *J. Am. Chem. Soc.* **2015**, *137*, 1774.
- (71) Ding, S.-Y.; Wang, W. *Chem. Soc. Rev.* **2013**, *42*, 548.
- (72) Segura, J. L.; Mancheno, M. J.; Zamora, F. *Chem. Soc. Rev.* **2016**, *45*, 5635.
- (73) Murray, L. J.; Dincă, M.; Long, J. R. *Chem. Soc. Rev.* **2009**, *38*, 1294.
- (74) Côté, A. P.; Benin, A. I.; Ockwig, N. W.; O'Keeffe, M.; Matzger, A. J.; Yaghi, O. *M. Science* **2005**, *310*, 1166.
- (75) Feng, X.; Ding, X.; Jiang, D. *Chem. Soc. Rev.* **2012**, *41*, 6010.
- (76) Colson, J. W.; Woll, A. R.; Mukherjee, A.; Levendorf, M. P.; Spitler, E. L.; Shields, V. B.; Spencer, M. G.; Park, J.; Dichtel, W. R. *Science* **2011**, *332*, 228.
- (77) Jin, S.; Furukawa, K.; Addicoat, M.; Chen, L.; Takahashi, S.; Irle, S.; Nakamura, T.; Jiang, D. *Chem. Sci.* **2013**, *4*, 4505.

- (78) Dogru, M.; Bein, T. *Chem. Commun.* **2014**, *50*, 5531.
- (79) Jin, S.; Sakurai, T.; Kowalczyk, T.; Dalapati, S.; Xu, F.; Wei, H.; Chen, X.; Gao, J.; Seki, S.; Irle, S.; Jiang, D. *Chem. Eur. J.* **2014**, *20*, 14608.
- (80) Cai, S.-L.; Zhang, Y.-B.; Pun, A. B.; He, B.; Yang, J.; Toma, F. M.; Sharp, I. D.; Yaghi, O. M.; Fan, J.; Zheng, S.-R.; Zhang, W.-G.; Liu, Y. *Chem. Sci.* **2014**, *5*, 4693.
- (81) Frere, P.; Skabara, P. J. *Chem. Soc. Rev.* **2005**, *34*, 69.
- (82) Roncali, J. *J. Mater. Chem.* **1997**, *7*, 2307.
- (83) Bellec, N.; Boubekeur, K.; Carlier, R.; Hapiot, P.; Lorcy, D.; Tallec, A. *J. Phys. Chem. A* **2000**, *104*, 9750.
- (84) Bryce, M. R.; Coffin, M. A.; Clegg, W. *J. Org. Chem.* **1992**, *57*, 1696.
- (85) Liang, S.; Zhao, Y.; Adronov, A. *J. Am. Chem. Soc.* **2014**, *136*, 970.
- (86) Liang, S.; Chen, G.; Peddle, J.; Zhao, Y. *Chem. Commun.* **2012**, *48*, 3100.
- (87) Liang, S.; Chen, G.; Zhao, Y. *J. Mater. Chem. C* **2013**, *1*, 5477.
- (88) Nish, A.; Hwang, J.-Y.; Doig, J.; Nicholas, R. J. *Nat. Nano* **2007**, *2*, 640.
- (89) Younes, E. A.; Williams, K.-L. M.; Walsh, J. C.; Schneider, C. M.; Bodwell, G. J.; Zhao, Y. *RSC Adv.* **2015**, *5*, 23952.
- (90) Figueira-Duarte, T. M.; Müllen, K. *Chem. Rev.* **2011**, *111*, 7260.
- (91) Winnik, F. M. *Chem. Rev.* **1993**, *93*, 587.
- (92) Mulla, K.; Shaik, H.; Thompson, D. W.; Zhao, Y. *Org. Lett.* **2013**, *15*, 4532.
- (93) Enozawa, H.; Hasegawa, M.; Takamatsu, D.; Fukui, K.-i.; Iyoda, M. *Org. Lett.* **2006**, *8*, 1917.
- (94) Hein, J. E.; Fokin, V. V. *Chem. Soc. Rev.* **2010**, *39*, 1302.

- (95) Meldal, M.; Tornøe, C. W. *Chem. Rev.* **2008**, *108*, 2952.
- (96) Lau, Y. H.; Rutledge, P. J.; Watkinson, M.; Todd, M. H. *Chem. Soc. Rev.* **2011**, *40*, 2848.
- (97) Mulla, K.; Zhao, Y. *Tetrahedron Lett.* **2014**, *55*, 382.
- (98) Mulla, K.; Dongare, P.; Thompson, D. W.; Zhao, Y. *Org. Biomol. Chem.* **2012**, *10*, 2542.
- (99) Georgakilas, V.; Perman, J. A.; Tucek, J.; Zboril, R. *Chem. Rev.* **2015**, *115*, 4744.
- (100) Chen, G.; Zhao, Y. *Org. Lett.* **2014**, *16*, 668.
- (101) Christensen, C. A.; Batsanov, A. S.; Bryce, M. R. *J. Org. Chem.* **2007**, *72*, 1301.
- (102) Hapiot, P.; Lorcy, D.; Tallec, A.; Carlier, R.; Robert, A. *J. Phys. Chem.* **1996**, *100*, 14823.

## Chapter 2

# Tetrathiafulvalene Vinylogue–Fluorene Co-oligomers: Synthesis, Properties, and Supramolecular Interactions with Carbon Nanotubes

The current chapter is based on my first paper published in the *Journal of Organic Chemistry (JOC)* with the same title and suitable modifications on compound, figure and scheme numbering. I am the first author to this paper and the principal investigator of the work described herein. I acknowledge Prof. A. Adronov and Mr. S. Liang at the Department of Chemistry, McMaster University for their kind assistance in GPC analysis.

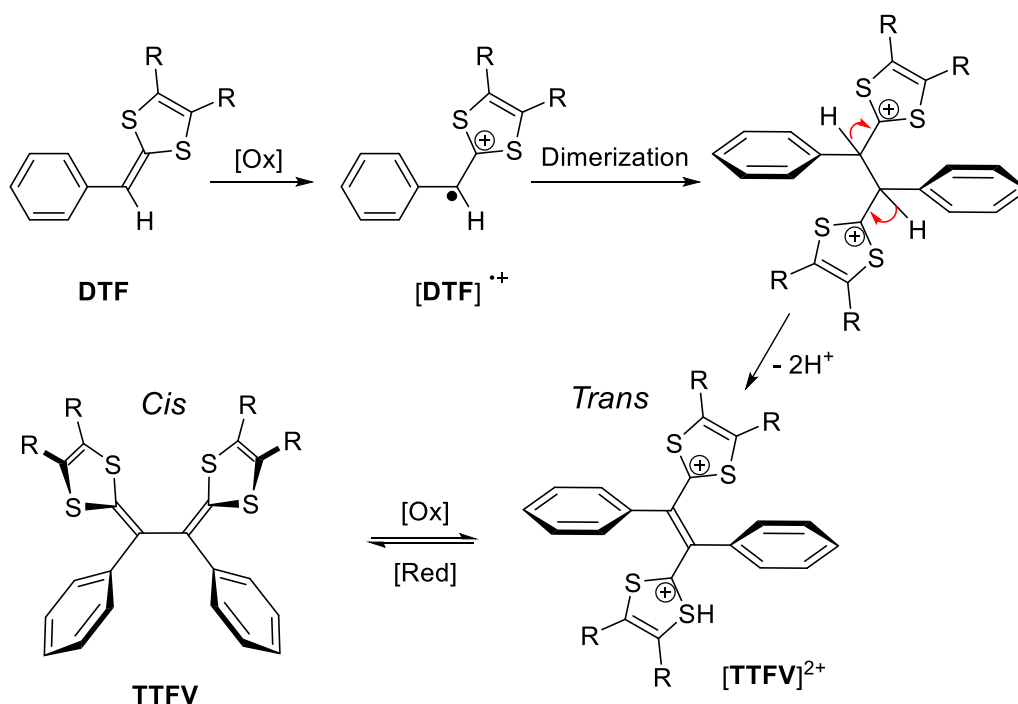
### 2.1 Introduction

Redox-active  $\pi$ -conjugated oligomers and polymers have offered numerous exciting prospects in the current materials science and nanotechnology,<sup>1-5</sup> on the basis of which active research has been dedicated to the development of molecular wires,<sup>6-9</sup> organic photovoltaics,<sup>10-14</sup> electrochromic devices,<sup>15-20</sup> molecular switches,<sup>21-23</sup> chemical sensors,<sup>24-27</sup> and stimuli-responsive materials and soft actuators,<sup>28-33</sup> in recent years. A

commonly employed strategy to impart desired redox-activity to  $\pi$ -conjugated oligomers and polymers is to have electron donors and/or acceptors either appended to the polymer side chain or placed directly in the repeat unit through  $\pi$ -conjugation.<sup>1-5</sup> Tetrathiafulvalene vinylogues (TTFVs) are a class of  $\pi$ -extended analogues of the well-known organic electron donor, tetrathiafulvalene (TTF).<sup>34-36</sup> TTFVs not only serve as excellent  $\pi$ -electron donors with tunable redox potentials but also show unique redox-triggered conformational switching properties.<sup>37-44</sup> The interesting molecular properties of TTFVs have sparked surging research interest in developing new TTFV-based functional materials over the past few years, including conjugated polymers,<sup>31-33,45-48</sup> macrocycles,<sup>19,20</sup> switchable ligands,<sup>49-52</sup> molecular rotors,<sup>53</sup> and chemosensors.<sup>54-57</sup> TTFV derivatives with aryl groups substituted at the vinylic positions are versatile building blocks for various TTFV-containing  $\pi$ -conjugated systems. The aryl-substituted TTFVs can be made via an oxidative coupling reaction in which a certain dithiafulvene (DTF) precursor is dimerized through a radical mechanism as exemplified by the dimerization of a phenyl-DTF in Scheme 2.1.<sup>58</sup> The synthetic scope of this methodology encompasses numerous aryl-substituted DTFs,<sup>59-63</sup> wherein the presence of aryl groups facilitates the formation of DTF radical cation in the first step of the mechanism and enables the molecular structure to be further elaborated into diverse  $\pi$ -conjugated motifs.

The DTF dimerization reaction provides an efficient C–C bond forming approach through which  $\pi$ -conjugated oligomers and polymers with diverse 1D and 2D structures can be conveniently assembled under either chemical or electrochemical conditions using suitably designed aryl-substituted DTFs as precursors.<sup>31-33,45-48,64,65</sup> Scheme 2.2 depicts

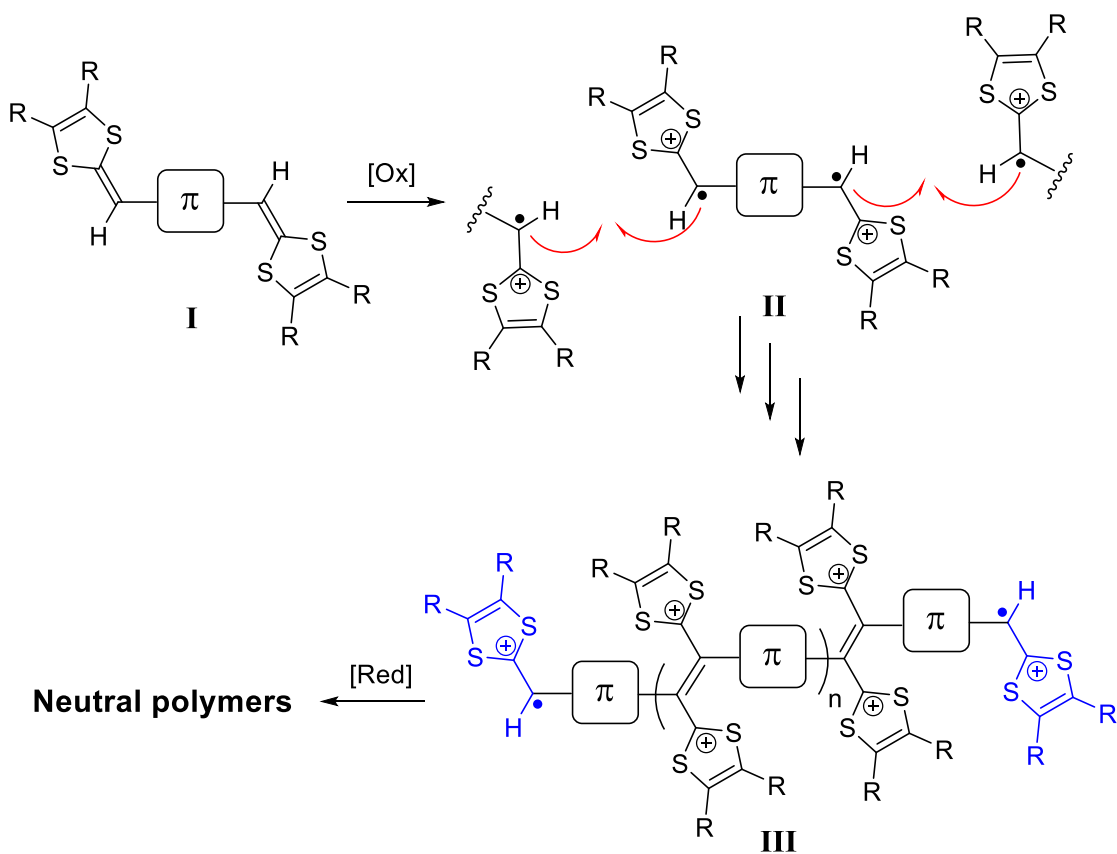
the oxidative polymerization of a generic bis(DTF)- $\pi$  building block **I**, which leads to the formation of a linear cationic polymer **III**.<sup>66</sup> Subsequent reductive workup yields the neutral polymer product with a TTFV moiety embedded in each of its repeat units. Typically, such a one-pot polymerization reaction as shown in Scheme 2.2 should give a mixture of polymers with varied chain lengths, whereas precise control over the degree of polymerization is usually not an easy task to accomplish. For instance, in our previous studies, bis(DTF)-end-capped  $\pi$ -conjugated butadiyne and octatetrayne derivatives were polymerized in solution using iodine as oxidant.<sup>19,20</sup> The reactions resulted in the formation of a number of relatively short oligomers rather than long-chain polymers. The observed low polymerization degree can be rationalized by noting that when the polymer chain is elongated the terminal DTF groups gradually lose the reactivity toward oxidative dimerization as a result of increased  $\pi$ -delocalization and intermolecular electrostatic repulsion.



**Scheme 2.1** General mechanism for the oxidative dimerization of phenyl-DTF

The poor efficiency found in DTF polymerization, on the other hand, might suggest a useful synthetic route to prepare relatively short, structurally defined TTFV-based  $\pi$ -oligomers. Hypothetically, if the bis(DTF)- $\pi$  precursor possesses a moderate reactivity toward DTF oxidative dimerization, it is likely for the terminal DTF radical cations (highlighted by blue color in Scheme 2.2) to become completely inert toward the oxidation dimerization when the oligomer chain arrives at a certain “critical length”. If such a scenario holds true, the polymerization after exhaustive reaction will yield  $\pi$ -oligomers with good monodispersity of chain length. One way to tune down the reactivity of a DTF radical cation is to increase the degree of  $\pi$ -delocalization. Linking the DTF group with  $\pi$ -extended arene units presents a feasible means to attain this goal. Another possible outcome for the one-pot polymerization is the formation of cyclic products,

namely macrocycles. TTFV-based macrocycles were rarely reported in the literature. In our recent work, we synthesized a series of trimeric TTFV macrocycles via a one-pot Pd/Cu-catalyzed alkynyl homocoupling of acetylenic TTFV precursors.<sup>19,20</sup> The DTF oxidative dimerization reaction, however, has not yet been demonstrated as a viable synthetic tool for direct construction of TTFV-containing macrocycles.



**Scheme 2.2** General polymerization route using DTF oxidative dimerization as the key step for polymer chain growth.

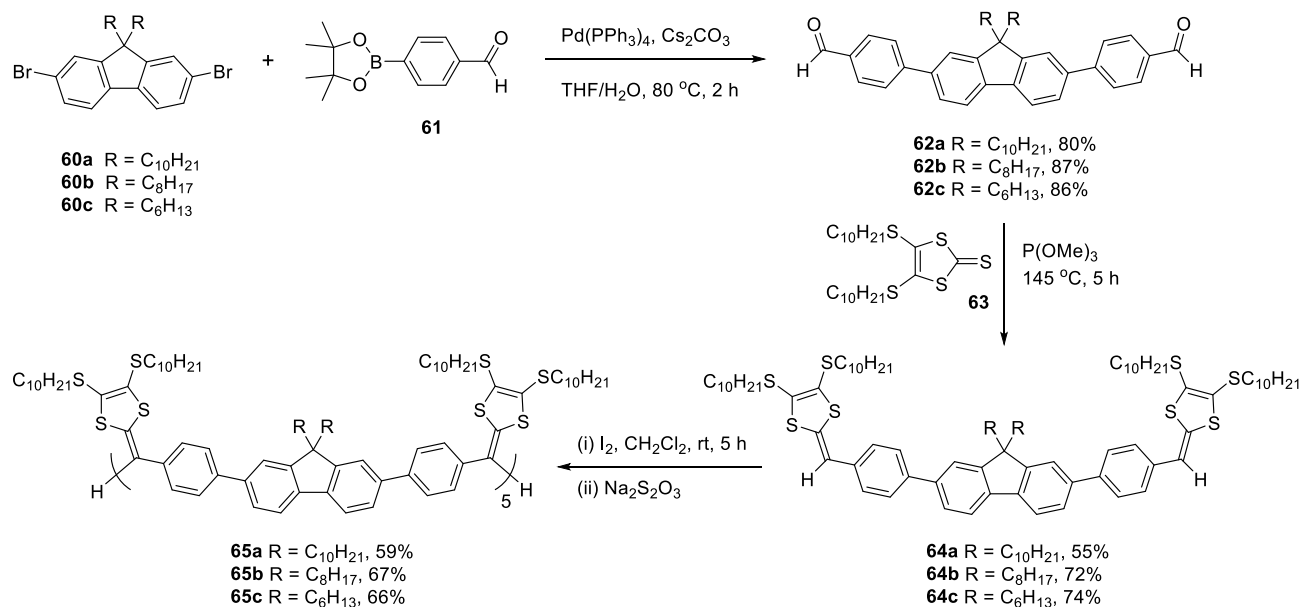
This Chapter addresses the synthetic scope of bis(DTF)-functionalized  $\pi$ -building blocks in terms of making various  $\pi$ -conjugated oligomers and macrocyclic structures. A series of fluorene-centered bis(DTF) derivatives was accordingly designed and synthesized. They were then subjected to a one-pot oxidative polymerization in the solution phase, and the resulting TTFV–fluorene co-oligomers were characterized by electrochemical and UV–vis analyses to understand their redox and electronic properties. Moreover, the supramolecular interactions of these electron-rich conjugated oligomers with single-walled carbon nanotubes (SWNTs) were investigated.  $\pi$ -Conjugated polymers containing TTFV units have been found to give rise to effective and selective dispersion of SWNTs in organic solvents.<sup>31-33</sup> Herein, the study of SWNT dispersion with TTFV–fluorene co-oligomers will further expand the application scope of TTFV-based  $\pi$ -oligomers in nanoscience and supramolecular chemistry.

## 2.2 Result and discussion

### 2.2.1 Synthesis

The synthetic routes to bis(DTF)-fluorenes **64a–c** are described in Scheme 2.3 2,7-Dibromofluorenes **60a–c** were, respectively, reacted with boronate **61** via the Suzuki coupling<sup>67</sup> to give dialdehydes **62a–c** in very good yields. Compounds **62a–c** were then subjected to a phosphite-induced olefination reaction<sup>68</sup> with thione **63** to produce bis(DTF)-fluorene derivatives **64a–c**. With **64a–c** in hand, iodine-promoted (ca. 2.8 equiv) oxidative polymerization reactions were undertaken in CH<sub>2</sub>Cl<sub>2</sub> at room temperature. The reactions in general completed within 5 h, as monitored by thin-layer

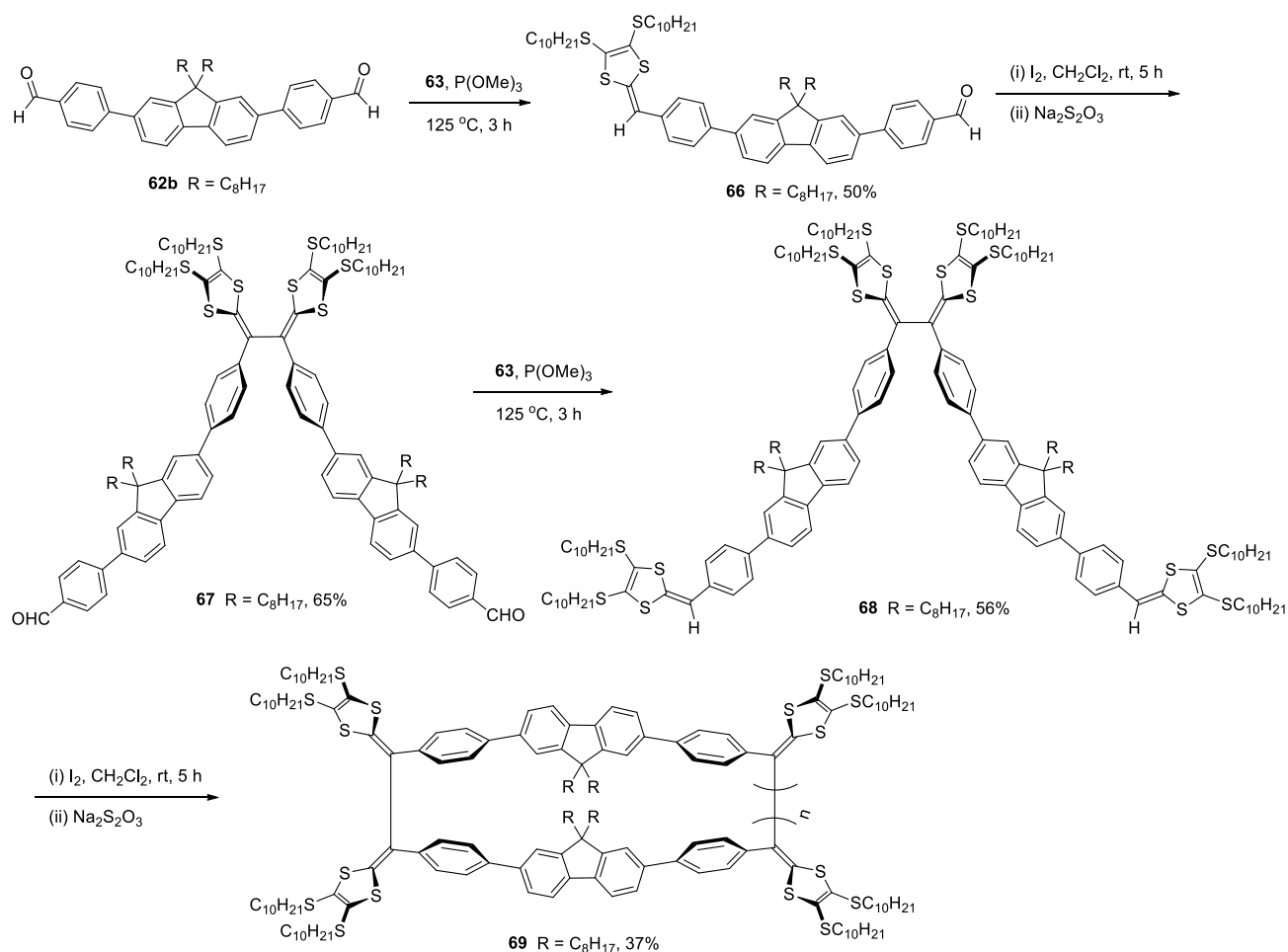
chromatographic (TLC) analysis. The major products of the polymerization reactions (oligomers **65a–c**) were obtained after a brief reductive aqueous workup with  $\text{Na}_2\text{S}_2\text{O}_3$ . Careful flash column chromatographic purification then afforded oligomers **65a–c** as brown semisolids in good yields. The molecular structures of these compounds were characterized as the acyclic TTFV–fluorene  $\pi$ -oligomers presented in Scheme 2.3 on the basis of  $^1\text{H}$  NMR, gel-permeation chromatographic (GPC), and cyclic voltammetric (CV) analyses (*vide infra*).



**Scheme 2.3** Synthesis of fluorene-cored bis(DTF) derivatives **64a–c** and acyclic TTFV-fluorene oligomers **65a–c**.

In addition to the bis(DTF)–fluorenes **64a–c**, the one-pot polymerization was expected to work in a similar way when using bis(DTF)- $\pi$  precursors with more extended

$\pi$ -skeletons. The resulting oligomers, however, were predicted to have relative higher degrees of polymerization due to the enlarged sizes of the monomers used for polymerization. To further explore this topic, the synthesis of an extended bis(DTF)-fluorene **68** was pursued as outlined in Scheme 2.4. Structurally, compound **68** is the dimer of **64b**, but synthetically it is challenging to acquire **68** from direct oxidative dimerization of bis(DTF)-fluorene **64b** due to the presence of two equally reactive DTF groups in **64b**. A multistep synthetic route was hence devised and executed. The synthesis began with an olefination reaction between compound **62b** and with 0.9 equiv of thione **63** in the presence of  $\text{P}(\text{OMe})_3$  under heating. The major product of this reaction was mono-DTF-substituted compound **66**, which could be easily separated from other byproducts by silica column chromatography. Compound **66** was then subjected to the iodine-induced oxidative dimerization to afford TTFV-centered oligomer **67**. Repetition of the  $\text{P}(\text{OMe})_3$ -promoted olefination on oligomer **67** with thione **63** gave bis(DTF)-oligomer **68** in a satisfactory yield of 56%. Finally, the iodine-induced one-pot polymerization of **68** was performed. To our surprise, there were no significant amounts of acyclic  $\pi$ -oligomers formed out of this reaction; instead, the major products were identified to be in the macrocyclic structure (see **69** in Scheme 2.4), which was characterized by  $^1\text{H}$  NMR, GPC, and CV characterizations (vide infra). Such a synthetic outcome sharply contrasts with the polymerization reactions using relatively shorter bis(DTF)-fluorenes **64a–c** as monomers, while a detailed rationalization for this is made in the later section based on kinetic considerations (see Figure 2.5).



**Scheme 2.4** Synthesis of cyclic TTFV-fluorene oligomers **69** using bis(DTF)-oligomer **68** as precursor.

### 2.2.2 Electronic and Redox Properties

The electronic absorption properties of the bis(DTF)-fluorene derivatives and related TTFV-fluorene co-oligomers were investigated by UV-vis spectroscopic analysis. Figure 2.1A shows the UV-vis absorption spectra of bis(DTF)-fluorenes **64a-c**. All of the spectra of the three compounds exhibit a nearly superimposable absorption

profile featuring a  $\pi \rightarrow \pi^*$  band at 396 nm. Clearly, the side chains attached to the fluorene core barely have any effect on the electronic absorption behavior of the bis(DTF)-fluorene  $\pi$ -framework. The UV-vis spectra of TTFV-fluorene co-oligomers **65a–c** (Figure 2.1B) show the same absorption band at 396 nm in the low energy region, indicating that the degrees of  $\pi$ -delocalization of the co-oligomers are virtually unchanged in comparison with their bis(DTF)-fluorene precursors. In addition, each of the spectra of **65a–c** exhibits a notable absorption shoulder at 343 nm, which can be assigned to the  $\pi \rightarrow \pi^*$  transition of the TTFV units in the oligomer backbones. The UV-vis spectrum of dimer **68** gives a spectral pattern similar to those of co-oligomers **65a–c** (see Figure 2.1C). In the UV-vis spectrum of macrocyclic oligomer **69** (Figure 2.1C), the same low energy absorption band at 396 nm can be observed. Unlike the acyclic oligomers **65a–c** and **68**, the shoulder band of macrocycle **69** at 343 nm appears to be significantly stronger in relative intensity, which very likely results from the constraint cyclic  $\pi$ -framework of the macrocycle (see Figure 2.4). In a comparative study of two dinaphthyl-substituted TTFV isomers we recently reported,<sup>61</sup> enlargement of the dihedral bond angle between the two vinyl units of TTFV was found to result in significantly increased absorptivity in the spectral range of ca. 330–350 nm. It is therefore deduced that the varied intensity of the shoulder band at 343 nm in the UV-vis spectra of **65a–c** and **69** is tied to the different TTFV conformations in these compounds.

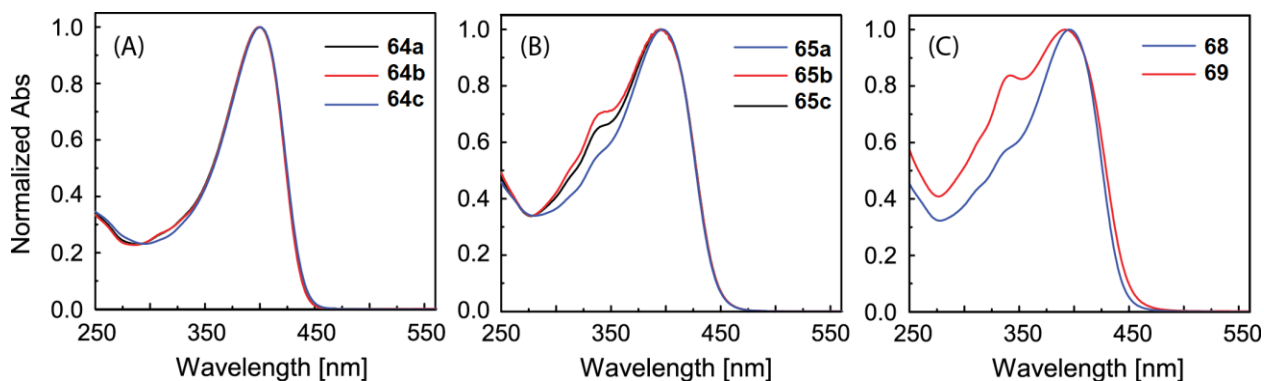


**Figure 2.1** UV-vis spectra of TTFV-fluorene co-oligomers and related  $\pi$ -precursors. All spectra were measured in  $\text{CHCl}_3$  at room temperature.

The electrochemical redox properties of the above-mentioned compounds were examined by CV experiments, and the detailed cyclic voltammograms are given in Figure 2.2. The cyclic voltammogram of bis(DTF)-fluorene **64a** (Figure 2.2 A) shows only one anodic peak at +0.78 V in the first cycle of CV scan, which is assigned to the one-electron oxidation of neutral DTF to its radical cation state.<sup>19,20,58</sup> In the reverse scan, a cathodic peak emerges at +0.46 V, the origin of which is attributed to the reduction of the TTFV dication resulting from the electrochemical dimerization taking place on the working electrode surface.<sup>19,20,58</sup> As the number of scan cycles increases, another anodic peak is observed to grow steadily at +0.52 V, which is due to the oxidation of the TTFV product accumulated on the working electrode surface. The CV profiles of bis(DTF)-fluorenes **64b** and **64c** (Figure 2.2 B,C) exhibit a similar pattern to that of **64a**, indicating that the three bis(DTF)-fluorene compounds have similar redox activities and electrochemical properties.

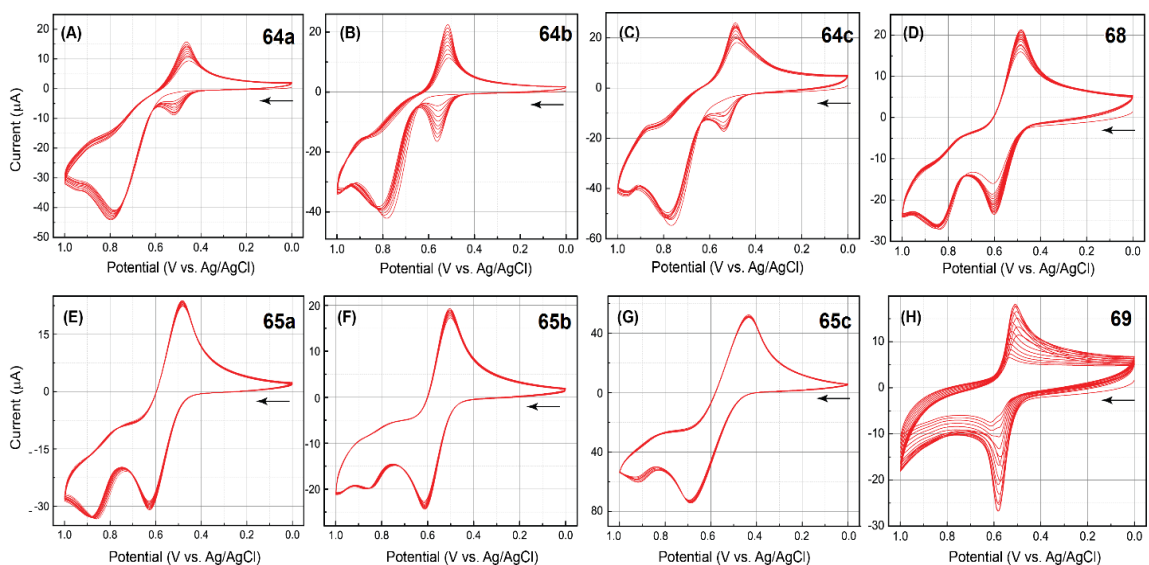


**Figure 2.2** Cyclic voltammograms of compounds **64a-c**, **65a-c**, **68**, and **69** measured in multiple scans. Electrolyte:  $\text{Bu}_4\text{NBF}_4$  (0.1 M); working electrode: glassy carbon; counter electrode: Pt wire; reference electrode: Ag/AgCl; scan rate:  $100 \text{ mV s}^{-1}$ .

The cyclic voltammogram of TTFV–fluorene co-oligomer **65a** gives two anodic peaks at +0.63 and +0.87 V respectively, while in the reverse scan a cathodic peak at +0.44 V is observed (Figure 2.2 E). The first anodic peak and the cathodic peak are due to the reversible redox couple of the TTFV moieties in the co-oligomer, and the second is assigned to the oxidation of the terminal DTF groups of **65a**.<sup>19,20,58</sup> After being scanned with multiple cycles, these redox peaks do not show any significant changes, indicating that the terminal DTF groups in **65a** are virtually unreactive toward oxidative dimerization. Similar electrochemical redox behavior can be observed in the CV profiles of co-oligomers **68**, **65b**, and **65c** (Figure 2.2\_D,F,G); however, the oxidation currents due to the TTFV and DTF moieties show notable differences in relative intensity in the cyclic

voltammograms of **65a–c**, and these results can be correlated with their different degrees of oligomerization (vide infra). The cyclic voltammogram of macrocycle **69** (Figure 2.2 H) shows only a reversible redox couple at  $E_{pa} = +0.58$  V and  $E_{pc} = +0.51$  V in the first cycle of CV scans, which is characteristic of the TTFV moieties in macrocycle **69**. There is no anodic peak due to DTF oxidation observed in the multicycle CV scans of **69**, which is congruous with a macrocyclic structure. It is also noted that the intensities of the redox wave pair give a significant decreasing trend with increasing number of CV scans, while the redox potentials appear to shift anodically in a slight degree. Such CV behavior alludes to a low degree of electrochemical stability for TTFV–fluorene macrocycle **69**.

### 2.2.3 Structural Elucidation of TTFV–Fluorene Co-oligomers

As manifested by the CV analysis, the structures of TTFV–fluorene co-oligomers **65a–c** take an acyclic structure with two DTF groups end-capped at the termini of each oligomer chain. The structure of co-oligomer **69**, on the other hand, is deduced to be in a macrocyclic motif based on the absence of DTF oxidation peaks in its cyclic voltammogram. For these co-oligomers, determination of the degrees of oligomerization ( $n$ , as indicated in the structures of co-oligomers shown in Schemes 2.3 and 2.4) is of great importance to better understanding their structural properties as well as gaining mechanistic insight into the oxidative polymerization reactions.

$^1\text{H}$  NMR analysis has proven to be an indispensable tool for determination of the  $n$  values in acyclic co-oligomers **65a–c**, given that the unique chemical shift of the vinylic protons ( $\text{H}_a$ ) on the terminal DTF groups is distinctively separated from the other

aromatic protons on the oligomer backbone. Figure 2.3 shows the partial  $^1\text{H}$  NMR spectra of **65a–c**, **68**, and **69**, highlighting the aromatic and vinylic regions. In each of the spectra, the vinylic protons of the terminal DTF groups ( $\text{H}_a$ ) give a singlet at 6.51 ppm. In addition, a pseudo doublet (labeled as  $\text{H}_b$ ) can be clearly seen at 7.31 ppm. The origin of  $\text{H}_b$  can be assigned to the *ortho*-protons on the phenyl ring adjacent to the terminal DTF group. Other aromatic protons located on the fluorene and phenyl rings ( $\text{H}_{\text{Ar}}$ ) collectively contribute to the signals in the range of 7.49–7.76 ppm, which are too significantly overlapped to attain detailed assignments. The integral ratio of  $\text{H}_a$  versus the sum of  $\text{H}_b$  and  $\text{H}_{\text{Ar}}$  thus allows the average degree of oligomerization ( $n$ ) for each co-oligomer to be calculated (see Table 1). The NMR results show that co-oligomers **6b** and **6c** have similar oligomerization degrees (i.e., at the stage of pentamer to hexamer). Comparatively, co-oligomer **65a** has a relatively lower degree of oligomerization ( $n = 2.87$ ), suggesting that the dominant component of **65a** is trimer. The relative lower oligomerization degree of **65a** can be ascribed to the long side chains on the fluorene units, the increased steric hindrance of which may retard the oxidative oligomerization.

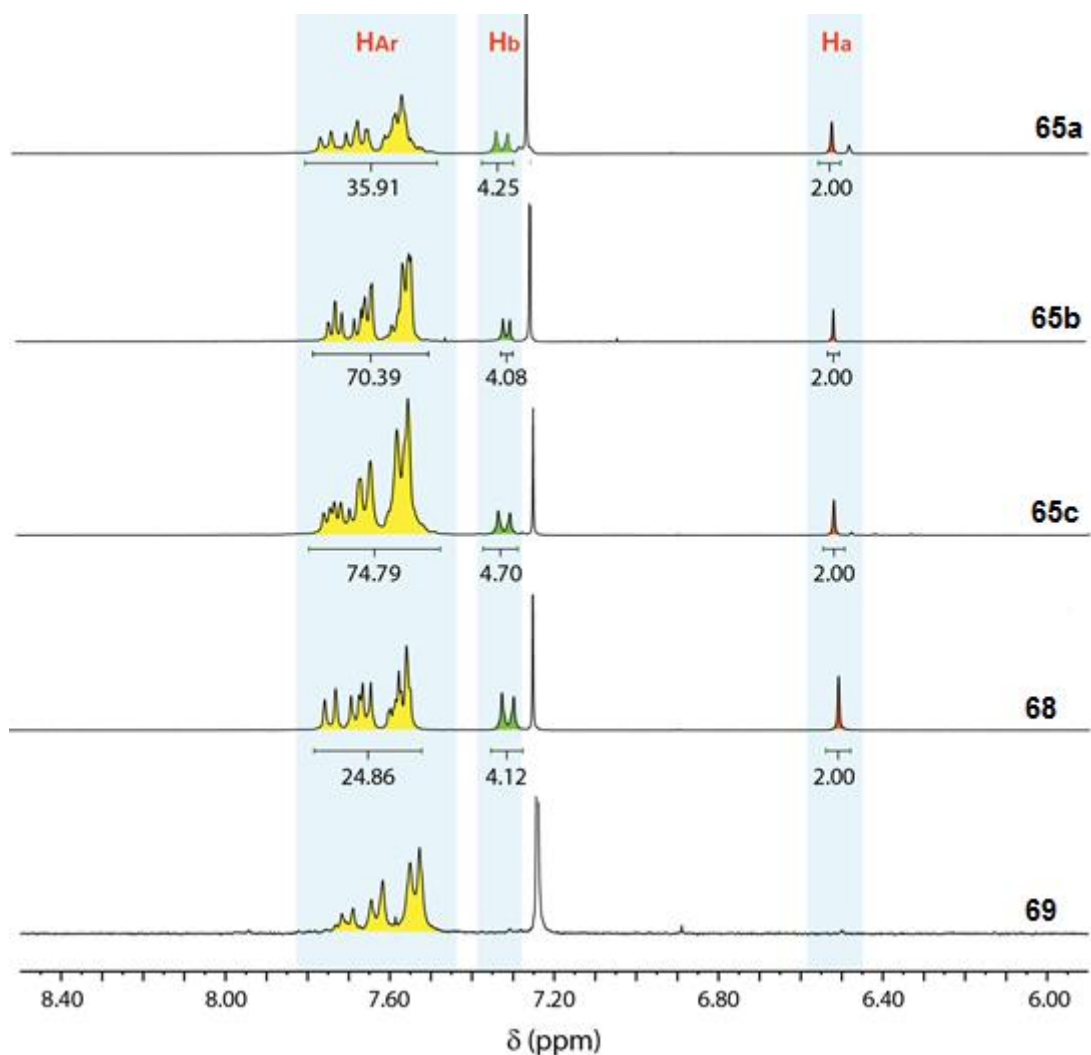


**Figure 2.3** Partial  $^1\text{H}$  NMR spectra of **65a-c**, **68** and **69** showing the aromatic and vinyl regions as well as relative integration values therein. The singlet at 7.24 ppm in each spectrum is due to residual  $\text{CHCl}_3$ .

The  $^1\text{H}$  NMR analysis on the average degree of oligomerization ( $n$ ) was then compared with gel permeation chromatographic (GPC) data. As listed in Table 1, TTFV–fluorene co-oligomers **65a–c** all exhibit relatively narrow polydispersity ( $\text{PDI} = 1.3\text{--}1.5$ ). The degree of oligomerization ( $n$ ) can be worked out using the formula  $n = M_n/M_0$ , where

in  $M_n$  is the number-average molecular weight determined by GPC and  $M_0$  is the molecular weight of the monomer used for the polymerization. The degrees of oligomerization calculated for **65a–c** based on GPC data show a good agreement with those derived from NMR analysis, testifying to the reliability of both methods in elucidating the structures of bis(DTF)-end-capped TTFV–fluorene co-oligomers. The GPC data for macrocycle **69** gave an  $M_n$  value very close the molecular weight of dimer **68**, indicating that the dominant reaction pathway in the macrocyclization of **68** was a ring closure resulting from intramolecular coupling of the two terminal DTF groups rather than intermolecular expansion. Nevertheless, the relatively wide polydispersity (PDI = 2.33) measured for **69** suggests that larger macrocycles were also formed via intermolecular cycloaddition pathways to a certain extent. The molecular structure of the macrocycle resulting from the intramolecular cyclization of **68** was simulated by the molecular mechanics (MM) approach using the MMFF force field implemented in Spartan'10 (Wave function, Inc.). As shown in Figure 2.4, the optimized geometry of the macrocycle shows that the dihedral angle between the two vinyl groups in each of the TTFV moieties is about 76–80°, which is larger than those observed for typical phenyl-substituted TTFV compounds<sup>60,61</sup> as a result of the macrocyclic strain energy. The two fluorene units are somehow parallelly oriented, but they are not close enough to induce significant van der Waals contact or  $\pi$ -stacking. Moreover, the central cavity of the macrocycle appears to be very small and therefore not suited to encapsulate meaningful molecular guests.

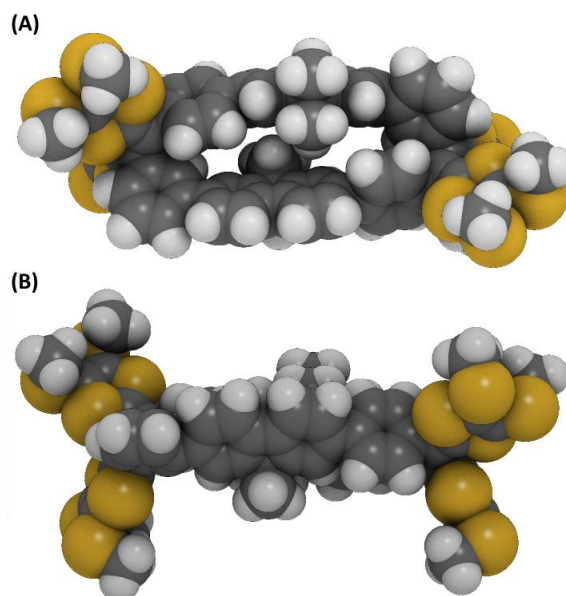


**Figure 2.4** Space-filling model of macrocycle **69** ( $n=1$ ) optimized using the MMFF force field: (A) side view, (B) top view. Long alkyl chains were replaced by CH<sub>3</sub> to save computational costs.

Apart from NMR and GPC analyses, the CV data could also serve as a meaningful way to assess the average degree of oligomerization ( $n$ ) for **65a–c**. As can be seen from Figure 2.2, the anodic peaks due to the oxidation of DTF and TTFV moieties are well separated from one another in the voltammogram of each oligomer. In principle, a DTF unit releases one electron and a TTFV unit loses two electrons during the oxidation processes. Assuming that the current intensity of each anodic peak is proportional to the number of electrons transferred,<sup>69</sup> the ratio of the current intensities for DTF and TTFV thus offers a quantitative measure for the degree of oligomerization ( $n$ ). To evaluate the usefulness of this method, the current intensities ( $i_{pa}$ ) of the DTF and TTFV anodic peaks

for TTFV–fluorene dimer **68** were first examined. The calculated  $n$  value (1.93) according to the CV data is satisfactorily close to the ideal value ( $n = 2$ ) for dimer **68**, corroborating the reliability of the electrochemical method (see Table 1). Indeed, the degrees of oligomerization ( $n$ ) calculated on the basis of the anodic peak currents are consistent with those determined by the GPC and NMR analyses in the cases of co-oligomers **65a** and **65b**. For co-oligomer **65c**, however, the electrochemical analysis yields a slightly larger  $n$  value than the other two methods, and the exact reason for such a discrepancy awaits more detailed investigation to clarify. It is worth mentioning that strenuous efforts were made in our work to characterize the TTFV–fluorene co-oligomers by MALDI-TOF MS analysis. Unfortunately, only dimer **68** was reasonably characterized by MS, whereas the other co-oligomers only gave the mass peaks due to smaller fragment ions in their mass spectra. It is therefore reasoned that these oligomers are unstable to the laser shots under the MALDI conditions, resulting in rapid decomposition and fragmentation which in turn obscured the MALDI-TOF MS analysis.

**Table 2.1** Summary of GPC Data for TTFV–fluorene Co-Oligomers and Their Calculated Degrees of Oligomerization ( $n$ )

Entry	$M_n$	$M_w$	PDI	$M_n/M_0$	$n$ (calc, NMR)	$n$ (calc, CV)
<b>65a</b>	4392	6965	1.39	3.13	2.87	3.29
<b>65b</b>	7961	12303	1.54	5.45	5.32	5.45
<b>65c</b>	8200	11119	1.35	5.41	5.63	8.31
<b>68</b>					2.07	1.93
<b>69</b>	3126	7297	2.33	1.07		

## 2.2.4 Mechanisms of Polymerization

The various characterization data have congruously indicated that the one-pot oxidative polymerization of bis(DTF)-fluorenes **64a–c** led to the formation of acyclic TTFV–fluorene co-oligomers with relatively narrow polydispersity. In contrast, treatment of compound **68**, which is the dimer in the series of co-oligomer **65b**, under the same oxidative conditions yielded only cyclic products. The different synthetic outcomes suggest that the DTF oxidative polymerization does not follow a conventional polymerization mechanism in which the monomers and/or intermediary oligomers react with each other nonselectively. The fact that dimer **68** predominantly underwent an intramolecular cyclization reaction suggests that the intermolecular DTF coupling between dimers and/or higher oligomers is a sluggish and disfavored pathway in the polymerization mechanism. It is therefore reasonable to propose that the mechanism for the polymerization of **64a–c** predominantly follows the chain-length growth pathway illustrated in Figure 2.5, in which the monomer is added to each of the termini of the intermediary oligomers in a stepwise fashion. When the oligomer is grown to a “critical chain length” where the terminal DTFs become completely inert to the oxidative dimerization reaction, the polymerization reaction is terminated. As such, the final products of the polymerization should converge toward a peculiar chain length with much better monodispersity than the outcome of a conventional polymerization pathway. Experimentally, the narrow polydispersity of co-oligomers **65a–c** determined by GPC analysis attests to the proposed selective chain length growth mechanism. Another valid argument supporting the proposed mechanism is that in the oxidative polymerization

of **64b** the first intermediate formed was actually dimer **68** in its oxidized state. If the conventional polymerization mechanism took place in a significant degree, the polymerization of **64b** would also produce macrocyclic oligomer **69** as one of the major products, but this scenario was not observed experimentally.

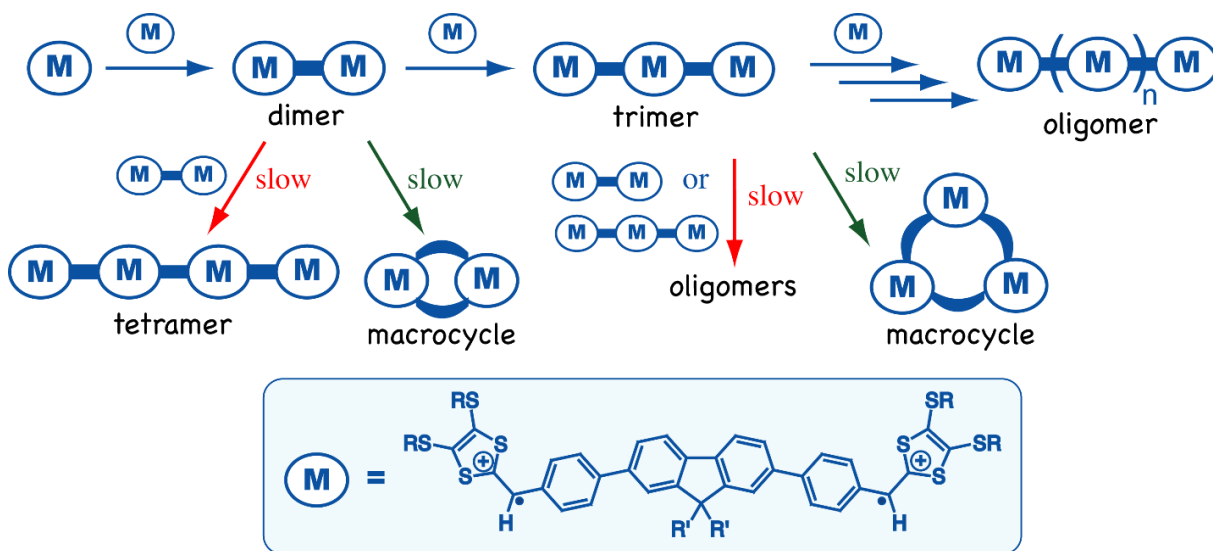


**Figure 2.5** Illustration of different reaction pathways involved in the one-pot oxidative polymerization of bis(DTF)-fluorenes.

### 2.2.5 Supramolecular Interactions of TTFV–Fluorene Co-oligomers with Single-Walled Carbon Nanotubes

The conformational properties of TTFV–fluorene co-oligomers **65a–c** were investigated by molecular mechanics (MM) simulations, where a model co-oligomer featuring the same  $\pi$ -framework as those of **65a–c** but without alkyl side chains was examined. The chain length of the model oligomer was set at the pentamer stage ( $n = 5$ ) to be consistent with the average oligomerization degrees of co-oligomers **65b** and **65c**.

As can be seen from Figure 2.6 A,B, the optimized geometry of the model oligomer adopts a “squarelike” folding structure with a central cavity of ca. 1–2 nm in diameter. Our previous studies have demonstrated that TTFV-containing  $\pi$ -conjugated polymers and bis(DTF) end-capped  $\pi$ -oligomers were able to wrap around or stick to the surface of single-walled carbon nanotubes (SWNTs), resulting in effective and selective dispersion of SWNTs in various organic solvents.<sup>31-33</sup> Along this line, we further envisioned that the unique folding features of the TTFV–fluorene co-oligomers together with their  $\pi$ -rich conjugated backbones should engender favorable supramolecular interactions with SWNTs. MM simulations of the interactions between the model oligomer and a segmental (10,0) SWNT have revealed a wrapping mode (Figure 2.6 C,D) dictated by intimate  $\pi$ -stacking between the oligomer  $\pi$ -framework and the SWNT surface.

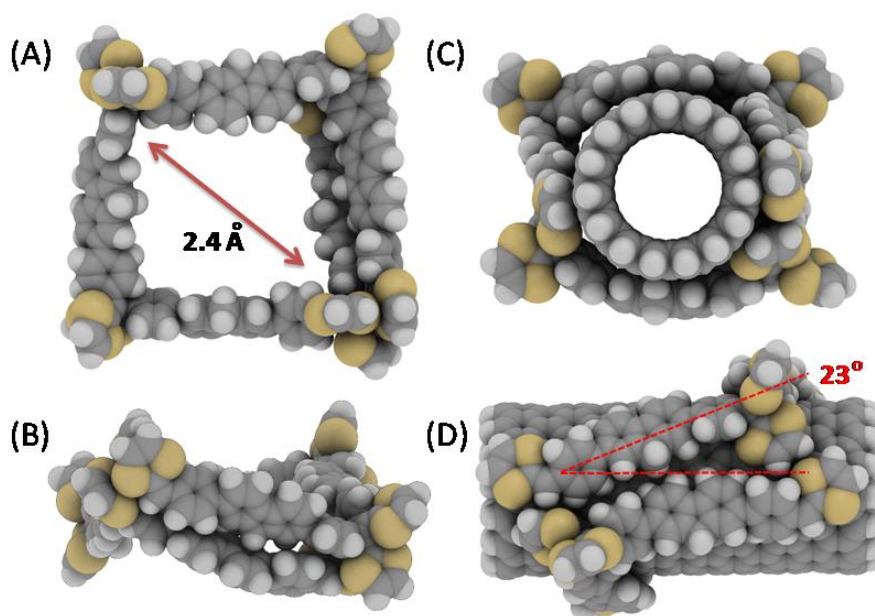


**Figure 2.6** Optimized geometries of a TTFV-fluorene pentamer (A: front view; B: side view) and the oligomer wrapping around a (10,0) nanotube (C: front view; D: side view).

To validate the prediction by the molecular modeling studies, two commercially available SWNT samples (namely, HiPCO and CoMoCAT) were acquired and subjected to dispersion experiments in organic solvents using co-oligomers **65a–c** as dispersing agents. In this work, SWNT dispersion was conducted by the ultrasonication/filtration procedures we reported previously.<sup>31–33</sup> It was found that all the co-oligomers could effectively disperse HiPCO nanotubes into two common organic solvents, CHCl<sub>3</sub> and THF, to form stable suspensions. The effectiveness of dispersion in CHCl<sub>3</sub> appeared to be better than in THF. For the CoMoCAT nanotubes, however, there was no significant dispersion observed in common organic solvents.

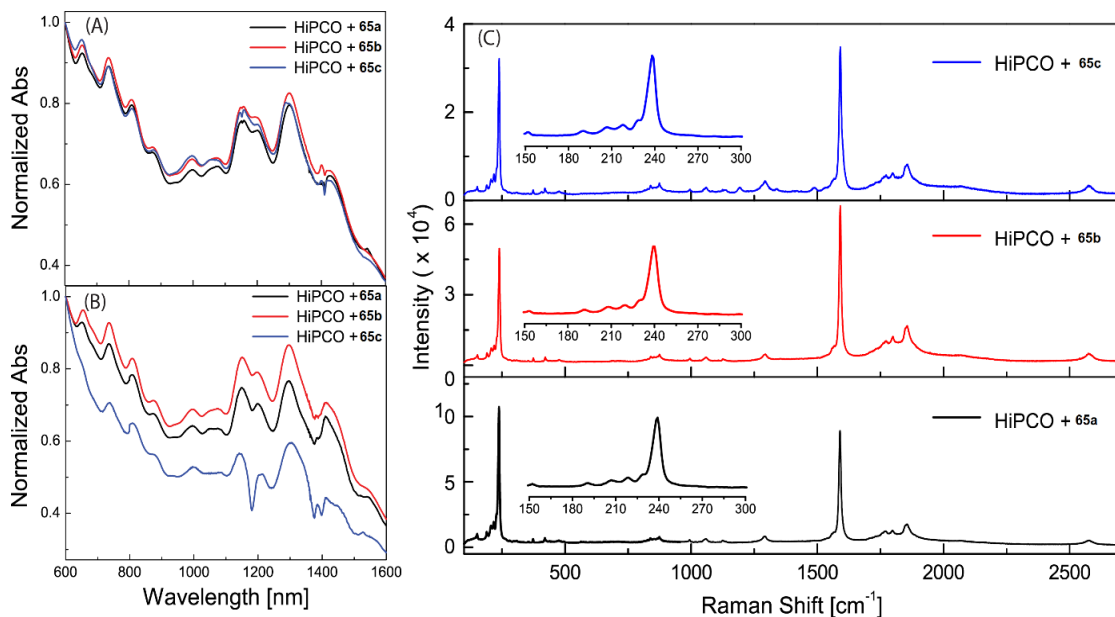


**Figure 2.7** (A) UV-Vis-NIR spectra of HiPCO SWNTs dispersed with co-oligomers **65a–c** in CHCl<sub>3</sub>. (B) UV-Vis-NIR spectra of HiPCO SWNTs dispersed with co-oligomers **65a–c** in THF. (C) Raman spectra of SWNTs dispersed with co-oligomers **65a–c**. Inset: Expanded spectra showing the radical breathing mode (RBM) region.

The HiPCO SWNT suspensions dispersed with co-oligomers **65a–c** in  $\text{CHCl}_3$  were characterized by UV–Vis–NIR analysis, and the results are shown in Figure 2.7A. The variously distinct absorption bands in the Vis–NIR region are characteristic of the interband transitions of debundled SWNTs in the solution.<sup>70</sup> The SWNTs dispersed by the three TTFV–fluorene co-oligomers give nearly superposable spectral patterns in Figure 2.7A, suggesting that the three  $\pi$ -oligomers have similar selectivity for the types of SWNTs dispersed in  $\text{CHCl}_3$ . In THF, the vis–NIR absorption spectra of the SWNTs dispersed by **65a** and **65b** (see Figure 2.7B) bear similar features to one another as well as to those determined in  $\text{CHCl}_3$ . For the SWNTs dispersed with oligomer **6c** in THF, however, the Vis–NIR spectrum is notably different in comparison with the others. The relatively lower solubility of **6c** than the other two co-oligomers in THF, due to the short alkyl chains attached to the fluorene moieties, could be a reason for the different spectral features in the Vis–NIR region.

To shed more light on the selectivity issue, Raman spectroscopic analysis was conducted. Figure 2.7C shows the Raman spectra of SWNTs dispersed with **65a–c**. Overall, the three Raman spectra bear close resemblance to one another, in which the dominant features are the tangential G band of SWNTs at  $1590\text{ cm}^{-1}$  and a sharp band at  $239\text{ cm}^{-1}$  in the radial breathing mode (RBM) region. The two characteristic Raman bands testify to the efficient dispersion of SWNTs by the three co-oligomers.

Figure 2.8 compares the spectra of oligomer **65b**, raw HiPCO SWNTs, and SWNTs dispersed with **65b**. The Raman spectrum of raw HiPCO SWNTs clearly shows a significant  $G^-$  band together with the  $G^+$  band in the tangential mode region. In addition,

the D band is discernible at  $1329\text{ cm}^{-1}$ . In sharp contrast, the SWNTs dispersed with TTFV–fluorene co-oligomers do not give any significant G<sup>-</sup> band. Moreover, the RBM bands of dispersed SWNTs appear to be much narrower than those of the raw HiPCO SWNTs. The Raman data corroborate that the dispersed SWNTs possess a better quality than raw SWNTs in terms of structural homogeneity; in particular, the diameters of the dispersed SWNTs are found to be narrowly distributed, given that RBM frequency ( $\omega$ ) is inversely proportional to the diameter of SWNT ( $d$ ).<sup>71,72</sup> Using the equation  $\omega_{\text{RBM}} = 248/d$ , developed by Dresselhaus et al.,<sup>73</sup> the average diameter ( $d$ ) of the SWNTs selectively dispersed by **65a–c** in  $\text{CHCl}_3$  is estimated to be ca. 1.0 nm. Such a good diameter selectivity is believed to arise from the unique wrapping mode of the oligomers with SWNTs as disclosed by the molecular modeling studies. The development of stimuli-responsive oligomers and polymers as SWNT dispersants has become a topic of research recently, and one advantage of this approach that particularly appeals to the application in SWNT-based devices is the ease and effectiveness in regenerating “additive-free” SWNTs after solution-phase processing.<sup>31-33,74-77</sup> Along this vein, we expect that the redox-active TTFV–fluorene co-oligomers **65a–c** will find further application in SWNT-based nanodevices and materials.

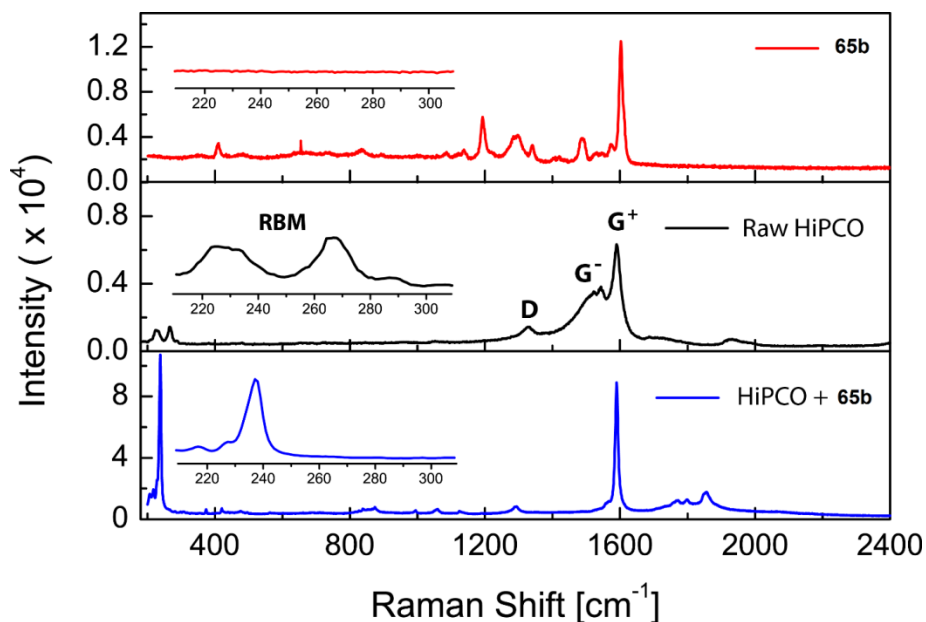


**Figure 2.8** Comparison of the Raman spectra of co-oligomer **65**, raw HiPCO SWNTs dispersed with **65**. Insets: Expanded spectra showing the radial breathing mode (RBM) region.

## 2.2.6 Conclusions

Oxidative dimerization of aryl-substituted DTFs offers a direct C–C bond-forming approach through which various extended  $\pi$ -conjugated systems can be generated. In this work, bis(DTF)-end-capped fluorenes **64a–c** were used as monomers for the iodine-induced oxidative DTF polymerization, yielding acyclic TTFV–fluorene co-oligomers with narrow polydispersity. The same oxidative reaction conditions applied to the bis(DTF) dimer **68**, however, led to a completely different synthetic outcome, wherein only cyclic oligomer products were formed as a result of the favored intramolecular DTF coupling. Our synthetic work has confirmed that the reactivity of a DTF group toward the

oxidative dimerization is highly dependent on the degree of  $\pi$ -conjugation of the aryl group attached to it. Another intriguing discovery is that the mechanism for the oxidative polymerization of bis(DTF)-fluorenes **65a–c** follows a selective chain length growth pathway, in which the oligomer intermediates favor to react with the bis(DTF)-fluorene monomers. This unique reactivity has enabled relatively monodisperse  $\pi$ -oligomers to be generated as the major products through the one-pot polymerization approach. Finally, the TTFV–fluorene co-oligomers were demonstrated to give rise to strong supramolecular interactions with SWNTs, which in turn allowed for effective and selective dispersion of SWNTs in the organic solutions of TTFV–fluorene co-oligomers. In summary, the findings disclosed in this work have contributed useful knowledge to the development of new redox-active functional materials based on  $\pi$ -conjugated oligomers and macrocycles.

## **2.3 Experimental Section**

### **2.3.1 General Information**

Commercially available chemicals were used directly without purification. All reactions were conducted in standard, dry glassware and under an inert atmosphere of nitrogen or argon unless otherwise noted.  $^1\text{H}$  and  $^{13}\text{C}$  NMR spectra were recorded on a 500 MHz or a 300 MHz multinuclear spectrometer. Chemical shifts ( $\delta$ ) are reported in ppm downfield relative to the signals of the internal reference  $\text{SiMe}_4$  or residual solvent signals from  $\text{CHCl}_3$   $\delta = 7.24$  ppm and  $\delta = 77.2$  ppm,  $\text{CH}_2\text{Cl}_2$   $\delta = 5.32$  ppm and  $\delta = 54.0$  ppm, respectively. Coupling constants ( $J$ ) are reported in hertz. MALDI-TOF MS

analysis was performed in the positive mode using dithranol as the matrix. High-resolution EI-TOF MS analysis was performed in the positive mode. Raman spectroscopic analysis was done on a Raman microscope equipped with a laser source at the wavelength of 830 nm. Gel permeation chromatographic (GPC) analysis was performed using THF as the eluent at a flow rate of 1.0 mL/min and monitored by a photodiode array detector and a refractive-index detector. Polystyrene standards were used for calibration.

#### 4,4'-(9,9-Didecyl-9H-fluorene-2,7-diyl)dibenzaldehyde (**62a**)



2,7-Dibromo-9,9-didecyl-9H-fluorene (**60a**) (1.70 g, 2.81 mmol), benzaldehyde **2** (1.60 g, 6.89 mmol), Cs<sub>2</sub>CO<sub>3</sub> (14.6 g, 44.8 mmol), and Pd(PPh<sub>3</sub>)<sub>4</sub> (0.33 g, 0.29 mmol) were added to a 100 mL round-bottom flask. THF (35 mL) and deionized water (15 mL) were added to the flask under an atmosphere of argon. The mixture was refluxed for 2 h under argon. After that, the mixture was cooled to room temperature and then poured into brine. The resulting mixture was extracted twice with CH<sub>2</sub>Cl<sub>2</sub>. The combined organic layers were dried over MgSO<sub>4</sub>, and the solvent was evaporated off under vacuum. The residue was crude product **62a**, which was further purified through silica column chromatography (Et<sub>2</sub>O/EtOAc 1:4) to give pure **62a** (1.50 g, 2.30 mmol, 80%) as a pale yellow oil: IR (neat) 2921, 2850, 2728, 1697, 1600, 1249, 1210, 812 cm<sup>-1</sup>

<sup>1</sup>H NMR (300 MHz, CDCl<sub>3</sub>) δ 10.09 (s, 2H), 8.00 (d, *J* = 8.4 Hz, 4H), 7.86–7.83 (m, 6H), 7.69–7.61(m, 4H), 2.10–2.04 (m, 4H), 1.31–1.11 (m, 32H), 0.82 (t, *J* = 6.9 Hz, 6H); <sup>13</sup>C NMR (75 MHz, CDCl<sub>3</sub>) δ 191.9, 152.0, 147.5, 140.9, 138.8, 135.1, 130.3, 127.7, 126.5, 121.7, 120.54, 55.5, 40.3, 31.8, 29.9, 29.6, 29.5, 29.3, 29.2, 22.6, 14.1; HRMS [M]<sup>+</sup> calcd for C<sub>47</sub>H<sub>58</sub>O<sub>2</sub> 654.4437, found 654.4418.

#### 4,4'-(9,9-Dioctyl-9H-fluorene-2,7-diyl)dibenzaldehyde (**62b**)



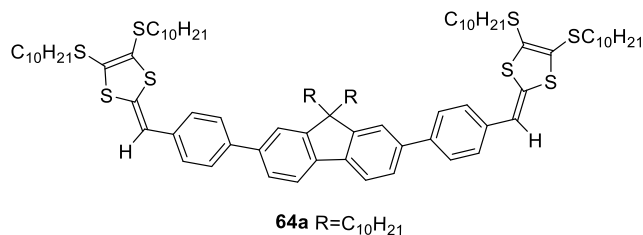
2,7-Dibromo-9,9-dioctyl-9H-fluorene (**60b**) (1.15 g, 2.09 mmol), benzaldehyde **61** (1.13 g, 4.87 mmol), Cs<sub>2</sub>CO<sub>3</sub> (9.70 g, 30.0 mmol), and Pd(PPh<sub>3</sub>)<sub>4</sub> (0.28 g, 0.24 mmol) were reacted under the same conditions as described in the synthesis of **62a** to yield compound **62b** (1.10 g, 1.83 mmol, 87%) as a pale yellow solid: <sup>1</sup>H NMR (300 MHz, CDCl<sub>3</sub>) δ 10.09 (s, 2H), 7.99 (d, *J* = 8.1 Hz, 4H), 7.86–7.83 (m, 6H), 7.68–7.61 (m, 4H), 2.10–2.04 (m, 4H), 1.19–1.03 (m, 24H), 0.78 (t, *J* = 6.8 Hz, 6H). The <sup>1</sup>H NMR data is consistent with the literature reported values.<sup>78</sup>

#### 4,4'-(9,9-Dihexyl-9H-fluorene-2,7-diyl)dibenzaldehyde (**62c**)



2,7-Dibromo-9,9-dihexyl-9H-fluorene (**60c**) (1.00 g, 2.03 mmol), benzaldehyde **2** (1.07 g, 4.60 mmol), Cs<sub>2</sub>CO<sub>3</sub> (4.40 g, 13.5 mmol), and Pd(PPh<sub>3</sub>)<sub>4</sub> (0.22 g, 0.19 mmol) were reacted under the same conditions as described in the synthesis of **62a** to yield compound **62c** (0.90 g, 1.66 mmol, 86%) a pale yellow solid: <sup>1</sup>H NMR (300 MHz, CDCl<sub>3</sub>) δ 10.08 (s, 2H), 7.99 (d, *J* = 8.4 Hz, 4H), 7.85–7.82 (m, 6H), 7.67–7.64 (m, 4H), 2.11–2.06 (m, 4H), 1.19–0.98 (m, 16H), 0.75 (t, *J* = 6.8 Hz, 6H). The <sup>1</sup>H NMR data is consistent with the literature reported values.<sup>78</sup>

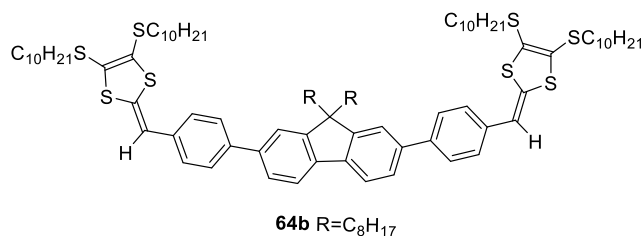
### Bis(DTF)-fluorene **64a**



Dibenzaldehyde **62a** (1.00 g, 1.52 mmol), thione **63** (1.75 g, 3.66 mmol), and P(OMe)<sub>3</sub> (30 mL) were added to a 100 mL round-bottom flask. The mixture was heated to 145 °C and kept at this temperature for 5 h. Then P(OMe)<sub>3</sub> was removed by vacuum distillation, and the crude product was purified through silica column chromatography (hexanes) to give **64a** (1.27 g, 0.83 mmol, 55%) as a yellow oil: IR (neat) 2952, 2919, 2849, 1569, 1544, 1463, 818 cm<sup>-1</sup>; <sup>1</sup>H NMR (300 MHz, CDCl<sub>3</sub>) δ 7.75 (d, *J* = 7.9 Hz, 2H), 7.68 (d, *J* = 8.4 Hz, 4H), 7.61–7.57 (m, 4H), 7.32 (d, *J* = 8.4 Hz, 4H), 6.52 (s, 2H), 2.86–2.81 (m, 8H), 1.73–1.59 (m, 8H), 1.48–1.00 (m, 96H), 0.90–0.78 (m, 18H); <sup>13</sup>C NMR (75 MHz, CD<sub>2</sub>Cl<sub>2</sub>) δ 151.9, 140.2, 139.5, 138.9, 135.4, 132.5, 127.7, 127.33,

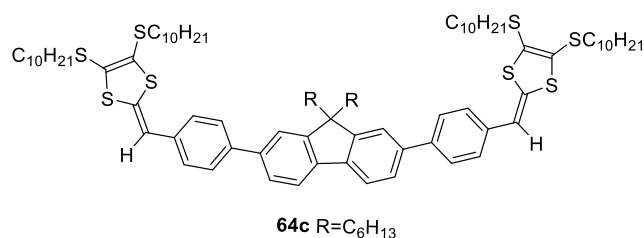
127.27, 125.9, 125.0, 121.3, 120.2, 114.1, 50.4, 40.6, 36.3, 36.2, 32.05, 32.04, 32.00, 31.7, 31.1, 30.2, 30.0, 29.9, 29.71, 29.68, 29.65, 29.47, 29.46, 29.40, 29.37, 29.3, 29.2, 28.73, 28.71, 22.82, 22.80, 22.78, 14.3, 14.2; HRMS  $[M + H]^+$  calcd for  $C_{93}H_{143}S_8$  1515.8955, found 1515.8929.

### Bis(DTF)-fluorene **64b**



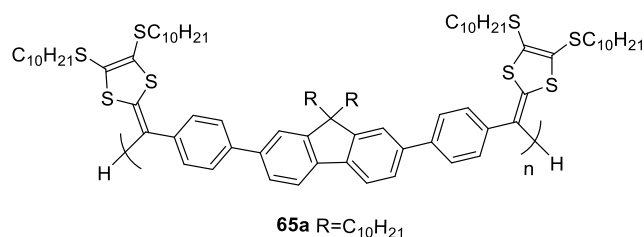
Dibenzaldehyde **62b** (0.40 g, 0.66 mmol), thione **63** (0.76 g, 1.60 mmol), and P(OMe)<sub>3</sub> (20 mL) were reacted under the same conditions as described in the synthesis of **64a** to give compound **64b** (0.70 g, 0.48 mmol, 72%) as a yellow oil: IR (neat) 2952, 2920, 2850, 1681, 1569, 1463, 1087, 819 cm<sup>-1</sup>; <sup>1</sup>H NMR (300 MHz, CDCl<sub>3</sub>) δ 7.76 (d, *J* = 7.9 Hz, 2H), 7.68 (d, *J* = 8.4 Hz, 4H), 7.61–7.57 (m, 4H), 7.32 (d, *J* = 8.4 Hz, 4H), 6.52 (s, 2H), 2.86–2.81 (m, 8H), 2.06–2.97 (m, 4H) 1.73–1.56 (m, 8H), 1.49–0.97 (m, 80H), 0.92–0.75 (m, 18H); <sup>13</sup>C NMR (75 MHz, CDCl<sub>3</sub>) δ 151.9, 140.2, 139.6, 138.9, 135.4, 132.56, 127.65, 127.33, 127.29, 125.90, 125.00, 121.31, 120.18, 114.11, 55.4, 40.6, 36.3, 36.2, 32.0, 31.9, 30.2, 30.0, 29.9, 29.71, 29.69, 29.48, 29.47, 29.4, 29.3, 28.7, 24.0, 22.8, 22.7, 14.3, 14.2; HRMS  $[M + H]^+$  calcd for  $C_{89}H_{135}S_8$  1459.8329, found 1459.8292.

### Bis(DTF)-fluorene **64c**



Dibenzaldehyde **62c** (0.57 g, 0.99 mmol), thione **63** (1.30 g, 2.25 mmol), and P(OMe)<sub>3</sub> (20 mL) were reacted under the same conditions as described in the synthesis of **64a** to give compound **64c** (0.95 g, 0.62 mmol, 62%) as a yellow oil: IR (neat) 3023, 2952, 2920, 2850, 1569, 1544, 1463, 818 cm<sup>-1</sup>; <sup>1</sup>H NMR (300 MHz, CDCl<sub>3</sub>) δ 7.75 (d, *J* = 8.0 Hz, 2H), 7.68 (d, *J* = 8.4 Hz, 4H), 7.63–7.54 (m, 4H), 7.32 (d, *J* = 8.4 Hz, 4H), 6.52 (s, 2H), 2.86–2.81 (m, 8H), 2.09–1.96 (m, 4H), 1.72–1.59 (m, 8H), 1.50–0.99 (m, 72H), 0.92–0.70 (m, 18H); <sup>13</sup>C NMR (75 MHz, CDCl<sub>3</sub>) δ 151.9, 140.2, 139.5, 138.9, 135.4, 132.6, 127.7, 127.33, 127.27, 125.5, 125.0, 121.3, 120.2, 114.1, 55.4, 40.6, 36.3, 36.2, 32.0, 31.6, 30.0, 29.9, 29.71, 29.68, 29.47, 29.46, 29.3, 28.73, 28.70, 23.9, 22.8, 22.7, 14.3, 14.1; HRMS [M + H]<sup>+</sup> calcd for C<sub>85</sub>H<sub>127</sub>S<sub>8</sub> 1403.7703, found 1403.7718.

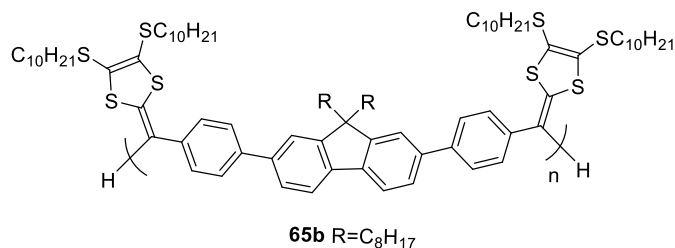
### TTFV-Fluorene Co-oligomer **65a**



To a solution of compound **64a** (0.11 g, 0.072 mmol) in CH<sub>2</sub>Cl<sub>2</sub> (10 mL) were added iodine chips (0.050 g, 0.20 mmol). The resulting dark solution was stirred at room

temperature for 5 h. After that, a saturated aqueous solution of Na<sub>2</sub>S<sub>2</sub>O<sub>3</sub> (10 mL) was added to the dark solution, and the mixture was stirred for another 3 h at room temperature. The resulting yellow organic layer was separated, washed with water, dried over MgSO<sub>4</sub>, and concentrated under reduced pressure. The resulting crude product was subjected to silica gel column chromatography (hexanes/CH<sub>2</sub>Cl<sub>2</sub>, 4:1), giving co-oligomer **65a** (0.066 g, 59%) as a yellow oil: IR (neat) 2953, 2920, 2850, 1463, 1054, 816 cm<sup>-1</sup>; <sup>1</sup>H NMR (300 MHz, CDCl<sub>3</sub>) δ 7.77–7.47 (m, 36H), 7.34–7.26 (m, 4H), 6.50 (s, 2H), 2.89–2.70 (m, 26H), 2.08–1.87 (m, 10H), 1.74–1.55 (m, 26H), 1.49–0.95 (m, 272H), 0.92–0.75 (m, 64H); <sup>13</sup>C NMR (75 MHz, CDCl<sub>3</sub>) δ 151.9, 151.8, 140.2, 139.8, 139.5, 138.9, 136.8, 136.0, 135.5, 135.4, 132.5, 129.0, 127.7, 127.32, 127.27, 127.1, 126.9, 125.9, 125.3, 125.0, 124.3, 121.3, 120.1, 114.1, 55.4, 40.7, 36.3, 36.2, 36.1, 32.08, 32.06, 32.0, 30.2, 30.0, 29.87, 29.85, 29.74, 29.72, 29.69, 29.64, 29.53, 29.48, 29.39, 29.35, 29.31, 28.75, 28.71, 24.0, 22.84, 22.79, 14.28, 14.26; GPC *M<sub>n</sub>* = 8200, *M<sub>w</sub>* = 11119, PDI = 1.35.

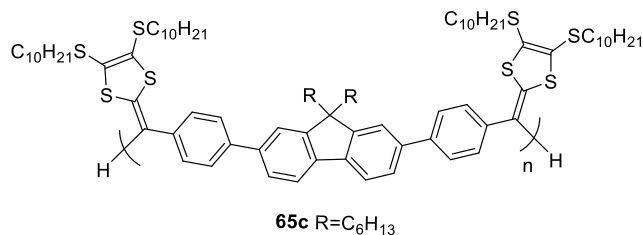
### TTFV–Fluorene Co-oligomer **65b**



Compound **64b** (0.10 g, 0.068 mmol) and iodine (0.050 g, 0.20 mmol) were reacted in CH<sub>2</sub>Cl<sub>2</sub>(10 mL) under the same conditions as described in the synthesis of **65a** to give

co-oligomer **65b** (0.067 g, 67%) as a yellow oil: IR (neat) 2952, 2920, 2850, 1463, 1434, 815  $\text{cm}^{-1}$ ;  $^1\text{H}$  NMR (300 MHz,  $\text{CDCl}_3$ )  $\delta$  7.74–7.45 (m, 70H), 7.32–7.28 (m, 4H), 6.50 (s, 2H), 2.88–2.73 (m, 42H), 2.06–1.92 (m, 20H), 1.70–1.54 (m, 48H), 1.44–0.96 (m, 460H), 0.89–0.72 (m, 120H);  $^{13}\text{C}$  NMR (75 MHz,  $\text{CDCl}_3$ )  $\delta$  151.84, 151.80, 140.2, 139.8, 139.5, 138.9, 136.8, 136.1, 136.0, 135.4, 132.6, 129.0, 127.33, 127.28, 127.1, 125.9, 125.3, 125.0, 124.3, 121.3, 120.2, 114.1, 55.4, 40.7, 36.3, 36.2, 36.1, 34.8, 32.1, 31.9, 31.8, 31.1, 30.2, 30.0, 29.9, 29.8, 29.72, 29.69, 29.53, 29.49, 29.4, 29.3, 29.2, 28.8, 28.7, 25.4, 24.0, 22.85, 22.82, 22.7, 20.9, 14.3, 14.2; GPC  $M_n = 7961$ ,  $M_w = 12303$ , PDI = 1.54.

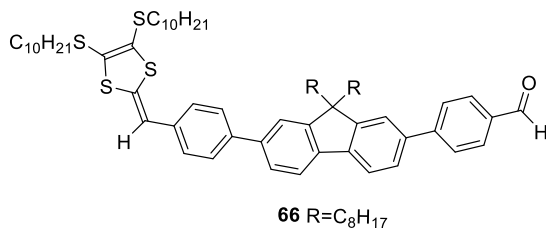
### TTFV–Fluorene Co-oligomer **65c**



Compound **64c** (0.060 g, 0.043 mmol) and iodine (0.030 g, 0.12 mmol) were reacted in  $\text{CH}_2\text{Cl}_2$  (10 mL) under the same conditions as described in the synthesis of **65a** to give co-oligomer **65c** (0.040 g, 66%) as a yellow oil: IR (neat) 2952, 2920, 2850, 1463, 1433, 815  $\text{cm}^{-1}$ ;  $^1\text{H}$  NMR (300 MHz,  $\text{CDCl}_3$ )  $\delta$  7.76–7.48 (m, 74H), 7.34–7.27 (m, 4H), 6.51 (s, 2H), 2.91–2.73 (m, 44H), 2.07–1.90 (m, 20H), 1.73–1.54 (m, 50H), 1.49–0.95 (m, 420H), 0.93–0.67 (m, 126H);  $^{13}\text{C}$  NMR (75 MHz,  $\text{CDCl}_3$ )  $\delta$  151.9, 151.8, 140.2, 139.8, 139.5, 138.9, 136.8, 136.0, 135.4, 132.6, 128.9, 127.6, 127.33, 127.27, 127.1, 125.9, 125.3, 125.0, 124.33, 121.27, 120.1, 114.1, 55.37, 55.35, 53.6, 40.7, 36.3, 36.2, 36.1, 32.1, 31.6,

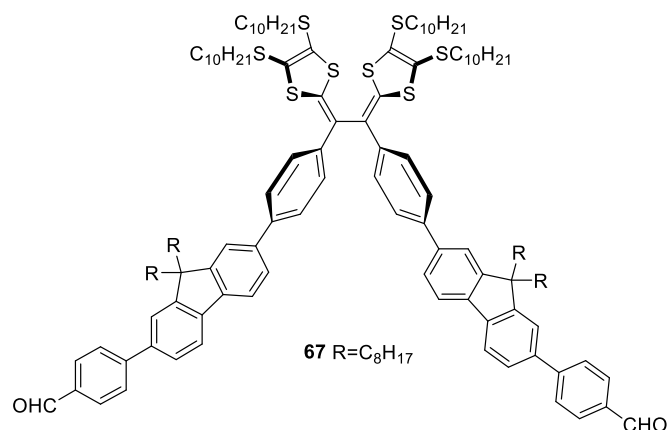
30.0, 29.9, 29.8, 29.74, 29.71, 29.68, 29.52, 29.48, 29.46, 29.37, 29.35, 29.30, 28.8, 28.74, 28.70, 24.0, 22.8, 22.7, 14.3, 14.1; GPC:  $M_n = 4932$ ,  $M_w = 6865$ , PDI = 1.39.

### DTF-Fluorene **66**



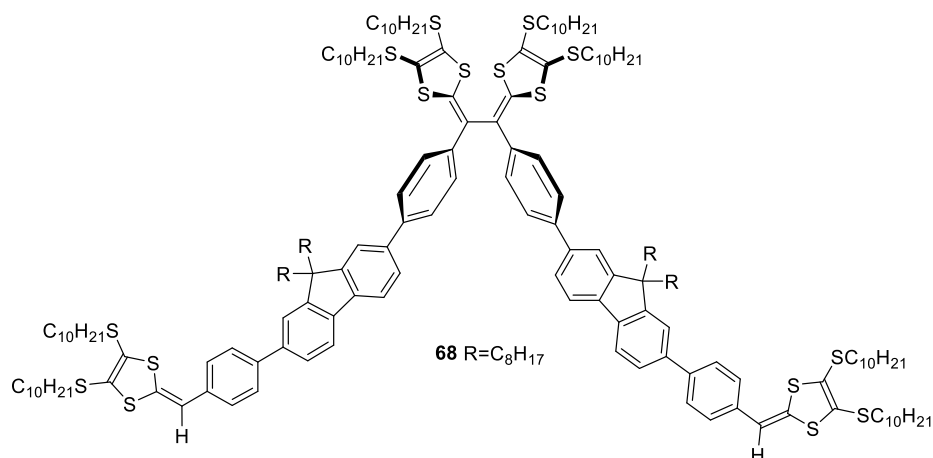
Compound **62b** (0.32 g, 0.53 mmol), thione **63** (0.23 g, 0.48 mmol), and P(OMe)<sub>3</sub> (15 mL) were reacted at 125 °C for 3 h under the same conditions as described in the synthesis of **64a**. The obtained crude product was purified by silica column chromatography (hexanes/CH<sub>2</sub>Cl<sub>2</sub>, 4:1) to afford compound **66** (0.27 g, 0.26 mmol, 50%) as a yellow oil: FTIR (neat) 2952, 2921, 2851, 1701, 1601, 1568, 1545, 1464, 1254, 1210, 844, 815 cm<sup>-1</sup>; <sup>1</sup>H NMR (300 MHz, CDCl<sub>3</sub>) δ 10.0(s, 1H), 7.98 (d, *J* = 8.3 Hz, 2H), 7.89–7.75 (m, 4H), 7.73–7.54 (m, 6H), 7.33 (d, *J* = 8.4 Hz, 2H), 6.53 (s, 1H), 2.84 (t, *J* = 7.3 Hz, 4H), 2.10–1.98 (m, 4H), 1.74–1.60 (m, 4H), 1.48–0.99 (m, 52H), 0.94–0.73 (m, 12H); <sup>13</sup>C NMR (75 MHz, CDCl<sub>3</sub>) δ 192.1, 152.1, 152.0, 147.8, 141.5, 140.05, 139.77, 138.76, 138.52, 135.54, 135.17, 132.7, 130.4, 127.8, 127.7, 127.34, 127.32, 126.6, 126.0, 125.0, 121.8, 121.4, 120.5, 120.4, 114.0, 55.5, 40.5, 36.3, 36.2, 32.1, 31.9, 30.1, 30.0, 29.9, 29.72, 29.69, 29.5, 29.33, 29.31, 28.74, 28.72, 23.9, 22.8, 22.7, 14.3, 14.2; HRMS [M + H]<sup>+</sup> calcd for C<sub>66</sub>H<sub>93</sub>OS<sub>4</sub> 1029.6109, found 1029.6112.

## TTFV-Fluorene **67**



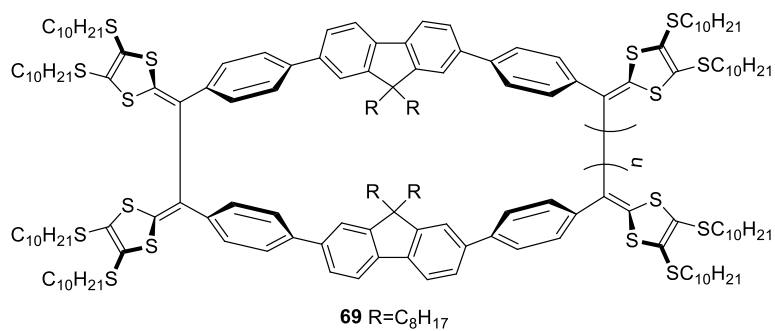
Compound **66** (0.90 g, 0.87 mmol) and iodine (0.66 g, 2.6 mmol) were added in CH<sub>2</sub>Cl<sub>2</sub> (15 mL), and the mixture was stirred at room temperature for 5 h. A saturated aqueous solution of Na<sub>2</sub>S<sub>2</sub>O<sub>3</sub> was added, and the resulting mixture was stirred at room temperature for another 1 h. The organic layer was separated, washed with H<sub>2</sub>O, dried over MgSO<sub>4</sub>, and concentrated under vacuum. The crude product obtained was purified through silica column chromatography (hexanes/CH<sub>2</sub>Cl<sub>2</sub>, 2:3) to yield compound **67** (0.58 g, 0.28 mmol, 65%) as a yellow oil: FTIR (neat) 2953, 2924, 2853, 1702, 1602, 1465, 1210, 1168, 815 cm<sup>-1</sup>; <sup>1</sup>H NMR (300 MHz, CDCl<sub>3</sub>) δ 10.0 (s, 2H), 7.98 (d, *J* = 8.4 Hz, 4H), 7.88–7.74 (m, 8H), 7.68–7.65 (m, 6H), 7.60–7.56 (m, 10H), 2.90–2.76 (m, 8H), 2.09–1.97 (m, 8H), 9.83–1.58 (m, 8H), 1.49–0.98 (m, 104H), 0.92–0.72 (m, 24H); <sup>13</sup>C NMR (75 MHz, CDCl<sub>3</sub>) δ 192.1, 152.1, 151.9, 147.8, 141.5, 140.0, 139.8, 139.6, 138.5, 137.0, 136.2, 135.2, 130.4, 129.0, 128.9, 127.8, 127.4, 127.1, 126.6, 126.0, 125.3, 124.2, 121.8, 121.4, 120.45, 120.36, 55.5, 40.6, 36.3, 36.2, 32.1, 31.9, 30.1, 29.9, 29.8, 29.53, 29.49, 29.3, 28.8, 28.7, 24.0, 22.8, 22.7, 14.3, 14.2.; HRMS [M + H]<sup>+</sup> calcd for C<sub>132</sub>H<sub>183</sub>O<sub>2</sub>S<sub>8</sub> 2056.1984, found 2056.1924.

## TTFV-Fluorene **68**



Compound **67** (0.35 g, 0.17 mmol), thione **63** (0.24 g, 0.51 mmol), and P(OMe)<sub>3</sub> (15 mL) were reacted under the same conditions as described in the synthesis of **66** to afford compound **68** (0.28 g, 0.096 mmol, 56%) as a yellow oil: FTIR (neat) 2953, 2923, 1464, 817 cm<sup>-1</sup>; <sup>1</sup>H NMR (300 MHz, CDCl<sub>3</sub>) δ 7.74 (d, *J* = 7.8 Hz, 4H), 7.69–7.56 (m, 20H), 7.32 (d, *J* = 8.5 Hz, 4H), 6.52 (s, 2H), 2.88–2.78 (m, 16H), 2.06–1.95 (m, 8H), 1.75–1.57 (m, 16H), 1.49–0.99 (m, 160H), 0.94–0.76 (m, 36H); <sup>13</sup>C NMR (75 MHz, CDCl<sub>3</sub>) δ 151.9, 151.8, 140.2, 139.8, 139.5, 138.9, 136.8, 136.0, 135.4, 132.5, 129.0, 127.6, 127.32, 127.28, 127.1, 125.9, 125.3, 125.0, 124.3, 121.31, 121.28, 120.2, 114.1, 55.4, 40.7, 36.3, 36.2, 36.1, 34.8, 34.7, 32.1, 31.9, 31.7, 30.2, 30.0, 29.8, 29.74, 29.71, 29.68, 29.52, 29.48, 29.46, 29.36, 29.34, 29.30, 29.2, 28.8, 28.73, 28.70, 27.1, 25.4, 23.9, 22.84, 22.81, 22.7, 14.3, 14.2; HRMS [M + H]<sup>+</sup> calcd for C<sub>178</sub>H<sub>267</sub>S<sub>16</sub> 2916.6424, found 2916.6499.

## TTFV-Fluorene Macrocycle **69**



Compound **68** (0.080 g, 0.027 mmol) and iodine (0.020 g, 0.081 mmol) were reacted in CH<sub>2</sub>Cl<sub>2</sub> (5 mL) under the same conditions as described in the synthesis of **65a** to yield compound **69** (0.030 g, 37%) as a yellow oil: FTIR (neat) 2953, 2923, 2852, 1464, 1260, 1092, 1017, 814, 803 cm<sup>-1</sup>; <sup>1</sup>H NMR (300 MHz, CDCl<sub>3</sub>) δ 7.71–7.46 (m, 7H), 2.96–2.64 (m, 8H), 1.92–0.92 (m, 40H), 0.86–0.74 (m, 9H); GPC  $M_n = 3126$ ,  $M_w = 7297$ , PDI = 2.33.

### 2.3.2 NMR Spectra for New Compounds

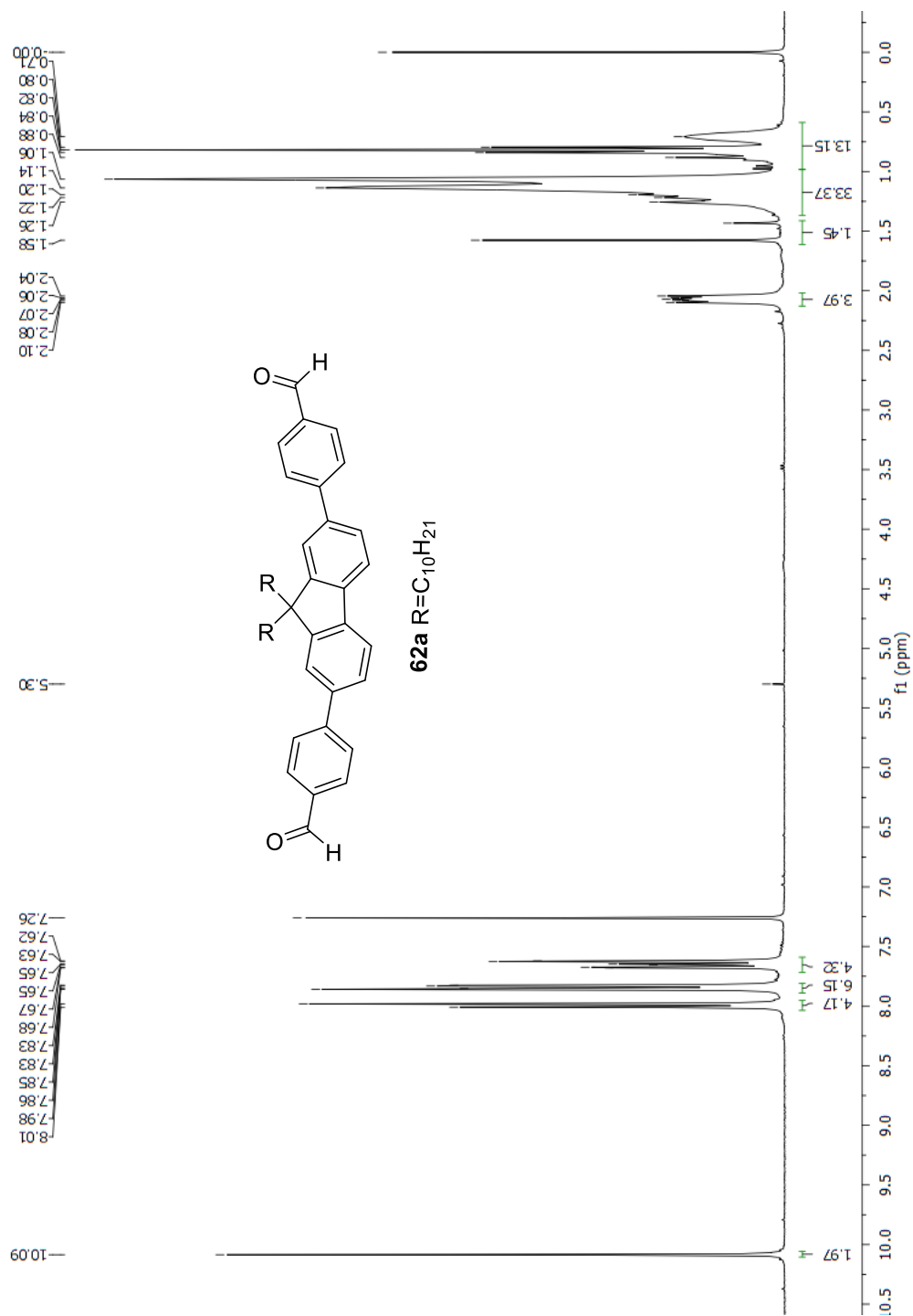


**Fig. 2-9:**  $^1\text{H}$  NMR (300 MHz,  $\text{CDCl}_3$ ) spectrum of compound **62a**.

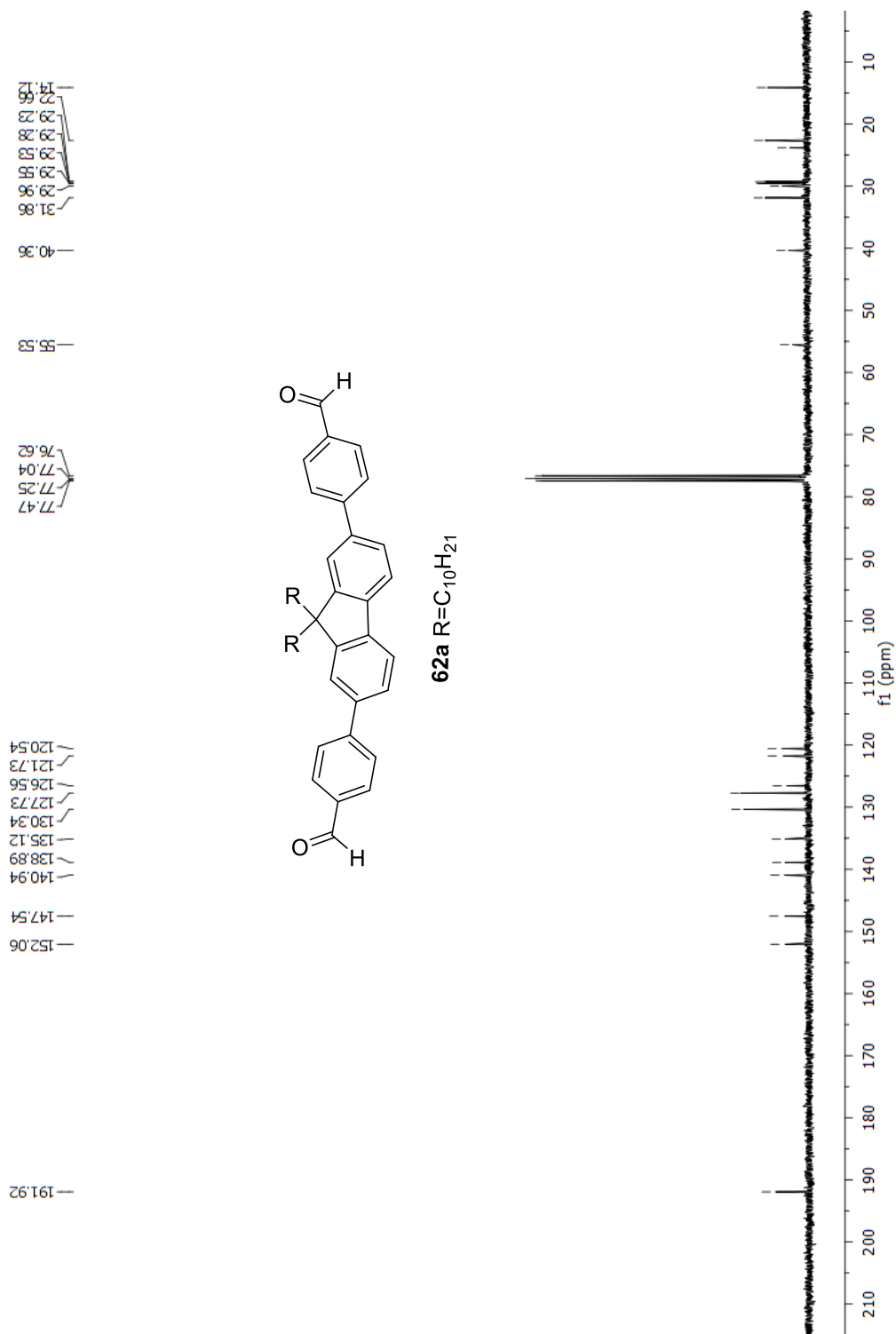


**Fig. 2-10:** <sup>13</sup>C NMR (75 MHz, CDCl<sub>3</sub>) spectrum of compound **62a**.

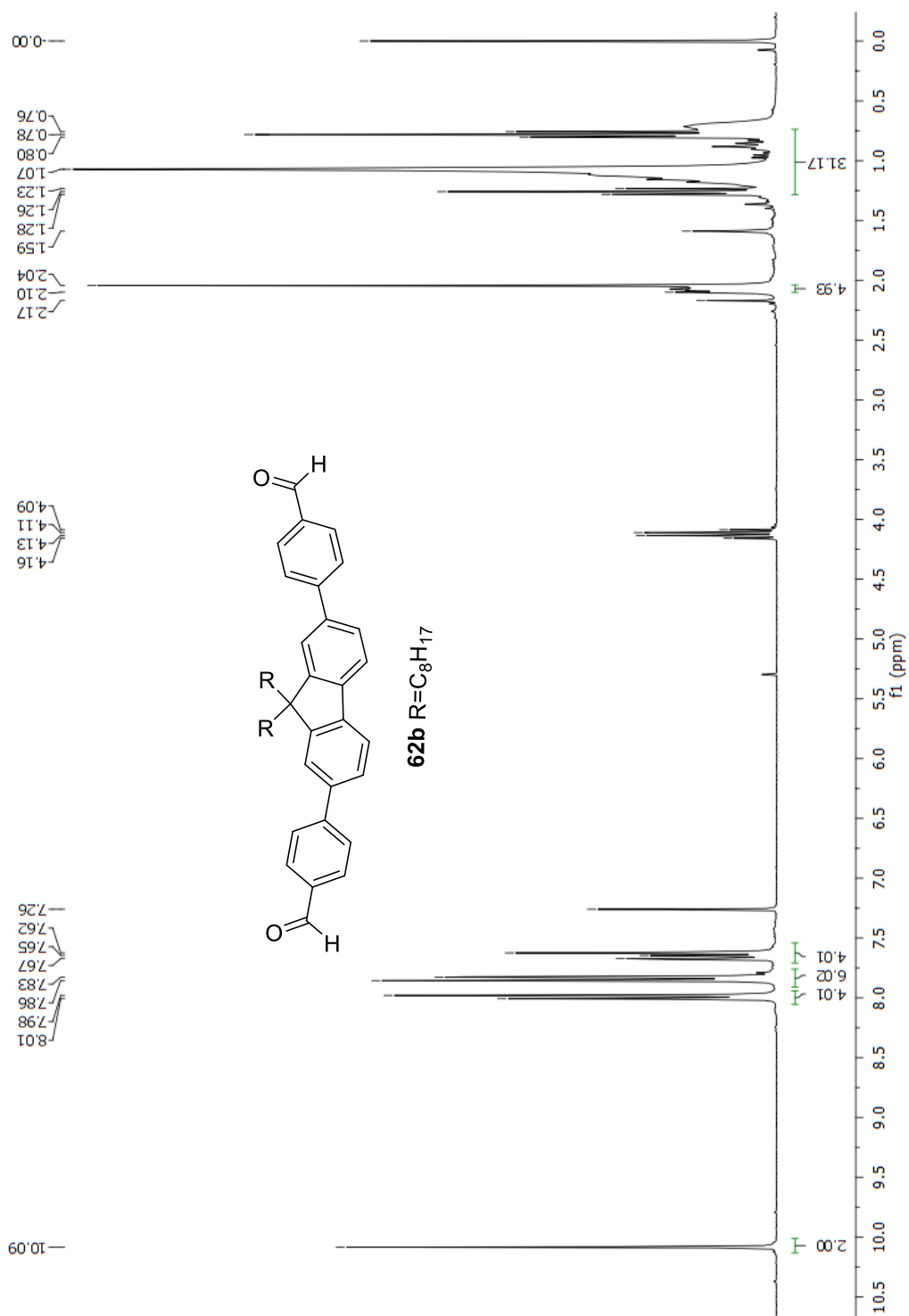


**Fig. 2-11:** <sup>1</sup>H NMR (300 MHz, CDCl<sub>3</sub>) spectrum of compound **62b**.

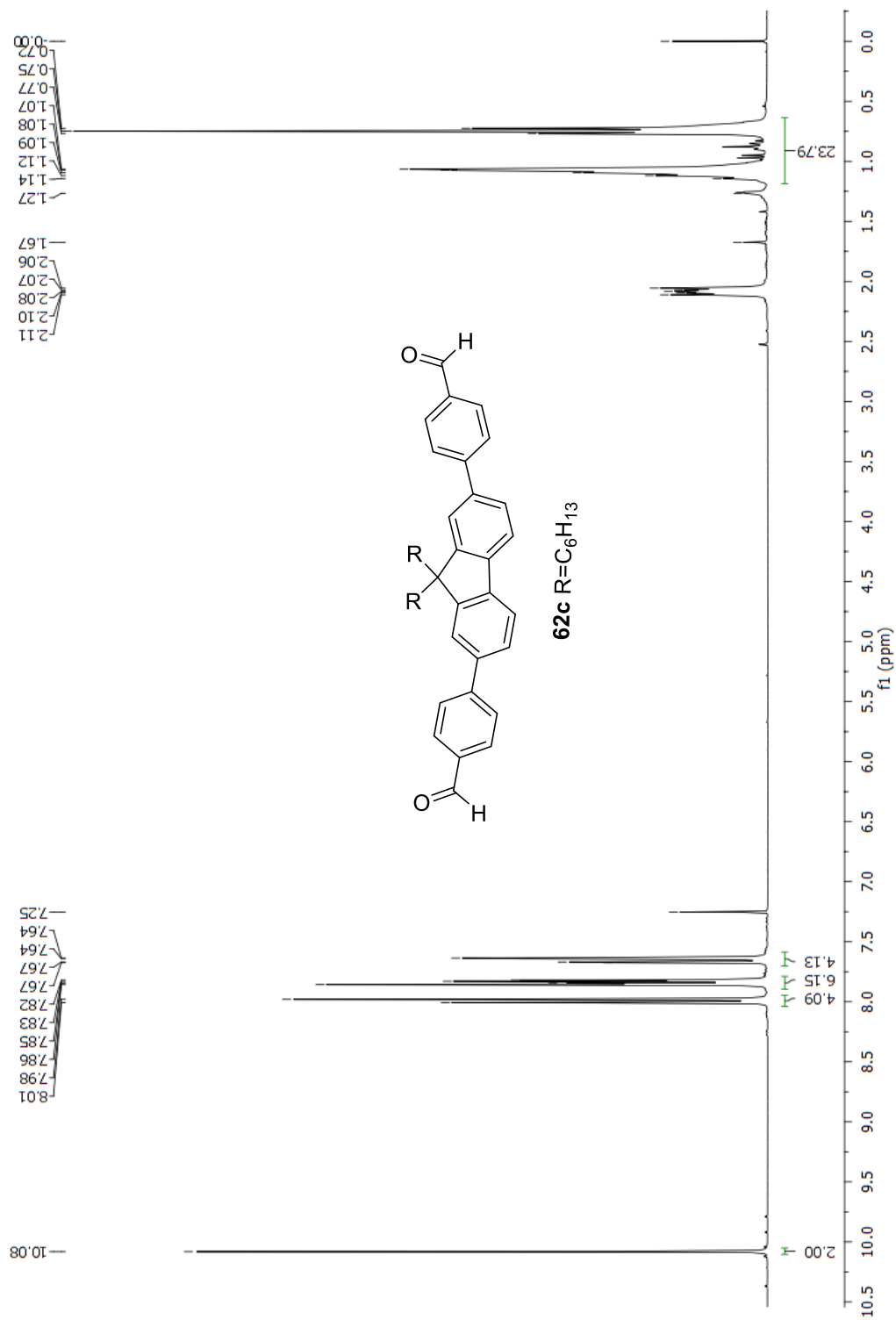


**Fig. 2-12:** <sup>1</sup>H NMR (300 MHz, CDCl<sub>3</sub>) spectrum of compound **62c**.

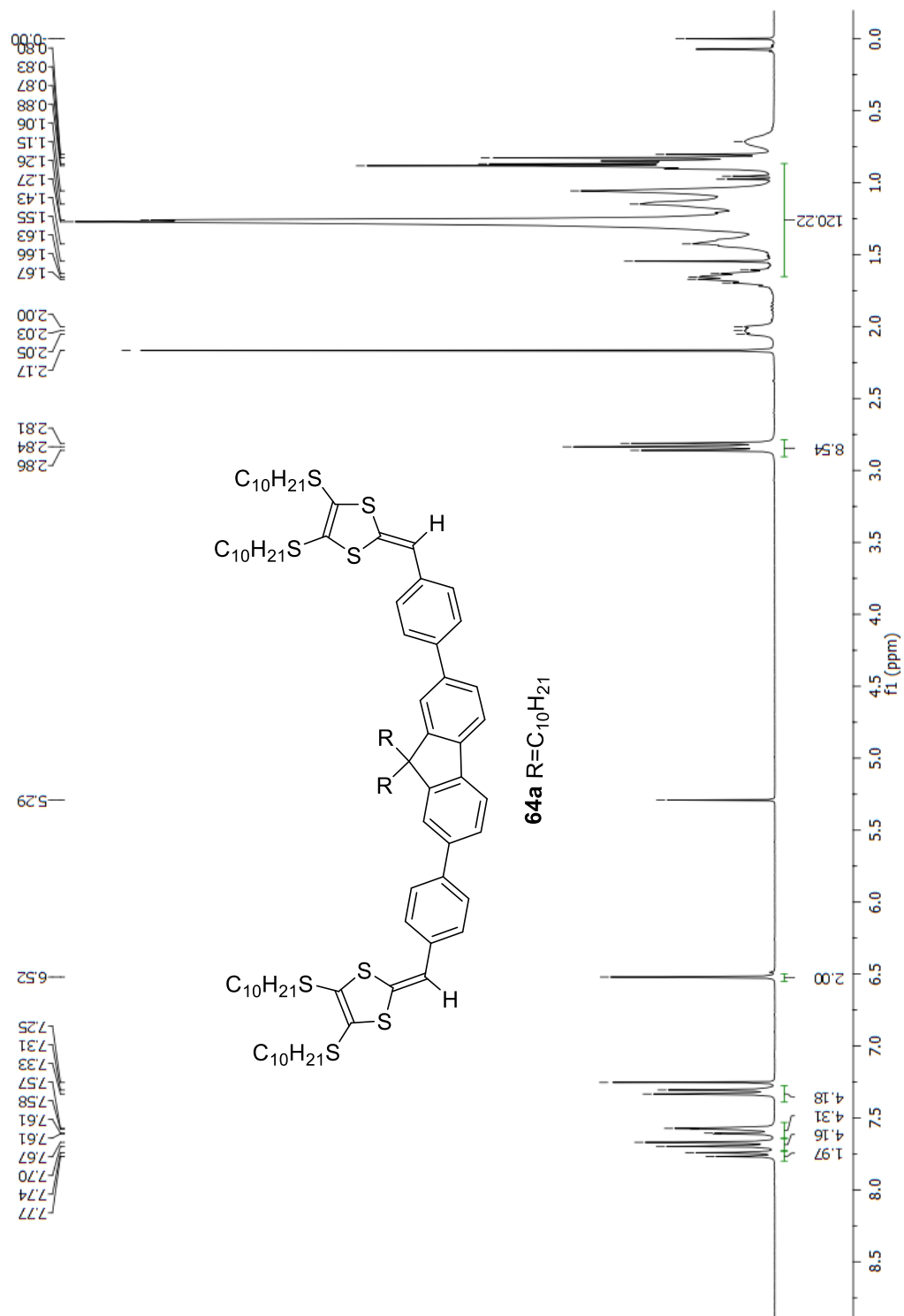


**Fig. 2-13:**  $^1H$  NMR (300 MHz,  $CDCl_3$ ) spectrum of compound **64a**.

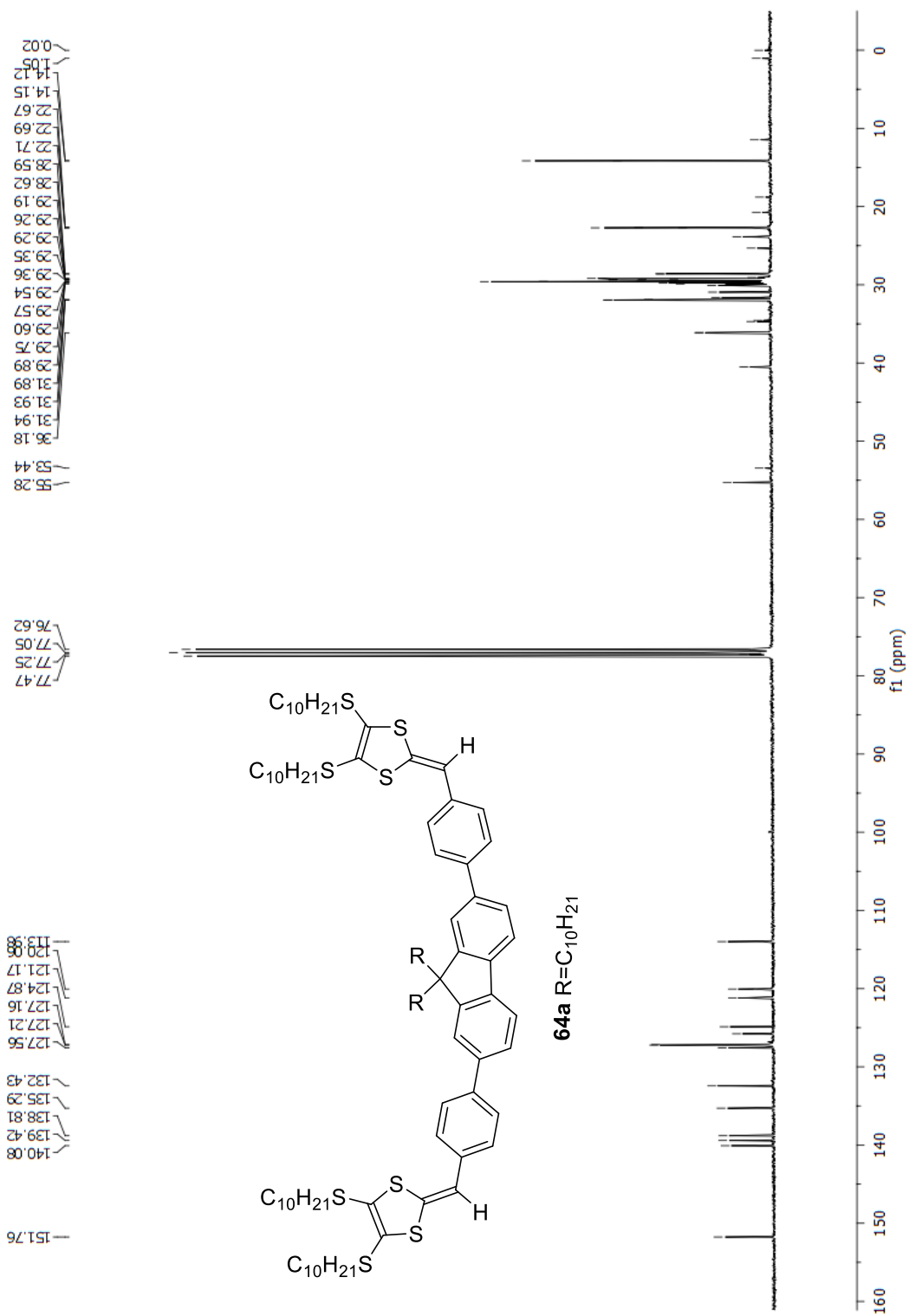


**Fig. 2-14:**  $^{13}C$  NMR (75 MHz,  $CDCl_3$ ) spectrum of compound **64a**.





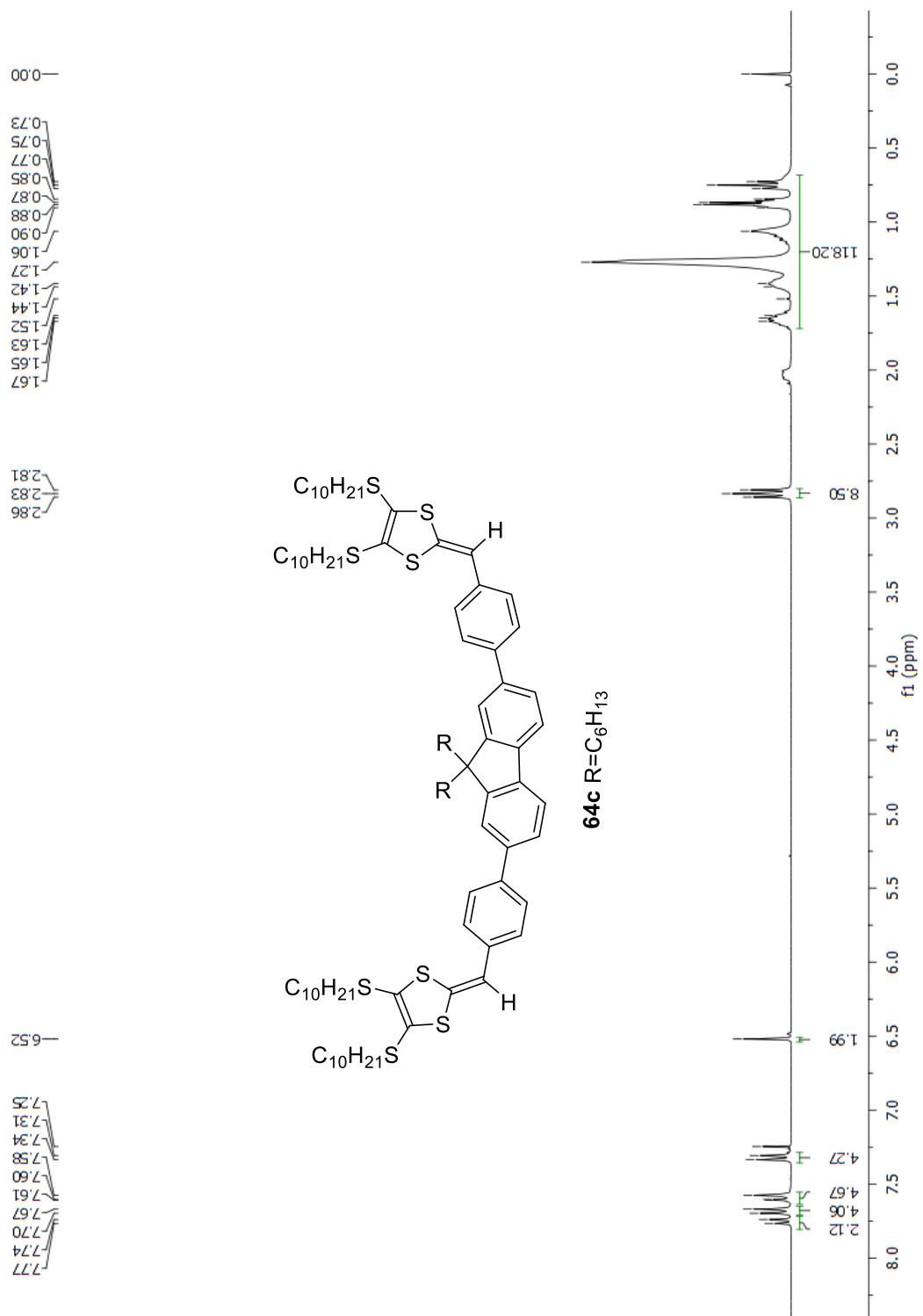


**Fig. 2-17:**  $^1H$  NMR (300 MHz,  $CDCl_3$ ) spectrum of compound **64c**.

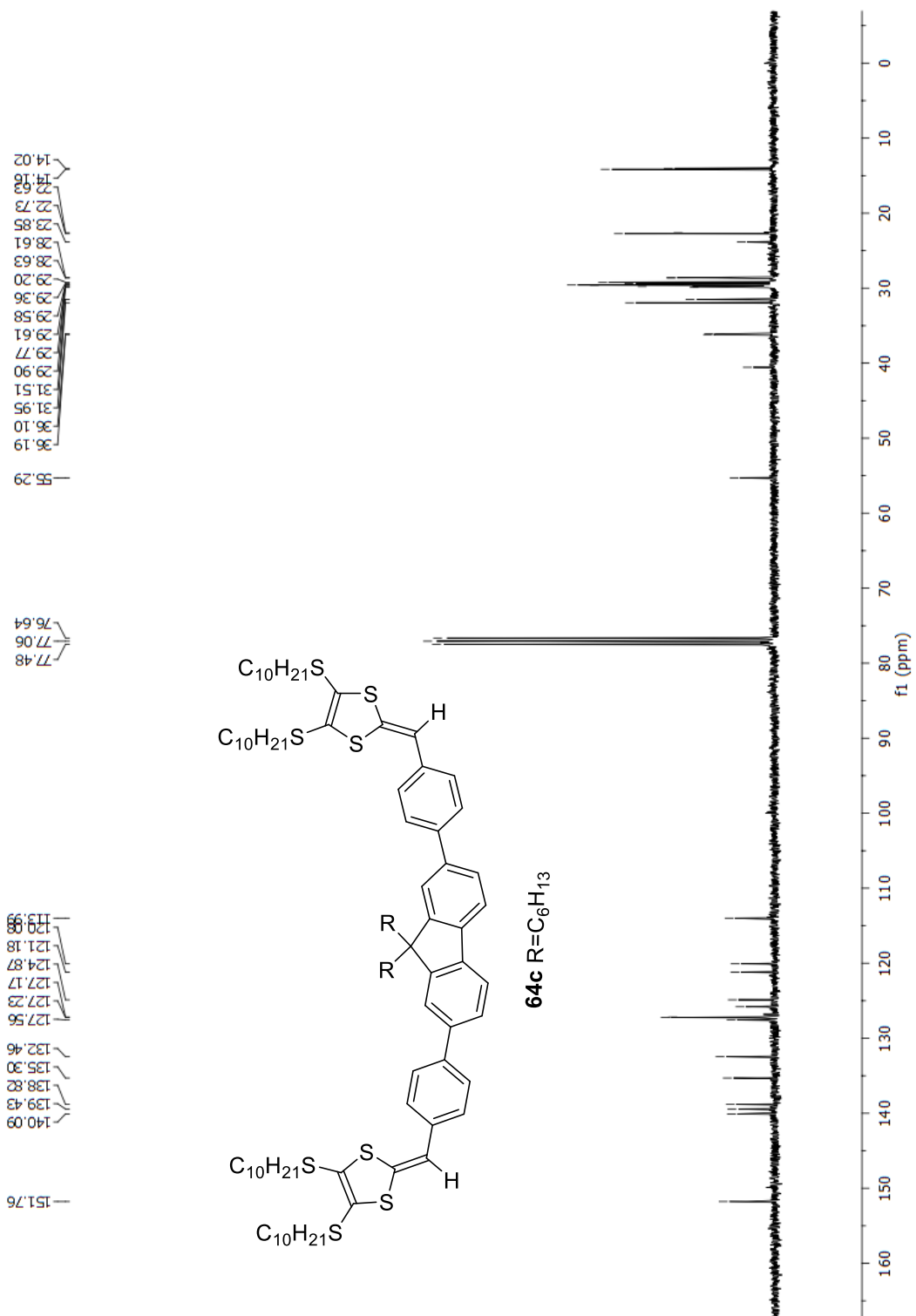


**Fig. 2-18:**  $^{13}C$  NMR (75 MHz,  $CDCl_3$ ) spectrum of compound **64c**.

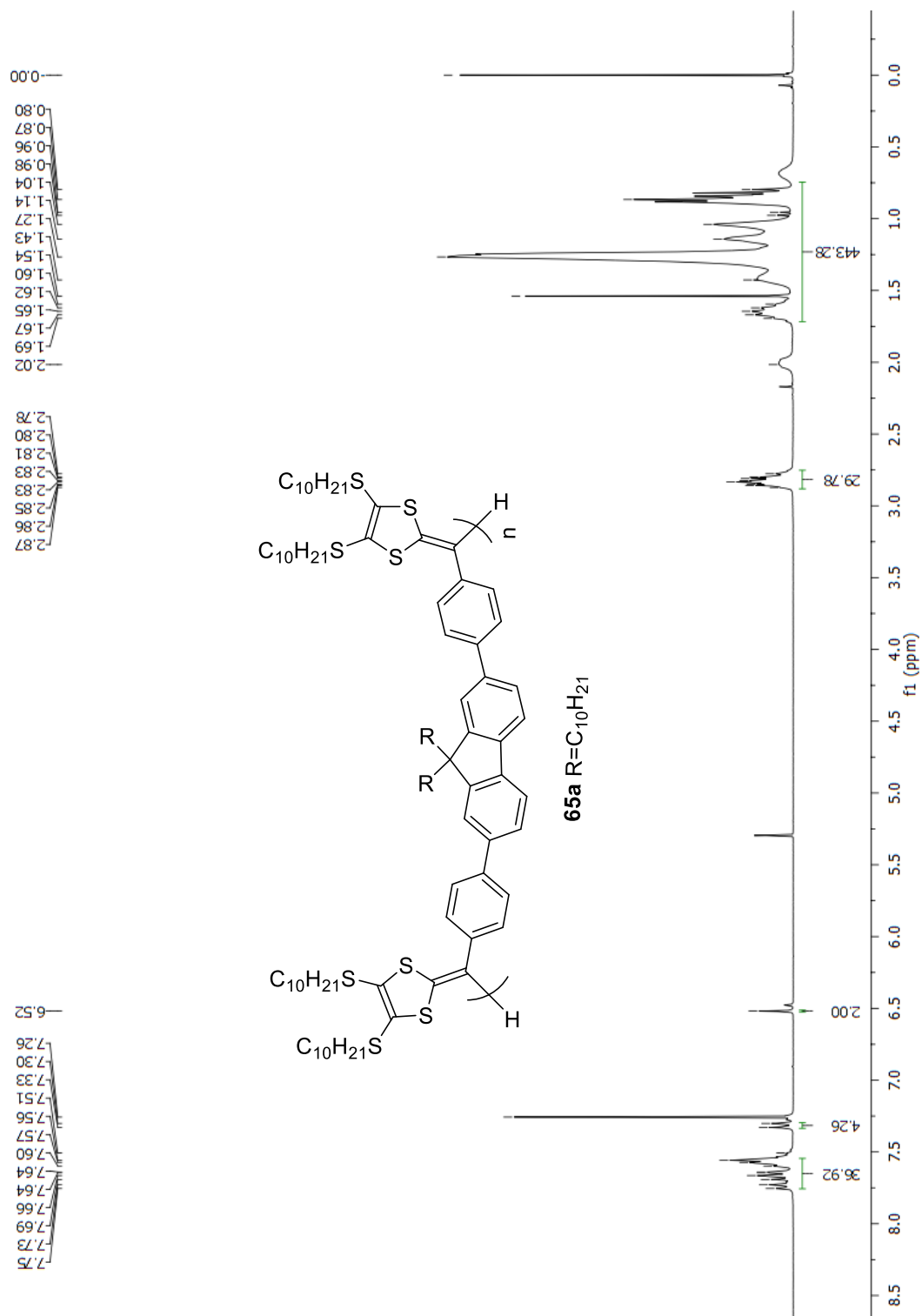


**Fig. 2-19:**  $^1H$  NMR (300 MHz,  $CDCl_3$ ) spectrum of compound **65a**.

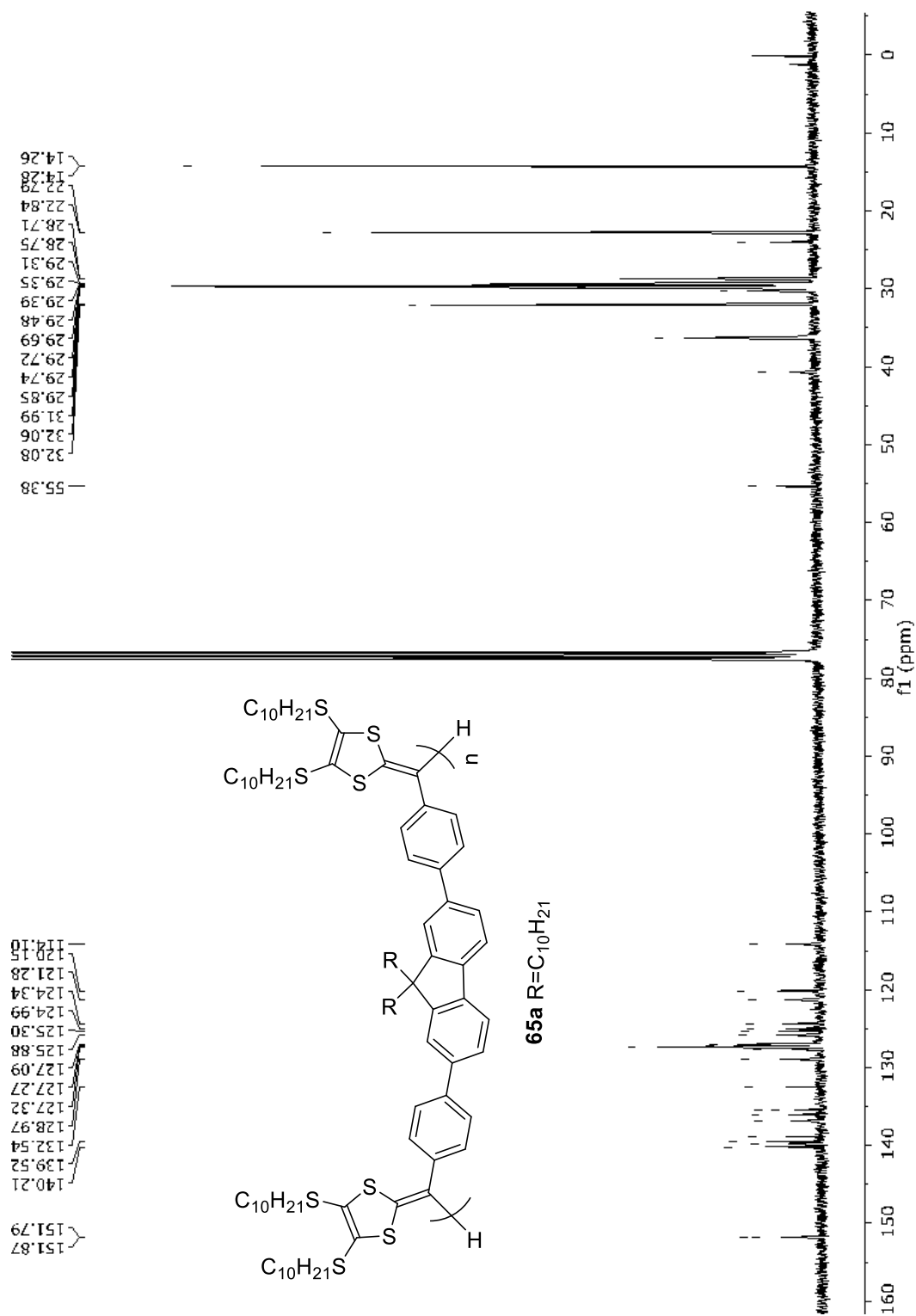


**Fig. 2-20:**  $^{13}C$  NMR (75 MHz,  $CDCl_3$ ) spectrum of compound **65a**.

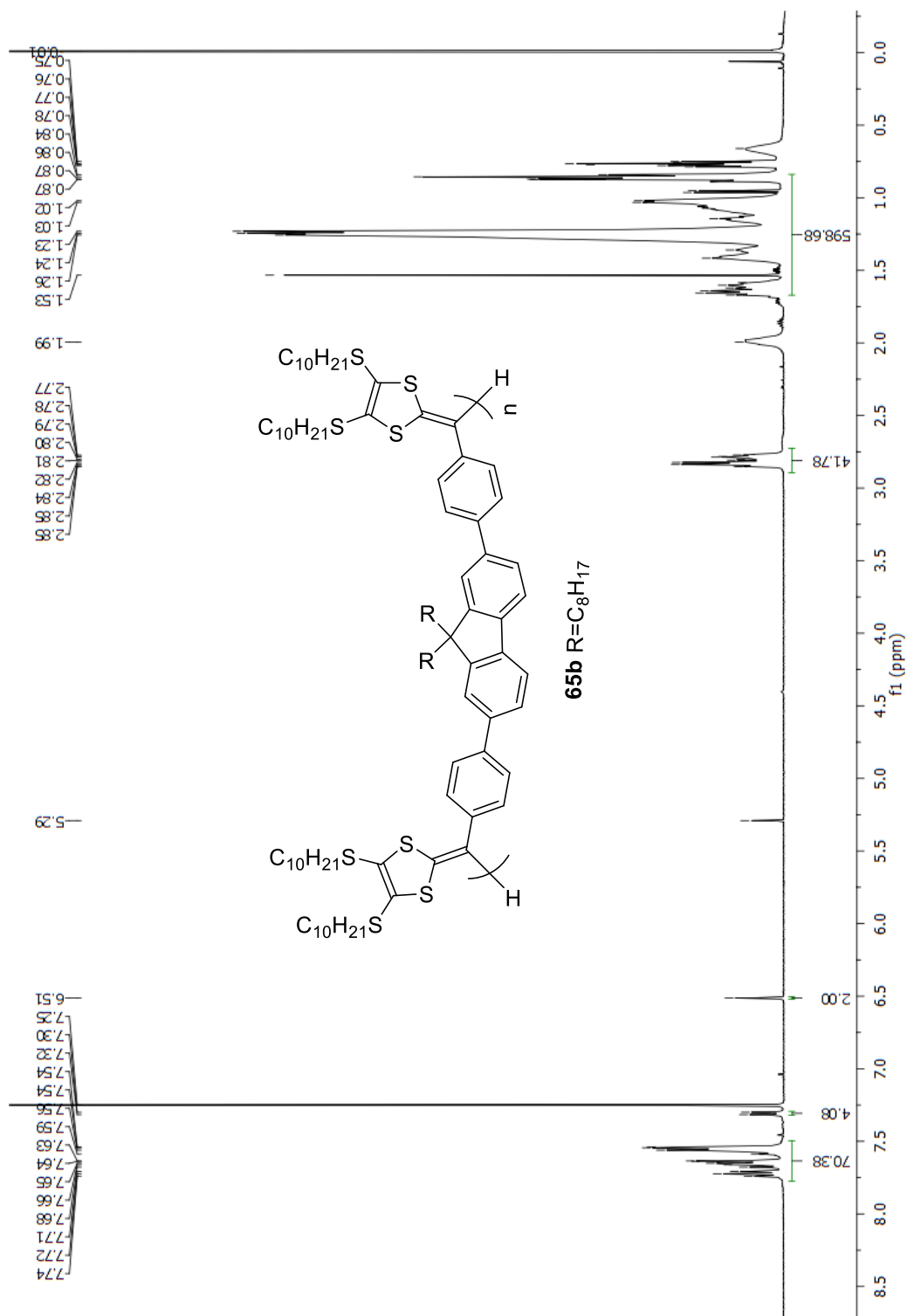


**Fig. 2-21:**  $^1H$  NMR (300 MHz,  $CDCl_3$ ) spectrum of compound **65b**.

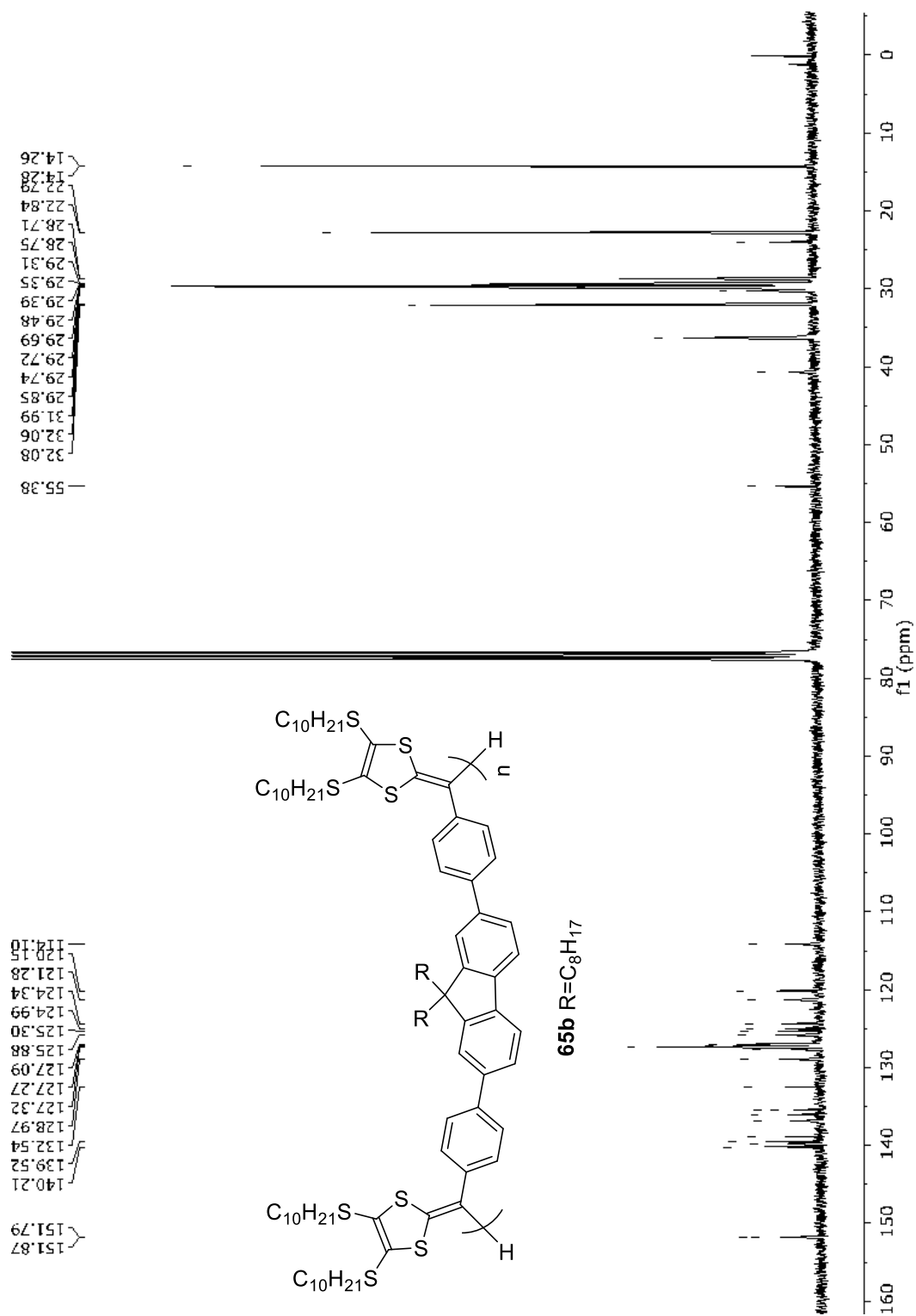


**Fig. 2-22:**  $^{13}C$  NMR (75 MHz,  $CDCl_3$ ) spectrum of compound **65b**.

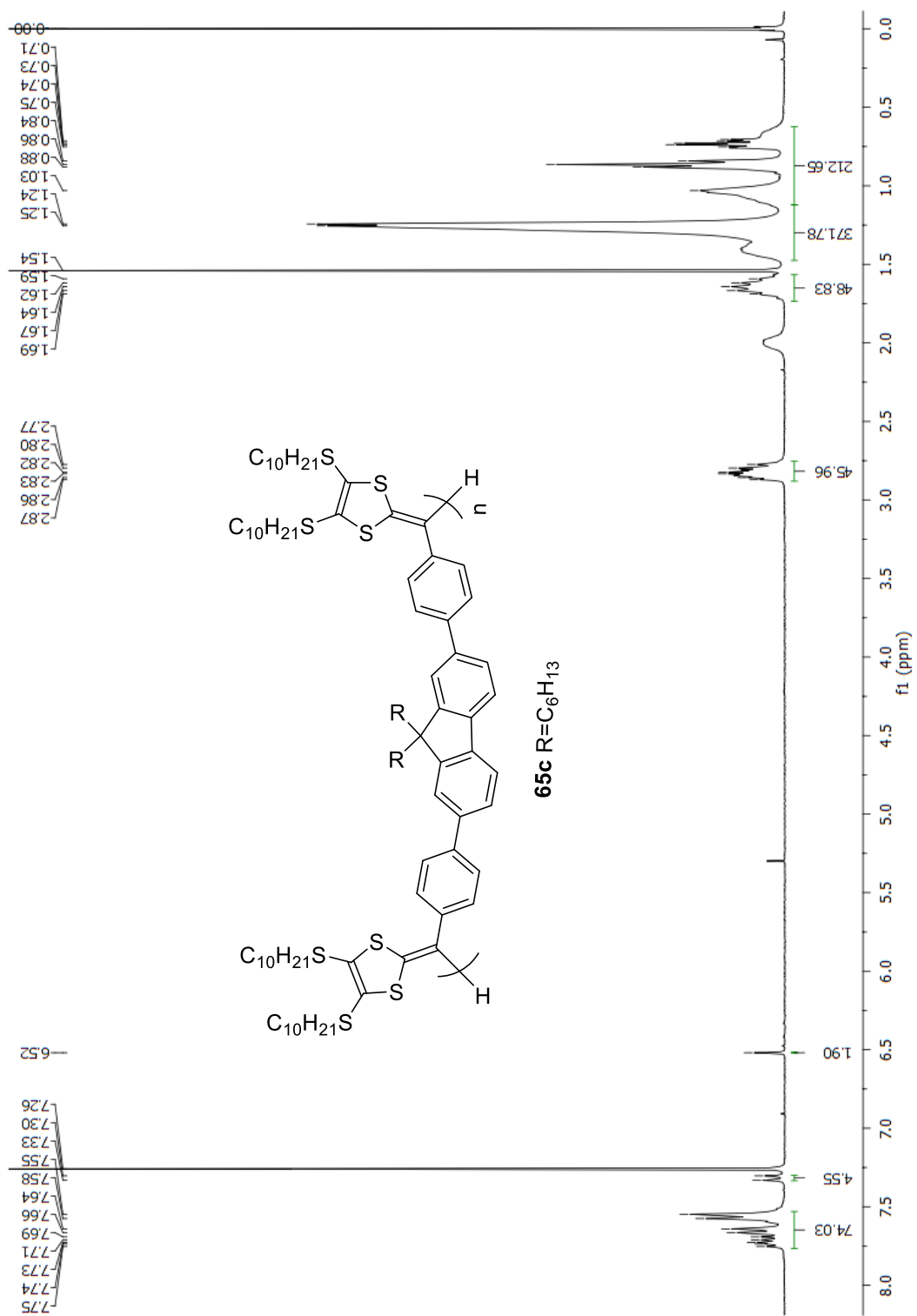


**Fig. 2-23:**  $^1H$  NMR (300 MHz,  $CDCl_3$ ) spectrum of compound **65c**.

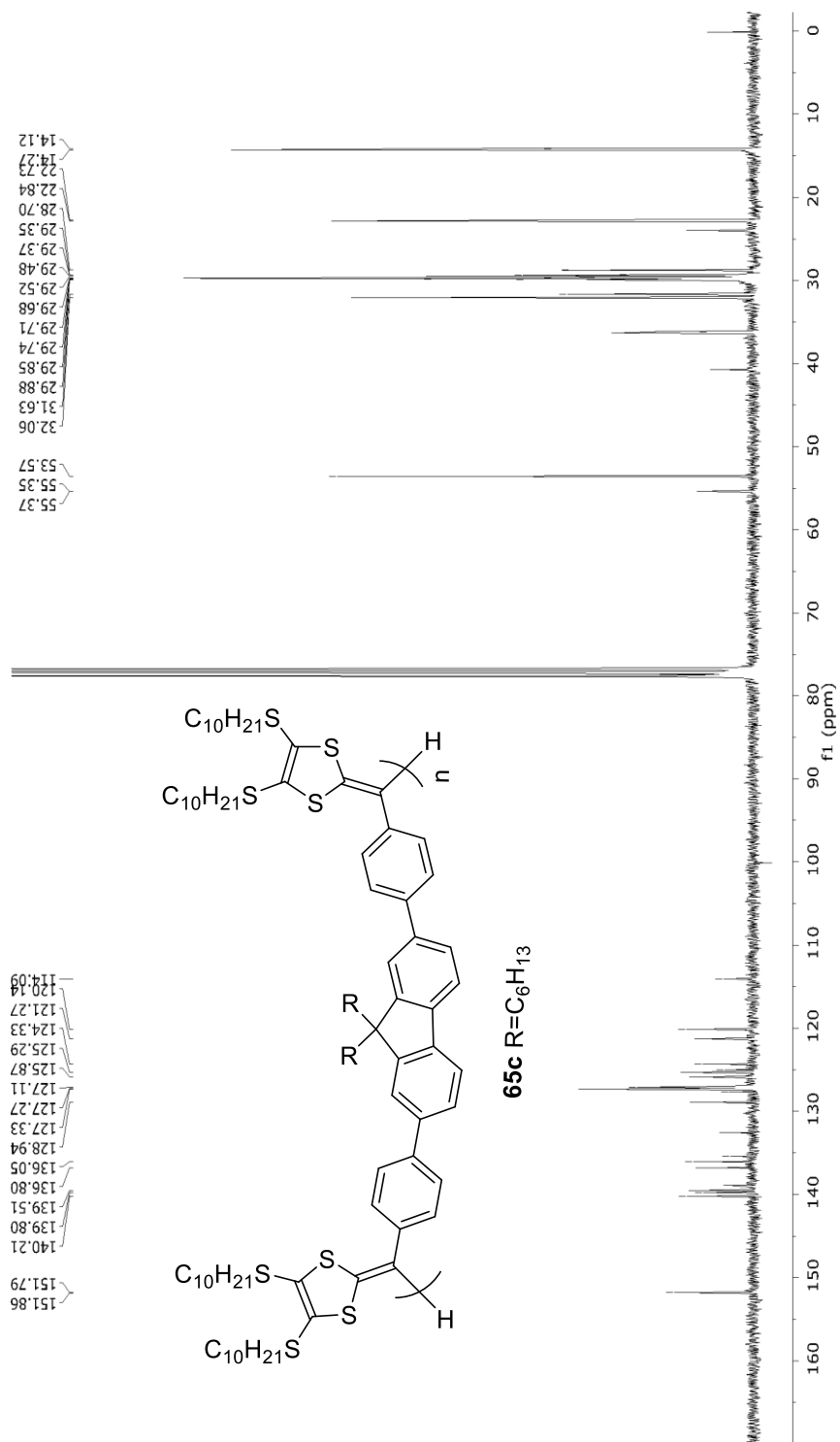


**Fig. 2-24:**  $^{13}C$  NMR (75 MHz,  $CDCl_3$ ) spectrum of compound **65c**.

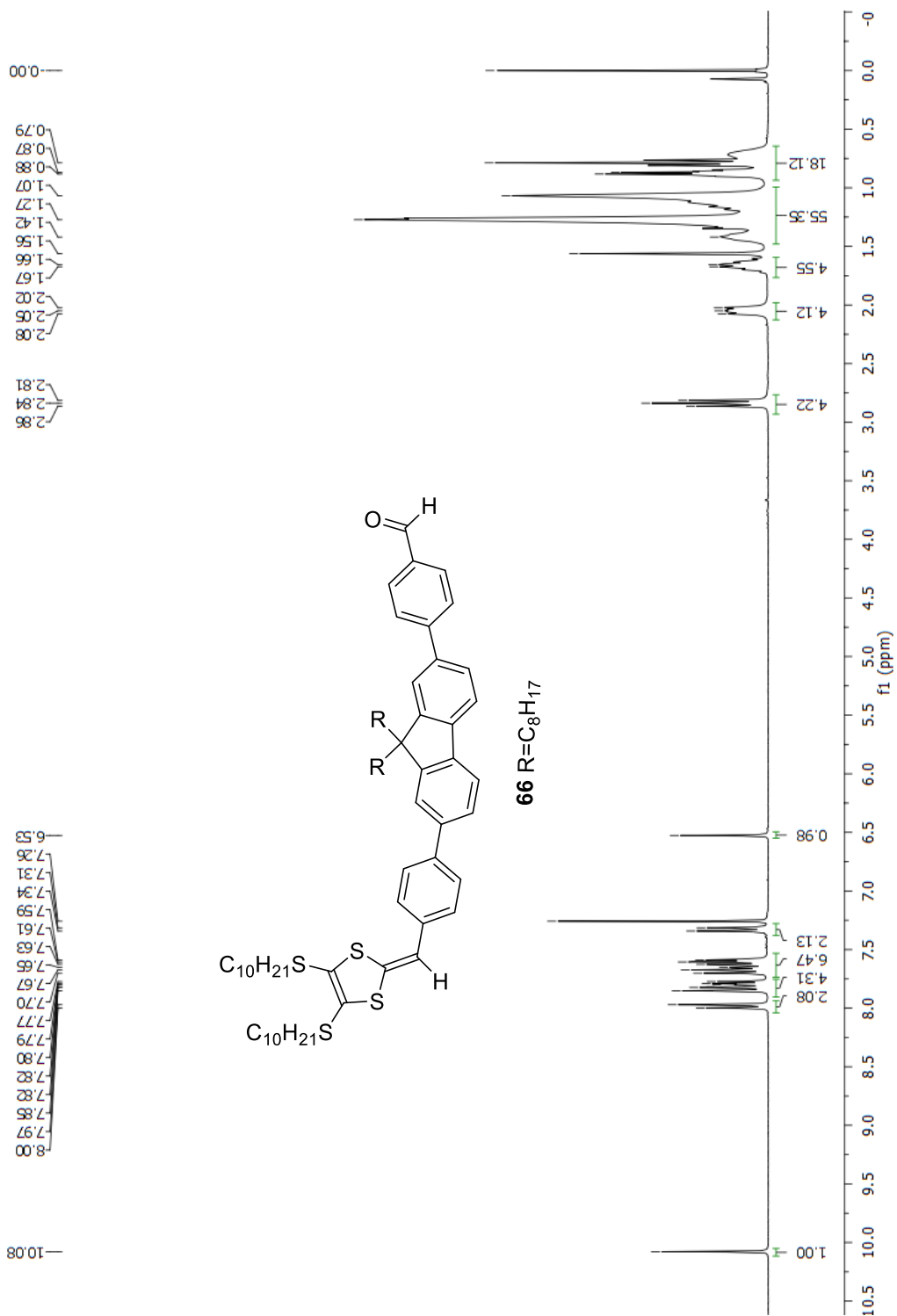


**Fig. 2-25:**  $^1H$  NMR (300 MHz,  $CDCl_3$ ) spectrum of compound **66**.



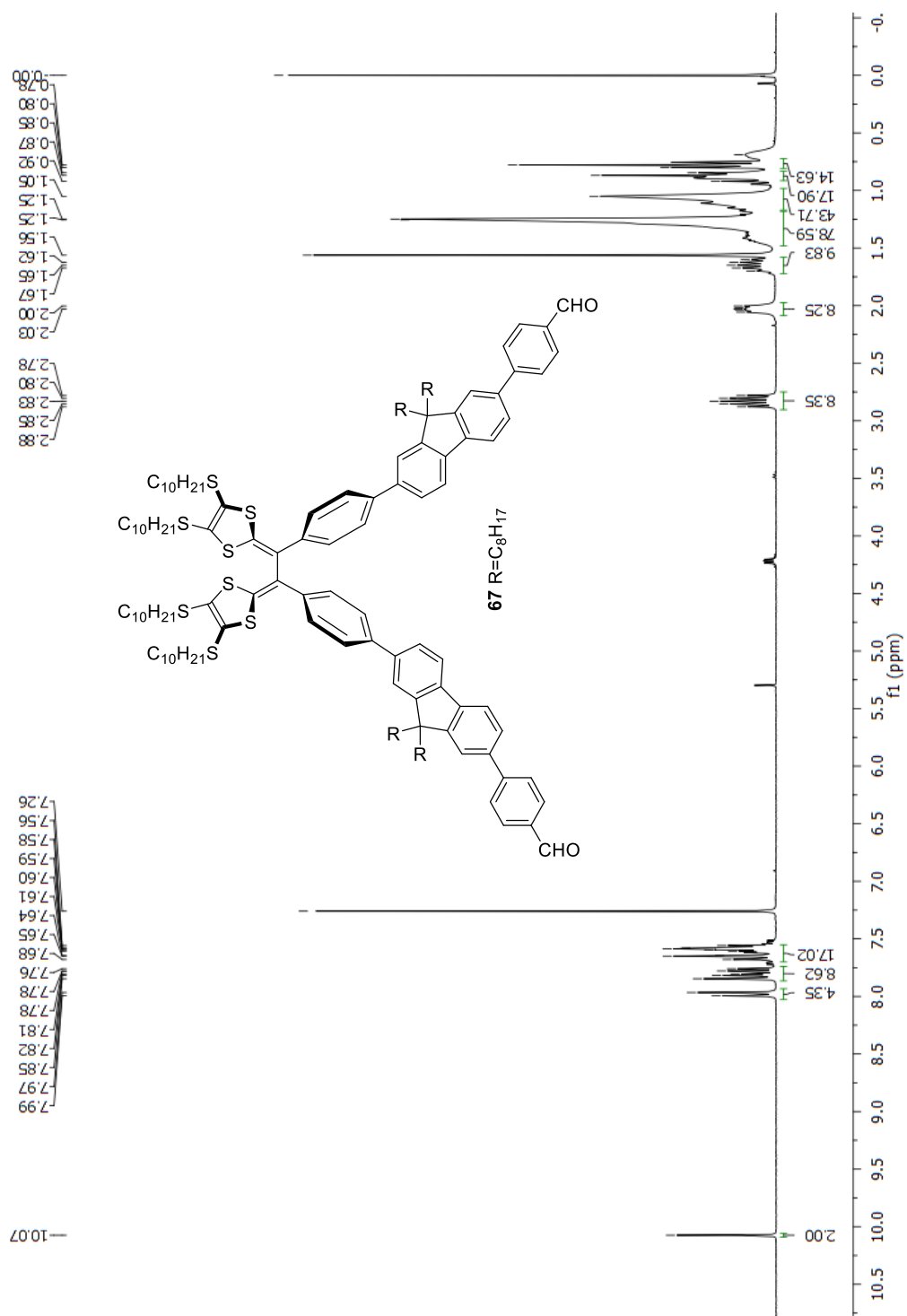


**Fig. 2-27:**  $^1H$  NMR (300 MHz,  $CDCl_3$ ) spectrum of compound **67**.

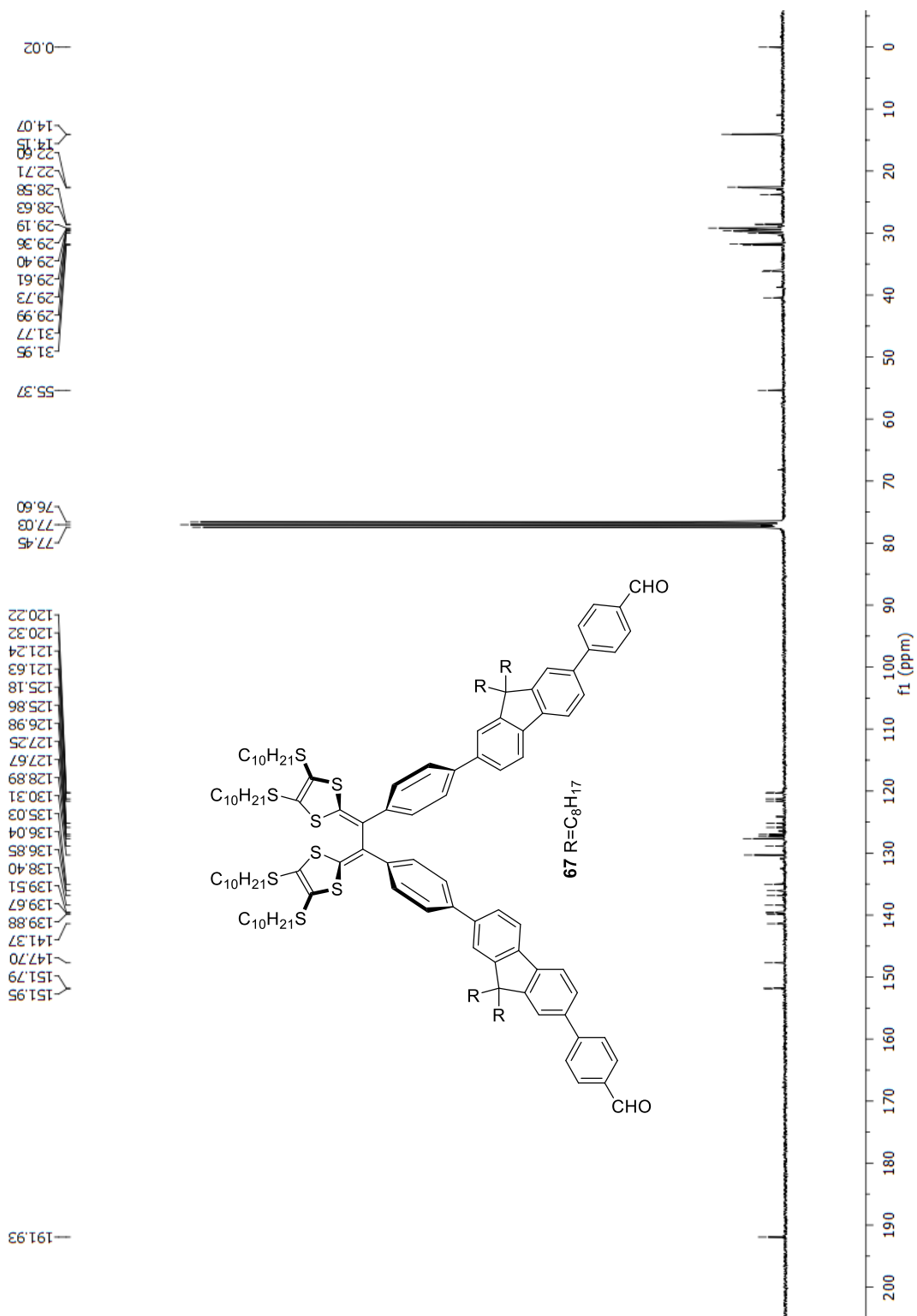


**Fig. 2-28:**  $^{13}C$  NMR (75 MHz,  $CDCl_3$ ) spectrum of compound **67**.

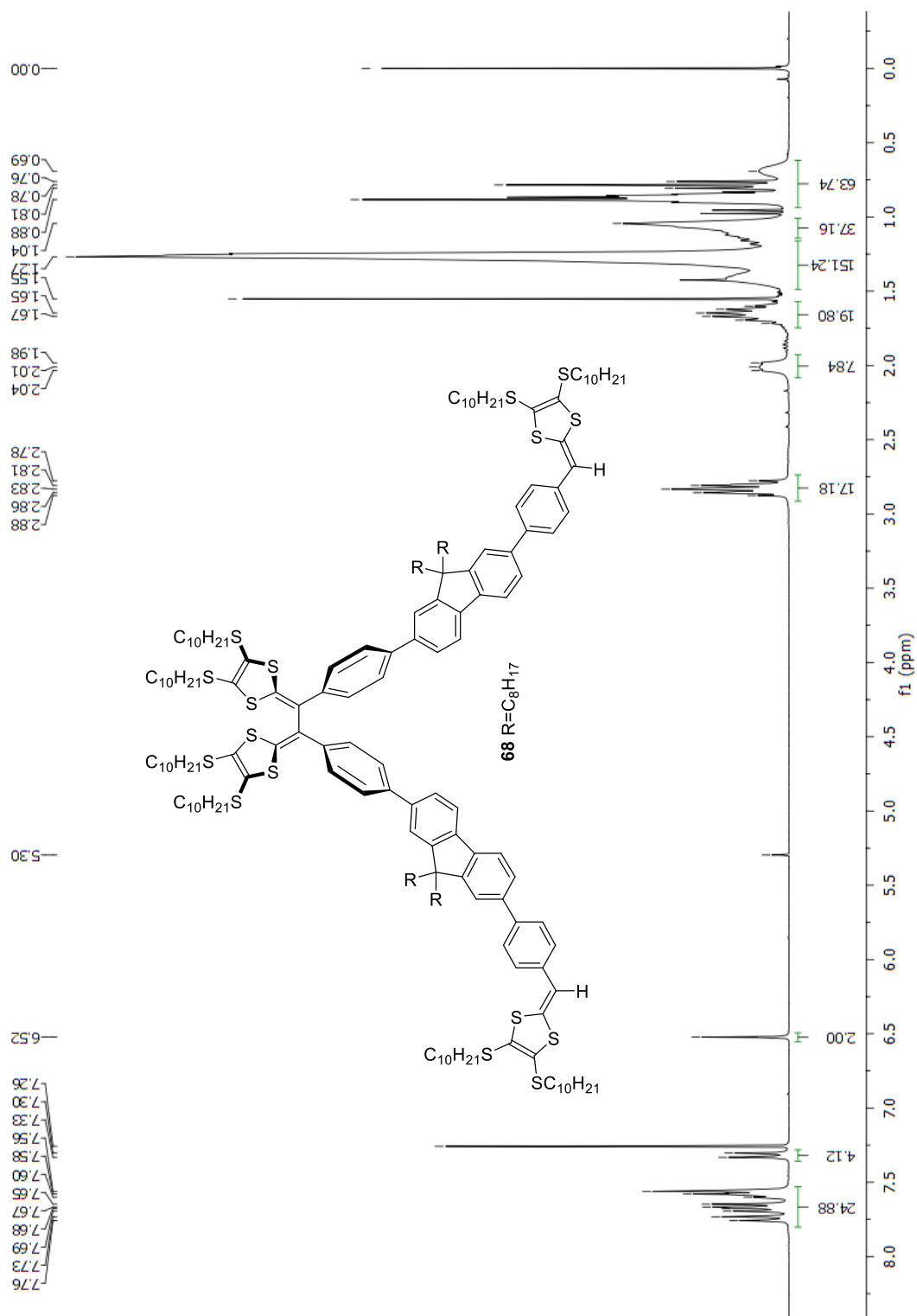


**Fig. 2-29:**  $^1H$  NMR (300 MHz,  $CDCl_3$ ) spectrum of compound **68**.

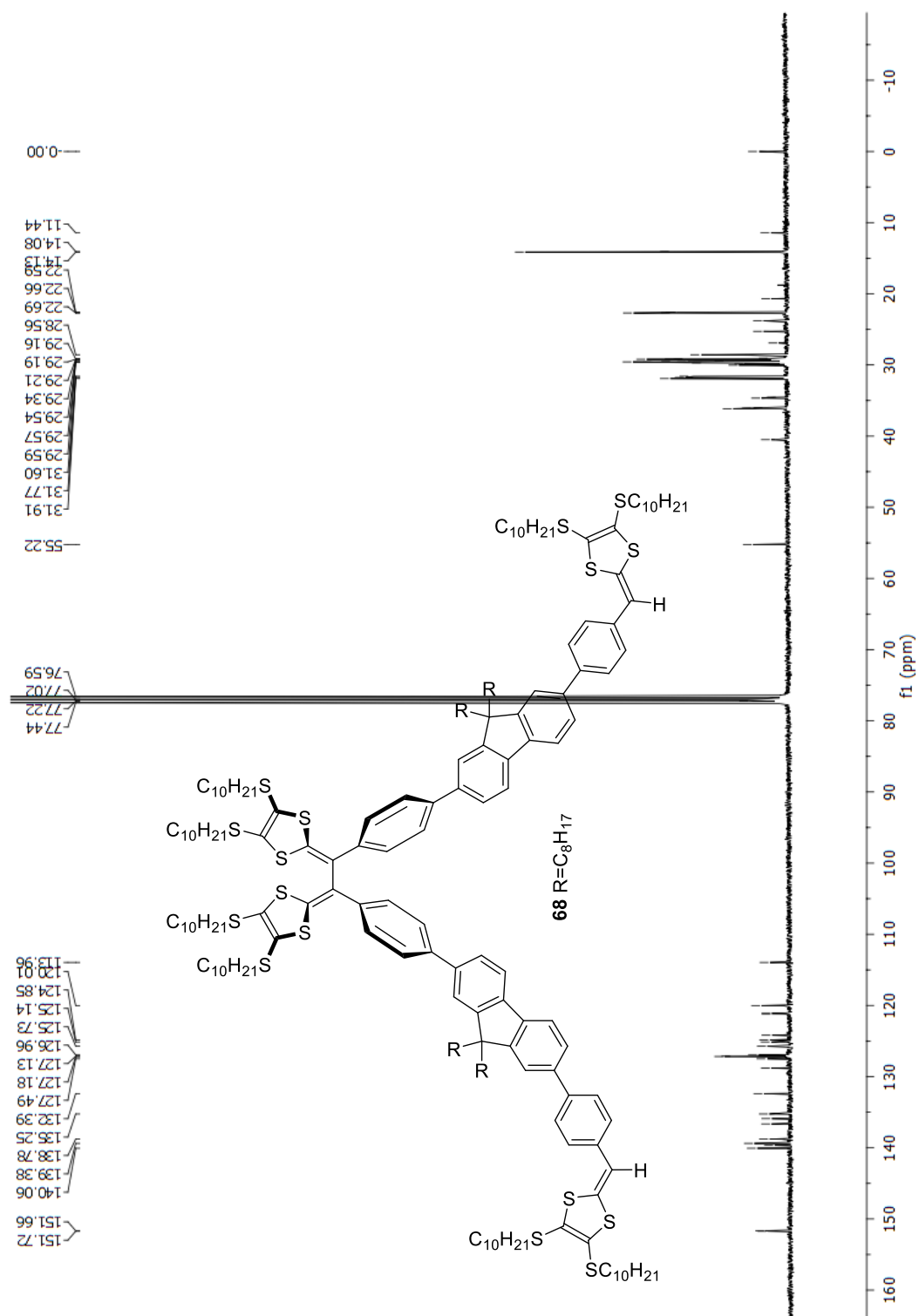


**Fig. 2-30:**  $^{13}C$  NMR (75 MHz,  $CDCl_3$ ) spectrum of compound **68**.

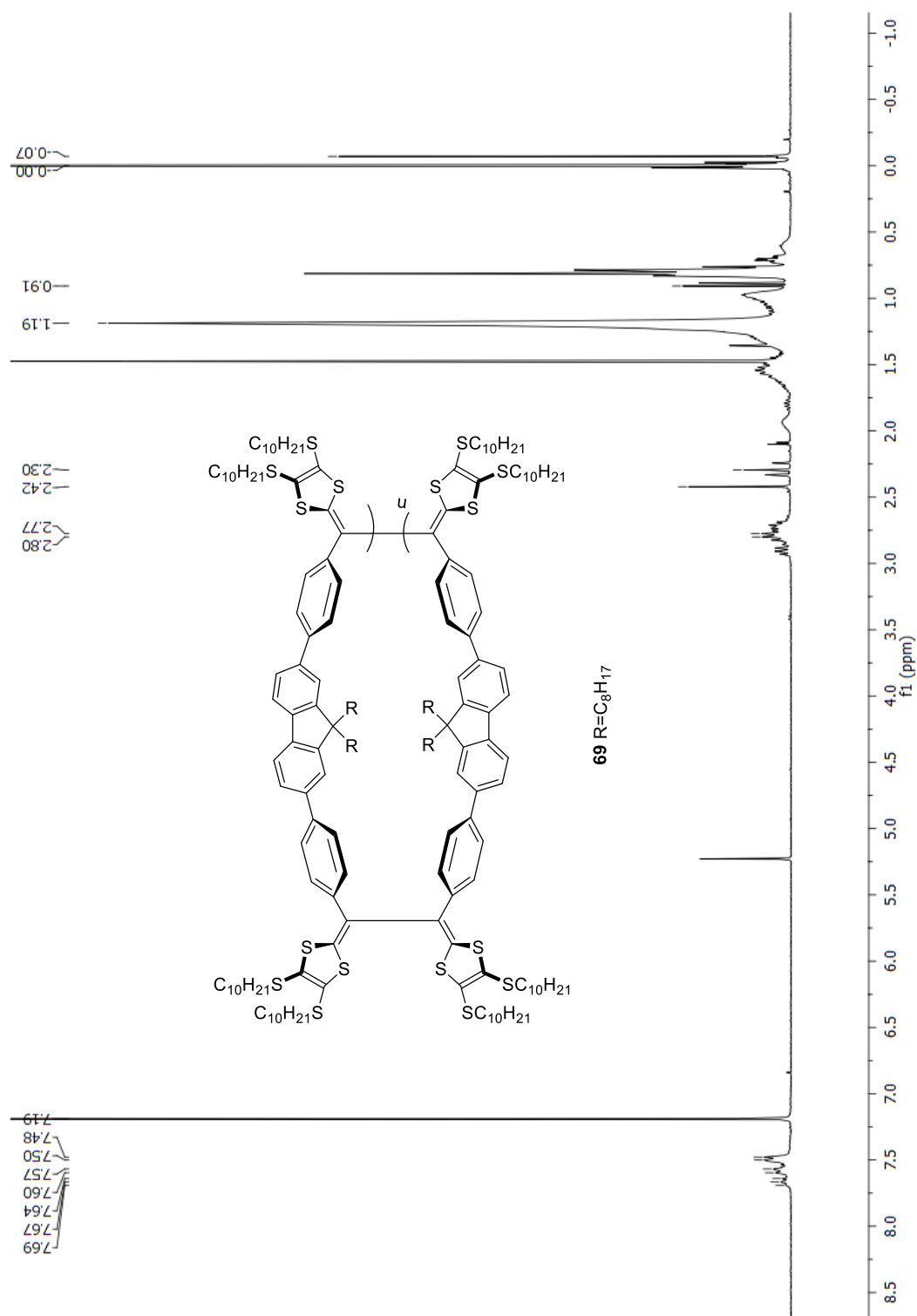


**Fig. 2-31:**  $^1H$  NMR (300 MHz,  $CDCl_3$ ) spectrum of compound **69**.

## 2.4 References

- (1) Skotheim, T. A., Elsenbaumer, R. L., Reynolds, J. R., Eds. *Handbook of conducting polymers*, 2<sup>nd</sup> ed.; Marcel Dekker: New York, 1997.
- (2) Hirao, T., Ed. *Redox systems under nano-space control: Nano-Space Control and its applications*; Springer, Berlin, 2006.
- (3) Mishra, A.; Ma, C.-Q.; Bäuerle, P. *Chem. Rev.* **2009**, *109*, 1141.
- (4) Inzelt, G. *Conducting polymers: a New Era in Electrochemistry*, 2<sup>nd</sup> ed.; Springer: Berlin, 2012.
- (5) Hirao, T., Ed. *Functionalized Redox Systems: Synthetic Reactions and Design of  $\pi$ -and bioconjugates*; Springer: Heidelberg, 2015.
- (6) Luo, L.; Benameur, A.; Brignou, P.; Choi, S. H.; Rigaut, S.; Frisbie, C. D. *J. Phys. Chem. C* **2011**, *115*, 19955.
- (7) Hortholary, C.; Coudret, C. *J. Org. Chem.* **2003**, *68*, 2167.
- (8) Chen, C.-P.; Luo, W.-R.; Chen, C.-N.; Wu, S.-M.; Hsieh, S.; Chiang, C.-M.; Dong, T.-Y. *Langmuir* **2013**, *29*, 3106.
- (9) Schubert, C.; Margraf, J. T.; Clark, T.; Guldi, D. M. *Chem. Soc. Rev.* **2015**, *44*, 988.
- (10) Shaibu, B. S.; Lin, S.-H.; Lin, C.-Y.; Wong, K.-T.; Liu, R.-S. *J. Org. Chem.* **2011**, *76*, 1054.
- (11) Segura, J. L.; Martín, N.; Guldi, D. M. *Chem. Soc. Rev.* **2005**, *34*, 31.
- (12) Alévêque, O.; Leriche, P.; Cocherel, N.; Frère, P.; Cravino, A.; Roncali, J. *Sol. Energy Mater. Sol. Cells* **2008**, *92*, 1170.

- (13) Guo, K.; Yan, K.; Lu, X.; Qiu, Y.; Liu, Z.; Sun, J.; Yan, F.; Guo, W.; Yang, S. *Org. Lett.* **2012**, *14*, 2214.
- (14) Wan, Z.; Jia, C.; Duan, Y.; Chen, X.; Lin, Y.; Shi, Y. *Org. Electron* **2013**, *14*, 2132.
- (15) Sönmez, G.; Schwendeman, I.; Schottland, P.; Zong, K.; Reynolds, J. R. *Macromolecules* **2003**, *36*, 639.
- (16) Nishida, J.-i.; Miyagawa, T.; Yamashita, Y. *Org. Lett.* **2004**, *6*, 2523.
- (17) Wang, X.; Ng, J. K.-P.; Jia, P.; Lin, T.; Cho, C. M.; Xu, J.; Lu, X.; He, C. *Macromolecules* **2009**, *42*, 5534.
- (18) Beaujuge, P. M.; Reynolds, J. R. *Chem. Rev.* **2010**, *110*, 268.
- (19) Chen, G.; Mahmud, I.; Dawe, L. N.; Zhao, Y. *Org. Lett.* **2010**, *12*, 704.
- (20) Chen, G.; Mahmud, I.; Dawe, L. N.; Daniels, L. M.; Zhao, Y. *J. Org. Chem.* **2011**, *76*, 2701.
- (21) Xu, B. Q.; Li, X. L.; Xiao, X. Y.; Sakaguchi, H.; Tao, N. J. *Nano Lett.* **2005**, *5*, 1491.
- (22) Tam, I. W.; Yan, J.; Breslow, R. *Org. Lett.* **2006**, *8*, 183.
- (23) Ohtake, T.; Tanaka, H.; Matsumoto, T.; Kimura, M.; Ohta, A. *J. Org. Chem.* **2014**, *79*, 6590.
- (24) McQuade, D. T.; Pullen, A. E.; Swager, T. M. *Chem. Rev.* **2000**, *100*, 2537.
- (25) Huang, J.; Virji, S.; Weiller, B. H.; Kaner, R. B. *J. Am. Chem. Soc.* **2003**, *125*, 314.
- (26) Liu, H.; Kameoka, J.; Czaplewski, D. A.; Craighead, H. G. *Nano Lett.* **2004**, *4*, 671.
- (27) Liu, B.; Bazan, G. C. *J. Am. Chem. Soc.* **2006**, *128*, 1188.
- (28) Wang, F.; Lai, Y.-H.; Han, M.-Y. *Macromolecules* **2004**, *37*, 3222.

- (29) Amir, E.; Amir, R. J.; Campos, L. M.; Hawker, C. J. *J. Am. Chem. Soc.* **2011**, *133*, 10046.
- (30) Ohtake, T.; Tanaka, H.; Matsumoto, T.; Ohta, A.; Kimura, M. *Langmuir* **2014**, *30*, 14680.
- (31) Liang, S.; Chen, G.; Peddle, J.; Zhao, Y. *Chem. Commun.* **2012**, *48*, 3100.
- (32) Liang, S.; Chen, G.; Zhao, Y. *J. Mater. Chem. C* **2013**, *1*, 5477.
- (33) Liang, S.; Zhao, Y.; Adronov, A. *J. Am. Chem. Soc.* **2014**, *136*, 970.
- (34) Yamada, J.-i.; Sugimoto, T. *TTF chemistry: fundamentals and applications of tetrathiafulvalene*; Springer: Berlin, 2004.
- (35) Segura, J. L.; Martín, N. *Angew. Chem., Int. Ed.* **2001**, *40*, 1372.
- (36) Canevet, D.; Salle, M.; Zhang, G.; Zhang, D.; Zhu, D. *Chem. Commun.* **2009**, 2245.
- (37) Moore, A. J.; Bryce, M. R.; Ando, D. J.; Hursthouse, M. B. *J. Chem. Soc., Chem. Commun.* **1991**, 320.
- (38) Moore, A. J.; Bryce, M. R. *Tetrahedron Lett.* **1992**, *33*, 1373.
- (39) Yu, L.; Zhu, D. *Chem. Commun.* **1997**, 787.
- (40) Bellec, N.; Boubekeur, K.; Carlier, R.; Hapiot, P.; Lorcy, D.; Tallec, A. *J. Phys. Chem. A* **2000**, *104*, 9750.
- (41) Carlier, R.; Hapiot, P.; Lorcy, D.; Robert, A.; Tallec, A. *Electrochim. Acta* **2001**, *46*, 3269.
- (42) Roncali, J. *J. Mater. Chem.* **1997**, *7*, 2307.
- (43) Bendikov, M.; Wudl, F.; Perepichka, D. F. *Chem. Rev.* **2004**, *104*, 4891.

- (44) Zhao, Y.; Chen, G.; Mulla, K.; Mahmud, I.; Liang, S.; Dongare, P.; Thompson, D. W.; Dawe, L. N.; Bouzan, S. *Pure Appl. Chem.* **2012**, *84*, 1005.
- (45) Inagi, S.; Naka, K.; Chujo, Y. *J. Mater. Chem.* **2007**, *17*, 4122.
- (46) Inagi, S.; Naka, K.; Iida, D.; Chujo, Y. *Polym. J.* **2006**, *38*, 1146.
- (47) Naka, K.; Inagi, S.; Chujo, Y. *J. Polym. Sci., Part A: Polym. Chem.* **2005**, *43*, 4600.
- (48) Lorcy, D.; Mattiello, L.; Poriel, C.; Rault-Berthelot, J. *J. of Electroanal. Chem.* **2002**, *530*, 33.
- (49) Guerro, M.; Carlier, R.; Boubekeur, K.; Lorcy, D.; Hapiot, P. *J. Am. Chem. Soc.* **2003**, *125*, 3159.
- (50) Guerro, M.; Roisnel, T.; Pellon, P.; Lorcy, D. *Inorg. Chem.* **2005**, *44*, 3347.
- (51) Gontier, E.; Bellec, N.; Brignou, P.; Gohier, A.; Guerro, M.; Roisnel, T.; Lorcy, D. *Org. Lett.* **2010**, *12*, 2386.
- (52) Lorcy, D.; Guerro, M.; Bergamini, J.-F.; Hapiot, P. *J. Phys. Chem. B* **2013**, *117*, 5188.
- (53) Chen, G.; Zhao, Y. *Org. Lett.* **2014**, *16*, 668.
- (54) Massue, J.; Bellec, N.; Guerro, M.; Bergamini, J.-F.; Hapiot, P.; Lorcy, D. *J. Org. Chem.* **2007**, *72*, 4655.
- (55) Mulla, K.; Dongare, P.; Thompson, D. W.; Zhao, Y. *Org. Biomol. Chem.* **2012**, *10*, 2542.
- (56) Mulla, K.; Shaik, H.; Thompson, D. W.; Zhao, Y. *Org. Lett.* **2013**, *15*, 4532.
- (57) Mulla, K.; Zhao, Y. *Tetrahedron Lett.* **2014**, *55*, 382.

- (58) Hapiot, P.; Lorcy, D.; Tallec, A.; Carlier, R.; Robert, A. *J. Phys. Chem.* **1996**, *100*, 14823.
- (59) Benahmed-Gasmi, A.; Frère, P.; Roncali, J.; Elandaloussi, E.; Orduna, J.; Garin, J.; Jubault, M.; Gorgues, A. *Tetrahedron Lett.* **1995**, *36*, 2983.
- (60) Yamashita, Y.; Tomura, M.; Badruz Zaman, M. *Chem. Commun.* **1998**, 1657.
- (61) Bouzan, S.; Chen, G.; Mulla, K.; Dawe, L. N.; Zhao, Y. *Org. Biomol. Chem.* **2012**, *10*, 7673.
- (62) Bouzan, S.; Dawe, L. N.; Zhao, Y. *Tetrahedron Lett.* **2013**, *54*, 4666.
- (63) Woolridge, K.; Goncalves, L. C.; Bouzan, S.; Chen, G.; Zhao, Y. *Tetrahedron Lett.* **2014**, *55*, 6362.
- (64) Massue, J.; Ghilane, J.; Bellec, N.; Lorcy, D.; Hapiot, P. *Electrochem. Commun.* **2007**, *9*, 677.
- (65) Younes, E. A.; Williams, K.-L. M.; Walsh, J. C.; Schneider, C. M.; Bodwell, G. J.; Zhao, Y. *RSC Adv.* **2015**, *5*, 23952.
- (66) González, S.; Martín, N.; Sánchez, L.; Segura, J. L.; Seoane, C.; Fonseca, I.; Cano, F. H.; Sedó, J.; Vidal-Gancedo, J.; Rovira, C. *J. Org. Chem.* **1999**, *64*, 3498.
- (67) Miyaura, N.; Suzuki, A. *Chem. Rev.* **1995**, *95*, 2457.
- (68) Christensen, C. A.; Batsanov, A. S.; Bryce, M. R. *J. Org. Chem.* **2007**, *72*, 1301.
- (69) Gosser, D. K. *Cyclic voltammetry: simulation and analysis of reaction mechanisms*; Wiley-VCH New York, 1993.
- (70) Saito, R.; Dresselhaus, G.; Dresselhaus, M. S. *Physical Properties of Carbon Nanotubes*; Imperial College Press: London, 1998. Meyyappan, M. *Carbon Nanotubes*:

- Science and Applications*; CRC Press: Boca Raton, 2005. Guldi, D. M.; Martín, N. *Carbon Nanotubes and Related Structures: Synthesis, Characterization, Functionalization, and Applications*; Wiley-VCH: Weinheim, 2010.
- (71) Kürti, J.; Kresse, G.; Kuzmany, H. *Phys. Rev. B* **1998**, *58*, R8869.
- (72) Maultzsch, J.; Telg, H.; Reich, S.; Thomsen, C. *Phys. Rev. B* **2005**, *72*, 205438.
- (73) Jorio, A.; Saito, R.; Hafner, J. H.; Lieber, C. M.; Hunter, M.; McClure, T.; Dresselhaus, G.; Dresselhaus, M. S. *Phys. Rev. Lett.* **2001**, *86*, 1118.
- (74) Mulla, K.; Zhao, Y. *J. Mater. Chem. C* **2013**, *1*, 5116.
- (75) Wang, D.; Chen, L. *Nano Lett.* **2007**, *7*, 1480.
- (76) Zhang, Z.; Che, Y.; Smaldone, R. A.; Xu, M.; Bunes, B. R.; Moore, J. S.; Zang, L. *J. Am. Chem. Soc.* **2010**, *132*, 14113.
- (77) Pochorovski, I.; Wang, H.; Feldblyum, J. I.; Zhang, X.; Antaris, A. L.; Bao, Z. *J. Am. Chem. Soc.* **2015**, *137*, 4328.
- (78) Long, Y.; Chen, H.; Yang, Y.; Wang, H.; Yang, Y.; Li, N.; Li, K.; Pei, J.; Liu, F. *Macromolecules* **2009**, *42*, 6501.

## Chapter 3

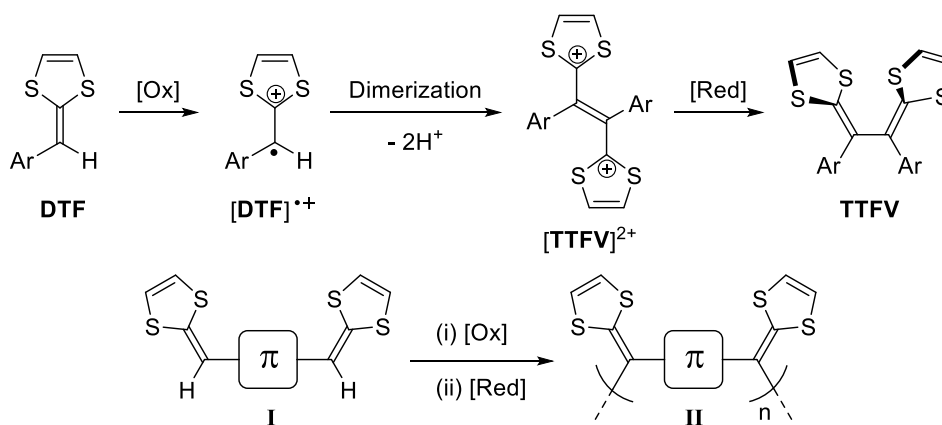
# A Macrocyclization of 1,8-Bis(dithiafulvenyl)pyrenes

The current chapter is the presentation and elaboration of my second published paper in *Organic Letters (Org. Lett.)* with the same above title. The preparation and characterization of compounds **70**, **71** and **73** was done by Joshua C. Walsh. I acknowledge his dedication and Prof. Graham J. Bodwell for his time and collaboration in this project. The current work is the best example of collaboration between Prof. Zhao and Prof. Bodwell from Memorial University. I also acknowledge Prof. Michael Katz for his assistance in the X-ray crystallographic analysis.

### 3.1 Introduction

Pyrene has been widely used as a functional molecular building block for various  $\pi$ -conjugated nanomaterials and devices.<sup>1-4</sup> Linear and cyclic oligomers and polymers<sup>5-14</sup> can be readily synthesized by coupling disubstituted pyrenes with suitable divalent  $\pi$ -counterparts, whereby the substitution pattern of pyrene unit plays an important role in determining the structures and properties of the resulting macromolecular systems. In our recent studies, the 1,8-pyrenylene motif was successfully exploited in constructing conjugated polymers<sup>6</sup> and shape-persistent macrocycles<sup>11</sup> through transition metal-catalyzed cross-coupling reactions.

Other types of direct C-C bond-forming methods could also be useful in the preparation of functional pyrene-based materials and therefore warrant exploration. One such reaction is the oxidative coupling of dithiafulvenyl (DTF) units to afford tetrathiafulvalene vinylologues (TTFVs) (Scheme 3.1).<sup>15,16</sup> This reaction has been investigated actively in recent years as a synthetic tool for generating a broad range of redox-active and conformationally switchable  $\pi$ -systems and devices.<sup>17-19</sup>



**Scheme 3.1** General Mechanism for Oxidative DTF Coupling and Polymerization of Bis(DTF)-endcapped Arenes

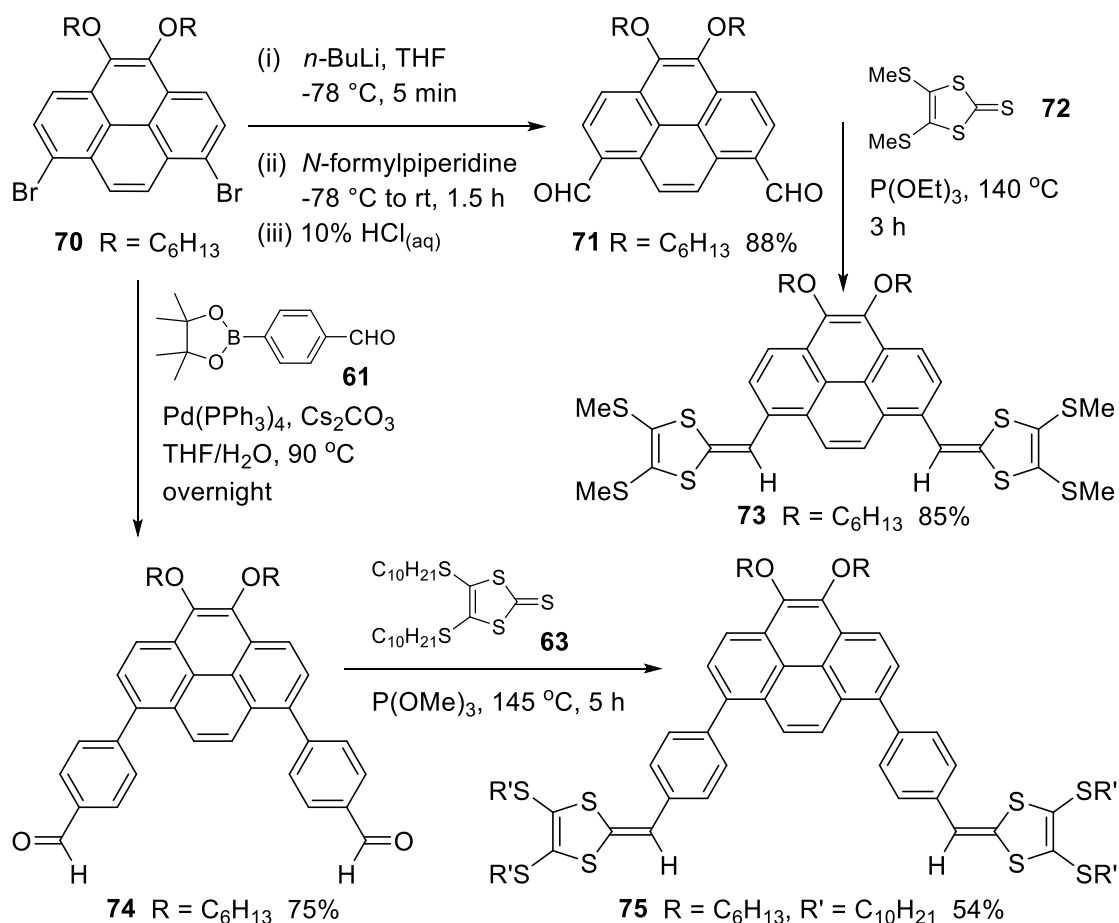
In general, DTF-  $\pi$  -DTF systems **I** would be expected to yield extended oligo-polymers **II** when subjected to oxidative coupling (Scheme 3.1). Although the possibility exists that cyclized products could also be generated, this is typically not the case.<sup>20,21</sup> Indeed, there is no precedent for direct macrocyclization from a DTF-  $\pi$  -DTF system **I** and only one clear example of macrocyclization through DTF oxidative coupling of oligomeric systems **II**, which afforded a mixture of cyclic products in low yields that

were difficult to purify.<sup>20</sup> Consequently, we became interested in the development of effective approaches to TTFV-containing macrocycles and we report herein the first successful macrocyclization *via* oxidative DTF coupling.

## 3.2 Result and Discussion

### 3.2.1 Synthesis and Characterization of Precursors

Pyrene derivatives with DTF units attached to the 1 and 8 positions were identified as suitable macrocyclization precursors due to their wedge-like molecular shapes (*ortho*-phenylene-like geometry) and potential for strong intermolecular aggregation. Initial work was centered on 1,8-bis(DTF)pyrene **73** (Scheme 3.2), which was synthesized from dibromide **70** in two steps *via* a lithiation–formylation reaction (88%) and then a phosphite-promoted olefination reaction (85%).<sup>17,21-23</sup> With the angular orientation (120° turn) of the two DTF groups and the rigid pyrenylene core, one can easily envision that oligomers arising from oxidative coupling of **73** could favor a folded conformation<sup>6</sup> as the chain length grows. When the folded oligomer chain arrives at a full turn (trimer:  $3 \times 120^\circ = 360^\circ$ ), cyclization might become favored.



**Scheme 3.2** Synthesis of Bis(DTF)pyrenes **73** and **75**

Unfortunately, bis(DTF)pyrene **73** was found to be persistently unreactive toward oxidative coupling using a variety of oxidants (I<sub>2</sub>, DDQ, CAN, AgNO<sub>3</sub>, Ag<sub>2</sub>O, CuSO<sub>4</sub>, FeCl<sub>3</sub>, HgCl<sub>2</sub>, and MoCl<sub>5</sub>) in CH<sub>2</sub>Cl<sub>2</sub>. Grinding neat **73** with excess iodine chips using a mortar and pestle for *ca.* 1 h was also tried, but this only ended up with nearly quantitative recovery of unreacted **73** after a reductive workup with aq. Na<sub>2</sub>S<sub>2</sub>O<sub>3</sub>. Alternatively, slow diffusion of iodine vapor into a CH<sub>2</sub>Cl<sub>2</sub> solution of **73** was performed, resulting in the formation of dark-colored crystalline needles, which may be

charge-transfer salt(s).<sup>24,25</sup> X-ray single crystallographic analysis of one of the crystals failed to give meaningful results. Some orange crystals were found to co-exist among the dark crystals and a single crystal X-ray structure determination showed them to be neutral **73** (Figure 3.1A). In the crystal structure of **73**, the two DTF groups form torsion angles of *ca.* 42° relative to the central pyrene unit. Such an orientation is in line with those observed in the single crystal structures of phenyl-substituted DTFs.<sup>26</sup> The moderate deviation from planarity in the DTF-pyrene-DTF skeleton suggests that  $\pi$ -delocalization is retained to a certain extent.

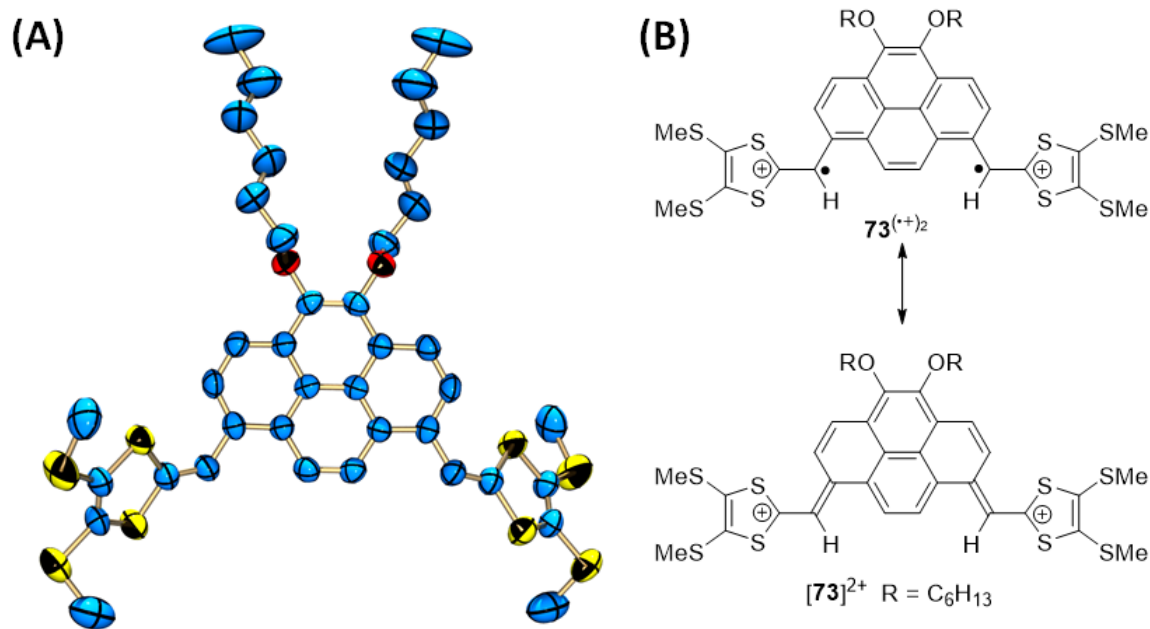


**Fig. 3.1** (A) ORTEP plot of compound **73** at 50% ellipsoid probability (CCDC#1450007). (B) Resonance structures for the singlet dication of **73**

The unsuccessful oxidative coupling of **73** can be understood by consideration of its cyclic voltammetric (CV) data. The oxidation of **73** proceeds through two prominent

anodic peaks at +0.57 V and +0.72 V (Figure 3.2A), which are assigned to sequential single-electron transfers in the two DTF groups. These oxidation potentials are considerably lower than those of typical arene-DTF derivatives (*ca.* +0.9 V to +1.1 V),<sup>16-21,26</sup> which can be attributed to an increasing degree of  $\pi$ -electron delocalization between the pyrene system in **73** and the two DTF units as they are oxidized. This is supported by UV-Vis absorption analysis (Figure 3.27) and density functional theory (DFT) calculations (see section 3.4) which show that the DTF/pyrene torsion angles in **73** decrease from 35.4° (neutral) to 18.6° (radical cation) and 4.3° (singlet dication) upon oxidation (Figures 3.19-3.21). The triplet dication of **73** (Figure 3.22) was calculated to be 33.55 kJ/mol higher in energy than the singlet form, which the calculations showed to be best represented by dication **73**<sup>2+</sup> resonance structure (unreactive toward oxidative coupling) rather than bis(radical cation) **73**<sup>(•+)</sup>2 (Figure 3.1B). Even the radical cation **73**<sup>•+</sup> was calculated to show very little spin density on the benzylic carbons (Figure 3.20), which is also consistent with the low reactivity toward oxidative coupling at this stage. This was corroborated experimentally by the multicycle CV scanning, where the CV profile of **73** remained nearly unchanged.

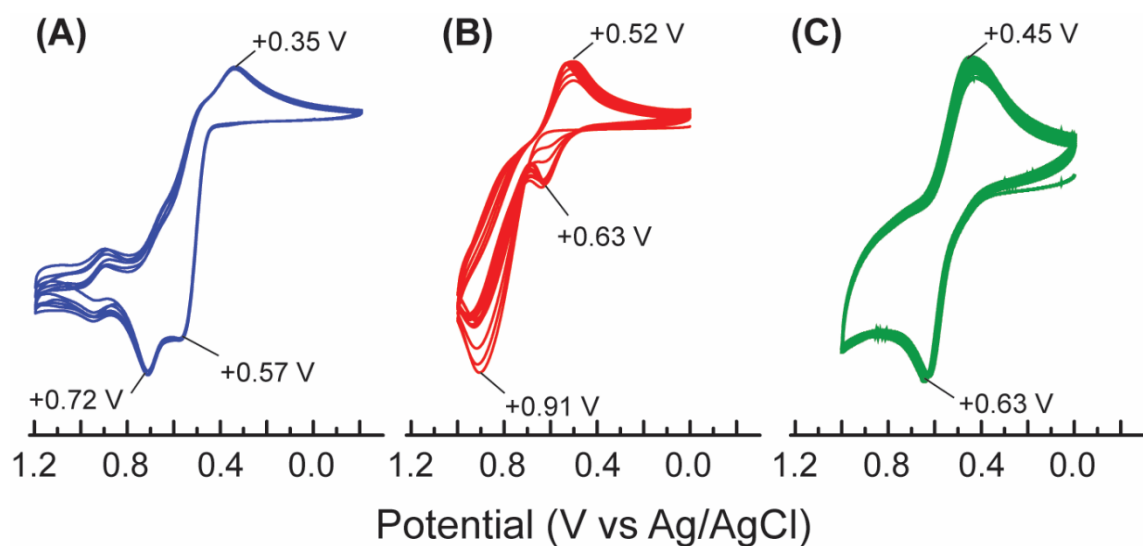


**Fig. 3.2** Cyclic voltammograms of (A) bis(DTF)pyrene **73**, (B) bis(DTF)pyrene **75**, and (C) macrocycle **77**. Solvent: CH<sub>2</sub>Cl<sub>2</sub>, electrolyte: Bu<sub>4</sub>NBF<sub>4</sub> (0.1 M), working electrode: glassy carbon, reference electrode: Ag/AgCl (3 M NaCl) counter electrode: Pt, scan rate: 0.3 V/s.

To circumvent the problems encountered with **73**, a modified bis(DTF)pyrene precursor **75** was designed (Scheme 3.2). Compound **75** differs from **73** in that a 1,4-phenylene unit has been inserted between each of the two DTF groups and the central pyrene core. This was intended to revive the DTF reactivity by reducing the electronic communication between the DTF units and the pyrene system.<sup>21</sup> The synthesis of **75** began with a twofold Suzuki-Miyaura coupling between 1,8-dibromopyrene **70** and boronate **61**, which yielded dialdehyde **74** (75%). Compound **74** was then converted into bis(DTF)pyrene **75** *via* the phosphite-mediated olefination reaction.<sup>17,21-23</sup> CV analysis of **75** confirmed that the DTF groups were indeed re-activated. The first cycle of anodic scan showed only one oxidation peak at +0.91 V, due to simultaneous electron

transfers at the two DTF groups (Figure 3.2B).<sup>15-21,26</sup> As of the second cycle of CV scans, a new oxidation peak emerged, which offers clear evidence for the DTF groups undergoing the oxidative coupling on the surface of the working electrode.<sup>15,16</sup>

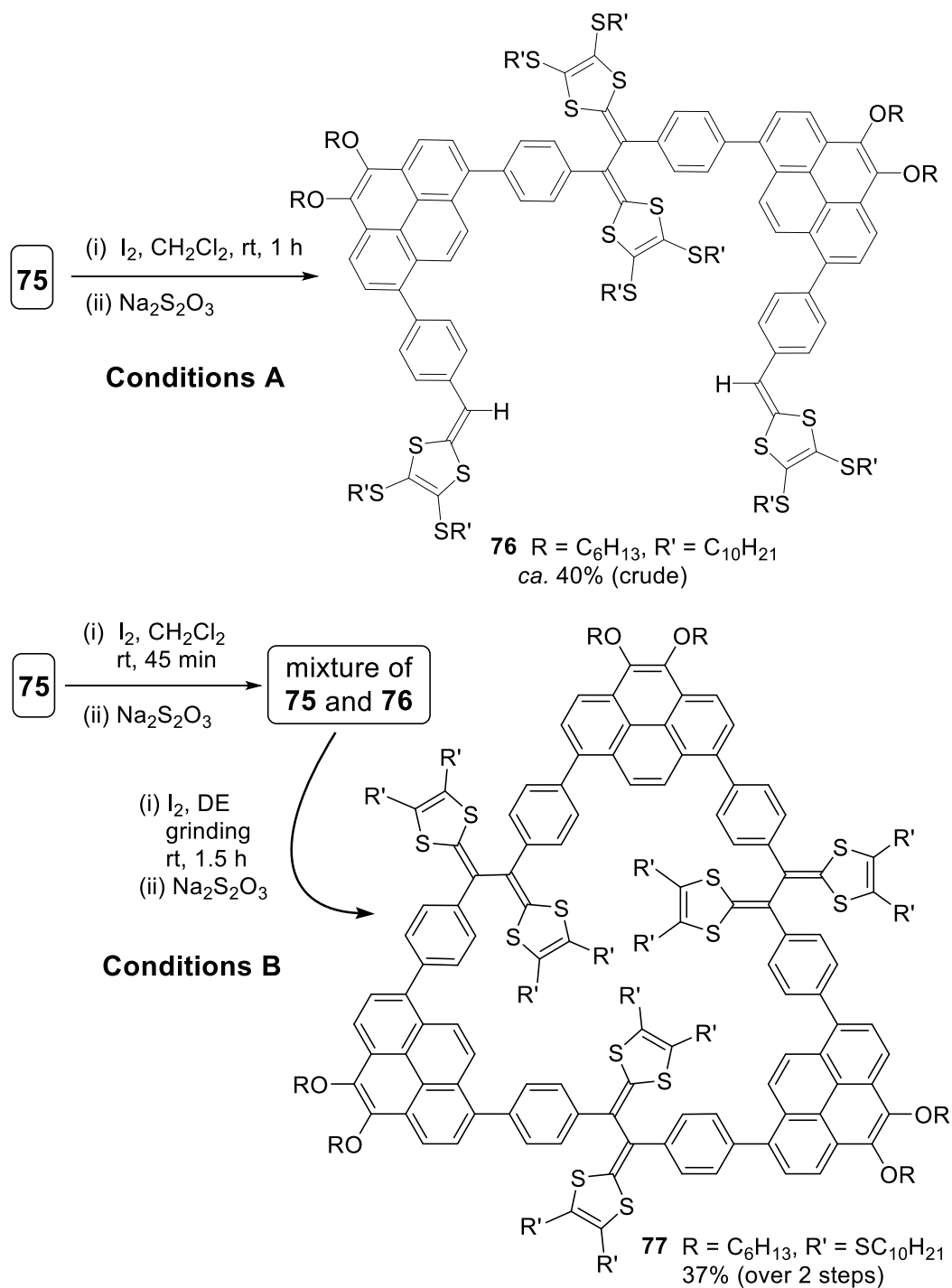
### 3.2.2 Synthesis of the Macrocycle: Obstacles and Solutions

Iodine-induced oxidative coupling of bis(DTF)pyrene **75** was then performed in a CH<sub>2</sub>Cl<sub>2</sub> solution (Conditions A, Scheme 3.3),<sup>27-29</sup> but the reaction was sluggish. After 1 h, the reaction mixture was found to consist of roughly equal amounts of dimerized product **76** and unreacted starting material **75** along with a small amount of a trimeric product (indicated by TLC, NMR, and especially MALDI-TOF MS analyses). When the reaction time was prolonged, higher oligomeric products were detected by MS analysis. Based on these results, it was concluded that solution phase conditions were unsuitable for macrocyclization.

Alternatively, solid-state conditions were investigated. Direct grinding of **75** with excess iodine using a mortar and pestle for 1 h led to the formation of a mixture of dimer **76**, a trimeric product, and unreacted **75** in similar amounts (TLC and MALDI-TOF MS analyses). Attempts to isolate the trimeric product in pure form by silica gel column chromatography were unsuccessful, so its structure (whether linear or cyclic) could not be determined. Nevertheless, the solid-state conditions seemed to induce more effective DTF coupling than solution conditions.

The addition of grinding aids such as diatomaceous earth (DE) or silica gel was investigated as a means to increase the ease and efficiency of grinding. After numerous

trials, a satisfactory two-step method for the synthesis of trimeric macrocycle **77** was established (Scheme 3.3). This method involves initial reaction of compound bis(DTF)pyrene **75** with iodine in CH<sub>2</sub>Cl<sub>2</sub> for 45 min. Work-up of this reaction yielded a solid mixture of roughly equal amounts of **75** and **76** (TLC analysis). Subjection of this mixture to grinding with iodine in the presence of DE for 1.5 h then furnished macrocycle **77** in 37% yield after preparative tlc. It appears that pre-mixing monomer **75** and dimer **76** in the solid state is key to the success of the macrocyclization. Semiempirical modeling suggested that **75** and **76** can form a 1:1 aggregate through complementary  $\pi$ -stacking (Figure 3.3), whereby they are preorganized to favor a [1+1] macrocyclization.



**Scheme 3.3** Oxidative Coupling Reactions of Bis(DTF)pyrene **75** under Different Conditions

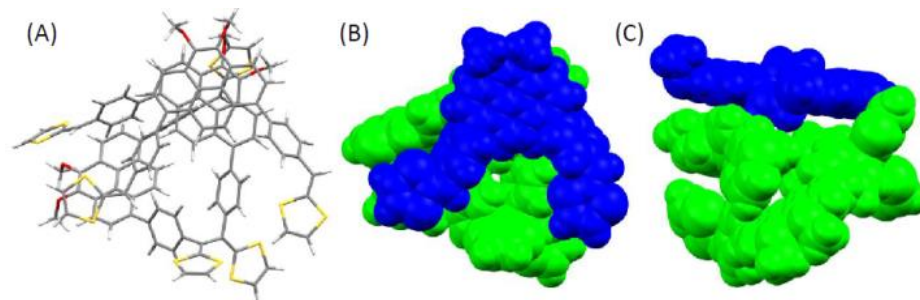


**Fig. 3.3** Molecular structure of a 1:1 aggregate of **75** and **76** optimized at the semiempirical RM1 level (Spartan'10). (A) Top view of the capped-stick model. Space-filling models showing (B) top and (C) side view. Color scheme: blue = **75**, green = **76**.  $\text{SC}_{10}\text{H}_{21}$  groups were replaced with hydrogen atoms and  $\text{OC}_6\text{H}_{13}$  groups with  $\text{OCH}_3$  groups to save computational expense.

Compound **77** was characterized by NMR, IR, and MALDI-TOF MS analyses. The former and latter of which clearly supported its cyclic trimeric nature (see section 3.3). The electrochemical redox properties of **77** were examined by CV analysis (Figure 3.2C) and oxidative UV-Vis titration (Figure 3.24). A quasi-reversible redox wave pair ( $E_{\text{pa}} = +0.63$  V,  $E_{\text{pc}} = +0.45$  V) characteristic of typical TTFV redox behavior<sup>15-21</sup> was observed in the CV of **77**. The absence of a DTF oxidation peak (*cf.* voltammograms of **73** and **75**) corroborated the macrocyclic structure of **77**. Molecular mechanics (*MM*) simulations indicated that macrocycle **77** can adopt a range of twisted, non-symmetrical conformations. The simplicity of the aromatic region of the  $^1\text{H}$  NMR spectrum of **77** (Figure 4A) points to rapid interconversion of conformers at room temperature, which

averages to a threefold-symmetric structure. Pulsed gradient spin-echo (PGSE) NMR analysis of **77** gave an average diffusion coefficient ( $D$ ) of  $3.07 \times 10^{-10} \text{ m}^2 \text{ s}^{-1}$  (based on the aromatic proton signals), which corresponds to a hydrodynamic diameter of 2.76 nm. This value is in good agreement with the calculated dimensions of the  $\pi$ -conjugated framework of **77** excluding the flexible alkyl chains (Figure 3.4B).

### 3.2.3 Binding Studies of the Macrocycle

The modeling results also suggest that macrocycle **77** has an inner cavity large enough to host  $\text{C}_{60}$  fullerene; however, no significant binding was observed experimentally. It may be that the 18 alkyl chains on the periphery of **77** block the entry of the relatively large guest molecule to the central cavity. Upon moving to nitrobenzene, a much smaller guest molecule than  $\text{C}_{60}$ , macrocycle **77** was found to form a 1:1 complex. The binding constant ( $K_{\text{assoc}}$ ) determined from a UV-Vis titration experiment is  $3644.6 \pm 0.4 \text{ M}^{-1}$  (Figure 3.23). The major driving force for the binding can be ascribed to  $\pi$ -stacking between pyrene and nitrobenzene.<sup>9</sup>

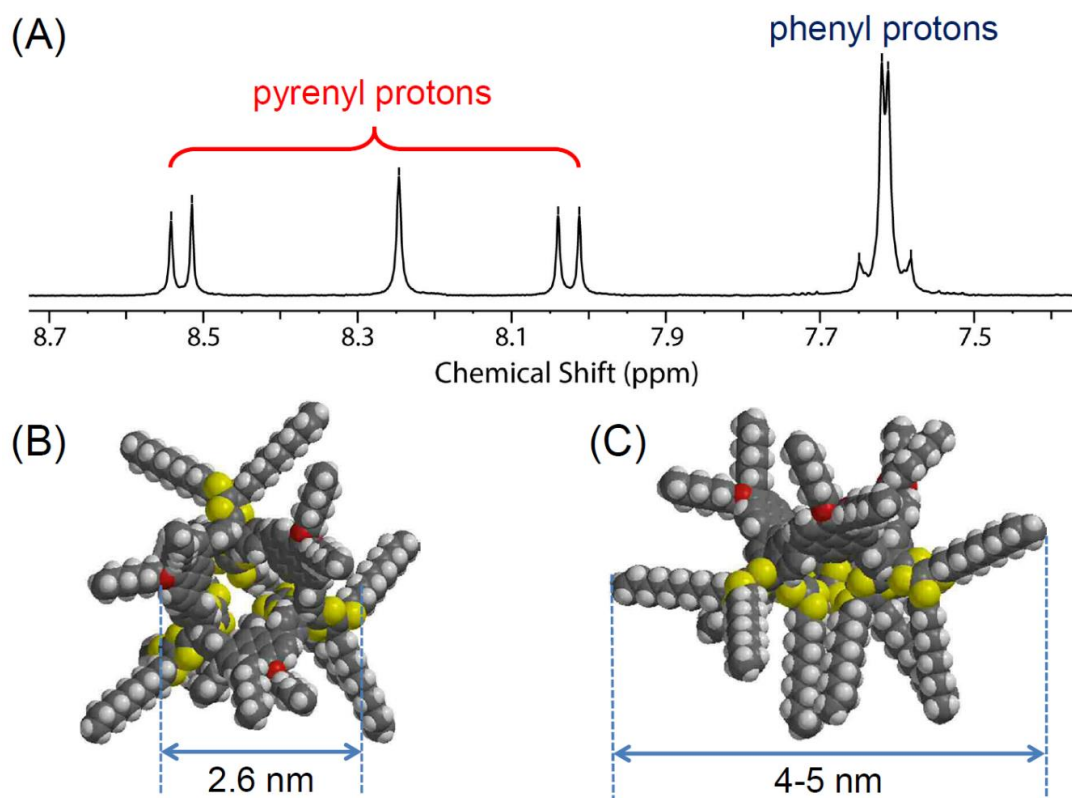


**Fig. 3.4** (A) Aromatic region of the <sup>1</sup>H NMR (500 MHz, CDCl<sub>3</sub>) spectrum of **77**. (B) Top and (C) side views of the optimized geometry of **77** using the *MMFF* force field.

### 3.2.4 Conclusions

In summary, we have developed a relatively effective two-stage synthetic method for the synthesis of a novel redox-active pyrene-TTFV macrocycle **77**, which involves sequential oxidative DTF coupling reactions in solution and the solid state. The success of this unique macrocyclization strategy can be explained by two key factors: (1) the solution-phase oxidative coupling of bis(DTF)pyrene **75** is sluggish and yields only a mixture of dimer and unreacted monomer; (2) modeling suggests that the monomer and dimer favor complementary  $\pi$ -stacking in the solid state. The TTFV-pyrene macrocycle

**77** and its bis(DTF)pyrene precursor **76** contribute useful building blocks for the preparation of redox-active supramolecular systems and functional molecular devices.

### 3.3. Experimental

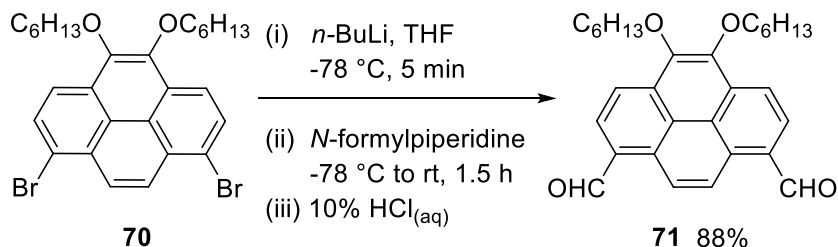
#### 3.3.1 General

Chemicals were purchased from commercial suppliers and used directly without purification. All reactions were conducted in standard, dry glassware and under an inert atmosphere of nitrogen or argon unless otherwise noted. Evaporation and concentration were carried out with a rotary evaporator. Flash column chromatography was performed with 240-400 mesh silica gel, and thin-layer chromatography (TLC) was carried out with silica gel F254 covered on plastic sheets and visualized by UV light. Melting points (m.p.) were measured using an SRS OptiMelt melting point apparatus and are uncorrected.  $^1\text{H}$  and  $^{13}\text{C}$  NMR spectra were measured on a Bruker Avance 500 MHz spectrometer and a Bruker Avance III 300 MHz multinuclear spectrometer. Chemical shifts ( $\delta$ ) are reported in ppm downfield relative to the signals of the internal reference  $\text{SiMe}_4$  or residual solvents ( $\text{CHCl}_3$ :  $\delta_{\text{H}} = 7.24$  ppm,  $\delta_{\text{C}} = 77.2$  ppm;  $\text{CH}_2\text{Cl}_2$ :  $\delta_{\text{H}} = 5.32$  ppm,  $\delta_{\text{C}} = 54.0$  ppm). Coupling constants ( $J$ ) are given in Hz. Infrared spectra (IR) were recorded on a Bruker Alfa spectrometer. MALDI-TOF MS analysis was performed on an Applied Biosystems Voyager instrument using dithranol as the matrix. HREI-TOF MS analysis was done on a GCT premier Micromass Technologies instrument.

1,3-Dithiole-2-thiones **72** and **63**,<sup>30,31</sup> and 4-(4,4,5,5-tetramethyl-1,3,2-dioxaborolan-2-yl)benzaldehyde **61**<sup>32</sup> were prepared according to the literature procedures.

### 3.3.2 Synthesis

#### 4,5-Dihexoxyppyrene-1,8-dicarbaldehyde (**71**)

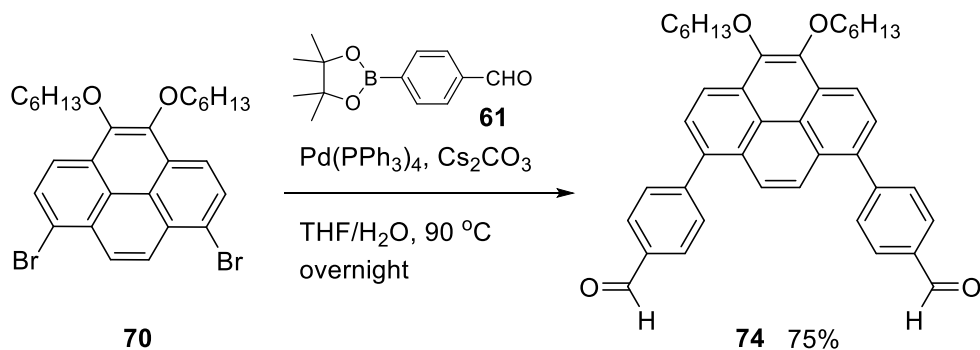


To a  $-78\text{ }^{\circ}\text{C}$  (cooled by a dry ice/acetone bath) nitrogen-purged solution of 1,8-dibromo-4,5-dihexoxyppyrene (**70**) (0.444 g, 0.792 mmol) in anhydrous THF (150 mL), *n*-BuLi (1.30 M, 4.87 mL, 6.33 mmol) was added dropwise. The reaction was allowed to stir at  $-78\text{ }^{\circ}\text{C}$  for 5 min. *N*-formylpiperidine (1.44 g, 12.7 mmol) was added and the dry ice/acetone bath was removed. The reaction mixture was allowed to warm to rt and stirred for a further 1.5 h. The reaction was quenched with 10% HCl<sub>(aq)</sub> (25 mL) and the organic solvents were removed under reduced pressure. The reaction mixture was extracted with CH<sub>2</sub>Cl<sub>2</sub> (2 × 50 mL). The combined organic layers were washed with 10% HCl<sub>(aq)</sub> (2 × 200 mL) and subsequently dried over anhydrous Na<sub>2</sub>SO<sub>4</sub>. The solvent was removed under reduced pressure to yield crude **71** as a dark orange oil. The crude product was subjected to silica gel column chromatography (CH<sub>2</sub>Cl<sub>2</sub>/hexanes, 3:1) to yield compound **71** as a canary yellow solid (0.320 g, 0.697 mmol, 88%). <sup>1</sup>H NMR (CDCl<sub>3</sub>, 300 MHz):  $\delta$  10.82 (s, 2H), 9.56 (s, 2H), 8.72 (d,  $J = 8.2$  Hz, 2H), 8.54 (d,  $J = 8.2$  Hz, 2H), 4.38 (t,  $J = 6.7$  Hz, 4H) 2.05-1.94 (m, 4H), 1.68-1.55 (m, 4H), 1.46-1.35 (m, 8H),



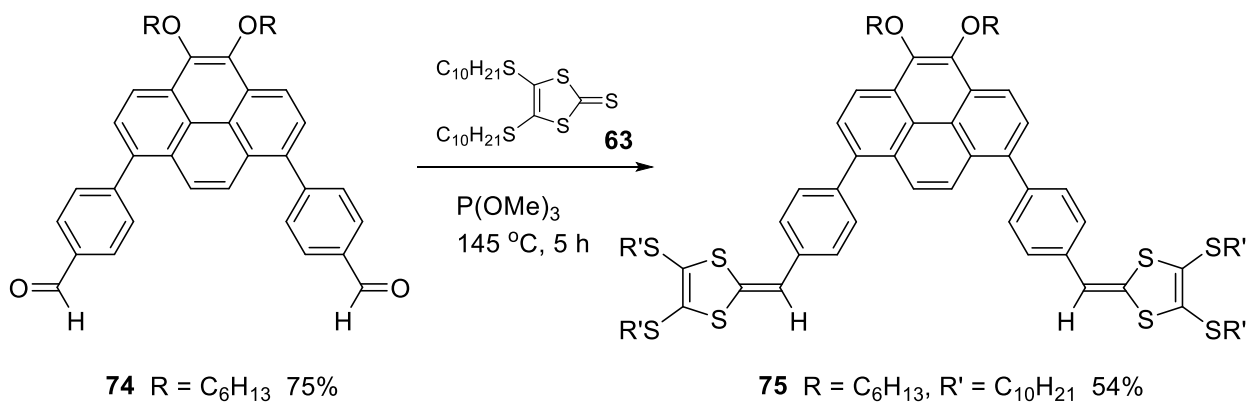
112.8, 74.0, 31.9, 30.7, 26.1, 22.8, 19.14, 19.09, 14.2; HRMS (APCI, positive mode)  $m/z$  calcd for  $C_{40}H_{46}O_2S_8$  814.1263, found 814.1244  $[M]^+$ .

### Compound 74



To a 100 mL round-bottomed flask were added 1,8-dibromo-4,5-dihexoxybenzene (**70**) (1.06 g, 1.88 mmol), boronic ester **61** (1.10 g, 4.74 mmol), cesium carbonate (4.28 g, 13.1 mmol),  $Pd(PPh_3)_4$  (0.22 g, 0.19 mmol), THF (20 mL), and deionized water (10 mL). The mixture was heated at reflux overnight. The mixture was cooled to rt, poured into brine, and then extracted twice with  $CH_2Cl_2$ . The organic layers were combined and dried over  $MgSO_4$ . After filtration and concentration under reduced pressure, the resulting residue was subjected to silica gel column chromatography (hexanes/EtOAc, 3:2) to give compound **74** (0.86 g, 0.52 mmol, 75%) as a pale yellow oil.  $R_f$  (40%  $CH_2Cl_2$ /hexanes) = 0.50; IR (neat):  $\tilde{\nu}$  2953, 2929, 2857, 1701, 1601, 1458, 1209, 1097, 1078, 829  $cm^{-1}$ ;  $^1H$  NMR (300 MHz,  $CDCl_3$ ):  $\delta$  10.14 (s, 2H), 8.62 (d,  $J = 8.1$  Hz, 2H), 8.08-8.01 (m, 8H), 7.79 (d,  $J = 8.1$  Hz, 4H), 4.42-4.38 (m, 4H), 2.06-0.93 (m, 22H);  $^{13}C$  NMR (75 MHz,  $CD_2Cl_2$ ):  $\delta$  192.0, 147.5, 144.1, 135.5, 135.2, 131.3, 129.8, 129.2, 128.1, 127.7, 125.2, 123.2, 119.7, 74.0, 31.7, 31.6, 30.5, 26.0, 22.7, 22.6, 14.14, 14.11; HRMS (EI-TOF, positive mode)  $m/z$  calcd for  $C_{42}H_{43}O_4$  611.3161, found 611.3168  $[M+H]^+$ .

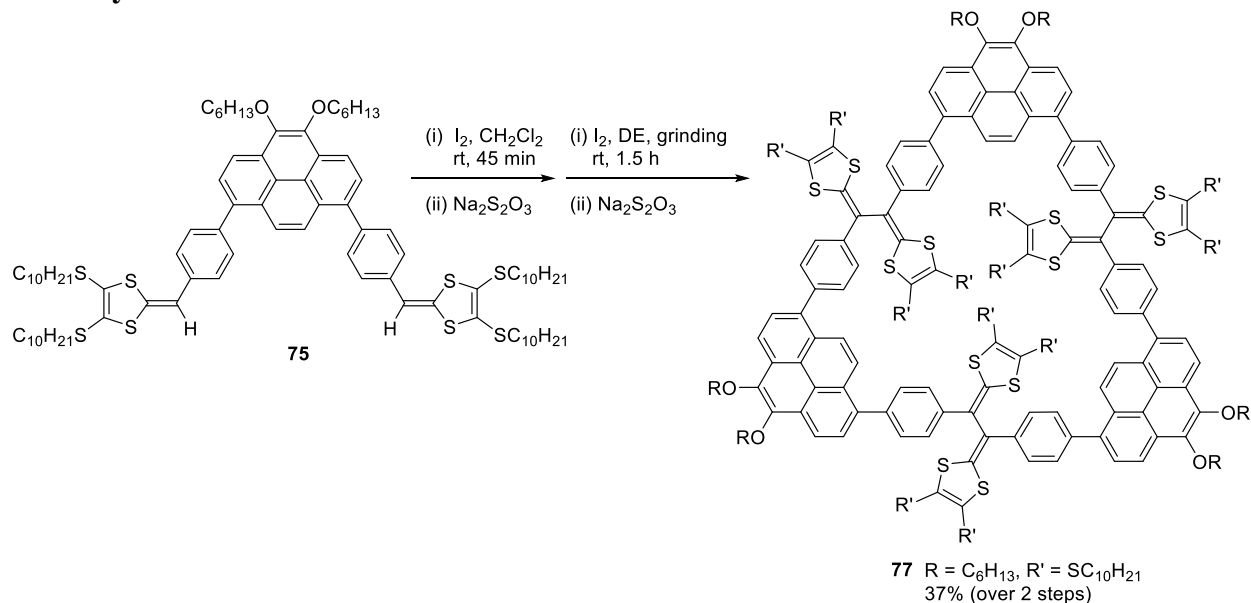
## Compound 75



Dialdehyde **74** (0.13 g, 0.21 mmol), 4,5-bis(decylthio)-1,3-dithiole-2-thione (**63**) (0.30 g, 0.63 mmol), and P(OMe)<sub>3</sub> (15 mL) were added to a 100 mL round-bottomed flask. The mixture was heated to 145 °C and kept at this temperature for 5 h. After cooling the unreacted P(OMe)<sub>3</sub> was then removed by vacuum distillation, and the residue was subjected to silica gel column chromatography (hexanes/CH<sub>2</sub>Cl<sub>2</sub>, 9:1) to give pure compound **75** (0.17 g, 0.83 mmol, 54%) as a yellow oil. *R<sub>f</sub>* (20% CH<sub>2</sub>Cl<sub>2</sub>/hexanes) = 0.34; IR (neat):  $\tilde{\nu}$  2953, 2922, 2852, 1571, 1458, 1302, 1097, 1080, 833 cm<sup>-1</sup>; <sup>1</sup>H NMR (300 MHz, CDCl<sub>3</sub>):  $\delta$  8.55 (d, *J* = 8.1 Hz, 2H), 8.16 (s, 2H), 8.01 (d, *J* = 8.1 Hz, 2H), 7.63 (d, *J* = 8.2 Hz, 4H), 7.39 (d, *J* = 8.3 Hz, 4H), 6.57 (s, 2H), 4.40-4.36 (m, 4H), 2.87-2.82 (m, 8H), 2.06-0.83 (m, 98H); <sup>13</sup>C NMR (75 MHz, CD<sub>2</sub>Cl<sub>2</sub>):  $\delta$  143.9, 138.5, 136.4, 135.3, 132.7, 130.8, 128.5, 128.3, 127.7, 127.6, 126.7, 125.3, 124.8, 123.5, 119.2, 113.9, 73.9, 36.2, 36.1, 31.94, 31.92, 31.8, 30.6, 29.8, 29.7, 29.59, 29.57, 29.36, 29.34, 29.1, 28.6,

28.5, 26.0, 22.73, 22.70, 14.15, 14.13; HRMS (EI-TOF, positive mode)  $m/z$  calcd for  $C_{88}H_{127}O_2S_8$  1471.7602, found 1471.7564  $[M + H]^+$ .

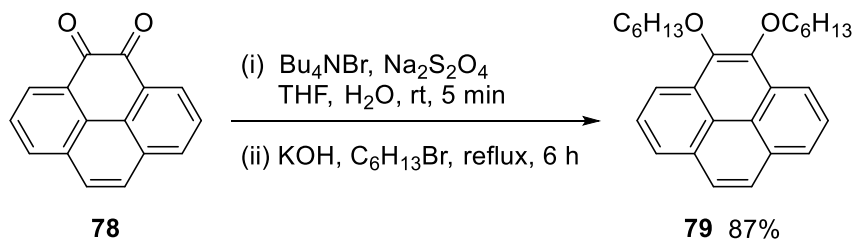
### Macrocycle **77**



Compound **75** (0.18 g, 0.12 mmol), I<sub>2</sub> (0.090 g, 0.37 mmol), CH<sub>2</sub>Cl<sub>2</sub> (5 mL) were added to a 25 mL round-bottomed flask. The mixture was stirred at rt for 45 min and quenched with aq. Na<sub>2</sub>S<sub>2</sub>O<sub>3</sub>. The organic layer was collected and evaporated to dryness under reduced pressure. The residue was transferred to a marble mortar using a small amount of CH<sub>2</sub>Cl<sub>2</sub>, which was evaporated under air. The residual solid was mixed with iodine chips (0.090 g) and diatomaceous earth (2.00 g), and the solid mixture was continually ground using a pestle for 1.5 h at rt. The mixture was then extracted with CH<sub>2</sub>Cl<sub>2</sub> (10 mL), and to the resulting mixture was added satd aq. Na<sub>2</sub>S<sub>2</sub>O<sub>3</sub> (10 mL). The mixture was stirred for 3 h at rt and the organic layer was separated and concentrated under reduced pressure. The residue was subjected to preparative thin-layer

chromatography (hexanes/CH<sub>2</sub>Cl<sub>2</sub>, 4:1) to give macrocycle **77** (0.070 g, 0.016 mmol, 37%) as a yellow oil.  $R_f$  (20% CH<sub>2</sub>Cl<sub>2</sub>/hexanes) = 0.21; IR (neat):  $\tilde{\nu}$  2957, 2923, 2852, 1458, 1299, 1259, 1093, 1017, 906, 799, 731 cm<sup>-1</sup>; <sup>1</sup>H NMR (300 MHz, CDCl<sub>3</sub>):  $\delta$  8.53 (d,  $J$  = 8.2 Hz, 6H), 8.25 (s, 6H), 8.03 (d,  $J$  = 8.2 Hz, 6H), 7.65-7.58 (m, 24H), 4.39-4.34 (m, 12H), 2.76-2.71 (m, 12H), 2.60-2.55 (m, 12H), 2.05-0.79 (m, 294H); <sup>13</sup>C NMR (75 MHz, CDCl<sub>3</sub>):  $\delta$  143.9, 143.8, 139.2, 137.0, 136.3, 136.1, 130.9, 128.7, 128.4, 128.1, 127.7, 126.6, 125.2, 124.1, 123.5, 119.2, 73.8, 35.9, 31.8, 31.85, 31.81, 30.6, 29.6, 29.58, 29.55, 29.3, 29.1, 28.5, 28.4, 26.0, 22.7, 22.65, 22.64, 14.0; MALDI-TOF MS (positive mode)  $m/z$  calcd for C<sub>264</sub>H<sub>373</sub>O<sub>6</sub>S<sub>24</sub> 4409.2264, found 4409.2578 [M + H]<sup>+</sup>. Note that there were no other mobile compounds observed by tlc. Presumably, the material that remained on the baseline of tlc consisted of higher (likely linear) oligomeric products.

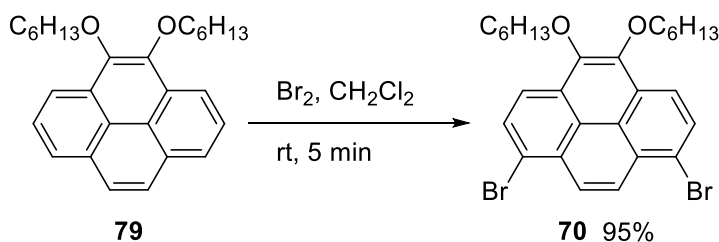
#### 4,5-Dihexoxyppyrene (79)



To a suspension of pyrene-4,5-dione (**78**)<sup>33</sup> (2.00 g, 8.64 mmol) in THF (100 mL) and H<sub>2</sub>O (100 mL) was added tetra-*n*-butylammonium bromide (0.835 g, 2.59 mmol) and Na<sub>2</sub>S<sub>2</sub>O<sub>4</sub> (4.51 g, 25.9 mmol). The reaction was stirred for 5 min at rt. KOH<sub>(aq)</sub> (3.88 g, 69.1 mmol in H<sub>2</sub>O (25 mL)) was added to the reaction mixture followed by 1-bromohexane (5.71 g, 34.6 mmol). The deep orange solution was heated at reflux for 6 h. The reaction was cooled and then extracted with EtOAc (100 mL). The layers were

separated and the aqueous phase was extracted with EtOAc (2 × 50 mL). The combined EtOAc extracts were washed with H<sub>2</sub>O (300 mL). The organic phase was dried over Na<sub>2</sub>SO<sub>4</sub> and the solvent removed under reduced pressure to yield a brown oil. The crude product was subjected to silica gel column chromatography (10% CH<sub>2</sub>Cl<sub>2</sub>/hexanes) to yield 4,5-dihexoxyppyrene (**79**) (3.02 g, 7.50 mmol, 87%) as a pale yellow solid. *R<sub>f</sub>* (10% CH<sub>2</sub>Cl<sub>2</sub>/hexanes) = 0.30; m.p. 40-45 °C; <sup>1</sup>H NMR (CDCl<sub>3</sub>, 300 MHz): δ 8.46 (dd, *J* = 6.2, 1.3 Hz, 2H), 8.15 (dd, *J* = 6.7, 1.3 Hz, 2H), 7.83 (s, 2H), 7.74 (t, *J* = 7.5 Hz, 2H); <sup>13</sup>C NMR (CDCl<sub>3</sub>, 75 MHz): δ 144.1, 131.1, 129.0, 127.3, 126.0, 124.3, 122.9, 119.5, 73.8, 31.8, 30.6, 26.0, 22.7, 14.1; MS (ESI, positive mode) *m/z* (%): 402 ([M]<sup>+</sup>, 100); HRMS (APCI, positive mode) calcd for C<sub>28</sub>H<sub>34</sub>O<sub>2</sub> 402.2559, found: 402.2541.

### 1,8-Dibromo-4,5-dihexoxyppyrene (**70**)



To a solution of 4,5-dihexoxyppyrene (**79**) (2.00 g, 5.00 mmol) in CH<sub>2</sub>Cl<sub>2</sub> (50 mL) was added bromine (1.75 g, 10.9 mmol, in CH<sub>2</sub>Cl<sub>2</sub> (10 mL)). The reaction was stirred for 5 min at rt. Excess bromine was quenched with saturated aq. Na<sub>2</sub>S<sub>2</sub>O<sub>3</sub> solution. The layers were separated and the aqueous phase was extracted with EtOAc (2 × 50 mL). The organic phase was dried over Na<sub>2</sub>SO<sub>4</sub> and the solvent was removed under reduced pressure to yield a brown solid. The crude product was subjected to silica gel column

chromatography (10% CH<sub>2</sub>Cl<sub>2</sub>/hexanes) to yield 1,8-dibromo-4,5-dihexoxypyrene (**70**) (2.65 g, 4.73 mmol, 95%) as a pale yellow solid. *R<sub>f</sub>* (10% CH<sub>2</sub>Cl<sub>2</sub>/hexanes) = 0.50; <sup>1</sup>H NMR (CDCl<sub>3</sub>, 300 MHz): δ 8.51 (s, 2H), 8.37 (d, *J* = 8.5, 2H), 8.27 (d, *J* = 8.5, 2H), 4.31 (t, *J* = 6.7 Hz, 2H) 1.95 (m, 4H), 1.60 (m, 4H), 1.40 (m, 8H), 0.93 (m, 6H); <sup>13</sup>C NMR (CDCl<sub>3</sub>, 75 MHz): δ 143.8, 130.7, 129.4, 128.7, 127.5, 123.5, 120.8, 119.9, 73.9, 31.8, 30.5, 25.9, 22.7, 14.1; MS (APCI, positive mode) *m/z* (%): 561 [M+H]<sup>+</sup>, 100. HRMS (APPI, positive mode) calcd for C<sub>28</sub>H<sub>32</sub><sup>79</sup>Br<sub>2</sub>O<sub>2</sub> 558.0769, found: 558.0753 [M<sup>+</sup>].

### 3.3.3 NMR Spectra for New Compounds

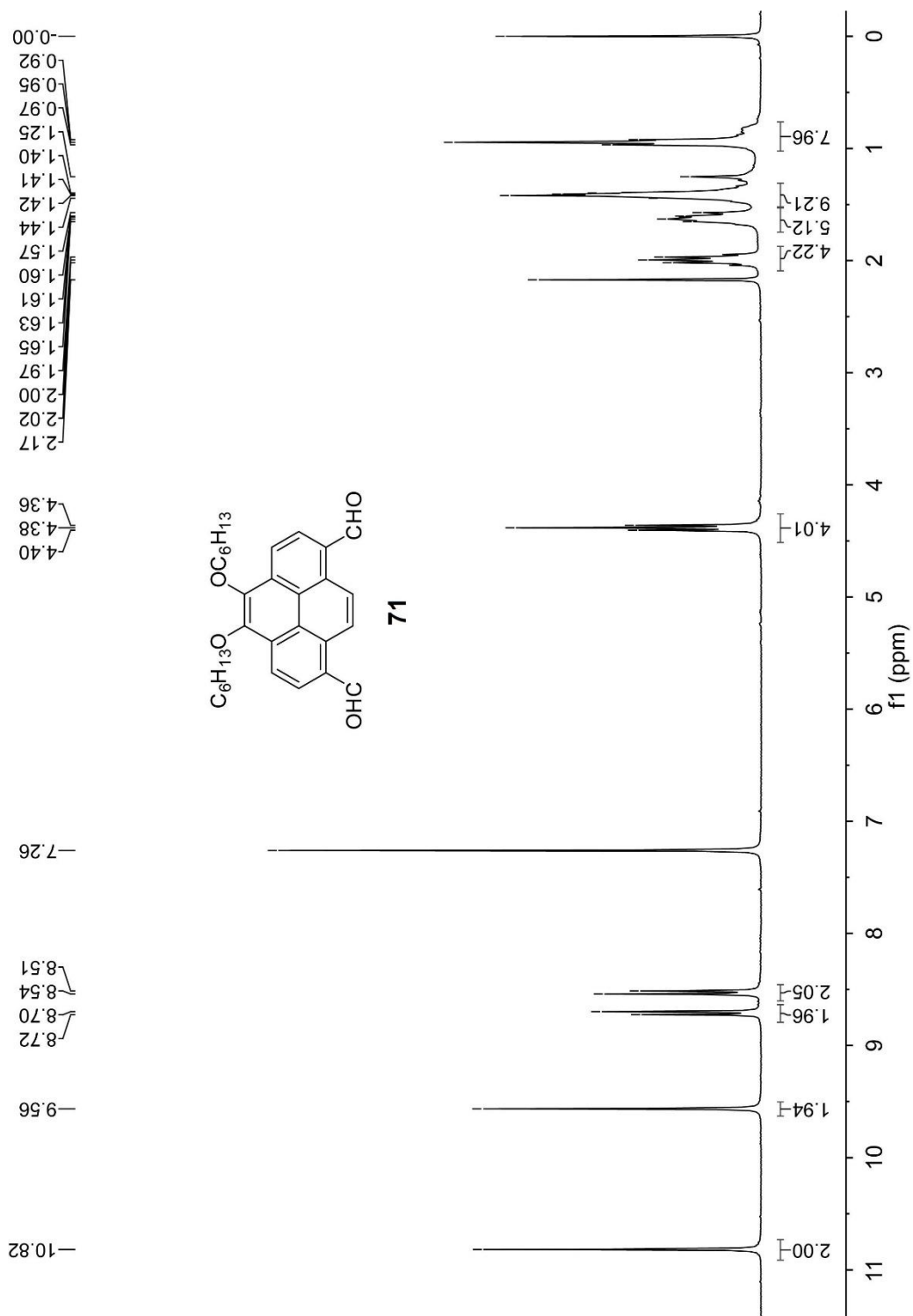


**Fig. 3.5** <sup>1</sup>H NMR (300 MHz, CDCl<sub>3</sub>) spectrum of compound **71**.

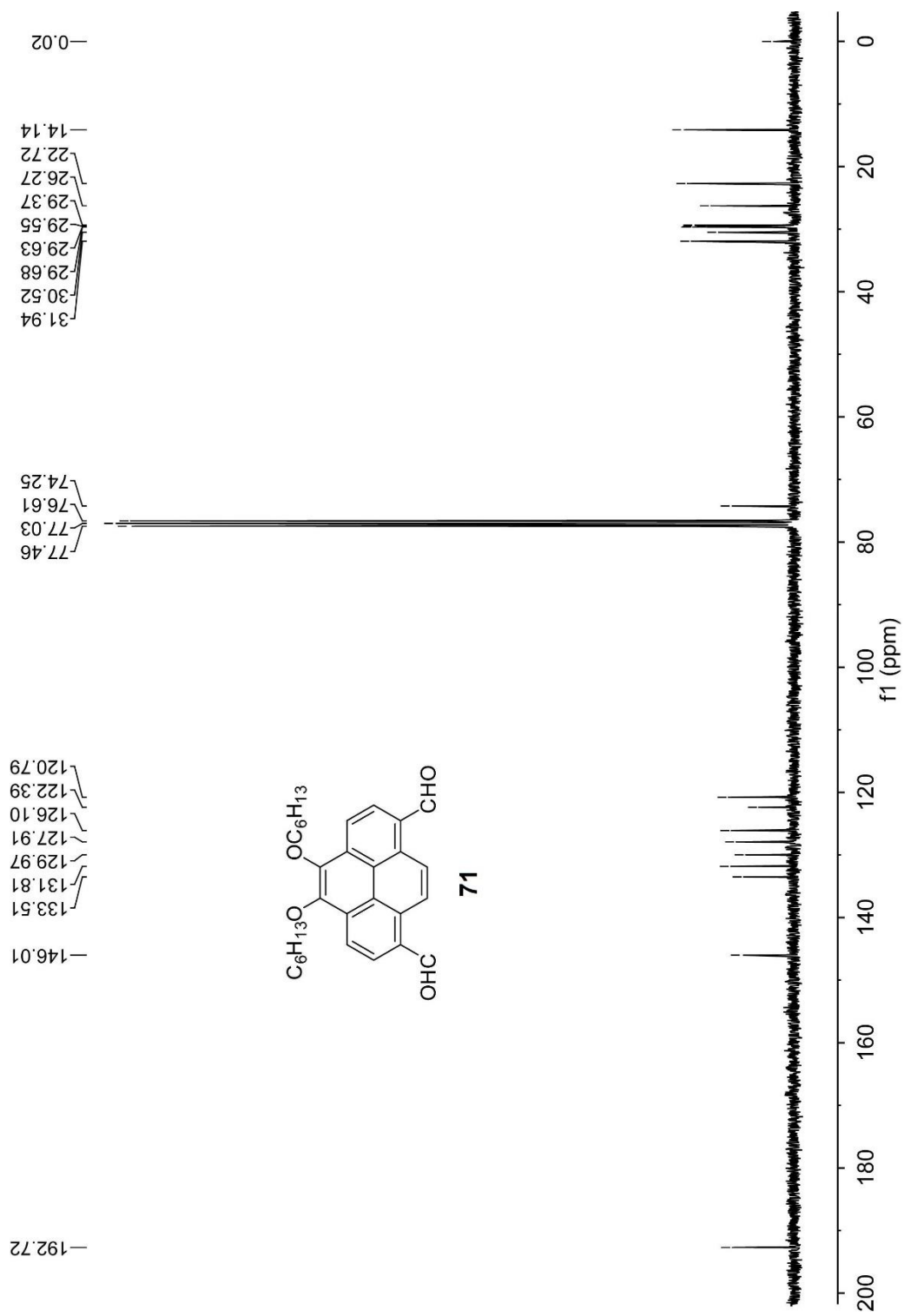


**Fig. 3.6** <sup>13</sup>C NMR (75 MHz, CDCl<sub>3</sub>) spectrum of compound 71.

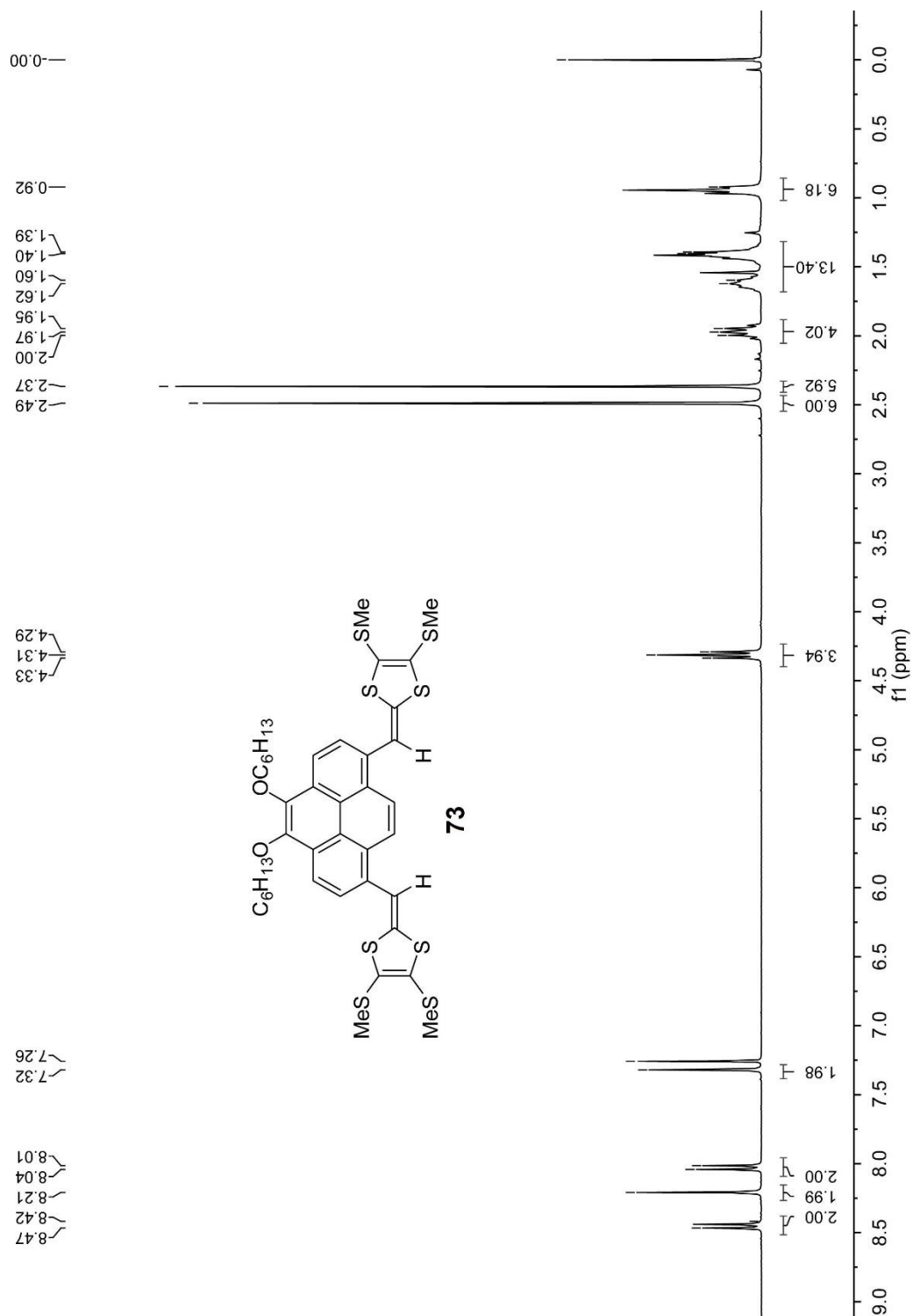


**Fig. 3.7** <sup>1</sup>H NMR (300 MHz, CDCl<sub>3</sub>) spectrum of compound **73**.

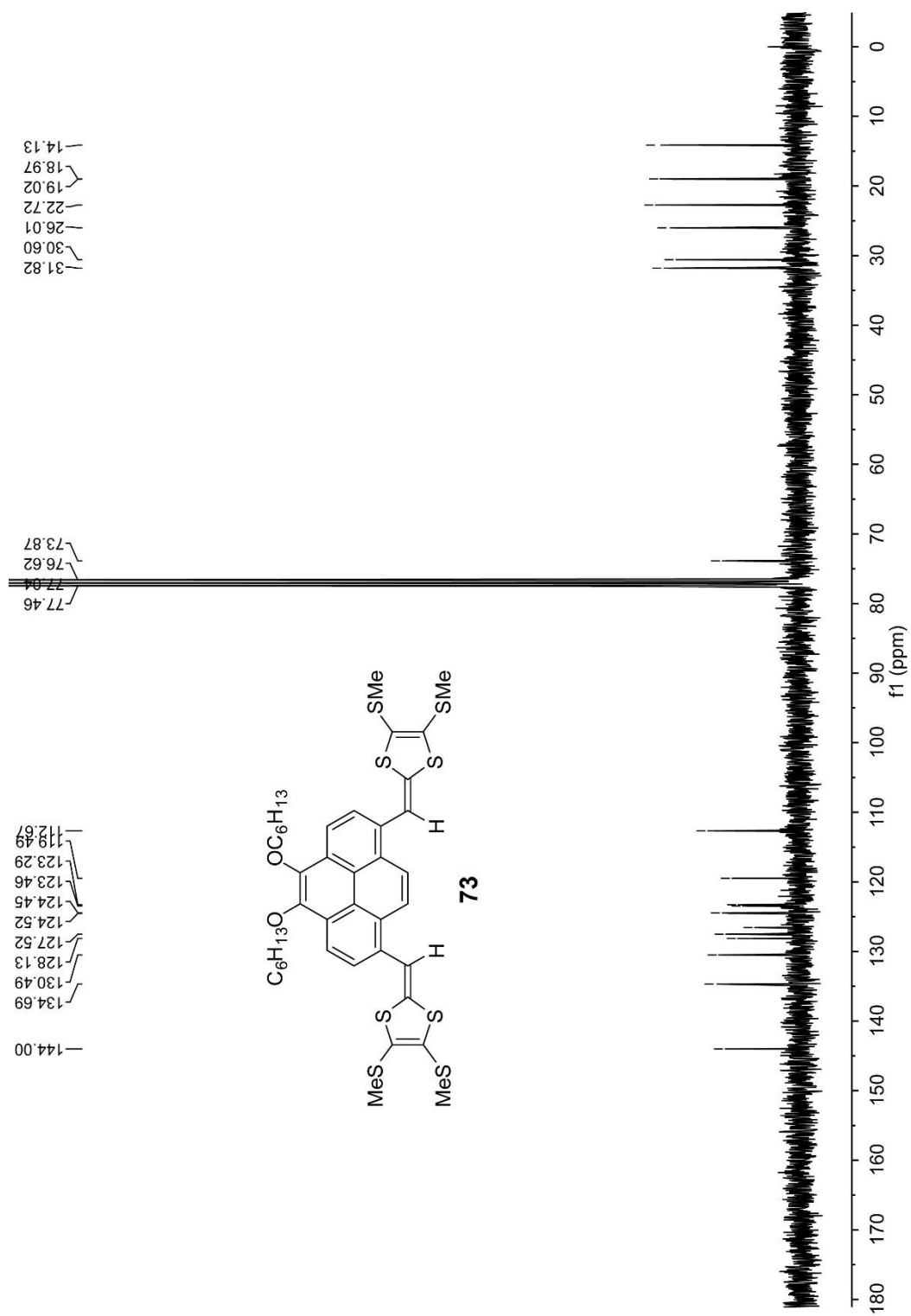


**Fig. 3.8**  $^{13}\text{C}$  NMR (75 MHz,  $\text{CDCl}_3$ ) spectrum of compound **73**.

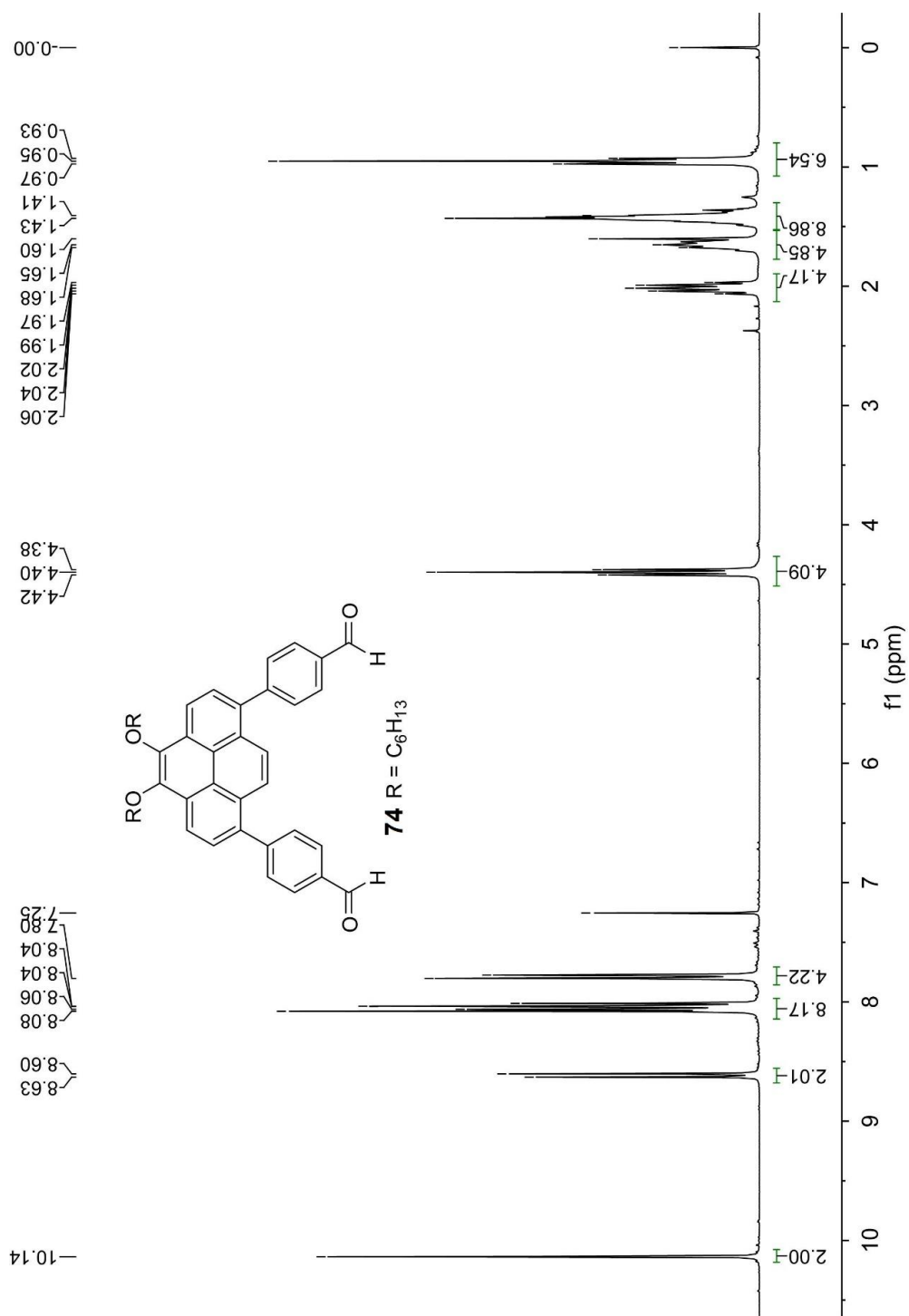


**Fig. 3.9**  $^1H$  NMR (300 MHz,  $CDCl_3$ ) spectrum of compound **74**.

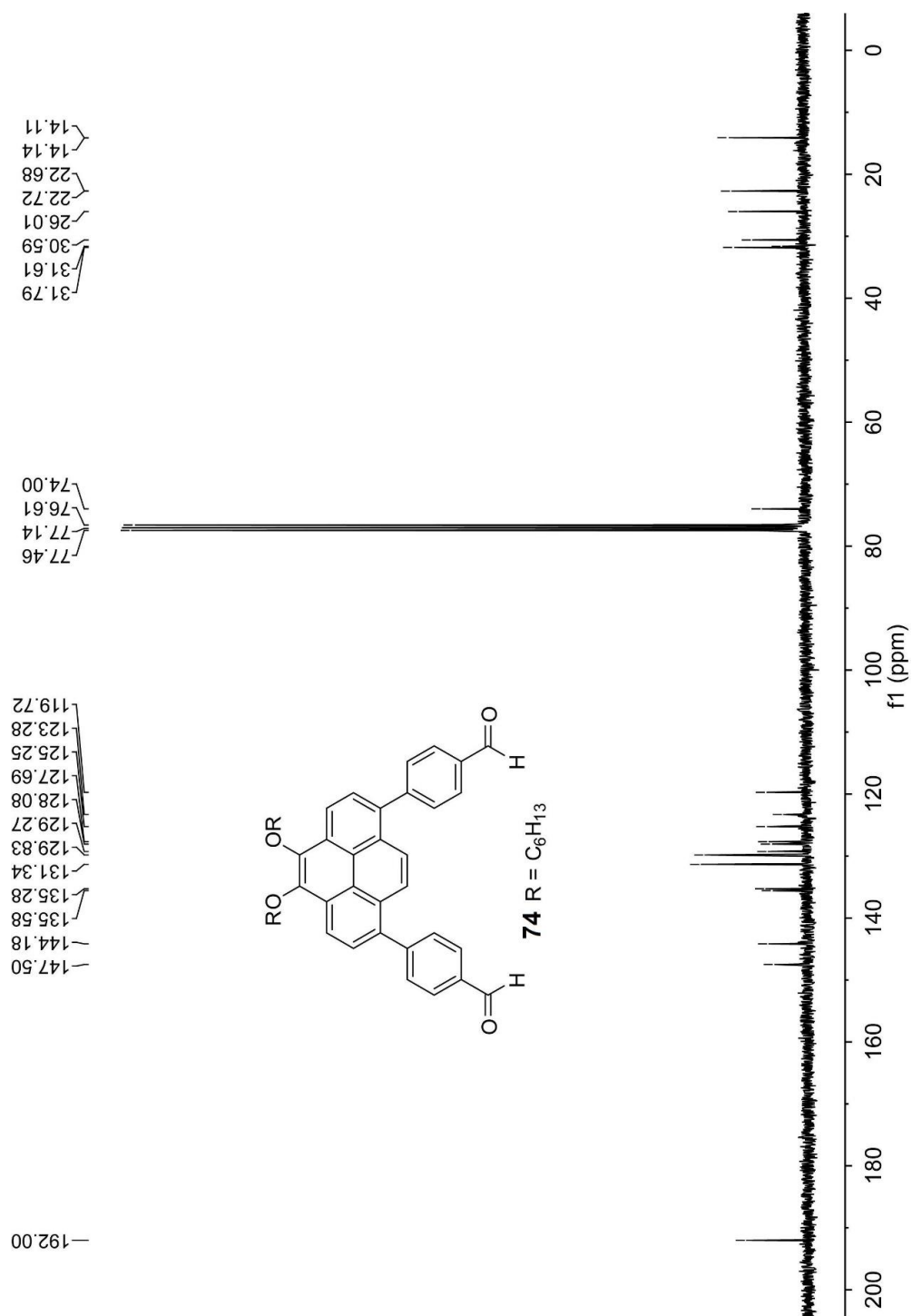


**Fig. 3.10**  $^{13}C$  NMR (75 MHz,  $CDCl_3$ ) spectrum of compound **74**.

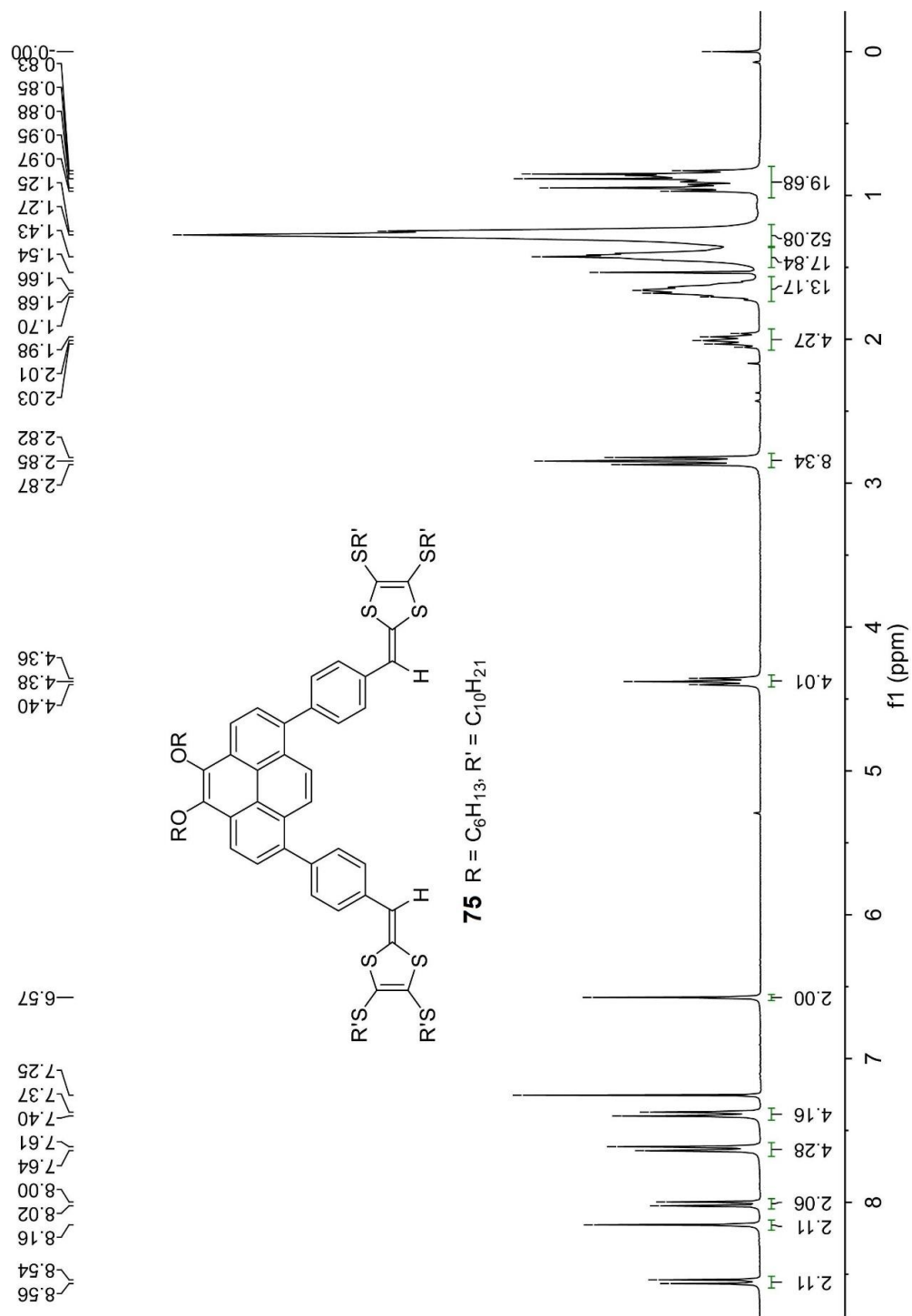


**Fig. 3.11**  $^1H$  NMR (300 MHz,  $CDCl_3$ ) spectrum of compound **75**.

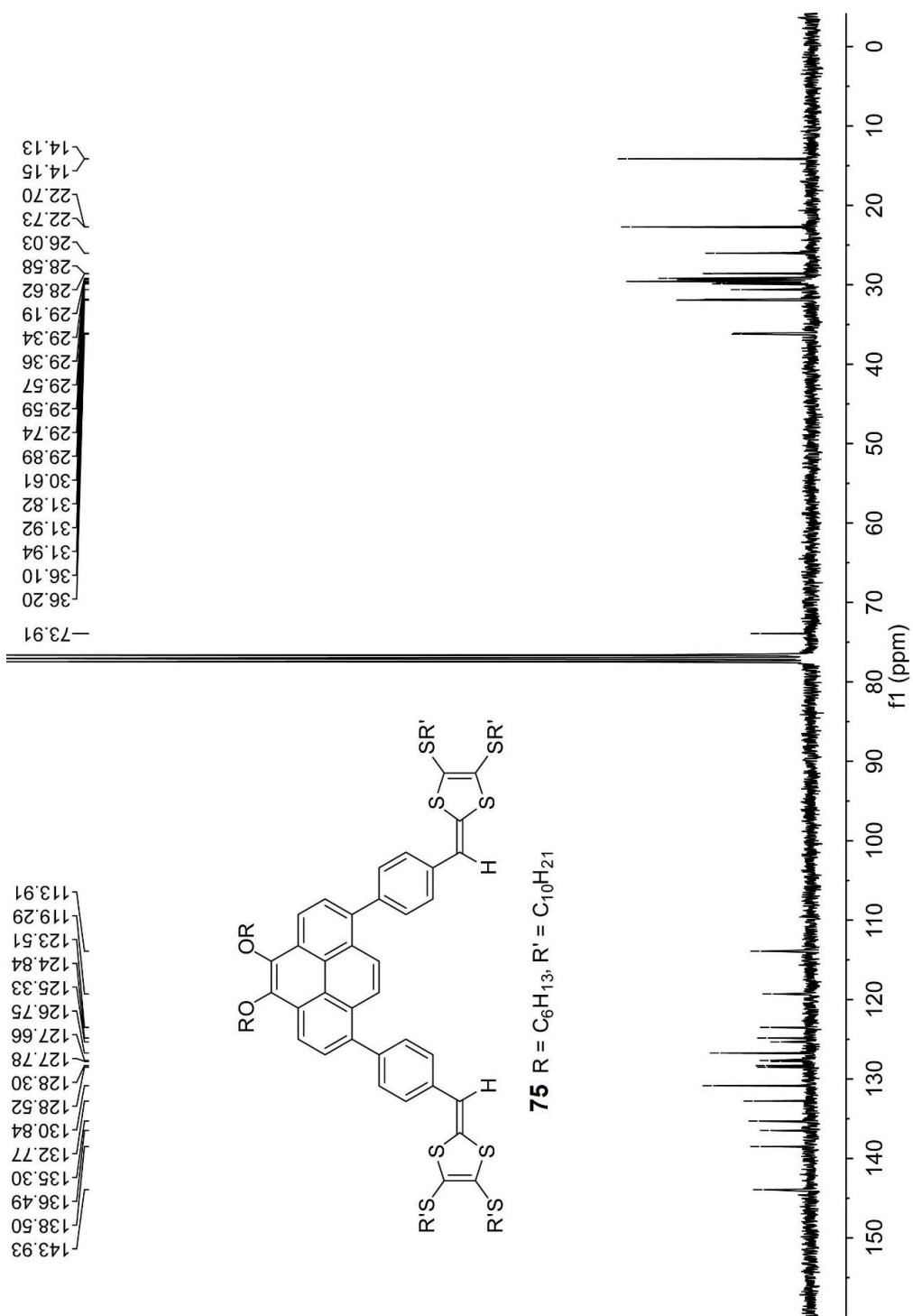


**Fig. 3.12** <sup>13</sup>C NMR (75 MHz, CDCl<sub>3</sub>) spectrum of compound **75**.

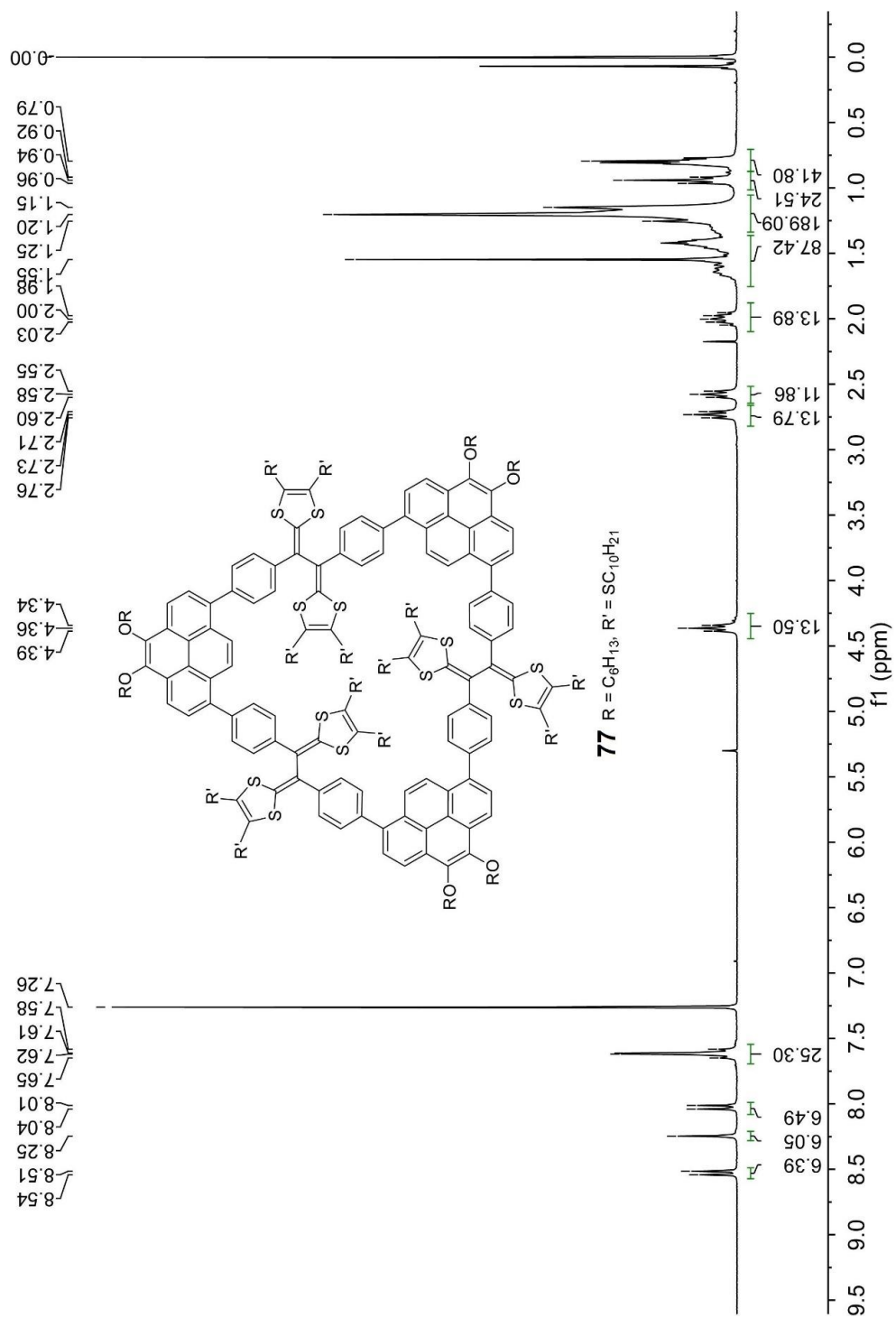


**Fig. 3.13** <sup>1</sup>H NMR (300 MHz, CDCl<sub>3</sub>) spectrum of compound **77**.

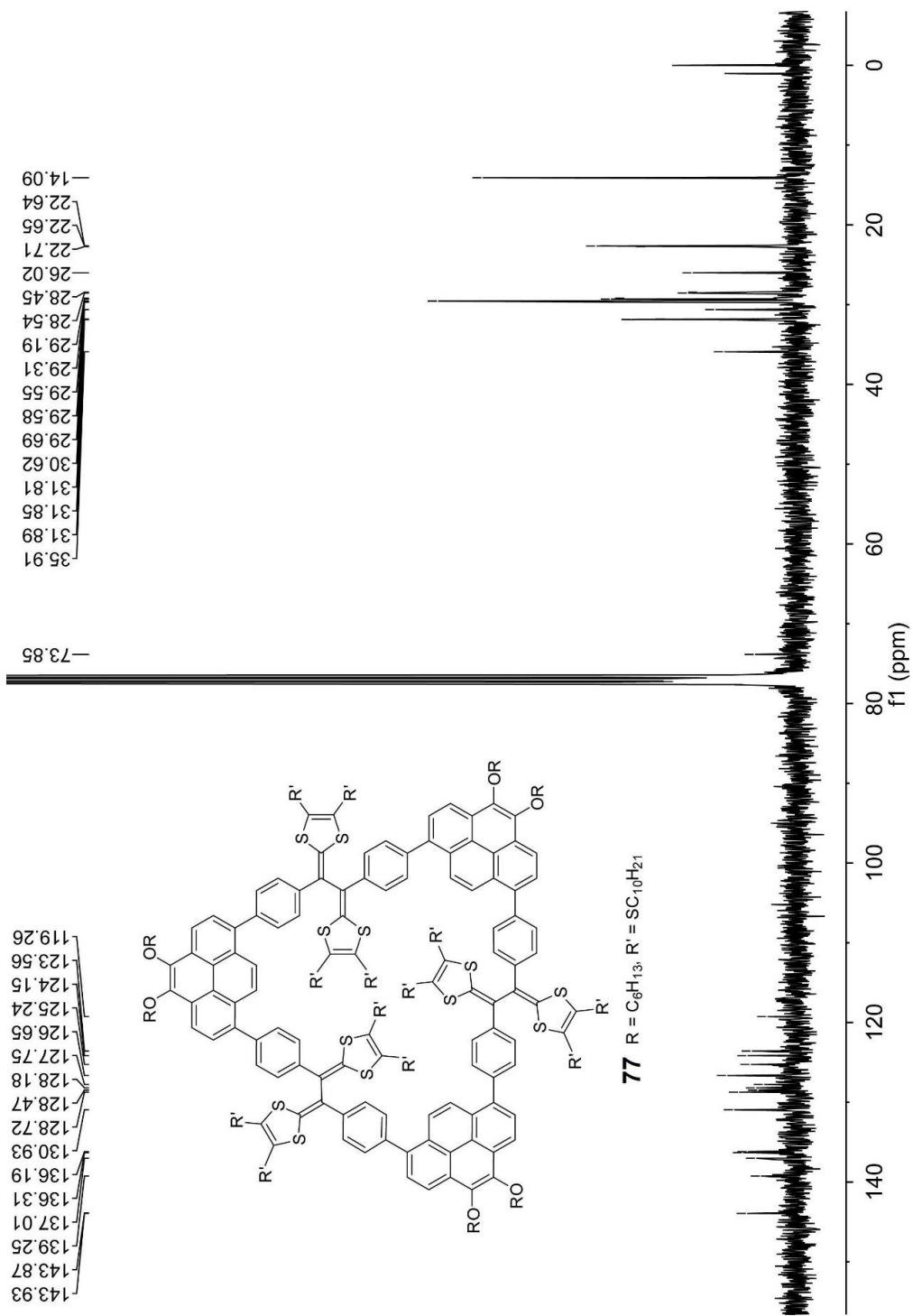


**Fig. 3.14** <sup>13</sup>C NMR (75 MHz, CDCl<sub>3</sub>) spectrum of compound **77**.

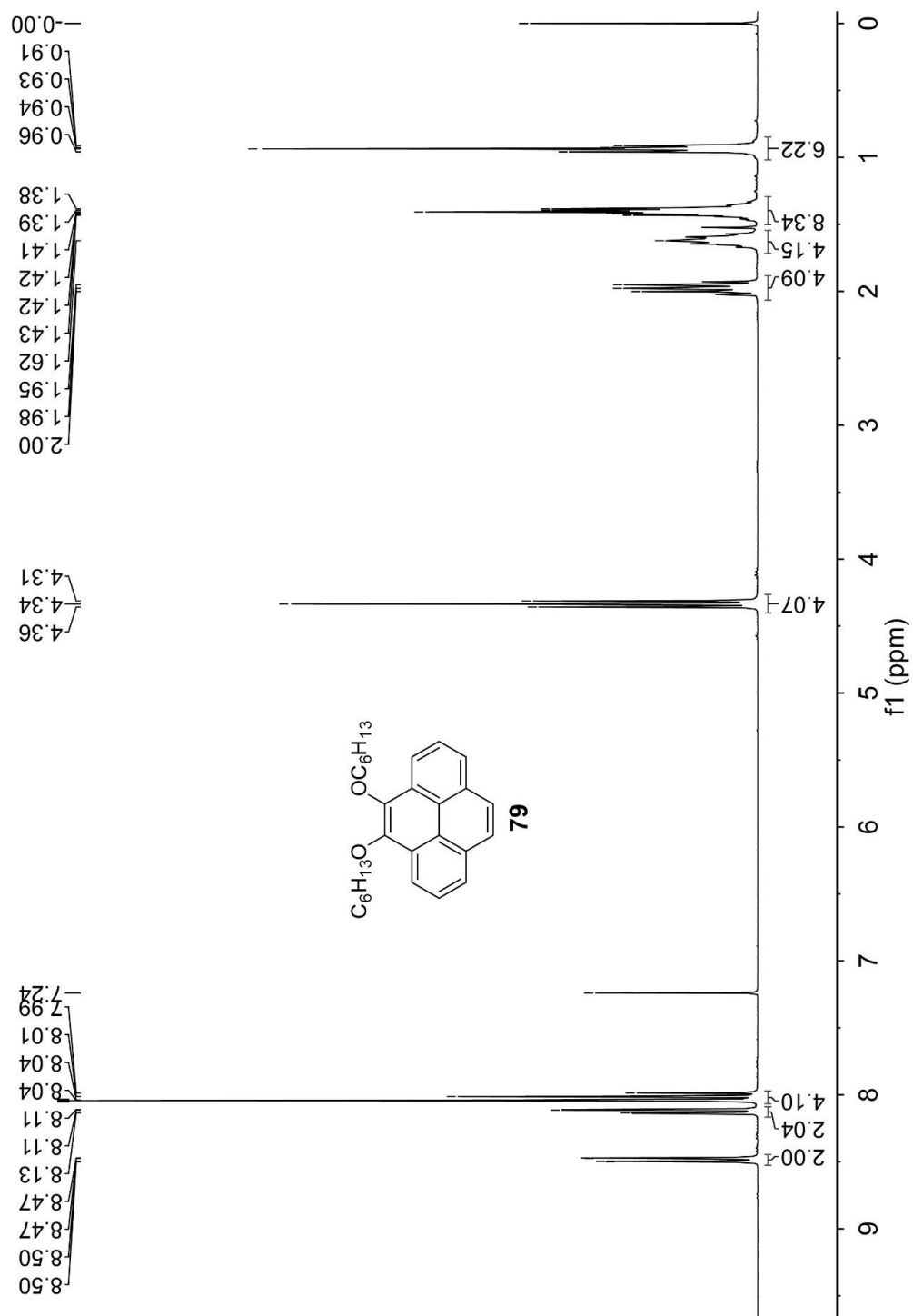


**Fig. 3.15**  $^1H$  NMR (300 MHz,  $CDCl_3$ ) spectrum of compound **79**.

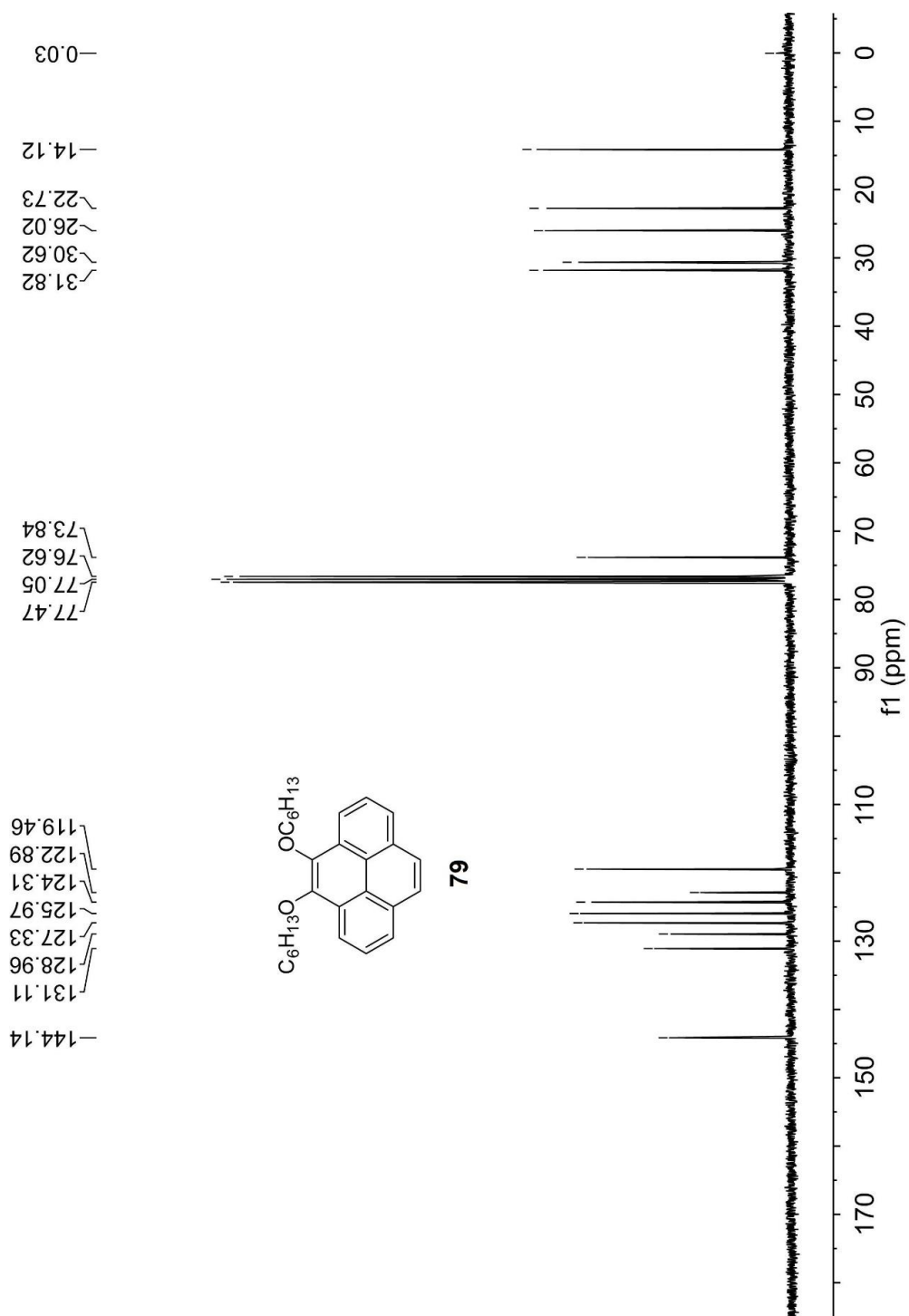


**Fig. 3.16**  $^{13}C$  NMR (75 MHz,  $CDCl_3$ ) spectrum of compound **79**.

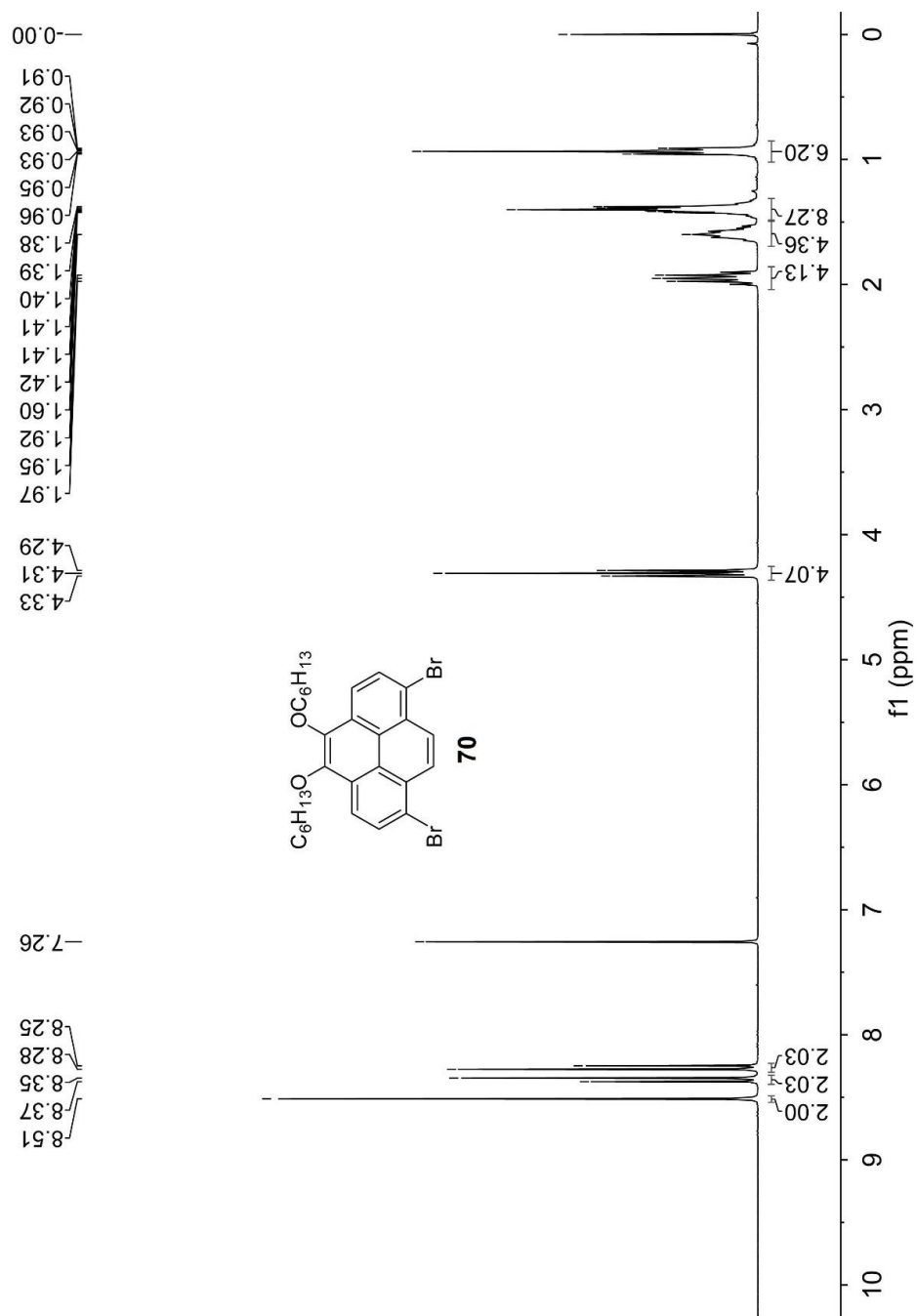


**Fig. 3.17**  $^1\text{H}$  NMR (300 MHz,  $\text{CDCl}_3$ ) spectrum of compound **70**.

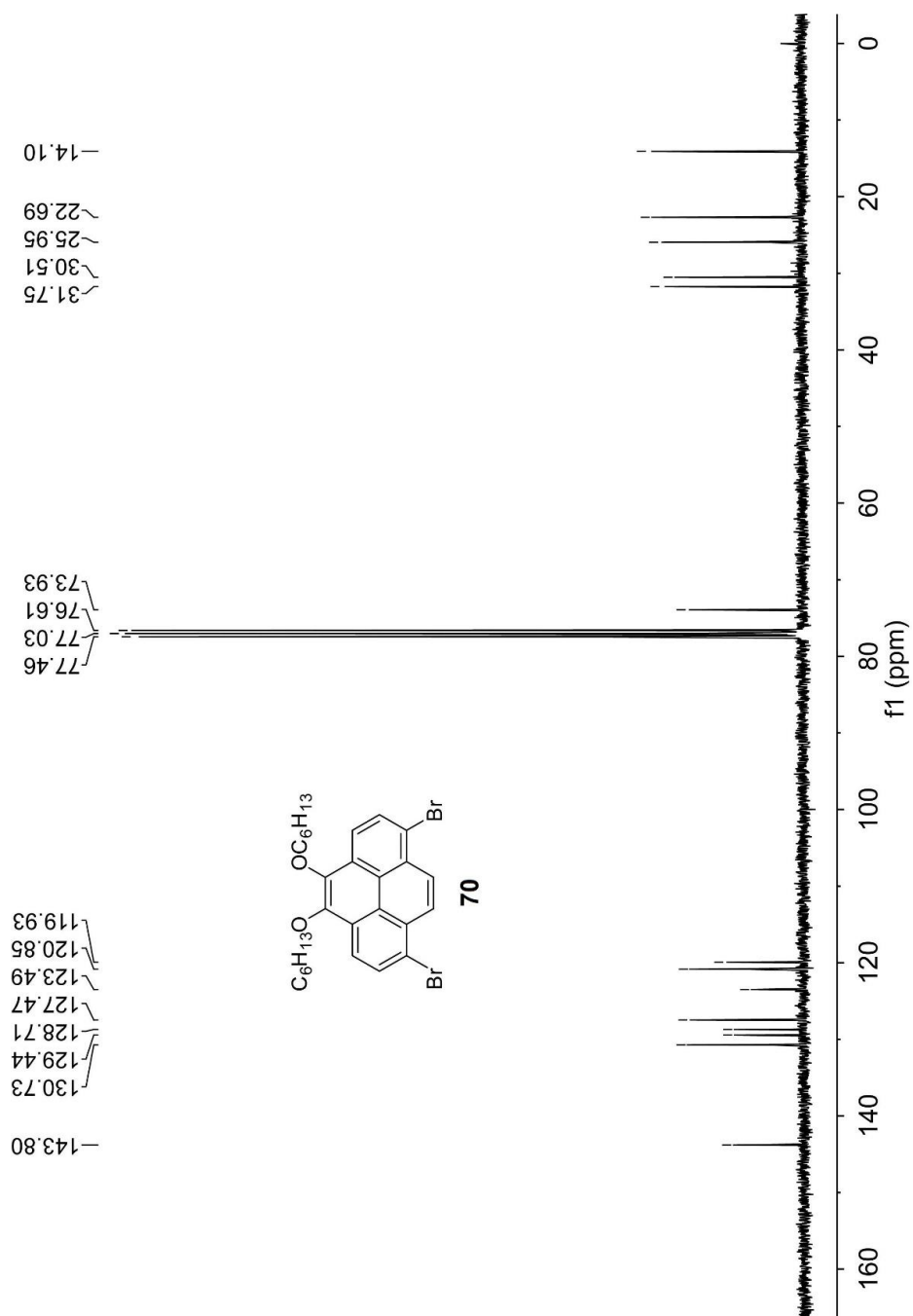


**Fig. 3.18**  $^{13}\text{C}$  NMR (75 MHz,  $\text{CDCl}_3$ ) spectrum of compound **70**.

### 3.4 Density Functional Theory (DFT) Modeling of **73**

The structures and molecular orbital (MO) properties of compound **73** in the neutral and oxidized states were calculated at the B3LYP/6-31G(d) level of theory using *Gaussian 09* software package.<sup>34</sup> The optimized molecular geometries, MOs, and density plots were visualized using *Gaussview 5*.<sup>35</sup>

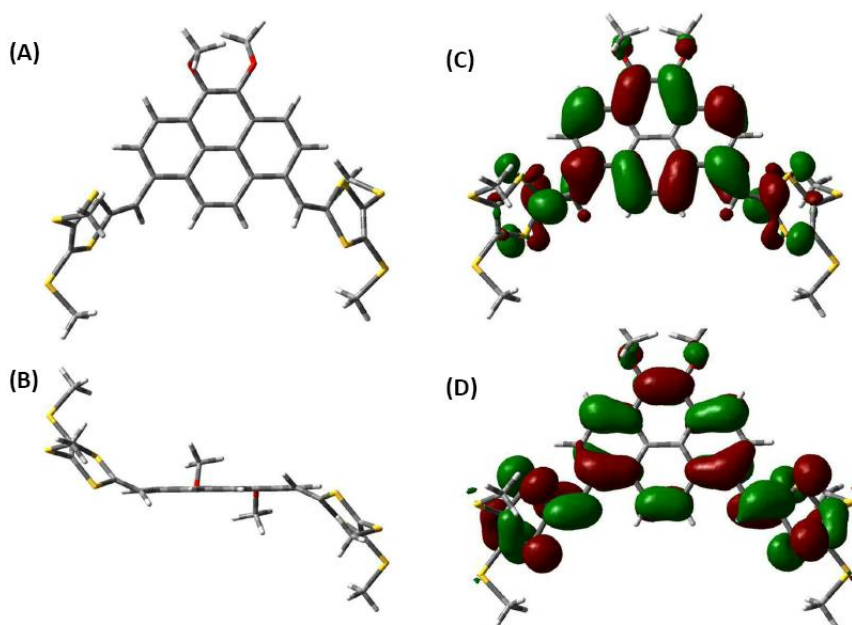


**Fig. 3.19** Optimized geometry of compound **73**: (A) front view, (B) side view. MO plots: (C) LUMO (-1.90 eV, isovalue = 0.02), (D) HOMO (-4.75 eV, isovalue = 0.02).

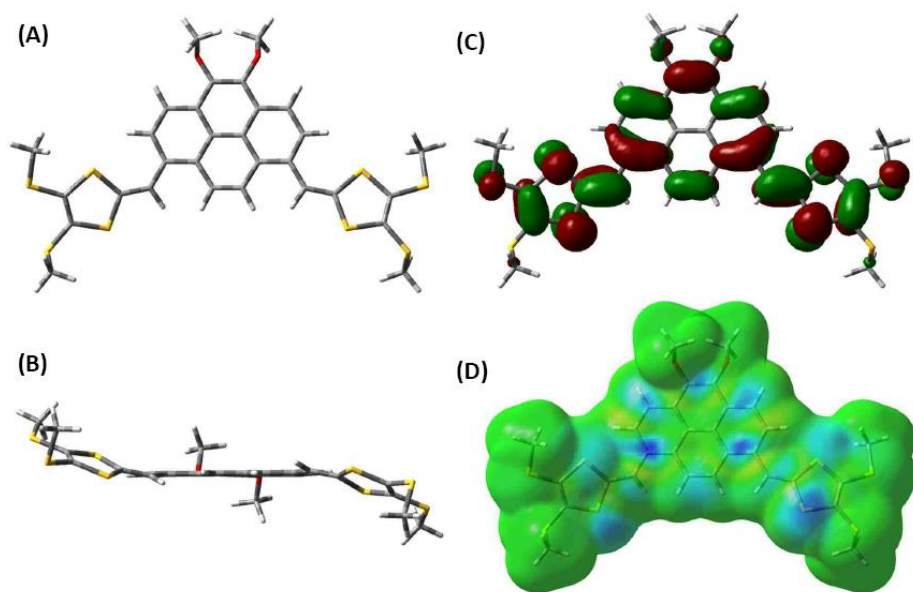


**Fig. 3.20** Optimized geometry of the radical cation of **73**: (A) front view, (B) side view. MO plots: (C) SOMO (-7.18 eV, isovalue = 0.02), (D) Spin density map (the blue color indicates the high spin density area).

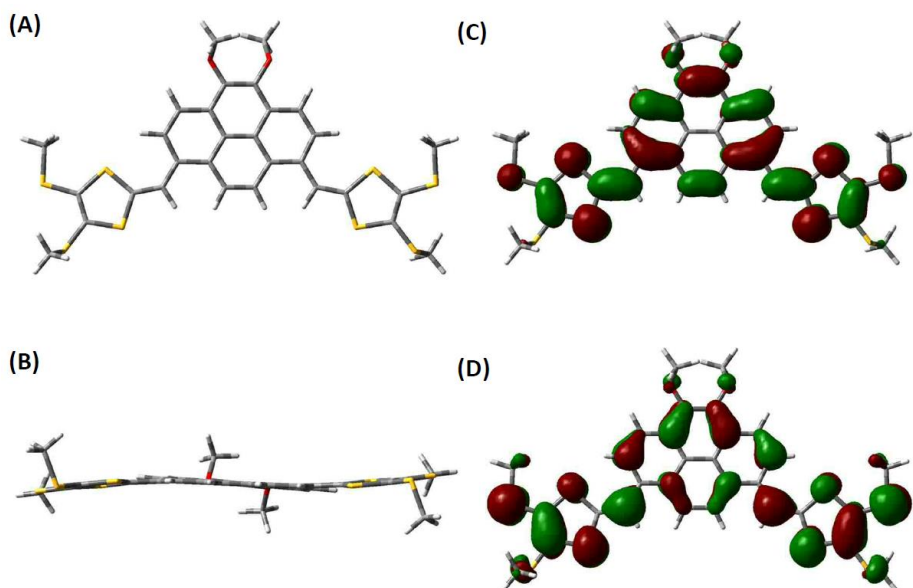


**Fig. 3.21** Optimized geometry of the singlet dication of **73**: (A) front view, (B) side view. MO plots: (C) LUMO (-10.04 eV, isovalue = 0.02), (D) HOMO (-10.66 eV, isovalue = 0.02).

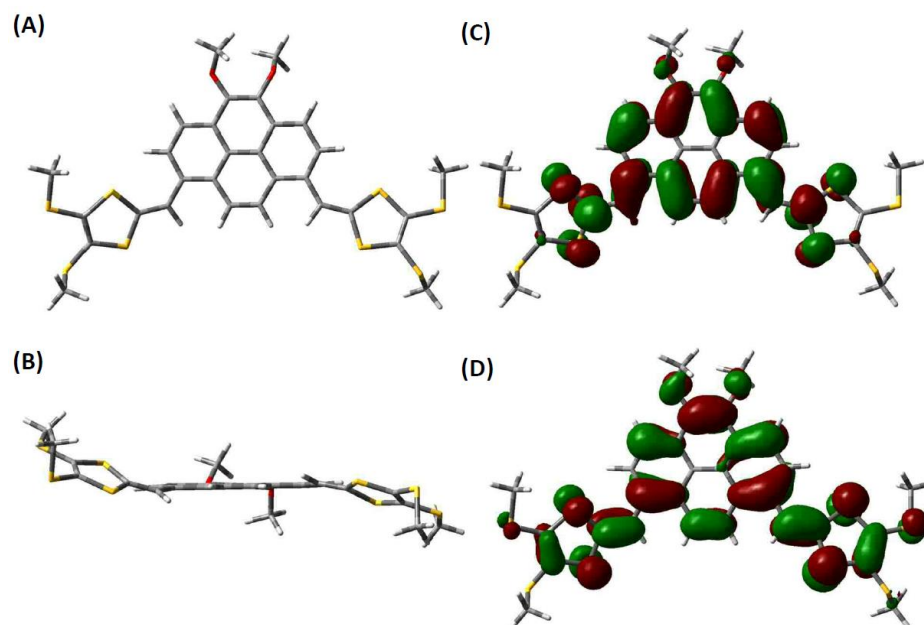


**Fig. 3.22** Optimized geometry of the triplet dication of **73**: (A) front view, (B) side view. MO plots: (C) SOMO 2 (-9.75 eV, isovalue = 0.02), (D) SOMO 1 (-10.43 eV, isovalue = 0.02).

Cartesian coordinates of compound **73**:

S	-5.96791941	0.11788599	-0.20597401
S	-5.47034536	-2.47438521	-1.51660111
S	-8.03470751	-3.75313731	-0.49557803
S	-8.60976258	-0.74687809	1.01479708
O	-1.35054606	5.44889141	-0.40002103
C	-1.36185705	3.04030623	-0.41224903

C	-0.68168599	1.79807613	-0.21667501
C	-0.65090299	-0.64711306	-0.20369201
H	-1.15616402	-1.59704913	-0.33930602
C	-1.37228104	0.56748804	-0.44211303
C	-4.75077629	-0.93823209	-0.96713307
C	-2.69896415	3.02685522	-0.83349106
H	-3.20230319	3.97094629	-1.00781207
C	-3.43857920	-0.66779407	-1.15460408
H	-2.84899715	-1.47800413	-1.57831711
C	-3.35746920	1.82678513	-1.06447507
H	-4.37022928	1.85698312	-1.45450511
C	-0.65995200	4.27575932	-0.18528901
C	-7.16275448	-1.17625612	0.09504101
C	-2.73244815	0.58300703	-0.87426306
C	-6.93278247	-2.37034621	-0.50380903
C	-7.89539552	-0.30634705	2.65022221
H	-7.41771648	-1.17410812	3.11022424
H	-8.74087259	0.01123897	3.26657425
H	-7.18235749	0.51620601	2.56665920
C	-6.95928446	-5.08477642	0.17284602
H	-6.09008040	-5.25734642	-0.46493703
H	-7.57957047	-5.98513651	0.18626102
H	-6.63958345	-4.85084139	1.19065710
S	5.96782251	0.11772003	0.20620802
S	5.47016947	-2.47470817	1.51649412
S	8.03448267	-3.75341126	0.49526704
S	8.60963573	-0.74697303	-1.01468507
O	1.35078315	5.44889744	0.39986304
C	1.36189716	3.04020723	0.41253304
C	0.68166511	1.79801914	0.21689902
C	0.65074412	-0.64716105	0.20381802
H	1.15594315	-1.59713412	0.33940803
C	1.37219017	0.56738804	0.44229104
C	4.75064043	-0.93847006	0.96720608
C	2.69897826	3.02667523	0.83386007
H	3.20234630	3.97073231	1.00829808
C	3.43844433	-0.66802804	1.15468209
H	2.84883828	-1.47827811	1.57828513
C	3.35741831	1.82656015	1.06479109
H	4.37015939	1.85668515	1.45487812
C	0.66010910	4.27567733	0.18547302
C	7.16261161	-1.17642507	-0.09499100
C	2.73235527	0.58281905	0.87445807
C	6.93260159	-2.37058716	0.50370104

C	7.89529466	-0.30620600	-2.65005820
H	7.41763165	-1.17390207	-3.11019923
H	8.74077972	0.01148003	-3.26634824
H	7.18224763	0.51632706	-2.56638319
C	6.95899060	-5.08494937	-0.17324501
H	6.08985052	-5.25761738	0.46459904
H	7.57927667	-5.98530542	-0.18685801
H	6.63918757	-4.85086235	-1.19098909
C	1.61770816	6.21453045	-0.78322905
H	0.68858810	6.53530548	-1.26389709
H	2.18814320	7.08669552	-0.45562403
H	2.21766822	5.63176141	-1.49313511
C	-1.61595308	6.21611449	0.78238606
H	-0.68624101	6.53674050	1.26196010
H	-2.18600813	7.08828856	0.45415604
H	-2.21581913	5.63461844	1.49341912

Total Energy = -4494.75426035 a.u.; Dipole Moment = 0.9443 Debye

Cartesian coordinates of the radical cation of **73**:

S	6.20939346	0.01582600	-0.02529600
S	5.51583143	-2.67597120	0.90551307
S	8.34544966	-3.75050629	0.65939905
S	9.17559572	-0.69908505	-0.40015103
O	1.40975011	5.27688041	0.13344301
C	1.40534611	2.88877322	0.16850401
C	0.70729106	1.64325813	0.10103001
C	0.67987805	-0.78523406	0.09601601
H	1.18081409	-1.74469813	0.14243501
C	1.42836211	0.41607803	0.21437102
C	4.92600738	-1.07175208	0.50926004
C	2.80801022	2.87876022	0.35185403
H	3.32528725	3.82777929	0.43101503
C	3.57886027	-0.79428006	0.59862005
H	2.98123523	-1.66243112	0.85762606
C	3.50247627	1.69699813	0.47136504
H	4.56356435	1.75199014	0.68227205
C	0.69371705	4.11633831	0.06002100
C	7.52706857	-1.16579509	0.02488600
C	2.86284722	0.43296903	0.41653803
C	7.20104157	-2.41922218	0.44480803
C	8.94794669	0.92816607	-1.20797709

H	8.30208866	0.85698707	-2.08617416
H	9.95127278	1.21914810	-1.52908111
H	8.57429267	1.68167113	-0.51017604
C	8.13513562	-4.66467336	-0.92428007
H	7.11074753	-5.02647538	-1.03464008
H	8.81457767	-5.51891542	-0.86364507
H	8.41676962	-4.03657131	-1.77131414
S	-6.20978950	0.01610000	0.02456200
S	-5.51578941	-2.67598521	-0.90498407
S	-8.34547564	-3.75056828	-0.65922105
S	-9.17603071	-0.69875006	0.39890703
O	-1.40963511	5.27691040	-0.13358901
C	-1.40530611	2.88879622	-0.16824301
C	-0.70730905	1.64326412	-0.10050801
C	-0.67999205	-0.78522506	-0.09498301
H	-1.18095509	-1.74468413	-0.14119101
C	-1.42843111	0.41609003	-0.21360502
C	-4.92614538	-1.07165208	-0.50891204
C	-2.80796621	2.87880322	-0.35162803
H	-3.32520426	3.82782829	-0.43097703
C	-3.57893828	-0.79425906	-0.59776304
H	-2.98126323	-1.66253313	-0.85622407
C	-3.50247727	1.69705313	-0.47095104
H	-4.56355435	1.75208413	-0.68188505
C	-0.69364205	4.11635931	-0.05997400
C	-7.52736856	-1.16567209	-0.02535200
C	-2.86291622	0.43299503	-0.41586003
C	-7.20112656	-2.41924419	-0.44468403
C	-8.94837871	0.92782907	1.20812209
H	-8.30290365	0.85579507	2.08652716
H	-9.95178175	1.21876609	1.52902712
H	-8.57427066	1.68182413	0.51109304
C	-8.13306961	-4.66629835	0.92326407
H	-7.10841454	-5.02779238	1.03216608
H	-8.81220770	-5.52076844	0.86245907
H	-8.41405262	-4.03920231	1.77125813
C	-1.39890211	6.10589248	1.04702908
H	-0.38462603	6.42690352	1.29655510
H	-2.01880516	6.97005052	0.80465906
H	-1.83601814	5.56262440	1.89228814
C	1.39896911	6.10565149	-1.04731408
H	0.38464203	6.42634148	-1.29704210
H	2.01859415	6.97003453	-0.80502806
H	1.83636714	5.56235140	-1.89240914

Total Energy = -4494.55055207 a.u.; Dipole Moment = 2.3302 Debye

Cartesian coordinates of the singlet dication of **73**:

S	-6.33422200	0.02315000	-0.15406800
S	-5.53747100	-2.75415400	0.06821600
S	-8.32169900	-3.88319700	-0.22120600
S	-9.31054700	-0.69313000	-0.43611300
O	-1.41461200	5.19081500	0.14786100
C	-1.40889900	2.82057400	0.08462200
C	-0.71314000	1.57197000	0.02615600
C	-0.69073200	-0.84482800	0.02240200
H	-1.17902900	-1.81106700	0.03898300
C	-1.44274500	0.34670700	0.05136300
C	-5.01228200	-1.10486800	0.01555800
C	-2.83201000	2.81381500	0.18071100
H	-3.34452000	3.76625000	0.24827100
C	-3.63528700	-0.83835900	0.07572200
H	-3.05208900	-1.75204300	0.09680700
C	-3.54212000	1.64718000	0.18055200
H	-4.61782100	1.71395600	0.27419500
C	-0.70418000	4.04183200	0.07344300
C	-7.63653400	-1.16287200	-0.21790900
C	-2.91173700	0.36727000	0.09934700
C	-7.25309900	-2.47846300	-0.10534900
C	-9.22861600	1.13320600	-0.49879900
H	-8.84747600	1.55356600	0.43536000
H	-10.26634500	1.45037400	-0.62802500
H	-8.64804500	1.48025400	-1.35741000
C	-8.95978900	-4.01132500	1.50397300
H	-8.14966600	-4.22512200	2.20331400
H	-9.65370200	-4.85570200	1.48442700
H	-9.50015900	-3.10789700	1.79064300
S	6.33413300	0.02309800	0.15449500
S	5.53754100	-2.75418900	-0.06861200
S	8.32183300	-3.88311600	0.22128700
S	9.31043000	-0.69312500	0.43699400
O	1.41479900	5.19078900	-0.14794500
C	1.40901500	2.82054300	-0.08498500
C	0.71321900	1.57195300	-0.02664900
C	0.69074400	-0.84484500	-0.02319800
H	1.17901900	-1.81109300	-0.03992500

C	1.44278700	0.34667300	-0.05199200
C	5.01229000	-1.10493400	-0.01580100
C	2.83212300	2.81375000	-0.18115700
H	3.34465400	3.76617400	-0.24870200
C	3.63530400	-0.83844000	-0.07627400
H	3.05210700	-1.75212000	-0.09756400
C	3.54219900	1.64709500	-0.18111300
H	4.61789200	1.71382500	-0.27490700
C	0.70433300	4.04182000	-0.07365400
C	7.63647400	-1.16289000	0.21839800
C	2.91177800	0.36720100	-0.09992700
C	7.25311700	-2.47847000	0.10545200
C	9.22836400	1.13318400	0.50034100
H	8.84735500	1.55387600	-0.43372300
H	10.26604900	1.45037500	0.62985400
H	8.64762500	1.47987100	1.35898500
C	8.95927000	-4.01165600	-1.50410500
H	8.14890100	-4.22566200	-2.20309800
H	9.65323100	-4.85599500	-1.48461700
H	9.49948600	-3.10826700	-1.79118900
C	1.14667100	6.07807400	-1.26548300
H	0.09566500	6.37021100	-1.29773700
H	1.77932000	6.94918900	-1.09808400
H	1.43027800	5.58340400	-2.19965000
C	-1.14645500	6.07795100	1.26551400
H	-0.09539800	6.36988900	1.29792600
H	-1.77892100	6.94919900	1.09811900
H	-1.43027200	5.58324400	2.19959700

Total Energy = -4494.25598236 a.u; Dipole Moment = 3.4722 Debye

Cartesian coordinates of the triplet dication of **73**:

S	6.25092800	-0.02822300	-0.08772900
S	5.37694100	-2.68383100	0.75457500
S	8.12864400	-3.90599800	0.74672200
S	9.18621400	-0.91138500	-0.23249800
O	1.31572800	5.38855500	0.09958200
C	1.35047200	2.99235800	0.14398000
C	0.67590600	1.73450900	0.05386200
C	0.69059100	-0.69399500	0.00112900
H	1.21282600	-1.64619800	0.03201600
C	1.41170100	0.52052000	0.14074200

C	4.89366600	-1.03936400	0.40458200
C	2.74704500	3.00530800	0.32958200
H	3.24969100	3.96000700	0.42995500
C	3.53638600	-0.69994000	0.48784700
H	2.90811100	-1.55948900	0.72034700
C	3.45883000	1.82093100	0.42718300
H	4.51437200	1.88712600	0.64542000
C	0.61958400	4.21904300	0.04927300
C	7.50076800	-1.25607300	0.06242200
C	2.83146200	0.55027900	0.33717000
C	7.08025100	-2.51204300	0.44570700
C	9.17656300	0.84542300	-0.73967700
H	8.60845500	0.99524100	-1.66119900
H	10.22600300	1.08429600	-0.92843700
H	8.80869000	1.48942100	0.06321100
C	8.38484600	-4.55642500	-0.96013400
H	7.43783200	-4.87561600	-1.39848800
H	9.03621200	-5.42486700	-0.83236400
H	8.88475400	-3.82071700	-1.59183900
S	-6.13010800	-0.08134400	0.24504900
S	-5.48797200	-2.64463200	-1.01716500
S	-8.27249300	-3.76873200	-0.80110600
S	-9.05853900	-0.88926500	0.65695100
O	-1.51421000	5.31036300	-0.08649700
C	-1.45590100	2.95199300	-0.18390700
C	-0.73623100	1.71820300	-0.14590600
C	-0.66239900	-0.71607100	-0.18781800
H	-1.14823300	-1.68246000	-0.24829700
C	-1.43397100	0.48214000	-0.28297900
C	-4.89535000	-1.07453500	-0.52545100
C	-2.85275600	2.92926800	-0.35613200
H	-3.38864400	3.86927400	-0.40257400
C	-3.56491500	-0.75294600	-0.70917400
H	-2.96951400	-1.57238800	-1.10298400
C	-3.53015500	1.73101200	-0.50361300
H	-4.59288100	1.76913600	-0.71400500
C	-0.75740200	4.20456800	-0.05175000
C	-7.44054300	-1.24297000	0.11135200
C	-2.86294900	0.48577200	-0.47735700
C	-7.12784100	-2.45897500	-0.47232400
C	-8.90002000	0.77690200	1.39390700
H	-8.21148800	0.77594400	2.24264900
H	-9.90377000	1.01824200	1.75192100
H	-8.60646300	1.51675400	0.64472400

C	-8.31138100	-4.64494400	0.82187100
H	-7.32651700	-5.04449300	1.06933700
H	-9.01134100	-5.47147300	0.67456500
H	-8.68439300	-3.99294500	1.61303000
C	-1.24812000	6.38947000	0.83983600
H	-0.57764300	7.12742700	0.39525800
H	-2.22006200	6.84403100	1.03528600
H	-0.81730300	6.00492400	1.76714100
C	1.40951100	6.10566100	-1.15199400
H	0.41671300	6.33746400	-1.54974400
H	1.94641900	7.02706900	-0.92509500
H	1.97230800	5.51702600	-1.88466600

Total Energy = -4494.24319695 a.u.; Dipole Moment = 0.6491 Debye

### 3.5 UV-Vis Titration Data

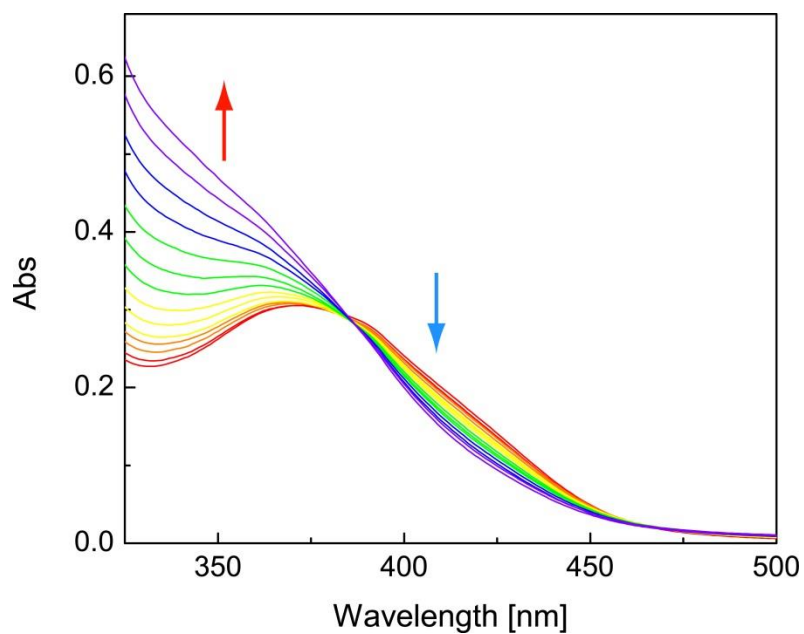


**Fig. 3.23** UV-Vis titration of macrocycle **77** ( $1.13 \times 10^{-5}$  M in  $\text{CHCl}_3$ ) with nitrobenzene (0.0 to 16.4 molar equivalents) at room temperature. The arrows indicate the trend of spectral change with increasing titration.

The UV-Vis titration curves in Fig. 3.23 clearly show an isosbestic point at 385 nm, indicating a 1:1 binding motif. The binding constant ( $K$ ) was determined as  $3644.6 \pm 0.4 \text{ M}^{-1}$  using the online *Bindfit* program (<http://www.supramolecular.org/>).

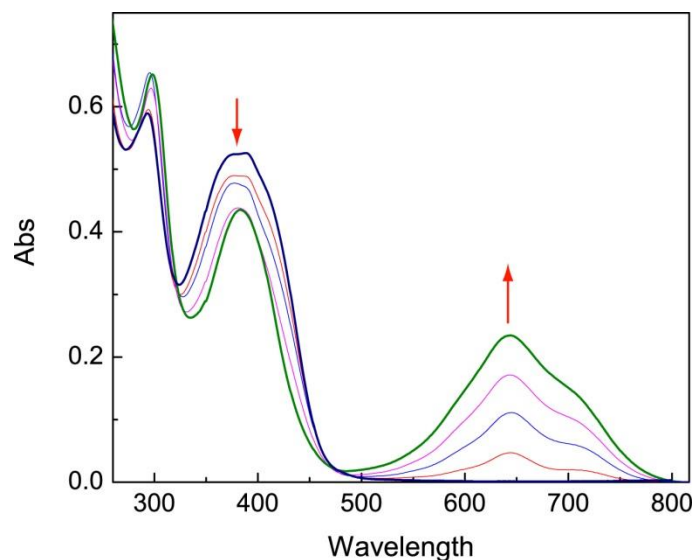


**Fig. 3.24** Oxidative UV-Vis titration of macrocycle **77** ( $2.27 \times 10^{-5} \text{ M}$  in  $\text{CHCl}_3$ ) with  $\text{PhI}(\text{OAc})_2/\text{CF}_3\text{SO}_3\text{H}$  (1:4 molar ratio) at room temperature. The arrows indicate the trend of spectral change with increasing titration. The addition of oxidant goes as follows: 0, 0.11, 0.33, 0.55, 0.76 molar equivalents of  $\text{PhI}(\text{OAc})_2$ .

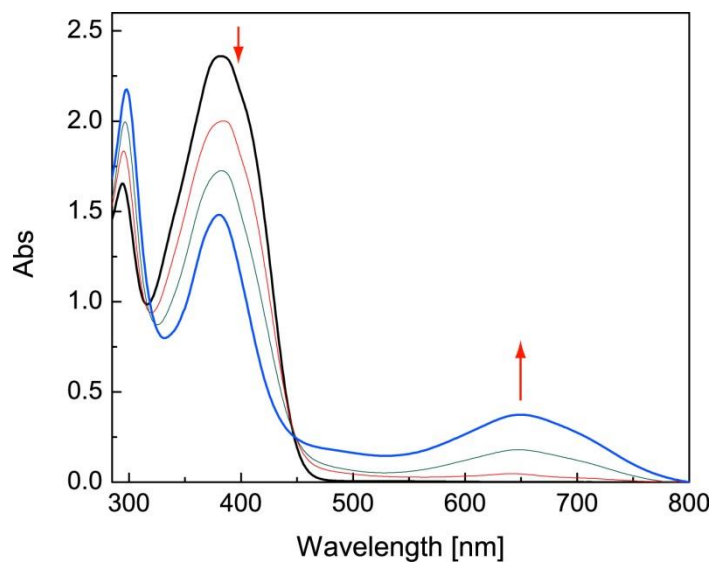


**Fig. 3.25** Oxidative UV-Vis titration of compound **75** ( $6.79 \times 10^{-5}$  M in  $\text{CHCl}_3$ ) with  $\text{PhI}(\text{OAc})_2/\text{CF}_3\text{SO}_3\text{H}$  (1:4 molar ratio) at room temperature. The arrows indicate the trend of spectral change with increasing titration. The addition of oxidant goes as follows: 0, 0.04, 0.11, 0.18 molar equivalents of  $\text{PhI}(\text{OAc})_2$ .

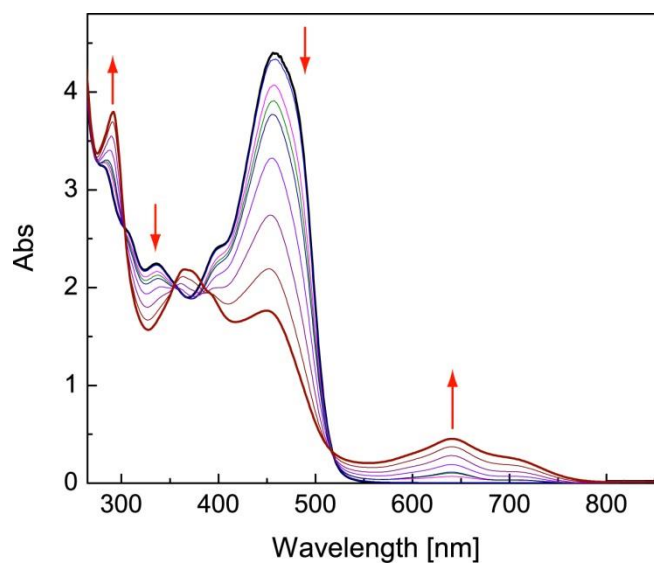


**Fig. 3.26** Oxidative UV-Vis titration of compound **73** ( $1.22 \times 10^{-4}$  M in  $\text{CHCl}_3$ ) with  $\text{PhI}(\text{OAc})_2/\text{CF}_3\text{SO}_3\text{H}$  (1:4 molar ratio) at room temperature. The arrows indicate the trend of spectral change with increasing titration. The addition of oxidant goes as follows: 0, 0.03, 0.08, 0.13, 0.18, 0.25, 0.35, 0.48, 0.62 molar equivalents of  $\text{PhI}(\text{OAc})_2$ .

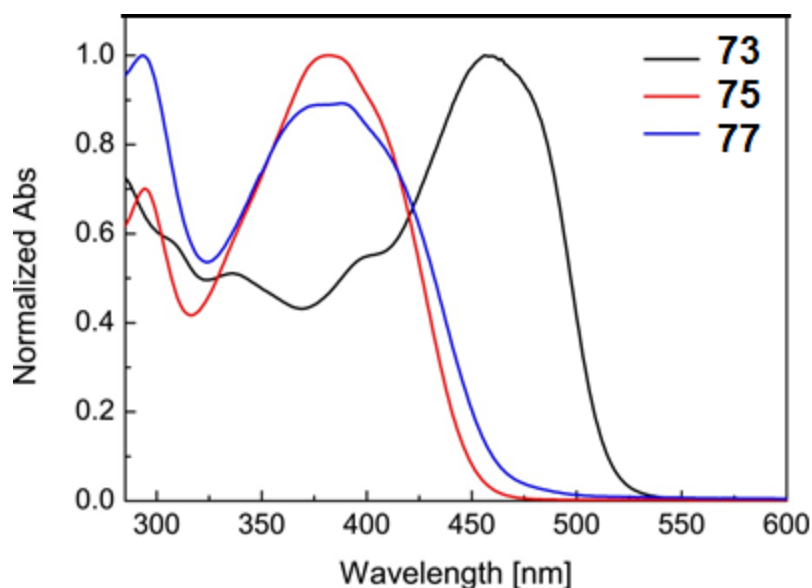


**Fig. 3.27** Normalized UV-Vis absorption spectra of compounds **73**, **75**, and **77**.

**Fig. 3.27** compares the normalized UV-Vis absorption spectra of compounds **73**, **75**, and macrocycle **77**. From the spectra, the maximum absorption wavelengths ( $\lambda_{\text{max}}$ ) of these compounds show a trend as follows: **73** (459 nm) > **75**  $\approx$  **77** (382 nm). The significantly redshifted  $\lambda_{\text{max}}$  of **73** relative to those of **75** and **77** indicates that there is a greater degree of  $\pi$ -delocalization between the DTF and pyrene units in **73** than the other two

compounds. Clearly, the presence of phenylene spacers between the DTF and pyrene units in compound **75** and macrocycle **77** attenuates the electronic communications.

### 3.6 Variable Temperature (VT) NMR Analysis of **77**

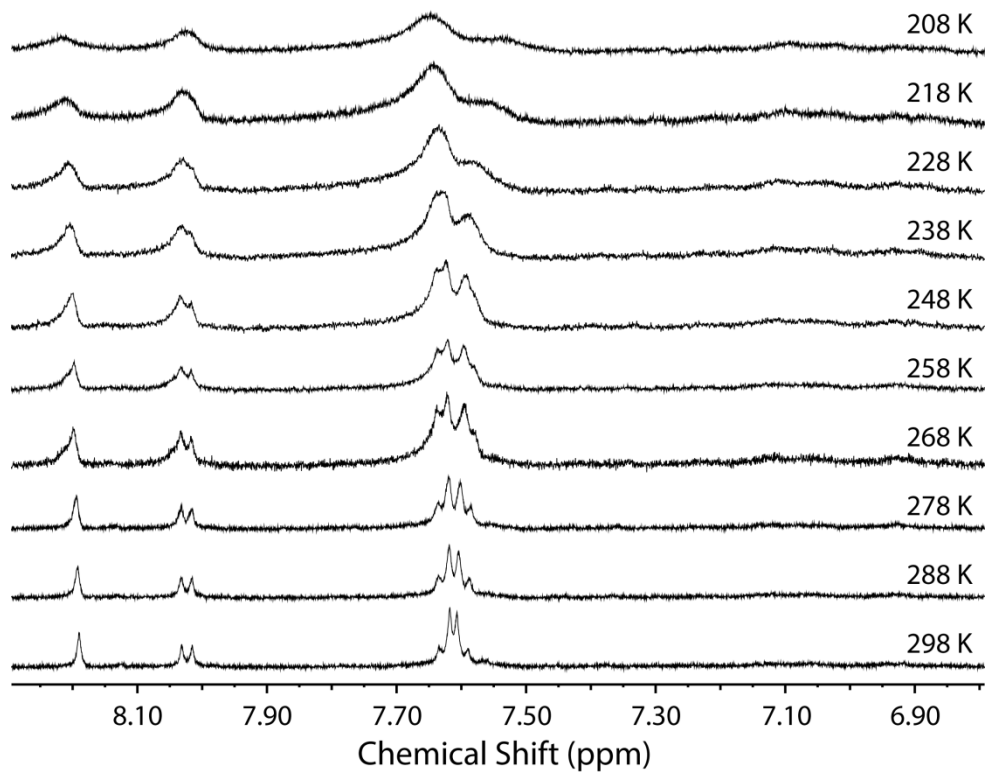


**Fig. 3.28** Expanded <sup>1</sup>H NMR (500 MHz, CD<sub>2</sub>Cl<sub>2</sub>) spectra of macrocycle **77** measured at different temperatures.

### 3.7 References

- (1) Figueira-Duarte, T. M.; Müllen, K. *Chem. Rev.* **2011**, *111*, 7260
- (2) Duhamel, J. *Langmuir* **2012**, *28*, 6527
- (3) Mateo-Alonso, A. *Chem. Soc. Rev.* **2014**, *43*, 6311
- (4) Ghasemabadi, P. G.; Yao, T.; Bodwell, G. J. *Chem. Soc. Rev.* **2015**, *44*, 6494.
- (5) Recent examples of pyrene-based conjugated polymers, see: Bheemireddy, S. R.; Plunkett, K. N. *Polym. Chem.* **2016**, *7*, 292.
- (6) Younes, E. A.; Williams, K.-L. M.; Walsh, J. C.; Schneider, C. M.; Bodwell, G. J.; Zhao, Y. *RSC Adv.* **2015**, *5*, 23952.
- (7) Zhu, X.; Wu, Y.; Zhou, L.; Wang, Y.; Zhao, H.; Gao, B.; Ba, X. *Chin. J. Chem.* **2015**, *33*, 431.
- (8) Yang, D. S.; Kim, K. H.; Cho, M. J.; Jin, J.-I.; Choi, D. H. *J. Polym. Sci. Part A: Polym. Chem.* **2013**, *51*, 1457.
- (9) He, G.; Yan, N.; Yang, J.; Wang, H.; Ding, L.; Yin, S.; Fang, Y. *Macromolecules* **2011**, *44*, 4759
- (10) Kawano, S.-i.; Yang, C.; Ribas, M.; Balushev, S.; Baumgarten, M.; Müllen, K. *Macromolecules* **2008**, *41*, 7933.
- (11) Recent examples of pyrene-based conjugated macrocycles, see: Venkataramana, G.; Dongare, P.; Dawe, L. N.; Thompson, D. W.; Zhao, Y.; Bodwell, G. J. *Org. Lett.* **2011**, *13*, 2240.
- (12) Lorbach, D.; Keerthi, A.; Figueira-Duarte, T. M.; Baumgarten, M.; Wagner, M.; Müllen, K. *Angew. Chem. Int. Ed.* **2016**, *55*, 418.

- (13)(a) López-Moreno, A.; Pérez, E. M. *Chem. Commun.* **2015**, *51*, 5421; (b) Iwamoto, T.; Kayahara, E.; Yasuda, N.; Suzuki, T.; Yamago, S. *Angew. Chem. Int. Ed.* **2014**, *53*, 6430.
- (14) Fujitsuka, M.; Tojo, S.; Iwamoto, T.; Kayahara, E.; Yamago, S.; Majima, T. *J. Phys. Chem. A* **2015**, *119*, 4136.
- (15) Lorcy, D.; Carlier, R.; Robert, A.; Tallec, A.; Le Magueres, P.; Ouahab, L. *J. Org. Chem.* **1995**, *60*, 2443
- (16) Hapiot, P.; Lorcy, D.; Tallec, A.; Carlier, R.; Robert, A. *J. Phys. Chem.* **1996**, *100*, 14823.
- (17) Zhao, Y.; Chen, G.; Mulla, K.; Mahmud, I.; Liang, S.; Dongare, P.; Thompson, D. W.; Dawe, L. N.; Bouzan, S. *Pure Appl. Chem.* **2012**, *84*, 1005
- (18) Bendikov, M.; Wudl, F.; Perepichka, D. F. *Chem. Rev.* **2004**, *104*, 4891
- (19) Roncali, J. *J. Mater. Chem.* **1997**, *7*, 2307.
- (20) Bellec, N.; Boubekeur, K.; Carlier, R.; Hapiot, P.; Lorcy, D.; Tallec, A. *J. Phys. Chem. A* **2000**, *104*, 9750
- (21) Khadem, M.; Zhao, Y. *J. Org. Chem.* **2015**, *80*, 7419.
- (22) Christensen, C. A.; Batsanov, A. S.; Bryce, M. R. *J. Org. Chem.* **2007**, *72*, 1301
- (23) Schou, S. S.; Parker, C. R.; Lincke, K.; Jennum, K.; Vibenholt, J.; Kadziola, A.; Nielsen, M. B. *Synlett* **2013**, *24*, 231.
- (24) Naka, K.; Uemura, T.; Chujo, Y. *Polym. J.* **2000**, *32*, 435
- (25) Gelover-Santiago, A.; Naka, K.; Chujo, Y. *J. Polym. Sci. Part A: Polym. Chem.* **2005**, *43*, 6592.

- (26) Woolridge, K.; Goncalves, L. C.; Bouzan, S.; Chen, G.; Zhao, Y. *Tetrahedron Lett.* **2014**, *55*, 6362.
- (27) Wang, Y.; Zhao, Y. *Org. Biomol. Chem.* **2015**, *13*, 9575
- (28) Chen, G.; Mahmud, I.; Dawe, L. N.; Daniels, L. M.; Zhao, Y. *J. Org. Chem.* **2011**, *76*, 2701
- (29) Chen, G.; Mahmud, I.; Dawe, L. N.; Zhao, Y. *Org. Lett.* **2010**, *12*, 704.
- (30) Moore, A. J.; Bryce, M. R. *Tetrahedron Lett.* **1992**, *33*, 1373
- (31) Chen, G.; Zhao, Y. *Tetrahedron Lett.* **2006**, *47*, 5069.
- (32) Wang, Z.; Lu, P.; Chen, S.; Gao, Z.; Shen, F.; Zhang, W.; Xu, Y.; Kwok, H. S.; Ma, Y. *J. Mater. Chem.* **2011**, *21*, 5451.
- (33) Venkataramana, G.; Dongare, P.; Dawe, L. N.; Thompson, D. W.; Zhao, Y.; Bodwell, G. J. *Org. Lett.* **2011**, *13*, 2240.
- (34) Gaussian 09, Revision D.01, M. J. Frisch, G. W. Trucks, H. B. Schlegel, G. E. Scuseria, M. A. Robb, J. R. Cheeseman, G. Scalmani, V. Barone, B. Mennucci, G. A. Petersson, H. Nakatsuji, M. Caricato, X. Li, H. P. Hratchian, A. F. Izmaylov, J. Bloino, G. Zheng, J. L. Sonnenberg, M. Hada, M. Ehara, K. Toyota, R. Fukuda, J. Hasegawa, M. Ishida, T. Nakajima, Y. Honda, O. Kitao, H. Nakai, T. Vreven, J. A. Montgomery, Jr., J. E. Peralta, F. Ogliaro, M. Bearpark, J. J. Heyd, E. Brothers, K. N. Kudin, V. N. Staroverov, T. Keith, R. Kobayashi, J. Normand, K. Raghavachari, A. Rendell, J. C. Burant, S. S. Iyengar, J. Tomasi, M. Cossi, N. Rega, J. M. Millam, M. Klene, J. E. Knox, J. B. Cross, V. Bakken, C. Adamo, J. Jaramillo, R. Gomperts, R. E. Stratmann, O. Yazyev, A. J. Austin, R. Cammi, C. Pomelli, J. W. Ochterski, R. L. Martin, K.

Morokuma, V. G. Zakrzewski, G. A. Voth, P. Salvador, J. J. Dannenberg, S. Dapprich, A. D. Daniels, O. Farkas, J. B. Foresman, J. V. Ortiz, J. Cioslowski, and D. J. Fox, Gaussian, Inc., Wallingford CT, 2013.

(35) GaussView, Version 5, Dennington, Roy; Keith, Todd; Millam, John. Semichem Inc., Shawnee Mission, KS, 2009.

## Chapter 4

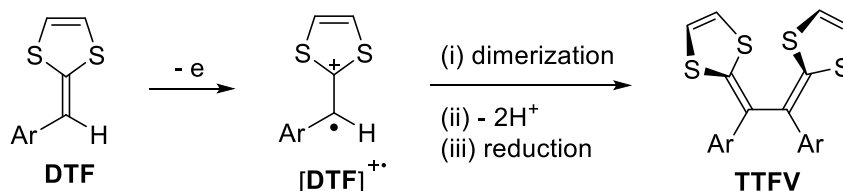
# Multivalent Dithiafulvenyl-functionalization of Dendritic Oligo(phenylene vinylene)s with an Anthraquinodimethane Core

The current chapter is the presentation and elaboration of my third published paper in *Chemical Communications (Chem. Commun.)* with the same above title. Prof. Rik R. Tykwinski and Dr. Frank Hampel of University of Erlangen-Nürnberg are acknowledged for assistance in X-ray structural analyses.

### 4.1 Introduction

Aryl-substituted dithiafulvenes (DTFs) have been investigated for more than two decades as a class of redox-active molecular building blocks in various functional molecular materials and devices.<sup>1-4</sup> Of particular interest is that the oxidative dimerization (depicted in Scheme 4.1) exhibit facile reactivity that numerous aryl-DTF derivatives tend to undergo.<sup>5-8</sup> Indeed, this reaction presents a concise, atomically economical C-C bond forming method, through which another class of redox-active  $\pi$ -systems, namely tetrathiafulvalene vinylogues (TTFVs), can be readily prepared. Over the past few years, a wide range of TTFV-based molecular

and supramolecular systems have been developed, with their excellent electronic and redox-regulated conformational properties being used in chemical sensors,<sup>9-11</sup> redox-active ligands,<sup>12,13</sup> functional nanomaterials,<sup>14-16</sup> and molecular machinery.<sup>17</sup>



**Scheme 4.1.** The general mechanism for the oxidative dimerization of an aryl-DTF

The applicability of DTF oxidative coupling in the synthesis of macromolecular materials has also been well-documented in the literature. In many of the studies bis(DTF)-substituted arenes were subjected to electropolymerization to form linear polymers in the form of solid films deposited on the surface of electrode.<sup>5-8,18,19</sup> Most recently, methods for making TTFV-based oligomers and macrocycles with well-defined molecular structures were successfully developed by our group.<sup>11,20-23</sup> The use of tris(DTF)- and poly(DTF)-substituted arenes for oxidative polymerization, on the other hand, has not yet been actively examined,<sup>24</sup> although it is a synthetic approach directly leading to 2D and/or 3D polymer networks with intrinsic microporosity and hence potential usefulness for gas adsorption and separation, catalysis, molecular recognition, and chemical sensing.<sup>25</sup> To cast more light in this respect, we have recently synthesized a new type of poly(DTF)-functionalized dendritic oligo(phenylene vinylene)s with an anthraquinodimethane unit serving as the core (**82** and **85** in Scheme 4.2A;

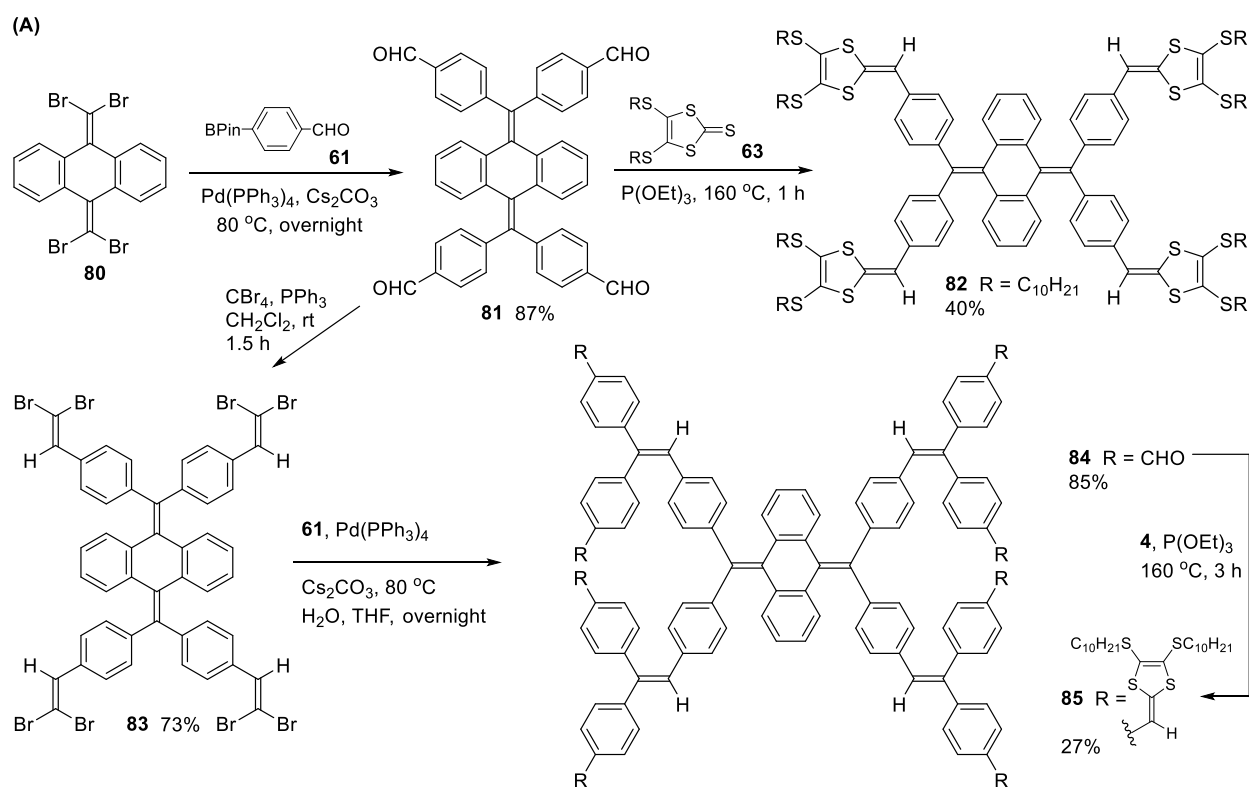
henceforth referred to as poly(DTF)-AQs). The designed systems herein were expected to act as functional materials with two key features. First, the central AQ core prefers a non-planar conformation as evidenced by both theoretical modelling and crystallographic analysis (*vide infra*). This property should be conducive to the generation of microporous polymer frameworks<sup>25-27</sup> in the case where compound **82** or **85** is subjected to oxidative DTF coupling. Second, the electron-donating nature of DTF and TTFV moieties should endow these compounds and their polymers with electron rich  $\pi$ -surfaces and cavities, which in turn would attract electron-deficient aromatic molecules (e.g., nitrobenzene) through  $\pi$ -stacking and charge-transfer (CT) interactions.<sup>11,28-30</sup> Demonstration of such supramolecular binding properties should have ramifications and applications in the development of polymer-based sensory devices for rapid detection of nitroaromatic explosives.

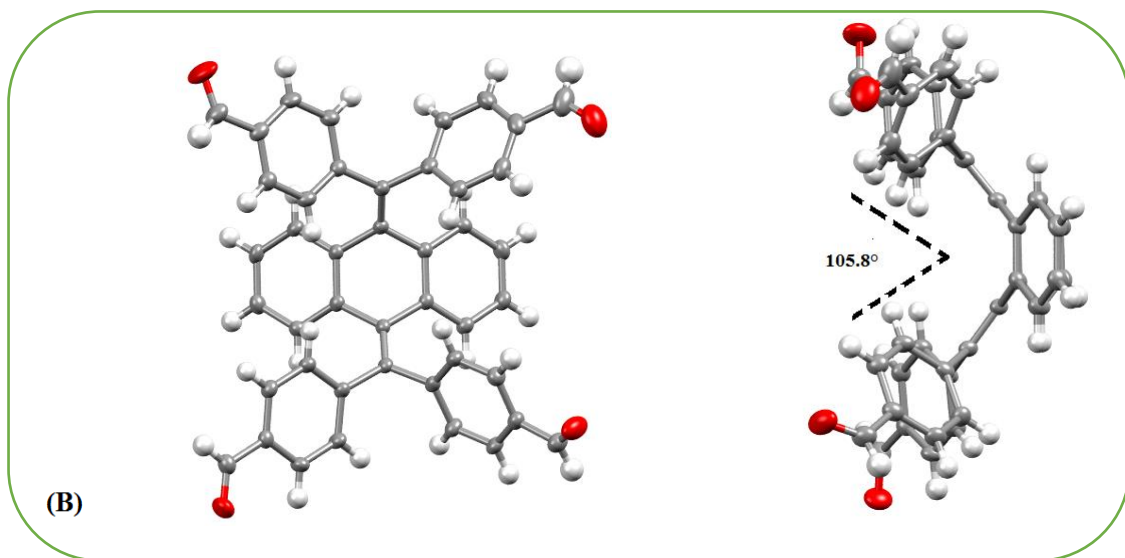
## 4.2 Result and Discussion

### 4.2.1 Synthesis and Characterization

The synthetic routes to poly(DTF)-AQs **82** and **85** are outlined in Scheme 4.2A. First, 9,10-bis(dibromomethylidene)-9,10-dihydroanthracene (**80**) was subjected to a four-fold Suzuki-Miyaura coupling with boronate ester **61** to give tetraaldehyde **81** in 87% yield. Compound **81** is a yellow coloured crystalline solid and its single-crystal X-ray structure shows a “butterfly-like” geometry (see Scheme 4.2B), in which the two phenyl rings of the central AQ moiety take an interplanar angle of 53.3° and the two vinyl units linked to the 9,10-positions of

AQ are at an angle of  $105.8^\circ$ . Compound **81** was then subjected to a  $\text{P}(\text{OEt})_3$ -promoted olefination reaction<sup>31</sup> with 1,3-dithiol-2-thione **63** at  $160^\circ\text{C}$ , affording tetrakis(DTF)-AQ **82** in 40% yield. Compound **81** underwent the Corey-Fuchs reaction to yield an octabromide product **83** in 73% yield. An 8-fold Suzuki-Miyaura coupling of **83** and **61** then led to octaaldehyde **84** in an excellent yield of 85%, testifying to the high efficacy of the Suzuki-Miyaura coupling in constructing large dendritic macromolecules. Finally, another iteration of  $\text{P}(\text{OEt})_3$ -promoted olefination gave octa(DTF)-AQ **85** in 27% yield. The yield of this reaction is actually very good, considering that totally eight steps of olefination sequentially took place in this one-pot synthetic process.





**Scheme 4.2.** (A) Synthesis of poly(DTF)-functionalized dendritic oligo(phenylene vinylene)s **82** and **85**. (B) ORTEP plots (50% ellipsoid probability, CCDC# 1518143) of the single crystal structure of compound **81** viewed from top and side.

Poly(DTF)-AQs **82** and **85** were characterized by IR, NMR, and MS analyses, and their geometries were modelled by the semi-empirical PM6 method (Fig. 4.1A, B). In both of the optimized structures, the central AQ cores adopt a shape resembling that in the single-crystal structure of **81**. The modelled structures were further substantiated by pulse gradient spin echo (PGSE) NMR analysis of **85**, in which a diffusion coefficient ( $D$ ) based on the vinylic protons next to the DTF groups was determined to be  $3.16 \times 10^{-10} \text{ m}^2/\text{s}$ . This  $D$  value corresponds to a hydrodynamic diameter of 2.68 nm which indeed is in a good agreement with the modelling results.

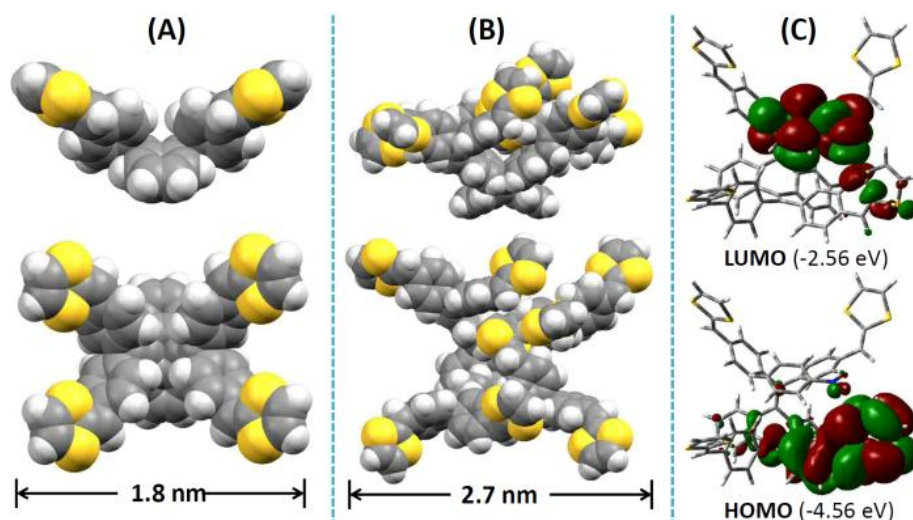


**Fig. 4.1** Space-filling models of poly(DTF)-AQs (A) **82** and (B) **85** optimized at the PM6 level. (C) Frontier molecular orbitals of the 1:1 complex of **82** with nitrobenzene calculated at the B3LYP-6-31G(d)//PM6 level. The SC10H21 side-chains were replaced with hydrogen atoms to save computational time.

The non-planar molecular shapes of **82** and **85** along with the electron-donating nature of the DTF endgroups were expected to create binding  $\pi$ -cavities for electron-deficient species through charge-transfer (C-T) interactions<sup>11,28-30</sup> and form stable guest-host complexes. Theoretically, a 1:1 complex of tetrakis(DTF)-AQ **82** and nitrobenzene (NB) were modelled (Fig. 4.1C) and its LUMO clearly shows orbital overlap between one of the DTF groups and NB. UV-Vis titration of **82** with NB in  $\text{CHCl}_3$  shows a hypochromic shift of the lowest-energy absorption band with an isosbestic point at 370 nm, indicating a 1:1 binding mode (Fig. 4.2A). Similar UV-Vis spectral changes are seen in the UV-Vis titration of **85** with NB (Fig. 4.2B). Further, the binding properties of **82** and **85** with three other NB

derivatives, DNT, TNT, and picric acid, were also revealed by UV-Vis titrations (see Fig. 4.15 and 4.16), attesting to the ability of poly(DTF)-AQs **82** and **85** to efficiently bind with electron-deficient aromatic compounds.

The reactivity of poly(DTF)-AQs **82** and **85** towards oxidative polymerization was investigated by two approaches. First, both compounds were subjected to oxidative polymerization using iodine as oxidant in CHCl<sub>3</sub> at room temperature. The reactions were allowed to proceed for two days and then quenched with Na<sub>2</sub>S<sub>2</sub>O<sub>3</sub>, affording polymeric products, poly-[**82**] and poly-[**85**], in the form of dark brown solids. The two polymers are reasonably soluble in CHCl<sub>3</sub>. Fig. 4.2C shows the UV-Vis spectra of the two polymers together with their precursors **82** and **85**. For each polymer there is no significant red-shift in low-energy bands relative to its precursor, suggesting a limited degree of  $\pi$ -delocalization within the polymer frameworks. Interestingly, the relative absorptivity of the low-energy bands in the polymers appears to be much weaker than those of their precursors. Such behaviour is in line with the characteristic  $\pi \rightarrow \pi^*$  transitions observed in TTFVs with a *s-trans* conformation.<sup>32</sup> <sup>1</sup>H NMR analysis was conducted to monitor the polymerization process of **82**. As can be seen in Fig. 4.2D, the vinylic protons adjacent to the DTF groups were greatly attenuated after the reaction proceeded for 3.5 h. In the meantime, NMR signal broadening was clearly seen, indicating the progress of polymerization. The polymerization appeared to be nearly complete after 48 h, as evidenced by the rather insignificant vinylic proton peak in the <sup>1</sup>H NMR spectrum. The fact that the

chemically polymerized products still retain sufficient solubility in common organic solvents such as  $\text{CHCl}_3$  suggests that the polymers may not possess a high degree of polymerization, and likely the DTF coupling occurred through both intermolecular and intramolecular pathways.

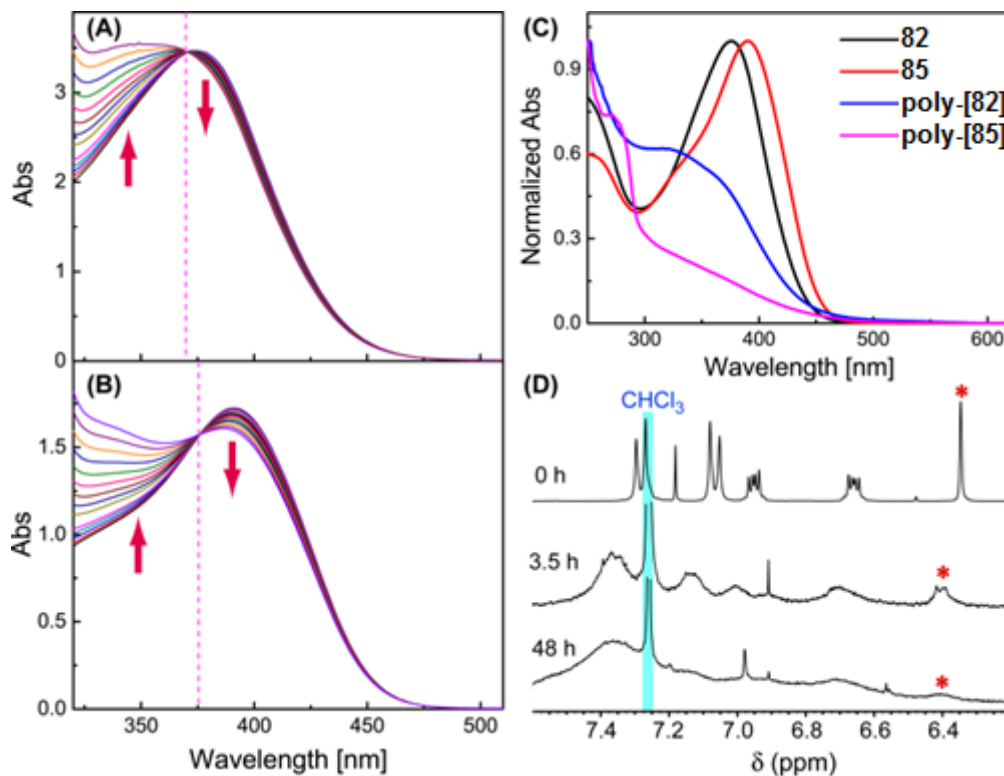


**Fig. 4.2** (A) UV-Vis spectra of **82** (42.7  $\mu\text{M}$ ) titrated with nitrobenzene (0 to 3.18 molar equivalents) in  $\text{CHCl}_3$  at room temperature. (B) UV-Vis spectra of **85** (20.4  $\mu\text{M}$ ) titrated with nitrobenzene (0 to 6.63 molar equivalents) in  $\text{CHCl}_3$  at room temperature. (C) Normalized UV-Vis spectra of **82**, **85**, poly-[**82**], and poly-[**85**] measured in  $\text{CHCl}_3$  at room temperature. (D) Partial  $^1\text{H}$  NMR (500 MHz,  $\text{CDCl}_3$ ) spectra monitoring the oxidative polymerization of **82** at different reaction times. The signals due to the vinylic protons adjacent to the DTF groups are highlighted by asterisk mark.

The polymerization of **82** and **85** was also performed under electrochemical conditions. In cyclic voltammetric (CV) analysis of tetrakis(DTF)-AQ **82**, an anodic peak appears at *ca.* +1.22 V during the first forward scan and a cathodic at +0.16 V in the reverse scan. The anodic peak can be ascribed to the single-electron transfer, oxidizing DTF group into a radical cation (Fig. 4.3A).<sup>5-8,18,19</sup> The radical cation would undergo swift dimerization to form TTFV dication (Scheme 4.1), the reduction of which in the reverse scan then gave rise to the cathodic peak. Upon multi-cycle CV scans, another anodic peak at +0.98 V can be seen to slightly emerge, which is possibly due to the polymerized product accumulated on the surface of the working electrode. However, the overall voltammetric profile does not show very significant variations. After multi-cycle CV scans of **82**, a blue coloured thin film could be observed depositing on the surface of working electrode. The thin film could be dissolved by rinsing with CH<sub>2</sub>Cl<sub>2</sub> or CHCl<sub>3</sub> exhaustively, but it sustained in CH<sub>3</sub>CN or other polar organic solvents. For this reason, the redox properties of the thin film were examined by multi-cycle CV scans in CH<sub>3</sub>CN (Figure 4.3B), which shows a reversible redox couple at  $E_{pa} = +0.65$  V and  $E_{pc} = +0.54$  V respectively. This redox wave pair is consistent with the simultaneous bielecronic transfer of typical TTFVs, indicating that the thin film is constituted of the polymer of **82** resulting from DTF coupling reactions.<sup>5-8,18-23</sup>

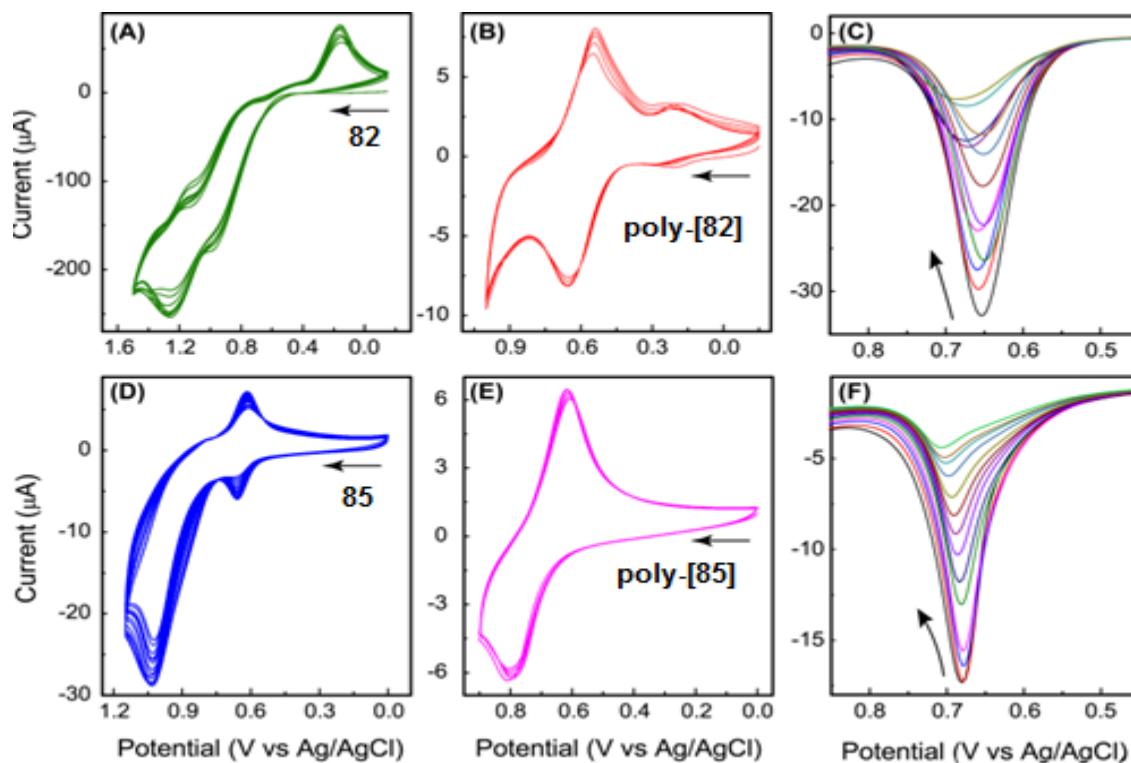


**Fig. 4.3** Multi-cycle CV scans of (A) **82**, (B) poly-[**82**] thin film, (D) **85**, and (E) of poly-[**85**] thin film. DPV responses of the thin films of (C) poly-[**82**] and (F) poly-[**85**] upon titration with nitrobenzene from 0 to 0.52 mM in CH<sub>3</sub>CN. Experimental conditions: electrolyte: Bu<sub>4</sub>NBF<sub>4</sub> (0.1 M); working electrode: glassy carbon; reference: Ag/AgCl (3M NaCl); counter electrode: Pt wire; CV scan rate: 100 mV/s; DPV step: 4 ms, pulse width: 50 ms, pulse period: 200 ms, pulse amplitude 50 mV.

The multi-cycle CV analysis of octa(DTF)-AQ **85** was also performed (Fig. 4.3D). In the first cycle of CV scan, an anodic peak at +1.02 V is observed due to the DTF oxidation. In the reverse scan, a cathodic peak shows up at +0.62 V. This peak along with another anodic peak at +0.66 V grow steadily in intensity

with increasing number of scan cycles, as a result of the formation of electropolymerized product (i.e., poly-[**85**]). Unlike the case of **82**, electropolymerization of **85** resulted in a robust thin film after multi-cycle CV scans, and the CV profile of poly-[**85**] thin film clearly exhibits a reversible redox couple at  $E_{pa} = +0.79$  V and  $E_{pc} = +0.61$  V (Fig. 4.3E). These values are relatively higher than those of poly-[**82**], and the shift can be rationalized by that the TTFV moieties in the two polymers may adopt different conformations due to their different degrees of twist and steric constraint in the polymer backbone.

To assess the performance of the two electrochemically generated polymers as sensitive electrochemical sensors for nitroaromatic compounds, the thin films of poly-[**82**] and poly-[**85**] on glassy carbon electrodes were subjected to differential pulse voltammetric (DPV) titrations with NB in CH<sub>3</sub>CN. Herein NB was chosen as a nitrobenzene explosive surrogate and its concentrations were controlled at the sub-mM level. The DPV profiles of poly-[**82**] generally shows a decreasing trend of current intensity ( $I$ ) and increasing oxidation potential ( $E_{ox}$ ) as the titration continues (Fig. 4.3C), but their correlations with the concentration of NB are not linear. It was also observed that the thin film showed slight detachment from the glassy carbon surface after a certain number of DPV scans, suggesting a relatively poor mechanical stability and adhesion.

#### 4.2.2 Characterization of The Thin Film

The thin film of poly-[**85**], in contrast, appeared to be more tolerant to multiple voltammetric scans and hence gave more meaningful results for the DPV titration experiments (Fig. 4.3F). Fig. 4.4A shows two very good linear correlations between the logarithmic concentration of NB and the DPV current of poly-[**85**], suggesting that the interactions of NB and poly-[**85**] involve two different stages. This point is further supported by the correlation diagram of NB concentration with the oxidation potential (Fig. 4.4B), where a decreasing trend is reversed to an increasing trend at the concentration of 24.1  $\mu\text{M}$ . Given the highly twisted nature of octa(DTF)-AQ **85**, the structure of poly-[**85**] is proposed to have rich intrinsic microporosity which is beneficial for trapping small NB molecules. Fig. 4.4C illustrates a two-stage mechanism. Stage I: the low concentration of NB molecules only causes the pores on surface of the film to be filled (i.e., surface adsorption). Stage II: NB molecules diffuse into the inner part of the film as the concentration of NB in the solution increases. It is worth noting that Stage II covers the concentration range of NB from  $\mu\text{M}$  to mM, and the excellent linear correlation ( $R^2$ ) manifests an ideal approach for rapid quantitative determination of NB at the sub-mM level.

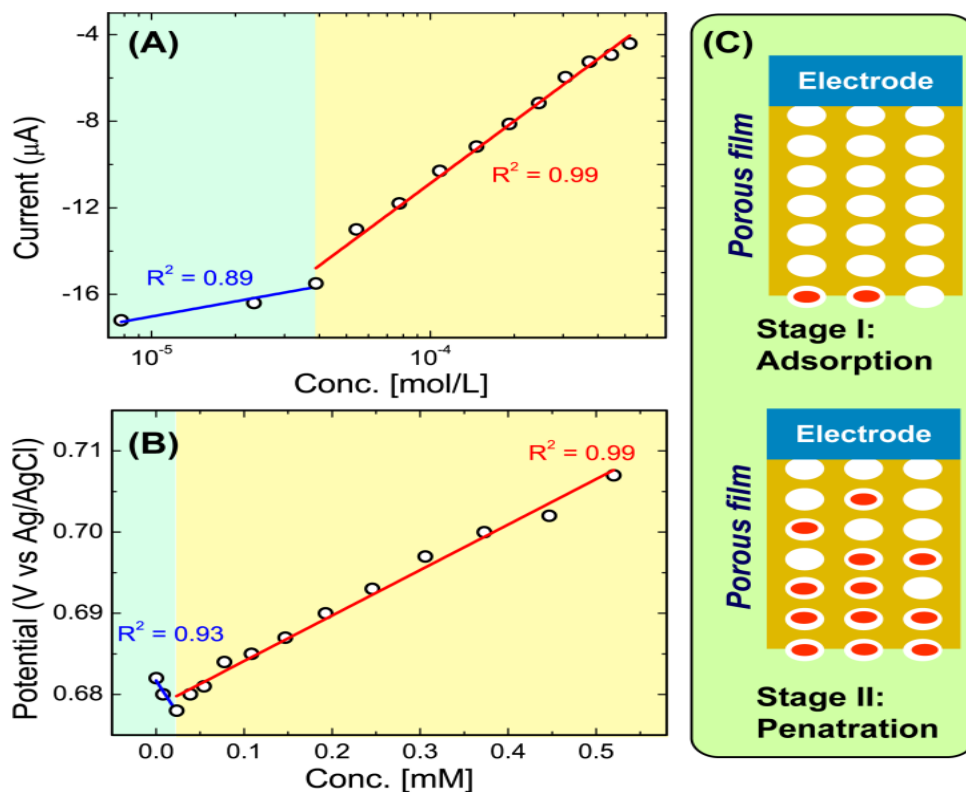


**Fig. 4.4** (A) Correlations of the concentration of NB with the DPV current intensity changes of poly-[85] during the titration. (B) Correlations of the concentration of NB with the oxidation potential changes of poly-[85] during the titration. (C) Schematic illustration of the two stages of interactions between NB molecules (red ovals) and the micropores in the thin film of poly-[85].

### 4.2.3 Conclusions

In summary, a new class of multivalent DTF functionalized  $\pi$ -conjugated dendritic systems were for the first time successfully synthesized and characterized. These compounds and their polymers are electron-rich and can serve as supramolecular hosts for electron-deficient small aromatic molecules. Investigations on the methods to prepare

more robust and better controlled polymer thin films for rapid and accurate electrochemical sensing of nitroaromatic explosives (e.g., TNT, DNT) are currently underway.

### **4.3. Experimental**

#### **4.3.1 General**

Chemicals were purchased from commercial suppliers and used directly without purification. All reactions were conducted in standard, dry glassware and under an inert atmosphere of nitrogen or argon unless otherwise noted. Evaporation and concentration were carried out with a rotary evaporator. Flash column chromatography was performed with 240-400 mesh silica gel, and thin-layer chromatography (TLC) was carried out with silica gel F254 covered on plastic sheets and visualized by UV light. Melting points (m.p.) were measured using an SRS OptiMelt melting point apparatus and are uncorrected.  $^1\text{H}$  and  $^{13}\text{C}$  NMR spectra were measured on a Bruker Avance III 300 MHz multinuclear spectrometer. Chemical shifts ( $\delta$ ) are reported in ppm downfield relative to the signals of the internal reference  $\text{SiMe}_4$  or residual solvents ( $\text{CHCl}_3$ :  $\delta_{\text{H}} = 7.24$  ppm,  $\delta_{\text{C}} = 77.2$  ppm;  $\text{CH}_2\text{Cl}_2$ :  $\delta_{\text{H}} = 5.32$  ppm,  $\delta_{\text{C}} = 54.0$  ppm). Coupling constants ( $J$ ) are given in Hz. Infrared spectra (IR) were recorded on a Bruker Alfa spectrometer. MALDI-TOF MS analysis was performed on an Applied Biosystems Voyager instrument using dithranol as the matrix. High resolution APPI-TOF MS analysis was done on a GCT premier Micromass Technologies instrument. UV-Vis absorption spectra were measured on a Cary 6000i spectrophotometer. Cyclic voltammetric (CV) and differential pulse

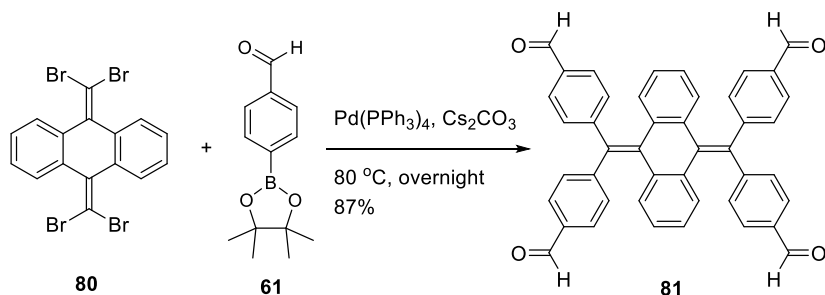
voltammetric (DPV) analyses were carried out in a standard three-electrode setup controlled by a BASi Epsilon potentiostat.

Molecular modeling studies were carried out using the Gaussian 09 software.<sup>33</sup> Visualization of the calculated molecular structures and orbitals were done by GaussView 5.<sup>34</sup>

### 4.3.2 Synthesis

Compound **61** was purchased from *Combi-Blocks, Inc.* (San Diego, USA). Compounds **80**,<sup>35,36</sup> and **63**<sup>37</sup> were prepared according to the literature procedures.

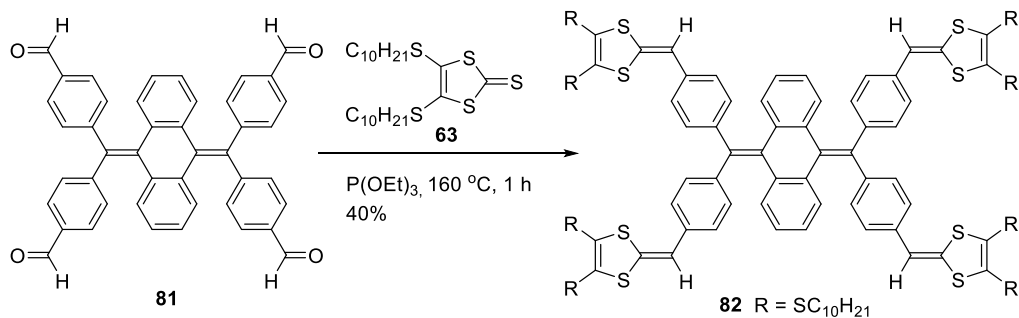
#### Tetraaldehyde-AQ **81**



To a 100 mL round-bottomed flask were added 9,10-bis(dibromomethylene)-9,10-dihydroanthracene (**61**) (1.00 g, 1.92 mmol), boronate ester **61** (2.68 g, 11.6 mmol), cesium carbonate (10.0 g, 30.7 mmol), Pd(PPh<sub>3</sub>)<sub>4</sub> (0.22 g, 0.19 mmol), THF (50 mL), and deionized water (20 mL). The reaction mixture was stirred and heated at reflux overnight. After that the mixture was cooled down to rt and then poured into brine and extracted twice with CH<sub>2</sub>Cl<sub>2</sub>. The organic layers were combined and dried over MgSO<sub>4</sub>. After filtration and concentration under reduced pressure, the resulting residue was subjected to silica gel column chromatography (hexanes/EtOAc, 4:6) to give compound **81** (1.04 g,

1.67 mmol, 87%) as a pale yellow solid. m.p. 268.2-269.8 °C; IR (neat): 3061, 2923, 2835, 2734, 1699, 1600, 1564 cm<sup>-1</sup>; <sup>1</sup>H NMR (300 MHz, CD<sub>2</sub>Cl<sub>2</sub>): δ 10.00 (s, 4H), 7.88 (d, *J* = 8.4 Hz, 8H), 7.64 (d, *J* = 8.1 Hz, 8H), 7.06–7.00 (m, 4H), 6.82–6.76 (m, 4H) ppm; <sup>13</sup>C NMR (75 MHz, CD<sub>2</sub>Cl<sub>2</sub>): δ 192.0, 148.1, 138.8, 137.4, 137.3, 135.8, 131.0, 130.4, 128.6, 126.6 ppm; HRMS (APPI-TOF, positive mode) *m/z* calcd for C<sub>44</sub>H<sub>29</sub>O<sub>4</sub> 621.2066, found 621.2011 [M + H]<sup>+</sup>.

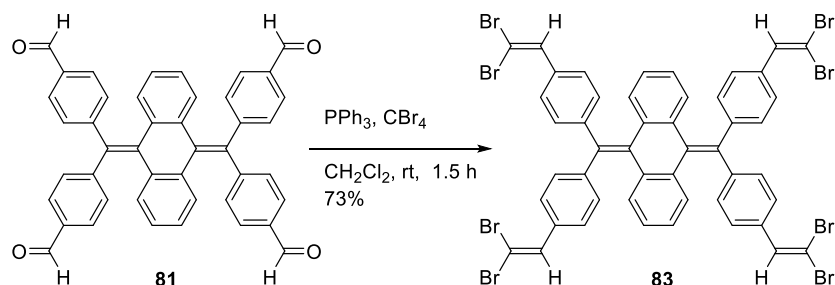
### Tetrakis(DTF)-AQ **82**



Tetraaldehyde **81** (0.10 g, 0.16 mmol), 1,3-dithiole-2-thione **63** (0.46 g, 0.96 mmol), and P(OEt)<sub>3</sub> (15 mL) were added to a 100 mL round-bottomed flask. The reaction mixture was stirred and heated to 160 °C and kept at this temperature for 1 h. After cooling down to rt, the unreacted P(OEt)<sub>3</sub> was removed by vacuum distillation, and the residue was subjected to silica gel column chromatography (hexanes/CH<sub>2</sub>Cl<sub>2</sub>, 4:1) to give compound **82** (0.15 g, 0.06 mmol, 40%) as a yellow oil. IR (neat): 2953, 2922, 2851, 1570, 1542, 1504, 1464 cm<sup>-1</sup>; <sup>1</sup>H NMR (300 MHz, CDCl<sub>3</sub>): δ 7.36 (d, *J* = 8.3 Hz, 8H), 7.15 (d, *J* = 8.3 Hz, 8H), 7.05-7.02 (m, 4H), 6.75-6.72 (m, 4H), 6.43 (s, 4H), 2.85-2.80 (m, 16H), 1.67-1.59 (m, 16H), 1.67-1.35 (m, 16H), 1.34-1.19 (m, 112H), 0.92-0.84 (m, 24H) ppm; <sup>13</sup>C NMR (75 MHz, CDCl<sub>3</sub>) δ 139.7, 139.1, 137.8, 135.8, 134.8, 132.4, 130.2,

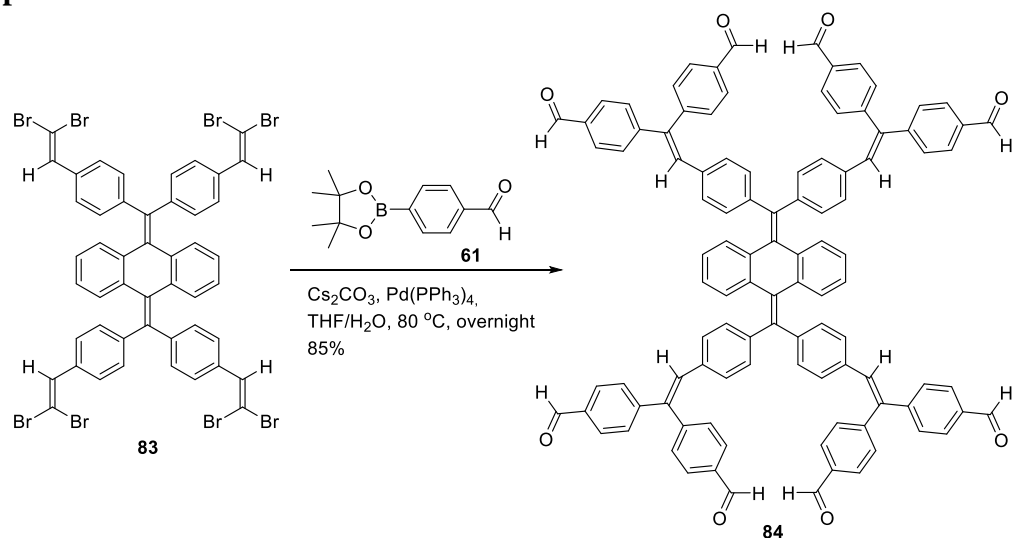
128.1, 127.7, 126.7, 125.4, 124.9, 114.0, 36.3, 36.1, 32.0, 29.9, 29.8, 29.7, 29.4, 29.3, 29.2, 28.72, 28.70, 22.8, 14.2 ppm. HRMS (APPI-TOF, positive mode)  $m/z$  calcd for  $C_{136}H_{196}S_{16}$  2342.0947, found 2342.0853  $[M + H]^+$ .

### Compound 83



A mixture of  $CBr_4$  (1.55 g, 4.67 mmol) and  $PPh_3$  (1.93 g, 0. mmol) in dry  $CH_2Cl_2$  (100 mL) was stirred at rt. To this solution tetraaldehyde **81** (0.29 g, 0.46 mmol) was slowly added in one portion, and the reaction mixture was kept under stirring at rt for 1.5 h. After that the reaction mixture was subjected to vacuum filtration and the solids collected were washed with  $CH_2Cl_2$ . The  $CH_2Cl_2$  layers were combined and evaporated to give the crude product of **83**, which was purified by silica gel column chromatography ( $CH_2Cl_2$ /hexanes, 1:4) to give **83** as a white solid (0.42 g, 0.34 mmol, 73%). m.p. > 274 °C (decomp.); IR (neat): 2955, 2923, 2854, 1504, 1459, 880, 865, 843, 760  $cm^{-1}$ ;  $^1H$  NMR (300 MHz,  $CD_2Cl_2$ ):  $\delta$  7.53 (d,  $J = 8.1$  Hz, 8H), 7.48 (s, 4H), 7.41 (d,  $J = 8.4$  Hz, 8H), 7.03-7.00 (m, 4H), 6.78-6.75 (m, 4H) ppm;  $^{13}C$  NMR (75 MHz,  $CD_2Cl_2$ ):  $\delta$  142.9, 139.4, 137.8, 137.0, 136.4, 134.4, 130.2, 128.9, 128.5, 126.0, 89.9 ppm. HRMS (APPI-TOF, positive mode)  $m/z$  calcd for  $C_{48}H_{29}Br_8$  1244.5654, found 1244.5630  $[M + H]^+$ .

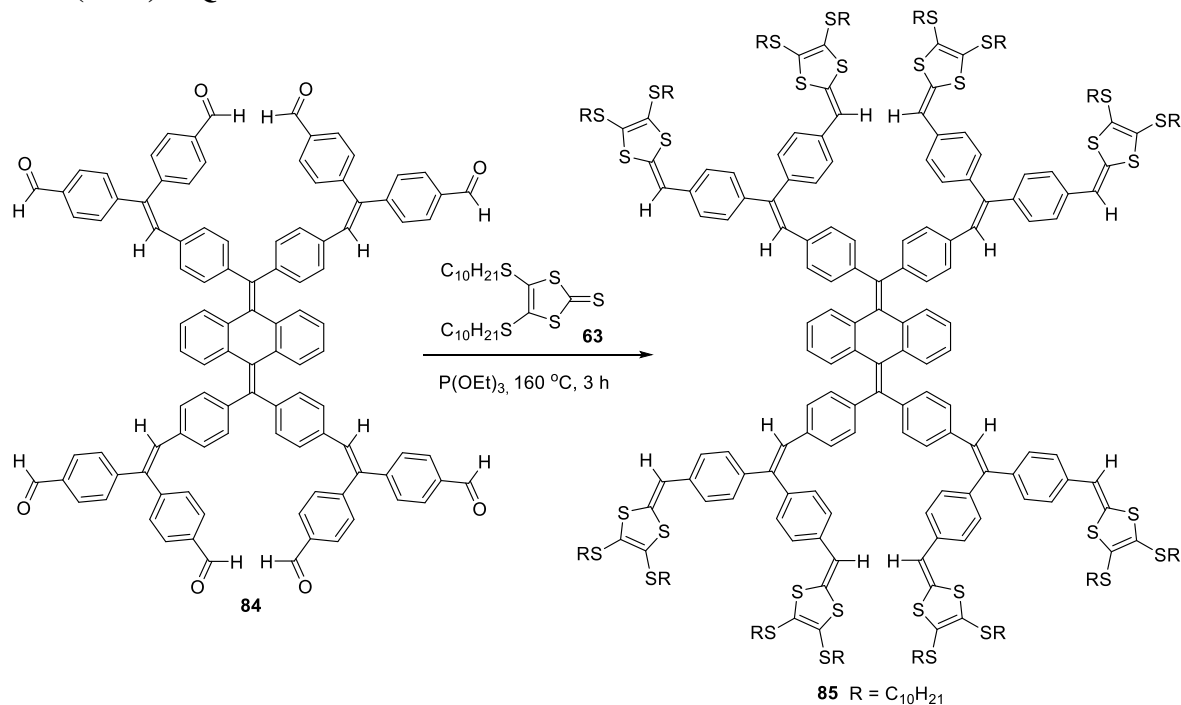
## Compound 84



To a 100 mL round-bottomed flask were added compound **83** (0.10 g, 0.080 mmol), boronic ester **61** (0.22 g, 0.96 mmol), cesium carbonate (0.18 g, 0.56 mmol),  $\text{Pd}(\text{PPh}_3)_4$  (0.03 g, 0.02 mmol), THF (20 mL), and deionized water (10 mL). The mixture was heated at reflux overnight. After that the mixture was cooled down to rt, poured into brine, and then extracted twice with  $\text{CH}_2\text{Cl}_2$ . The organic layers were combined and dried over  $\text{MgSO}_4$ . After filtration and concentration under reduced pressure, the resulting residue was subjected to silica gel column chromatography (hexanes/ $\text{EtOAc}$ , 2:3) to give compound **84** (0.98 g, 0.67 mmol, 85%) as yellow oil; IR (neat): 3026, 2827, 2733, 1697, 1595, 1562  $\text{cm}^{-1}$ ;  $^1\text{H}$  NMR (300 MHz,  $\text{CD}_2\text{Cl}_2$ ):  $\delta$  10.02 (s, 4H), 10.01 (s, 4H), 7.88–7.83 (m, 16H), 7.49 (d,  $J = 8.3$  Hz, 8H), 7.39 (d,  $J = 8.1$  Hz, 8H), 7.18 (s, 4H), 7.09 (d,  $J = 8.3$

Hz, 8H), 6.93-6.88 (m, 12H), 6.82-6.79 (m, 4 H) ppm;  $^{13}\text{C}$  NMR (75 MHz,  $\text{CD}_2\text{Cl}_2$ ):  $\delta$  192.1, 192.0, 148.7, 146.7, 142.0, 141.1, 139.4, 137.9, 136.3, 136.2, 135.6, 131.8, 131.7, 130.6, 130.2, 129.9, 128.6, 128.4, 125.8 ppm. HRMS (MALDI-TOF, positive mode)  $m/z$  calcd for  $\text{C}_{104}\text{H}_{68}\text{O}_8$  1444.4908, found 1444.4907  $[\text{M}]^+$ .

### Octa(DTF)-AQ 85



Octaaldehyde **84** (0.050 g, 0.034 mmol), 1,3-dithiole-2-thione **63** (0.20 g, 0.42 mmol), and  $\text{P(OEt)}_3$  (10 mL) were added to a 100 mL round-bottomed flask. The mixture was heated to 160 °C and kept stirring at this temperature for 3 h. After cooling the unreacted  $\text{P(OEt)}_3$  was removed by vacuum distillation, and the residue was subjected to silica gel column chromatography (hexanes/ $\text{CH}_2\text{Cl}_2$ , 4:1) to give compound **85** (0.045 g, 0.0092 mmol, 27%) as a yellow oil. IR (neat): 2953, 2923, 2852, 1571, 1544, 1504, 1464  $\text{cm}^{-1}$ ;  $^1\text{H}$  NMR (300 MHz,  $\text{CD}_2\text{Cl}_2$ ):  $\delta$  7.34-7.31 (m, 8H), 7.21-7.16 (m, 24H), 7.10-7.07 (m, 8H), 6.97-6.92 (m, 16H), 6.82-6.79 (m, 4H), 6.49 (s, 4H), 6.48 (s, 4H), 2.86-2.73 (m,

32H), 1.71-1.52 (m, 32H), 1.48-1.20 (m, 224H), 0.82-0.83 (m, 48H) ppm;  $^{13}\text{C}$  NMR (75 MHz,  $\text{CD}_2\text{Cl}_2$ ):  $\delta$  142.4, 141.2, 141.1, 139.9, 138.3, 138.1, 136.6, 136.18, 136.14, 136.0, 133.3, 133.2, 131.3, 129.9, 128.3, 128.1, 127.5, 127.1, 125.4, 125.2, 114.3, 36.68, 36.60, 32.5, 30.6, 30.4, 30.3, 30.2, 30.17, 30.14, 29.95, 29.93, 29.7, 29.17, 29.14, 29.10, 29.0, 23.3 ppm. HRMS (MALDI-TOF, positive mode)  $m/z$  calcd for  $\text{C}_{288}\text{H}_{405}\text{S}_{32}$  4887.2754, found 4887.2319  $[\text{M}+\text{H}]^+$ .

### 4.3.3 NMR Spectra for New Compounds

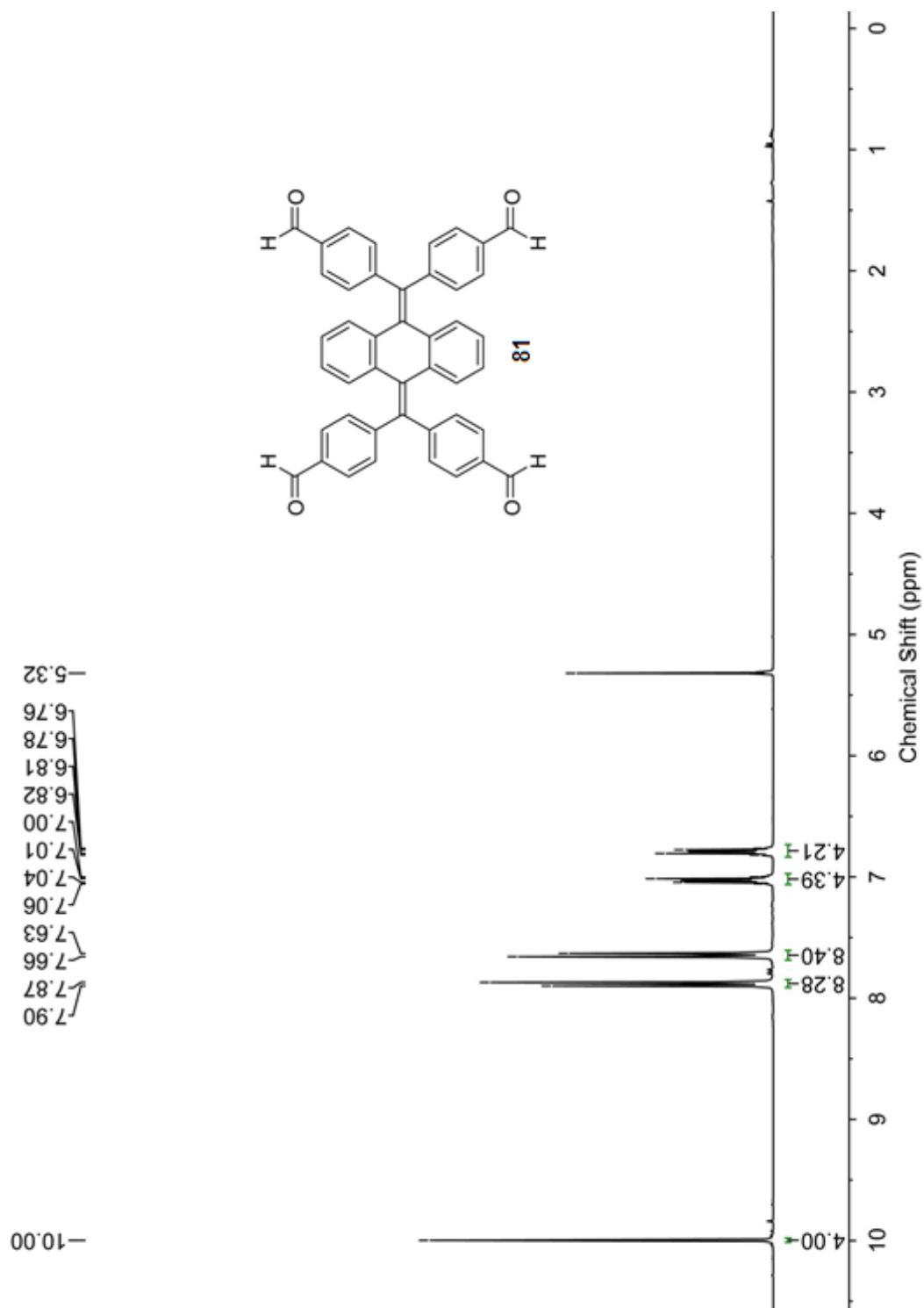


Fig. 4.5  $^1\text{H}$  NMR (300 MHz,  $\text{CD}_2\text{Cl}_2$ ) of compound **81**.

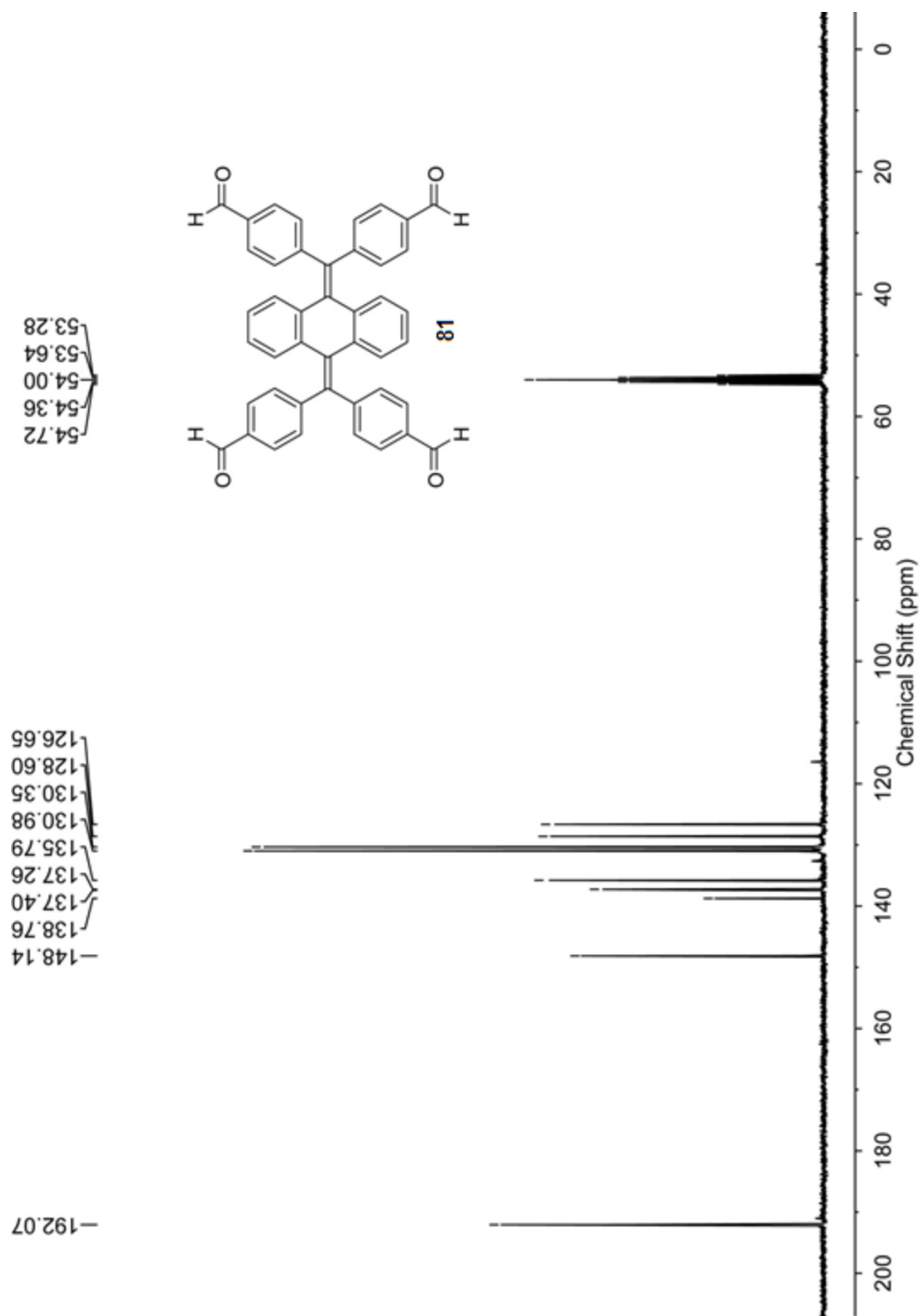


Fig. 4.6  $^{13}\text{C}$  NMR (75 MHz,  $\text{CD}_2\text{Cl}_2$ ) of compound **81**.

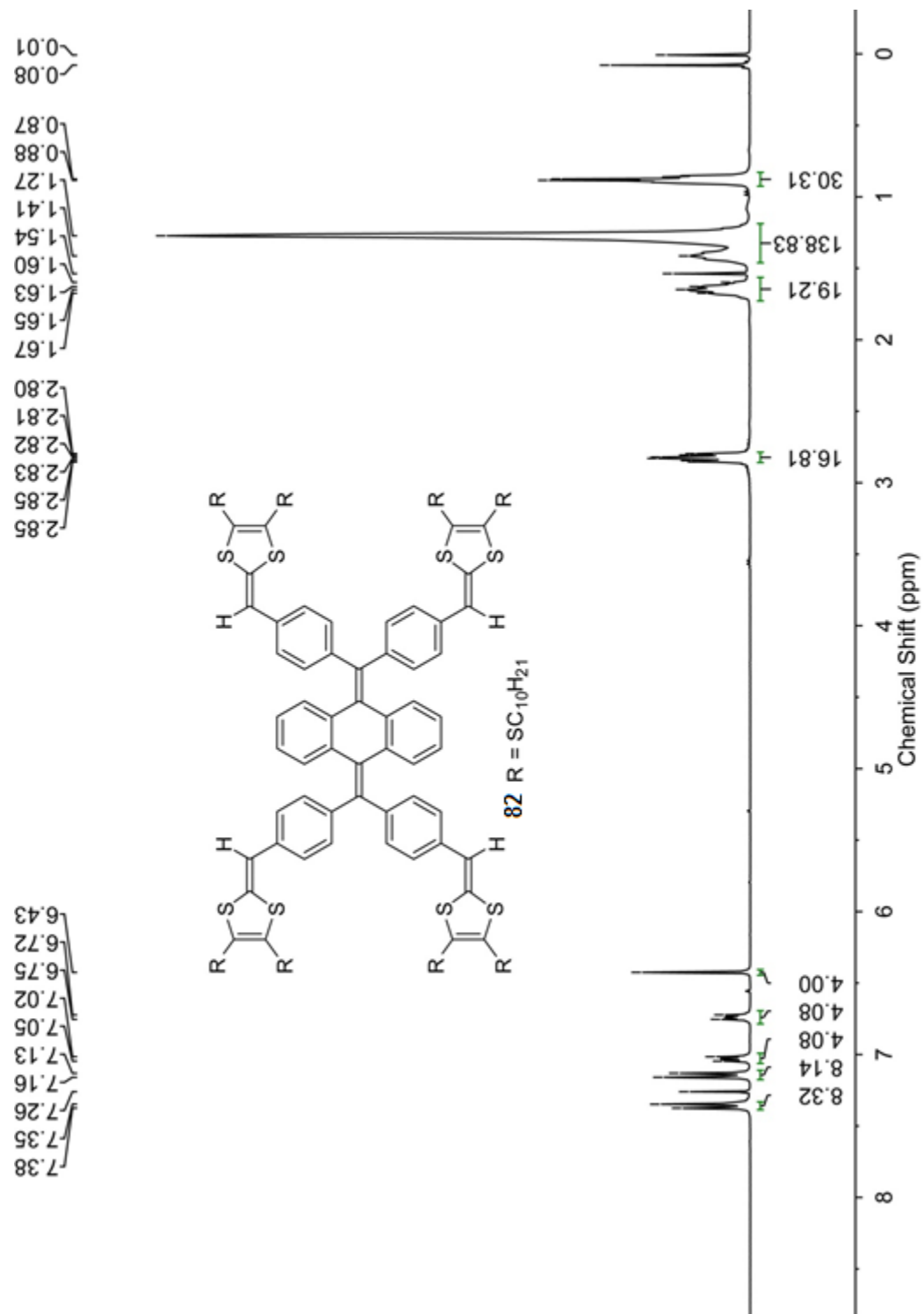


Fig. 4.7  $^1\text{H}$  NMR (300 MHz,  $\text{CDCl}_3$ ) of compound **82**.

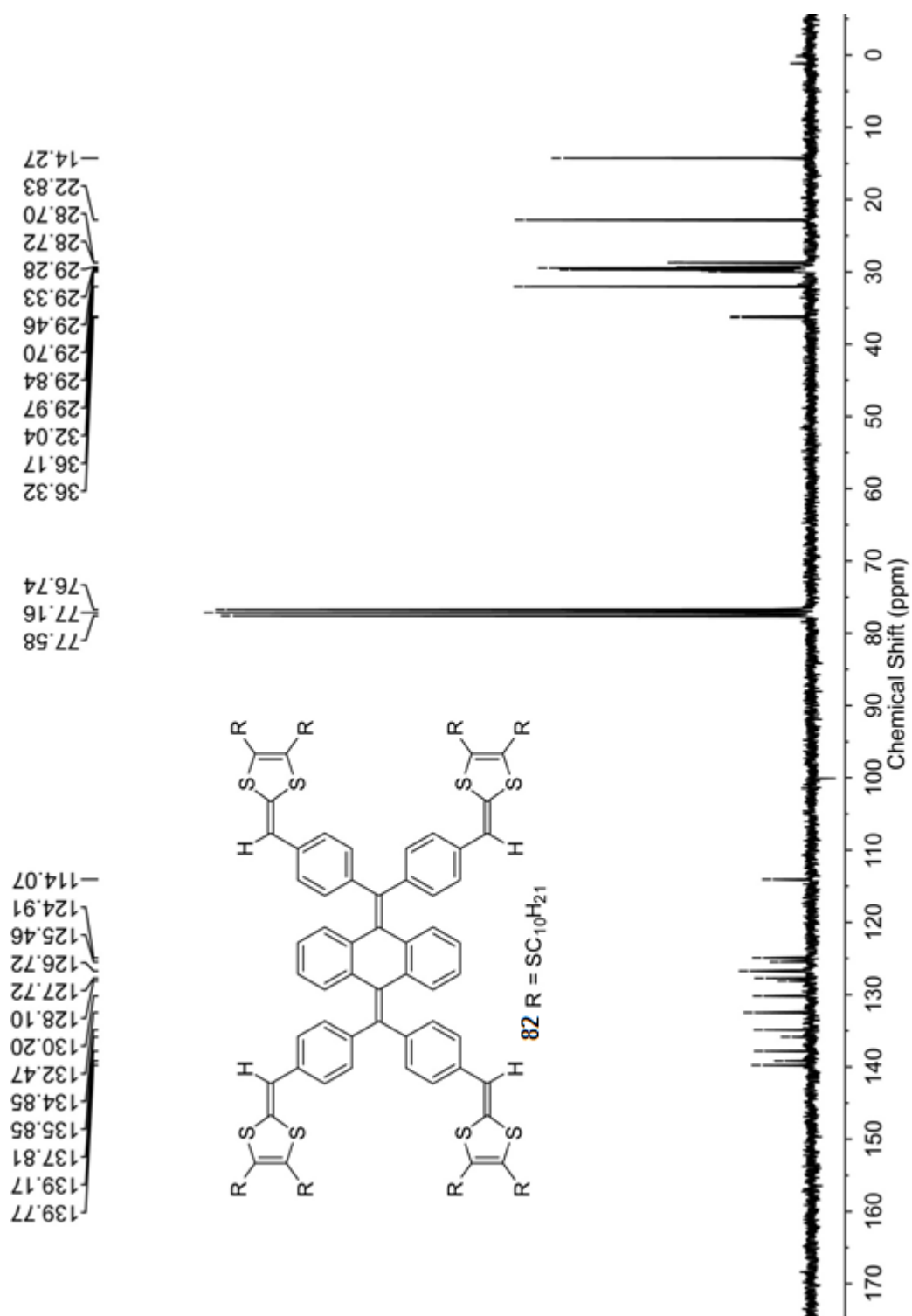
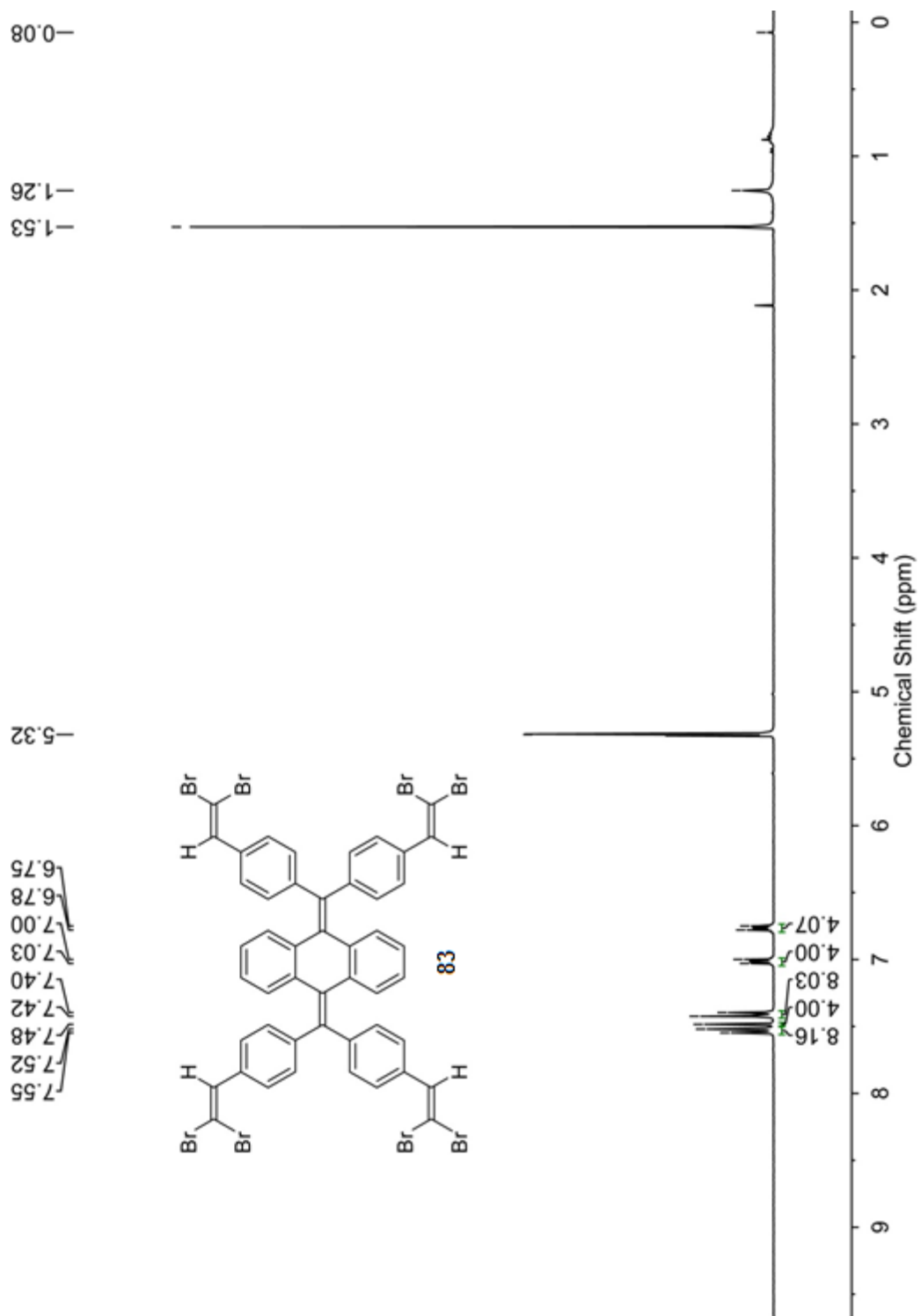
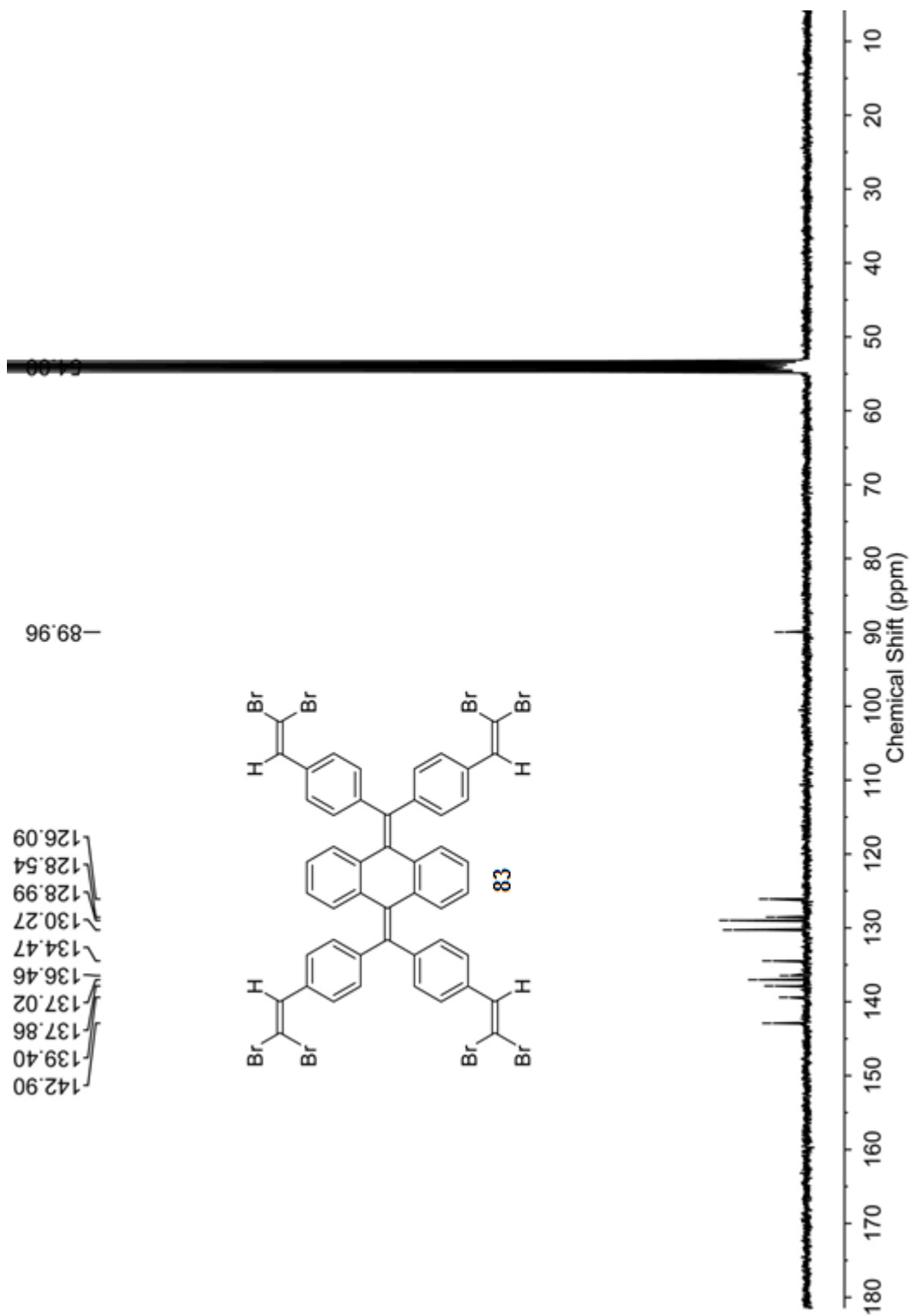


Fig. 4.8  $^{13}C$  NMR (75 MHz,  $CDCl_3$ ) of compound **82**.



**Fig. 4.9**  $^1\text{H}$  NMR (300 MHz,  $\text{CD}_2\text{Cl}_2$ ) of compound **83**.



**Fig. 4.10**  $^{13}\text{C}$  NMR (75 MHz,  $\text{CD}_2\text{Cl}_2$ ) of compound **83**.

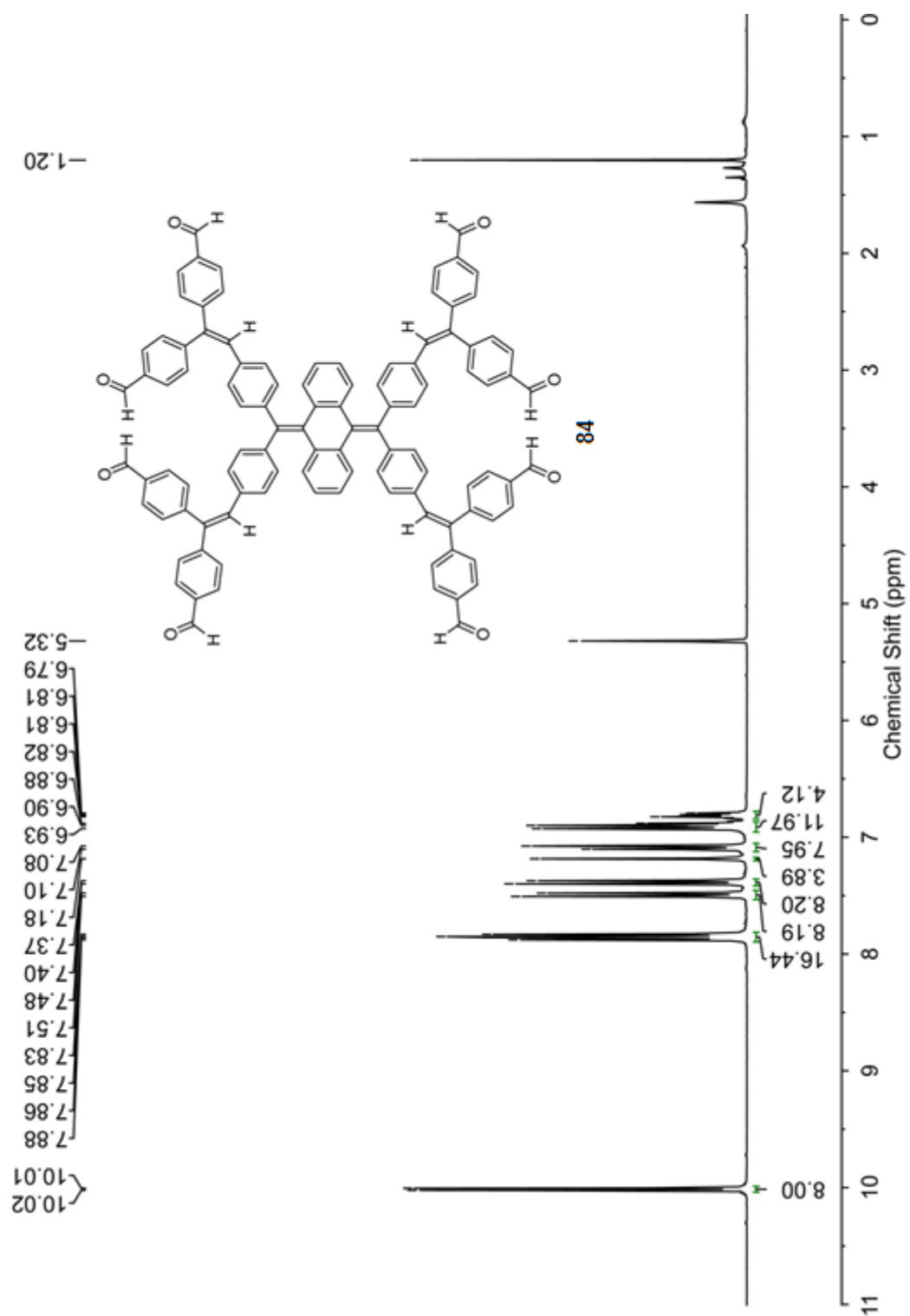
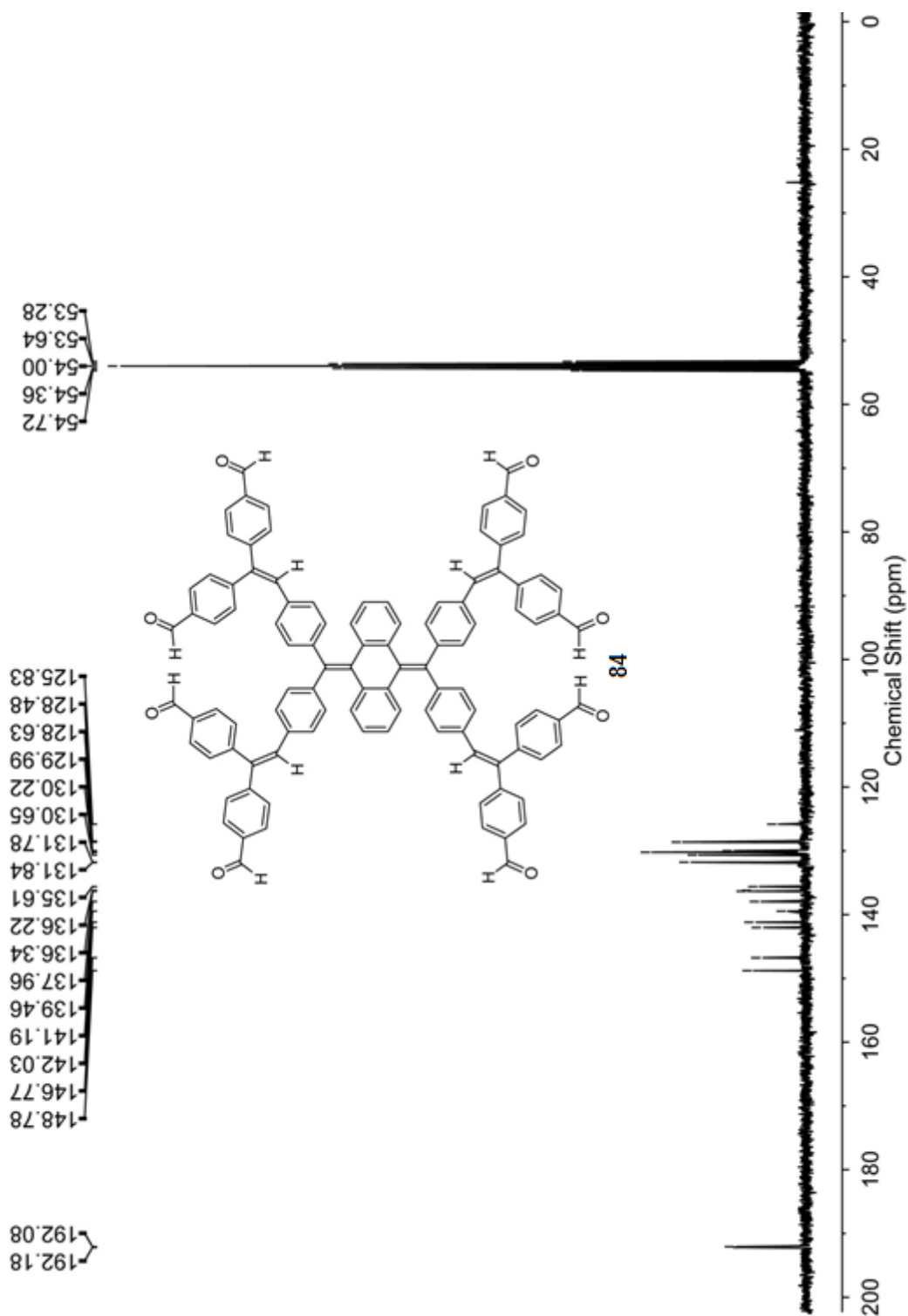


Fig. 4.11  $^1\text{H NMR}$  (300 MHz,  $\text{CD}_2\text{Cl}_2$ ) of compound **84**.



**Fig. 4.12**  $^{13}\text{C}$  NMR (75 MHz,  $\text{CD}_2\text{Cl}_2$ ) of compound **84**.

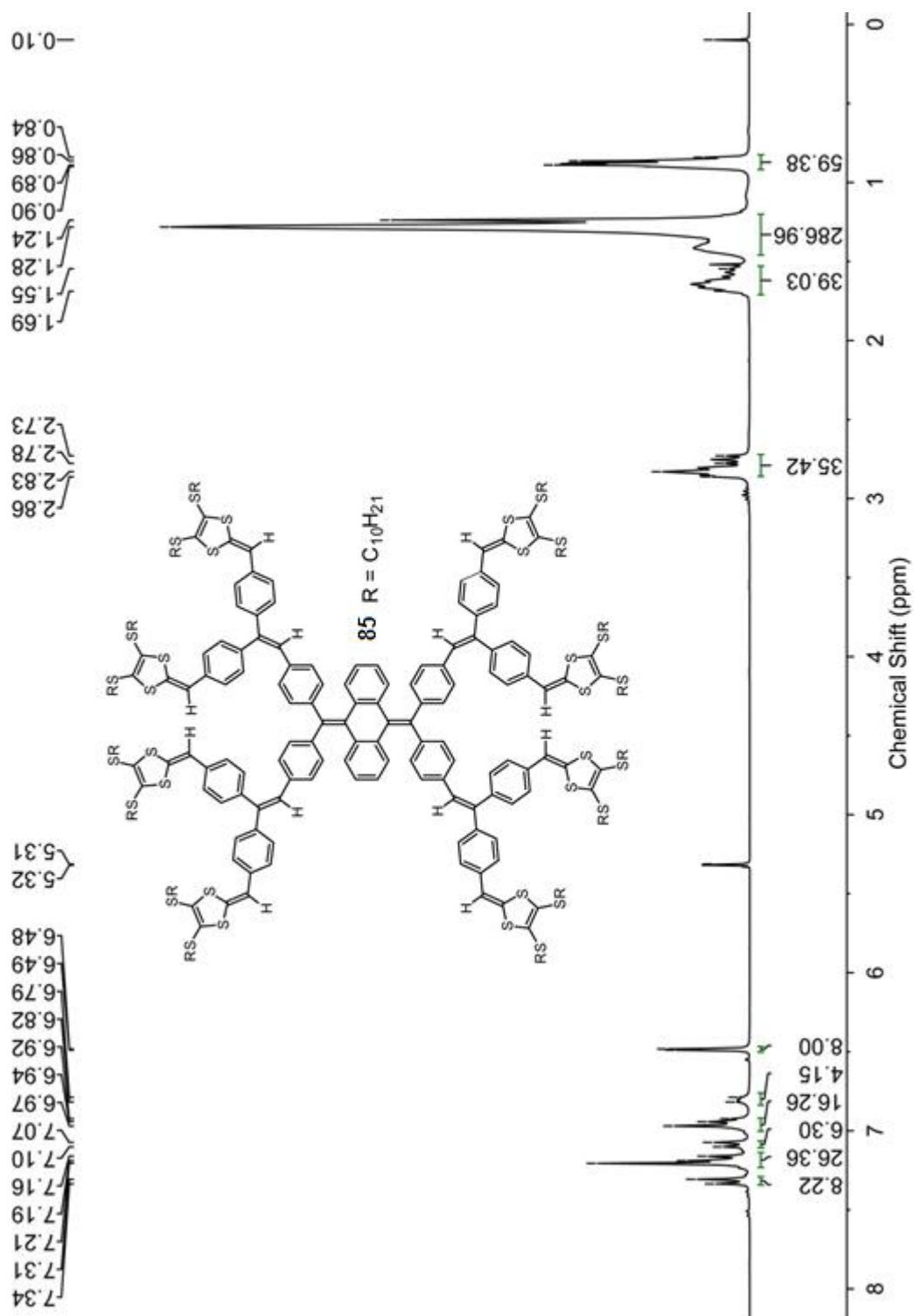


Fig. 4.13  $^1H$  NMR (300 MHz,  $CD_2Cl_2$ ) of compound **85**.

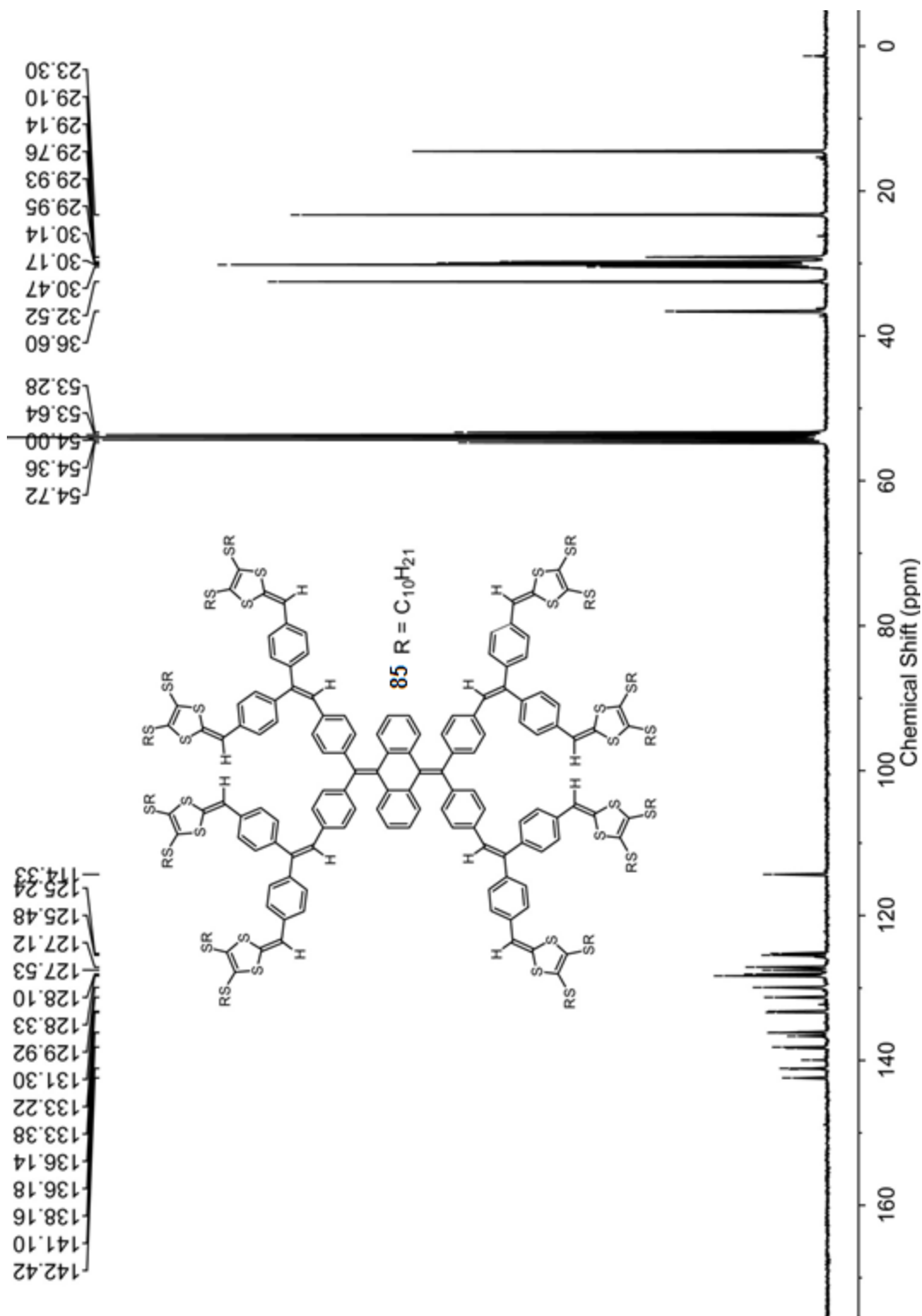
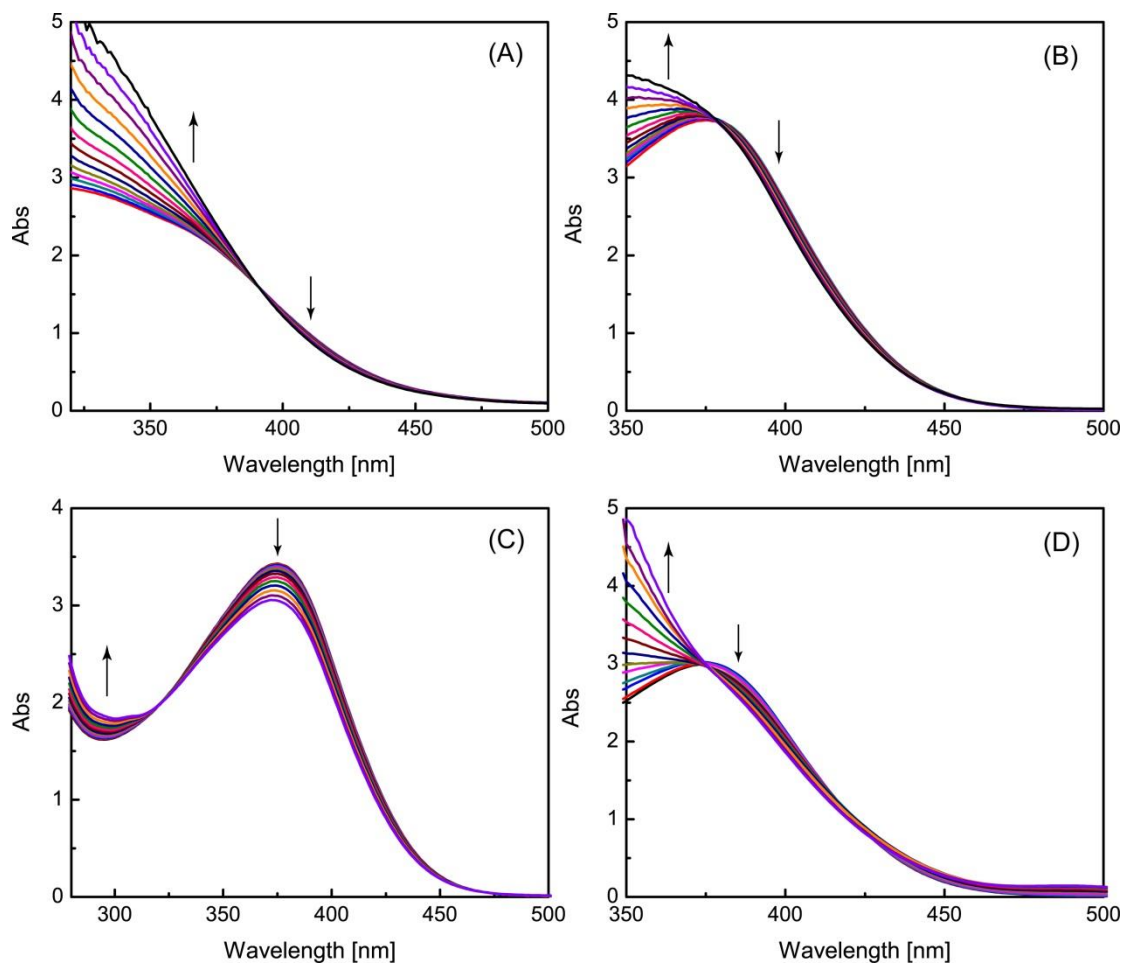


Fig. 4.14  $^{13}C$  NMR (75 MHz,  $CD_2Cl_2$ ) of compound **85**.

#### 4.3.4 UV-Vis Titration Studies

Tetrakis(DTF)-AQ **82** and Octa(DTF)-AQ **85** were subjected to UV-Vis titrations with nitrobenzene and three nitrobenzene derivatives (i.e., DNT, TNT, and picric acid) in  $\text{CHCl}_3$  respectively. The detailed results are summarized in Fig. 4.15 and Fig. 4.16.



**Fig. 4.15** UV-Vis titration profiles of compound **82** ( $42.7 \mu\text{M}$  in  $\text{CHCl}_3$ , 298 K) with (A) nitrobenzene (0 to 3.18 molar equiv), (B) 2,4-dinitrotoluene (0 to 2.15 molar equiv), (C) 2,4,6-trinitrotoluene (0 to 0.34 molar equiv), (D) picric acid (0 to 0.34 molar equiv).

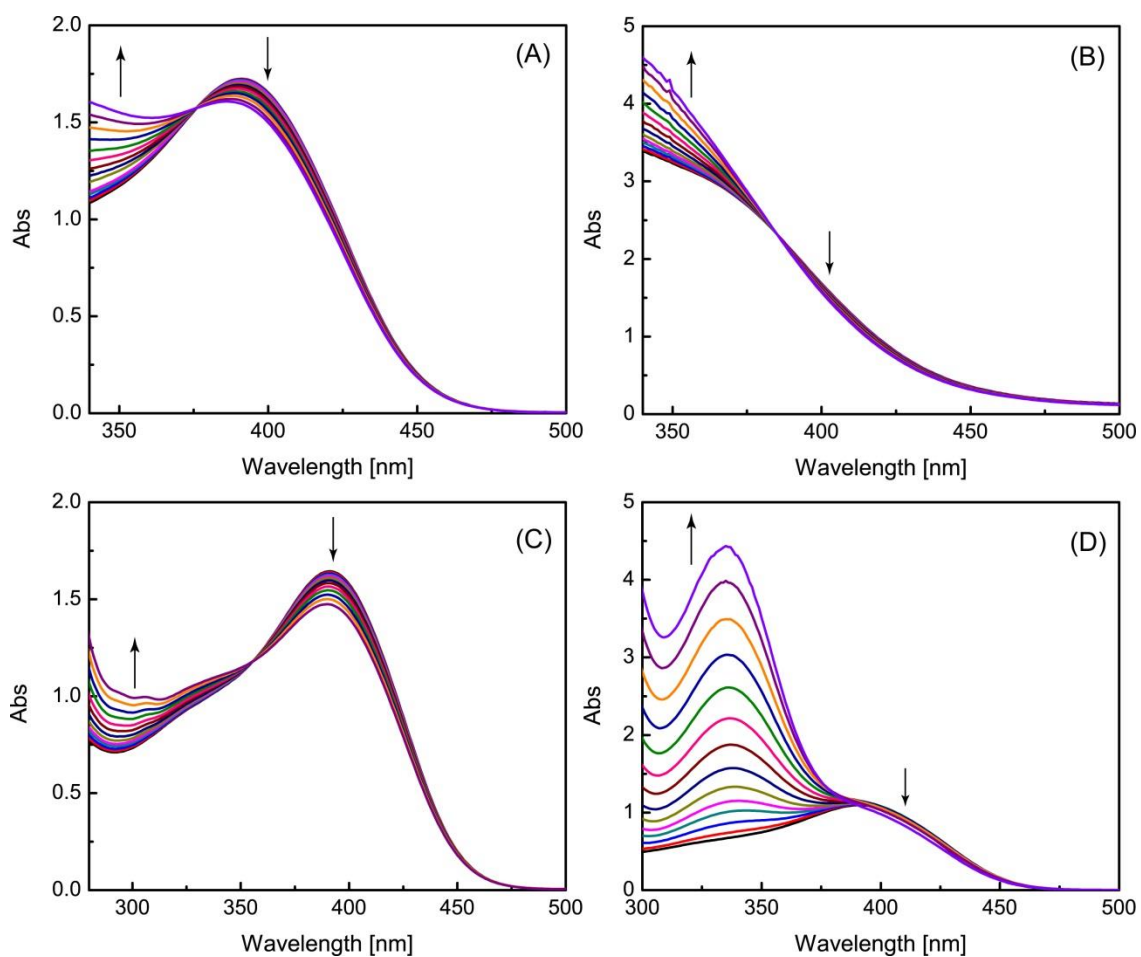


**Fig. 4.16** UV-Vis titration profiles of compound **85** (20.4  $\mu\text{M}$  in  $\text{CHCl}_3$ , 298 K) with (A) nitrobenzene (0 to 6.63 molar equiv), (B) 2,4-dinitrotoluene (0 to 4.48 molar equiv), (C) 2,4,6-trinitrotoluene (0 to 0.72 molar equiv), (D) picric acid (0 to 0.71 molar equiv).

### 4.3.5 Job Plot Analysis

Herein the binding stoichiometry of poly(DTF)-AQs with nitrobenzene derivatives was briefly studied by analyzing the Job's plot of oct-DTF **85** with nitrobenzene (NB) as a representative case, since not all the UV-Vis titration data in Fig. 4.15 and Fig. 4.16 show clear and significant spectral changes for detailed binding mode analysis. As shown in Fig. 4.17, the Job's plot was made by correlating  $A - \epsilon[\mathbf{85}]_0$  with the molar fraction of NB, where  $A$  is the observed absorbance at 390 nm,  $\epsilon$  is the extinction coefficient of **85**, and  $[\mathbf{85}]_0$  is the initial concentration of **85**.

Assuming that **85** and NB form a 1:1 complex (C) as shown in Eq. 4-1,



The observed absorbance at 390 nm can be expressed by Eq. 4-2, where  $\epsilon'$  and  $\epsilon''$  stand for the extinction coefficient of the complex (C) and NB respectively.

$$A = \epsilon [\mathbf{85}] + \epsilon'[\text{C}] + \epsilon''[\text{NB}] \quad (\text{Eq. 4-2})$$

Considering that  $\epsilon'' \approx 0$  at 390 nm and the actual concentration  $[\mathbf{85}] = [\mathbf{85}]_0 - [\text{C}]$ , the actual concentration of complex [C] can be thus expressed by Eq. 4-3, where the term,  $A - \epsilon [\mathbf{85}]_0$ , can be found to be directly proportional to [C].

$$[\text{C}] = (A - \epsilon [\mathbf{85}]_0) / (\epsilon' - \epsilon) \quad (\text{Eq. 4-3})$$

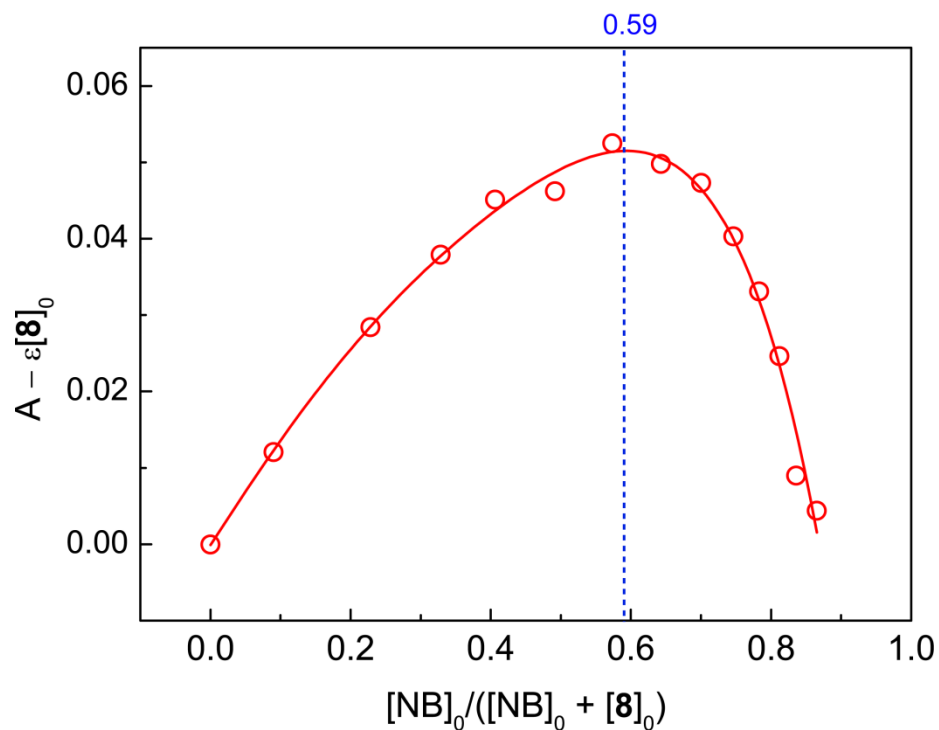


**Fig. 4.17** Job's plot for determination of the binding stoichiometry of octa(DTF)-AQ **85** with nitrobenzene (NB).

The Job's plot in Fig. 4.17 is fit with a polynomial function (5<sup>th</sup> order) and the maximum appears at the molar fraction = 0.59, which is slightly deviated from the ideal value of 0.5 for the 1:1 binding ratio. This result suggests that 1:1 is the dominant binding ratio, while 1:2 binding may also occur to some extent.

#### 4.4. Molecular Modeling Studies

The ground-state structures of tetrakis(DTF)-AQ **82**, octa(DTF) **85**, and the 1:1 complex of **82** and nitrobenzene (NB@**82**) were optimized by the semi-empirical PM6 method implemented in Gaussian 09 software package. The frontier molecular orbital (FMO) plots and eigenvalues of **82** and NB@**82** were computed by single-point density functional theory (DFT) calculations at the B3LYP/6-31G(d) level of theory. For all of the calculations, the SC<sub>10</sub>H<sub>21</sub> side chains in the compounds were replaced with hydrogen atoms to save computational expenses.

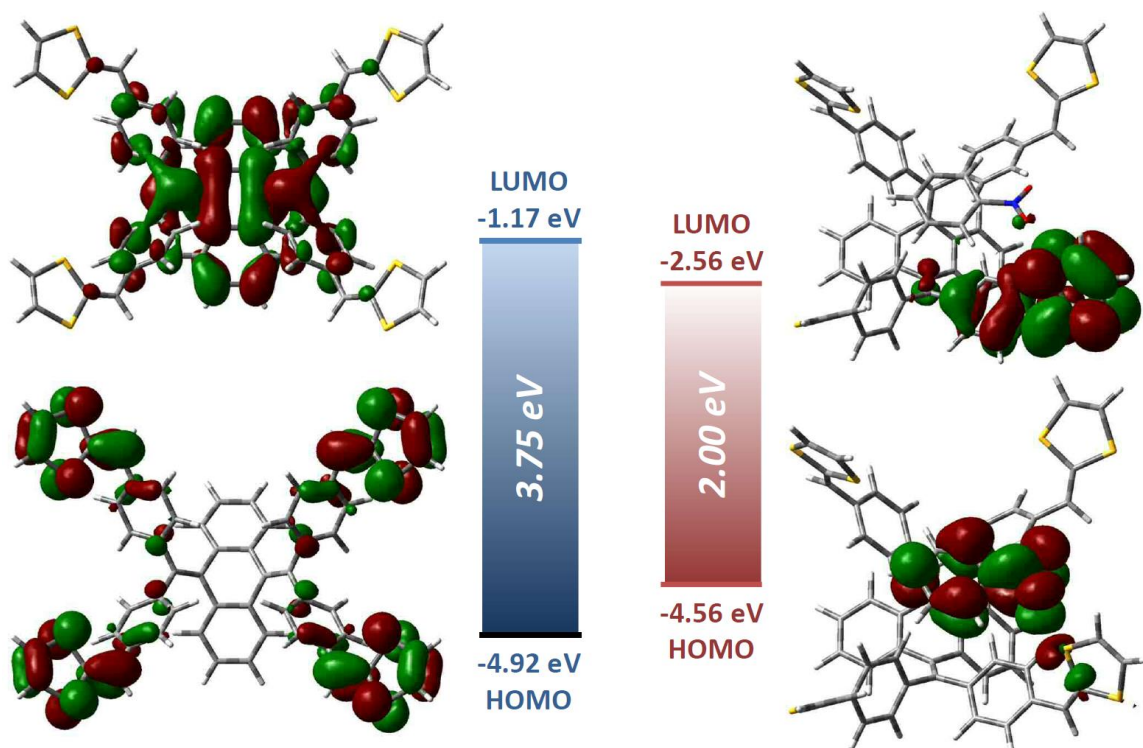


**Fig. 4.18** Optimized structures and FMOs of compound **82** (left) and the 1:1 supramolecular complex of NB@**82** (right). Structures optimized at the PM6 level and

single-point calculations done at the B3LYP/6-31G(d) level of theory. FMO countours are plotted at an isovalue of 0.02.

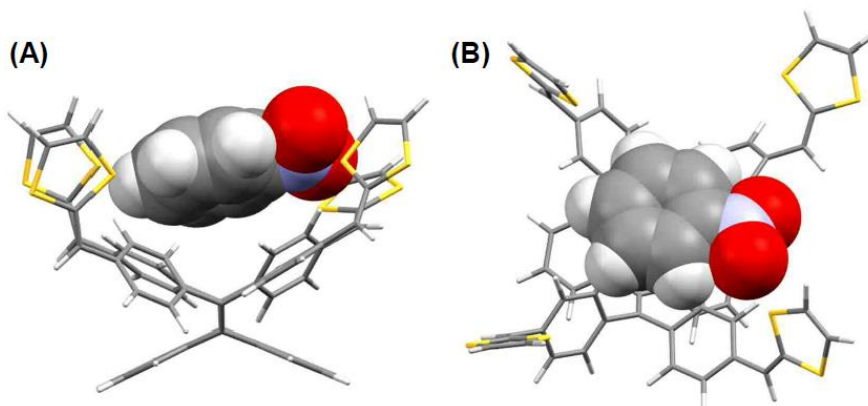


**Fig. 4.19** Molecular structure of the 1:1 complex of **82** and nitrobenzene (NB@**82**) optimized at the PM6 level. (A) Side view, (B) top view. The NB molecule is highlighted by the space-filling plot to better visualize the intermolecular interactions.

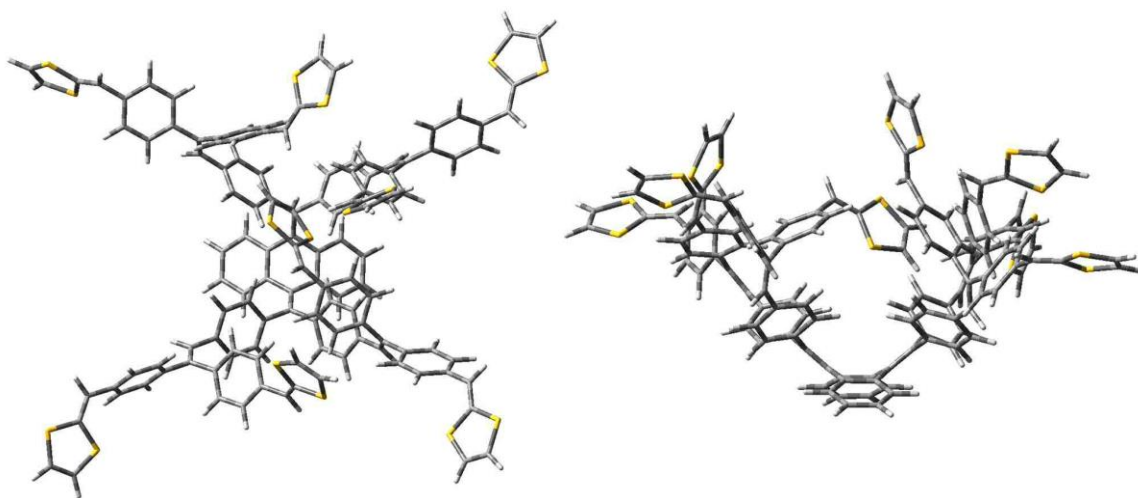


**Fig. 4.20** Molecular structure of compound **85** optimized at the PM6 level. (A) Top view, (B) side view.

#### 4.5. SEM Imaging of Poly-[82]

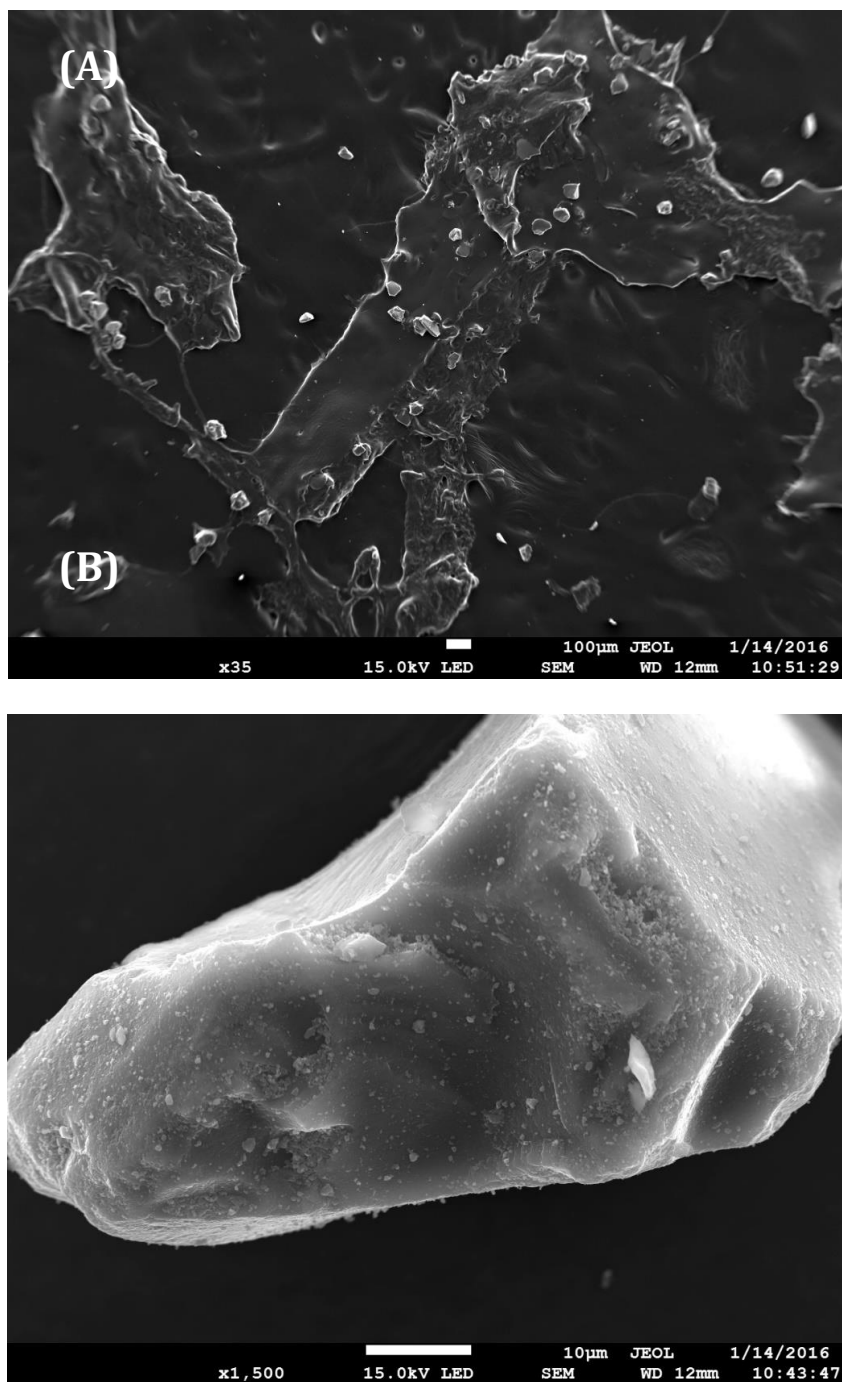


**Fig. 4.21** SEM images of poly-[82] generated by oxidative coupling reactions.

## 4.6 References

- (1) M. R. Bryce, *Chem. Soc. Rev.*, **1991**, 20, 355-390
- (2) S. Inagi, K. Naka and Y. Chujo, *J. Polym. Sci. Part A: Polym. Chem.*, **2007**, 45, 3770-3775
- (3) Y. Hou, G. Long, D. Sui, Y. Cai, X. Wan, A. Yu and Y. Chen, *Chem. Commun.*, **2011**, 47, 10401-10403
- (4) K. Guo, K. Yan, X. Lu, Y. Qiu, Z. Liu, J. Sun, F. Yan, W. Guo and S. Yang, *Org. Lett.*, **2012**, 14, 2214-2217.
- (5) A. Ohta and Y. Yamashita, *J. Chem. Soc., Chem. Commun.*, **1995**, 1761-1762
- (6) D. Lorcy, R. Carlier, A. Robert, A. Tallec, P. Le Magueres and L. Ouahab, *J. Org. Chem.*, **1995**, 60, 2443-2447
- (7) P. Hapiot, D. Lorcy, A. Tallec, R. Carlier and A. Robert, *J. Phys. Chem.*, **1996**, 100, 14823-14827
- (8) Y. Zhao, G. Chen, K. Mulla, I. Mahmud, S. Liang, P. Dongare, D. W. Thompson, L. N. Dawe and S. Bouzan, *Pure Appl. Chem.*, **2012**, 84, 1005-1025.
- (9) J. Massue, N. Bellec, M. Guerro, J.-F. Bergamini, P. Hapiot and D. Lorcy, *J. Org. Chem.*, **2007**, 72, 4655-4662
- (10) K. Mulla, H. Shaik, D. W. Thompson and Y. Zhao, *Org. Lett.*, **2013**, 15, 4532-4535
- (11) M. Khadem, J. C. Walsh, G. J. Bodwell and Y. Zhao, *Org. Lett.*, **2016**, 18, 2403-2406.

- (12) E. Gontier, N. Bellec, P. Brignou, A. Gohier, M. Guerro, T. Roisnel and D. Lorcy, *Org. Lett.*, **2010**, 12, 2386-2389
- (13) Y. Wang and Y. Zhao, *Beilstein J. Org. Chem.*, **2015**, 11, 957-965.
- (14) S. Liang, G. Chen, J. Peddle and Y. Zhao, *Chem. Commun.*, **2012**, 48, 3100-3102
- (15) S. Liang, Y. Zhao and A. Adronov, *J. Am. Chem. Soc.*, **2014**, 136, 970-977
- (16) S. Liang, G. Chen and Y. Zhao, *J. Mater. Chem. C*, **2013**, 1, 5477-5490.
- (17) G. Chen and Y. Zhao, *Org. Lett.*, **2014**, 16, 668-671.
- (18) D. Lorcy, L. Mattiello, C. Poriel and J. Rault-Berthelot, *J. Electroanal. Chem.*, **2002**, 530, 33-39
- (19) J. Roncali, *J. Mater. Chem.*, **1997**, 7, 2307-2321.
- (20) G. Chen, I. Mahmud, L. N. Dawe and Y. Zhao, *Org. Lett.*, **2010**, 12, 704-707
- (21) G. Chen, I. Mahmud, L. N. Dawe, L. M. Daniels and Y. Zhao, *J. Org. Chem.*, **2011**, 76, 2701-2715
- (22) Y. Wang and Y. Zhao, *Org. Biomol. Chem.*, **2015**, 13, 9575-9579
- (23) M. Khadem and Y. Zhao, *J. Org. Chem.*, **2015**, 80, 7419-7429.
- (24) E. Ripaud, P. Leriche, N. Cocherel, T. Cauchy, P. Frere and J. Roncali, *Org. Biomol. Chem.*, **2011**, 9, 1034-1040.
- (25) D. Wu, F. Xu, B. Sun, R. Fu, H. He and K. Matyjaszewski, *Chem. Rev.*, **2012**, 112, 3959-4015.
- (26) P. M. Budd, B. S. Ghanem, S. Makhseed, N. B. McKeown, K. J. Msayib and C. E. Tattershall, *Chem. Commun.*, **2004**, 230-231

- (27) A. Palma-Cando, G. Brunklaus and U. Scherf, *Macromolecules*, **2015**, 48, 6816-6824.
- (28) C. Gu, N. Huang, Y. Wu, H. Xu and D. Jiang, *Angew. Chem. Inter. Ed.*, **2015**, 54, 11540-11544
- (29) A. Raupke, A. Palma-Cando, E. Shkura, P. Teckhausen, A. Polywka, P. Gorrn, U. Scherf and T. Riedl, *Sci. Rep.*, **2016**, 6, 29118.
- (30) Y. Li, T. Liu, H. Liu, M.-Z. Tian and Y. Li, *Acc. Chem. Res.*, **2014**, 47, 1186.
- (31) C. A. Christensen, A. S. Batsanov and M. R. Bryce, *J. Org. Chem.*, **2007**, 72, 1301-1308.
- (32) S. Bouzan, G. Chen, K. Mulla, L. N. Dawe and Y. Zhao, *Org. Biomol. Chem.*, **2012**, 10, 7673-7676.
- (33) Gaussian 09, Revision E.01, M. J. Frisch, G. W. Trucks, H. B. Schlegel, G. E. Scuseria, M. A. Robb, J. R. Cheeseman, G. Scalmani, V. Barone, B. Mennucci, G. A. Petersson, H. Nakatsuji, M. Caricato, X. Li, H. P. Hratchian, A. F. Izmaylov, J. Bloino, G. Zheng, J. L. Sonnenberg, M. Hada, M. Ehara, K. Toyota, R. Fukuda, J. Hasegawa, M. Ishida, T. Nakajima, Y. Honda, O. Kitao, H. Nakai, T. Vreven, J. A. Montgomery, Jr., J. E. Peralta, F. Ogliaro, M. Bearpark, J. J. Heyd, E. Brothers, K. N. Kudin, V. N. Staroverov, R. Kobayashi, J. Normand, K. Raghavachari, A. Rendell, J. C. Burant, S. S. Iyengar, J. Tomasi, M. Cossi, N. Rega, J. M. Millam, M. Klene, J. E. Knox, J. B. Cross, V. Bakken, C. Adamo, J. Jaramillo, R. Gomperts, R. E. Stratmann, O. Yazyev, A. J. Austin, R. Cammi, C. Pomelli, J. W. Ochterski, R. L. Martin, K. Morokuma, V. G. Zakrzewski, G. A. Voth, P. Salvador, J. J. Dannenberg, S. Dapprich, A. D. Daniels, .

Farkas, J. B. Foresman, J. V. Ortiz, J. Cioslowski, and D. J. Fox, *Gaussian, Inc.*, Wallingford CT, **2009**.

(34) GaussView, Version 5, R. Dennington, T. Keith, and J. Millam, *Semichem Inc.*, Shawnee Mission, KS, **2009**.

(35) Z.-Q. Chen, T. Chen, J.-X. Liu, G.-F. Zhang, C. Li, W.-L. Gong, Z.-J. Xiong, N.-H. Xie, B. Z. Tang and M.-Q. Zhu, *Macromolecules*, **2015**, 48, 7823-7835

(36) S. Pola, C. Kuo, W. Peng, M. M. Islam, I. Chao and Y. Tao, *Chem. Mater.*, **2012**, 24, 2566–2571.

(37) A. J. Moore and M. R. Bryce, *Tetrahedron Lett.*, **1992**, 33, 1373-1376.

# Chapter 5

## Synthesis of New DTF and TTFV Derivatives

The current chapter describes other synthetic projects conducted during this PhD thesis work. Unlike the results reported in the previous three chapters, the projects outlined below have only attained preliminary and premature conclusions; however, these results show potential to be further developed to add new knowledge to DTF and TTFV-related synthetic and materials chemistry.

### 5.1 Introduction

As demonstrated in the previous chapters, DTF and TTFV groups have been functionalized to provide various  $\pi$ -rich molecular systems ranging from linearly conjugated polymers/oligomers to shape-persistent macrocycles and dendrimers. In the projects, transition metal-catalyzed coupling reactions are often used to assemble the major  $\pi$ -backbones in multiple steps. Electron-donating DTF and/or TTFV groups are attached to or embedded in the molecular backbones at different synthetic stages. According to the detailed synthetic targets and the compatibility of DTF/TTFV with the reaction conditions. Recent studies carried out in the Zhao group have shown that Sonogashira-Hagihara cross coupling reactions usually give low yields when the substrates are pre-installed with DTF groups. It is reasoned that the sulfur atoms of DTF may also act as ligands to interact with the Pd(0) and Cu(I) species to deactivate the

Pd/Cu catalytic system. As such, most of the successful synthetic routes to DTF/TTFV functionalized  $\pi$ -conjugated systems have the DTF and TTFV functionalization planned) as late as possible to avoid the poor compatibility of Sonogashira-Hagihara coupling with DTF/TTFV groups. Nevertheless, Pd-catalyzed cross-coupling reactions have been a very efficient methodology for assembling diverse  $\pi$ -conjugated systems. If a particular type of Pd-catalyzed coupling reaction can be found to well tolerate to the presence of DTF/TTFV groups, it will greatly enhance the synthetic flexibility and scope for DTF/TTFV containing  $\pi$ -conjugated molecular and macromolecular materials. Efforts to investigate in this respect will also be of great benefit to the applications of new DTF/TTFV derivatives in materials science and nanotechnology.

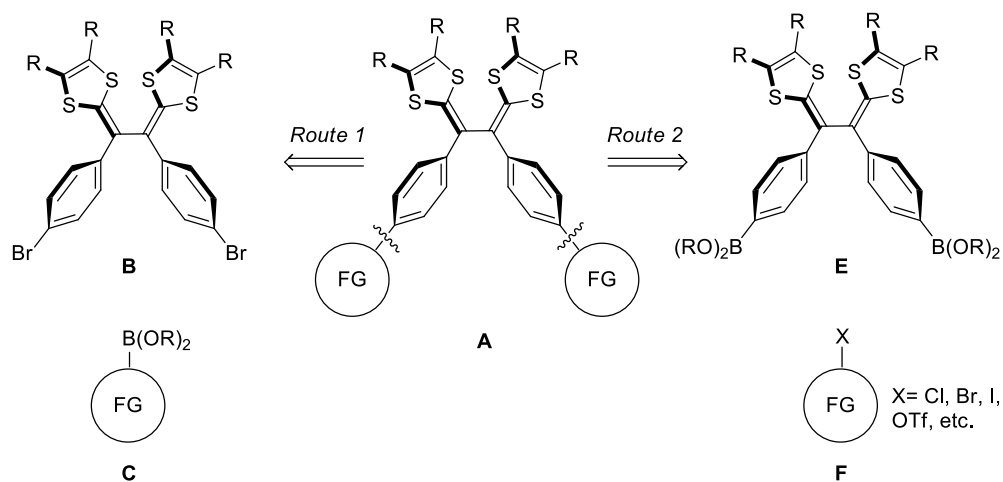
The Suzuki-Miyaura cross coupling<sup>1</sup> is well-established and abundantly utilized methodology in modern synthetic chemistry. The scope of this type of coupling reaction has encompassed many fields ranging from pharmaceuticals, synthetic polymers, biomolecules, to nanomaterials. Compared with Sonogashira-Hagihara coupling, the Suzuki reactions are more compatible with different substrates and reaction conditions (e.g., solvents, temperature). Based on the previous experimental results, it was envisioned that the Suzuki-Miyaura cross coupling after suitable modifications would become a useful methodology to directly link other organic functional groups (e.g., donors/acceptors, synthetic receptors, extended  $\pi$ -oligomers) to the substrates containing DTF and TTFV groups. If this goal can be achieved, the synthetic toolbox for DTF/TTFV based molecular materials will be considerably expanded. In this regard, synthetic efforts to functionalize TTF using the Suzuki reaction as the key ligation step have been made

during the process of this PhD thesis work. The following sections discuss results that have been achieved and some unexpected outcomes observed.

## 5.2. Results and Discussion

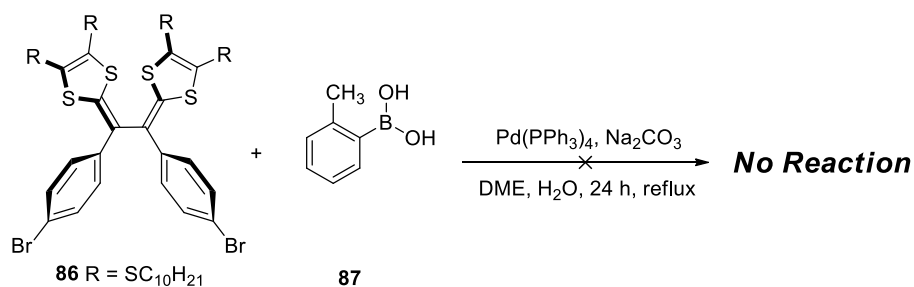
### 5.2.1 Direct Functionalization of Diphenyl-TTFV through Suzuki-Miyaura Cross Coupling

At the outset of the projects carried out in this chapter, two general and modular functionalization strategies were conceived for the synthesis of various functionalized TTFV derivatives through the Suzuki coupling reactions as illustrated Scheme 5.1. In the first approach (route 1), bis(*p*-bromophenyl)-TTFV **B** and a boron-based counterpart **C** constitute the two synthetic precursors for the coupling reaction. Compound **B** can be easily prepared from an inexpensive precursor, *p*-bromobenzaldehyde, *via* the phosphite-promoted olefination reaction successfully demonstrated in the previous chapters, while compound **C** can be of a large variety given the abundance of commercially available boronic acid and boronate building blocks. Alternatively, a second retrosynthetic approach can be executed through the Suzuki coupling of bis(boronic acid) or bis(boronate)-substituted TTFV **E** and an organohalide **F**.



**Scheme 5.1** Retrosynthesis of TTFV derivatives through two Suzuki coupling approaches.

Scheme 5.2 shows the Suzuki coupling between bis(*p*-bromophenyl)-TTFV **86** and *o*-tolylboronic acid (**87**) in the presence of tetrakis(triphenylphosphine)palladium(0) as catalyst.



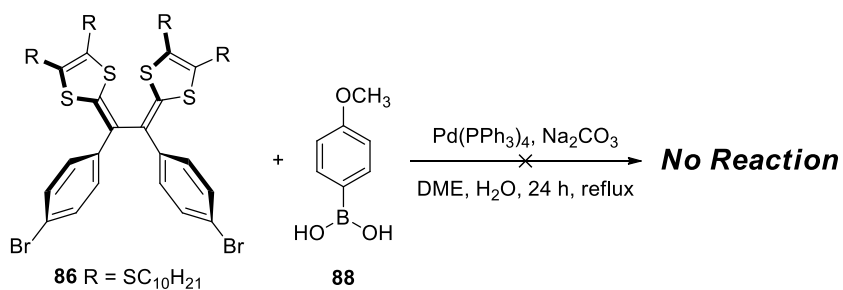
**Scheme 5.2** Attempted Suzuki coupling between TTFV **86** and boronic acid **87**.

The outcome of this reaction was, however, disappointing; there was no cross-coupling products formed. The unsuccessful synthesis can be ascribed to number of

reasons. First, the quality of the Pd(0) catalyst used could be poor, judged upon its color. The color of freshly prepared, active Pd(0) catalyst should be yellow to greenish. The actual color of Pd(0) catalyst used in the initial synthesis was brownish, which is indicative of somewhat degradation of the catalyst. Tetrakis(triphenylphosphine)palladium(0) was first prepared by Lamberto Malatesta *et al.*<sup>2</sup> in the 1950s by reduction of sodium chloropalladate with hydrazine in the presence of triphenylphosphine. Although commercially available, the use of directly purchased tetrakis(triphenylphosphine)palladium(0) needs to be treated with care. After exposure to air and moisture for a certain period of time, the Pd(0) catalyst can decompose significantly to be less active or even inactive in promoting cross-coupling reactions. Upon this consideration, fresh tetrakis(triphenylphosphine)palladium(0) was prepared and then used immediately as catalyst for the Suzuki coupling of **86** and **87**. The preparation of tetrakis(triphenylphosphine)palladium(0) was done in two steps from PdCl<sub>2</sub> as described in eq. 5.1 and 5.2. Experimentally, it was done in a one-pot manner under the protection of nitrogen or argon gas. Hydrazine was employed as an reducing agent. Once prepared, the catalyst was rapidly washed with ethanol and then diethyl ether to yield yellow-colored crystals. It was then kept in a vial under inert gas protection prior to use.



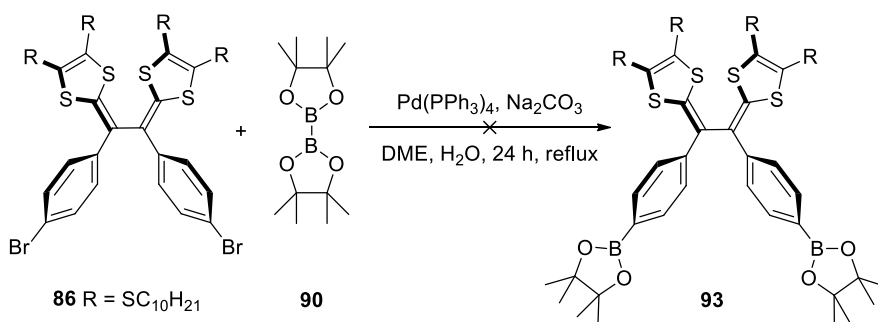
With the freshly prepared Pd(0) catalyst, the Suzuki coupling reaction between compound **86** and **87** was still unsuccessful. Clearly, the catalyst is not the reason for the failed synthesis. It was then reasoned that the boronic acid substrate **87** may have some “hindrance” coming from the *ortho*-methyl group, which impedes the cross-coupling reaction. To remove the steric effect, *p*-methoxyphenylboronic acid (**88**) was tested as a substrate to under Suzuki coupling with TTFV **86** (Scheme 5.3). which that was failed (Scheme 5.2). Unfortunately, this reaction ended with no yield of the desired cross-coupled products.



**Scheme 5.3** Attempted Suzuki coupling reaction for TTFV **86** with boronic acid **88** under the catalysis of freshly prepared Pd(0) catalyst.

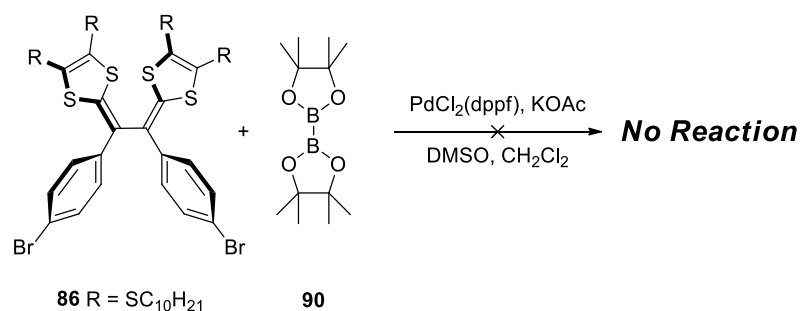


Alternatively, the second synthetic approach (route 2, Scheme 5.1) was investigated, in which the bromo groups on compound **86**<sup>3,4</sup> were switched to boronic acid ester. It was hoped that the boronate-substituted TTFV target **93** would react more efficiently with certain aryl halides (e.g., aryl iodide) to give reasonable yields for the cross-coupled products. The attempt to convert dibromo-TTFV **86** to bis(boronate)-TTFV **93** under the Pd(0) catalysis, however, ended with failure (Scheme 5.5).



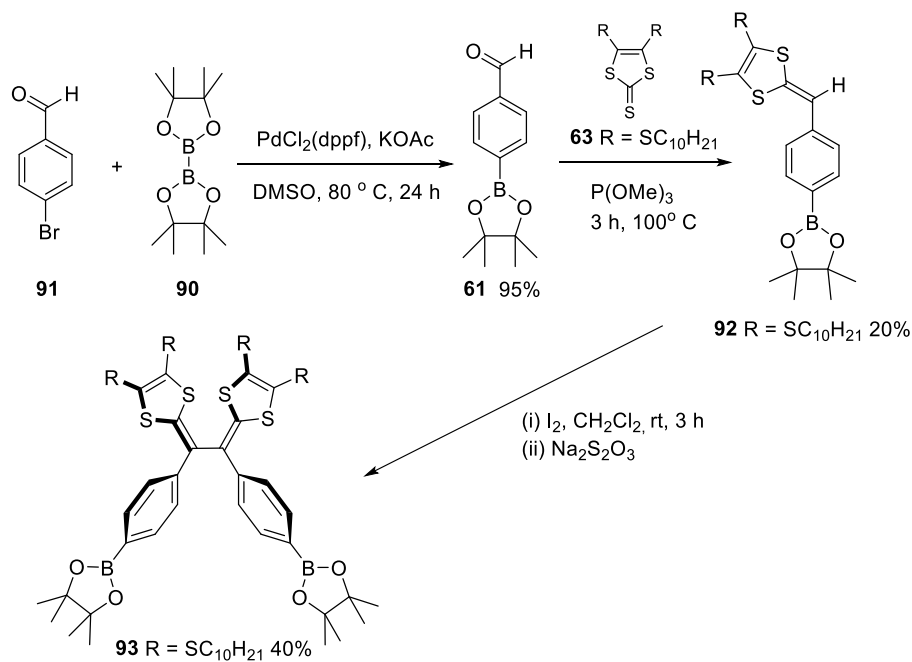
**Scheme 5.5** Attempted conversion of dibromo-TTFV **86** into bis(boronate)-TTFV **89** under the catalysis of freshly prepared Pd(0) catalyst.

It was reported the use of other Pd catalysts, for example 1,1'-Bis(diphenylphosphino)ferrocene]palladium(II) dichloride, could improve the yield of boronation reactions. As shown Scheme 5.6, the experimental results seems to suggest that such Pd(II) catalyst is not applicable to the boronation of **86**.



**Scheme 5.6** Attempted conversion of dibromo-TTFV **86** into bis(boronate)-TTFV **89** under the catalysis of PdCl<sub>2</sub>(dppf).

To circumvent the difficulty in direct boronation on TTFV **86**, the synthesis of **93** was re-routed to a lengthier approach as shown in Scheme 5.7. Herein, *p*-bromobenzaldehyde (**91**) was first converted into boronate **61** under the catalysis of PdCl<sub>2</sub>(dppf). The reaction was accomplished with an excellent yield of 95%. Compound **61** was then subjected to phosphite-promoted olefination with 1,3-dithio-2-thione **63** to give boronate-substituted DTF **92** in a mediocre yield of 20%. The low yield is tentatively ascribed to the high Lewis acidity of the boronate group in **61**, which may interact with P(OMe)<sub>3</sub> (a Lewis base). DTF **92** was then subjected to oxidative dimerization in the presence of iodine. The reaction did afford product **93**, but it was of low yield and could not be readily separated from numerous by-products to attain good purity. At this juncture, the low yield of intermediate **92** and the complex side-reactions concomitant with the formation of **93** made this synthetic approach not useful.

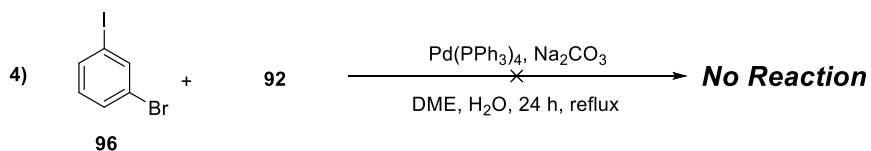
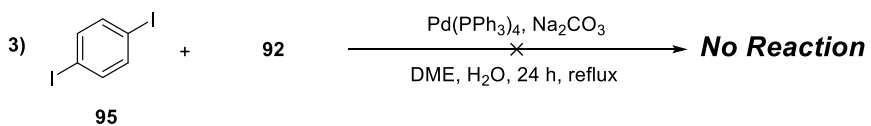
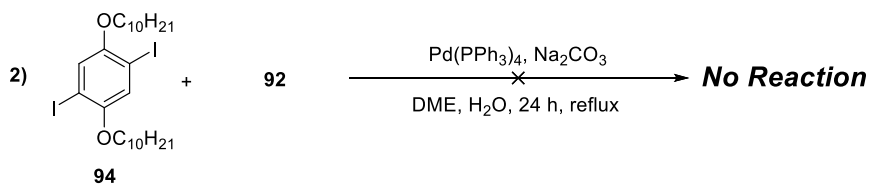
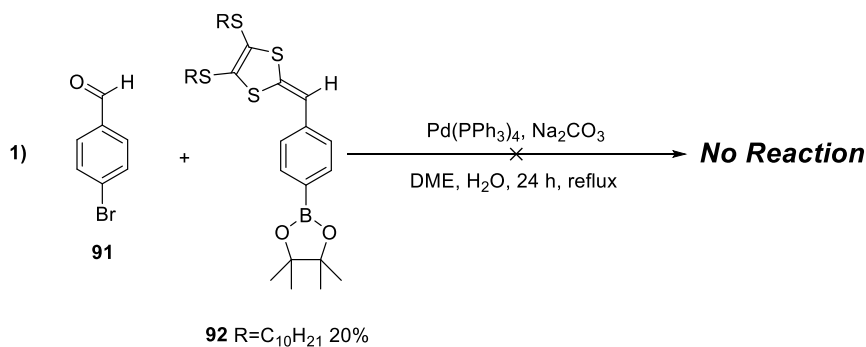


**Scheme 5.7** An alternative synthetic approach to bis(boronate)-TTFV **93**.

### 5.2.2 Direct Functionalization of Phenyl-DTF through Suzuki-Miyaura Cross Coupling

The major challenges in the above direct boronation reactions are tedious synthetic steps, low reactivity, and difficult purification.<sup>5,6</sup> In addition, the Pd-catalyzed conditions seem to be incompatible with the TTFV moiety. Should this problem persist in the case of substrates containing DTF groups? To address this concern, boronate-DTF **92** was subjected to a series of Suzuki coupling reactions with various aryl halides, and the results are summarized in Scheme 5.8. Again, like the previous synthetic attempts, these Suzuki coupling reactions were unsuccessful in producing desired cross-coupled products.

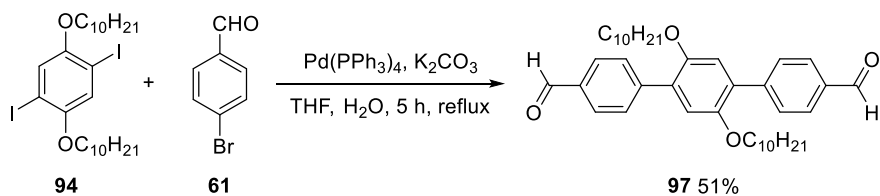
Since all above Suzuki-Miyaura cross-coupling reactions on DTF and TTFV containing substrates failed to give meaningful results, it was clear that typically used Suzuki coupling conditions (catalyst, base, solvent, etc.) are not compatible with the DTF and TTFV groups. The electron-donating properties and the strong ligand effects of the sulfur atoms are believed to be problematic in these reactions. Therefore, it is advised to avoid the use of Pd(0) catalyzed cross-coupling reactions (Sonogashira-Hagihara, Suzuki Miyaura) when the reactants contain DTF/TTFV groups. Methodological development is warranted in the future work; however, this is not expected to be an easy task to undertake.



**Scheme 5.8** Attempted Suzuki coupling reactions of boronate-DTF **92** with various aryl halides.

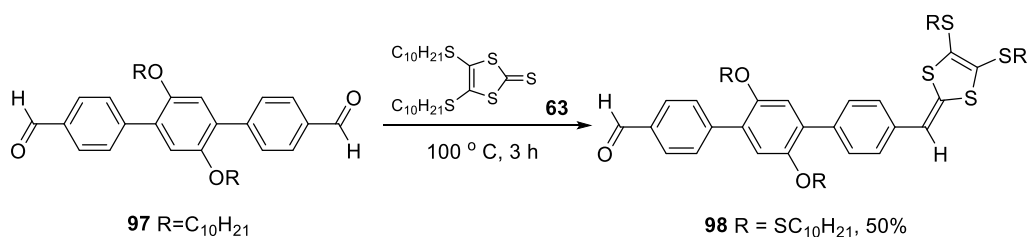
### 5.2.3 Functionalization of Phenylene Oligomers with DTF End Groups

Oligo(*p*-phenylene)s are an important class of  $\pi$ -conjugated oligomers that have attracted enormous research owing to their fascinating electronic and photophysical properties. Addition of electron-donating terminal groups, such as DTFs, to an oligo(*p*-phenylene) chain was expected to give novel redox-activity and charge transfer properties. To shed light on this issue, a synthetic project on DTF-endcapped oligo(*p*-phenylene)s was launched. Scheme 5.9 shows the synthesis of a phenylene trimer **97** through a Suzuki coupling reaction between *p*-bromobenzaldehyde (**61**) and 1,4-didecyloxy-2,5-diodobenzene (**94**). A successful Suzuki coupling in absence of TTFV or DTF groups (Scheme 5.9) was achieved.



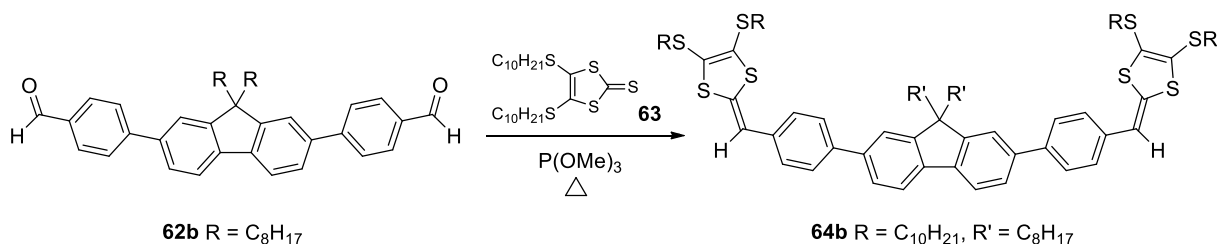
**Scheme 5.9** Synthesis of oligo(*p*-phenylene)s **97** through Suzuki coupling.

Compound **97** was carried on to the phosphite-promoted olefination reaction with 1,3-dithio-2-thione **63** at 100 °C to yield a mono-DTF compound **98** (Scheme 5.10).



**Scheme 5.10** Synthesis of mono-DTF functionalized oligo(*p*-phenylene)s **98**.

Chronologically, this selective mono-olefination reaction preceded similar olefination reactions reported in Chapters 2-4 and it actually formed the synthetic strategy recurrently used therein. In Chapter 2, the initial synthesis of fluorene-based dialdehyde **62b** through Suzuki coupling was very successful, but the subsequent olefination reaction was problematic when performed at 100 °C. Optimization of the reaction conditions for this olefination was investigated (Scheme 5.11 and Table 5.1). The results show that the olefination of **62b** performed at 145 °C for 2 hours gives the highest yield.<sup>7</sup>



**Scheme 5.11** Phosphite-promoted olefination reaction of compound **62b**.

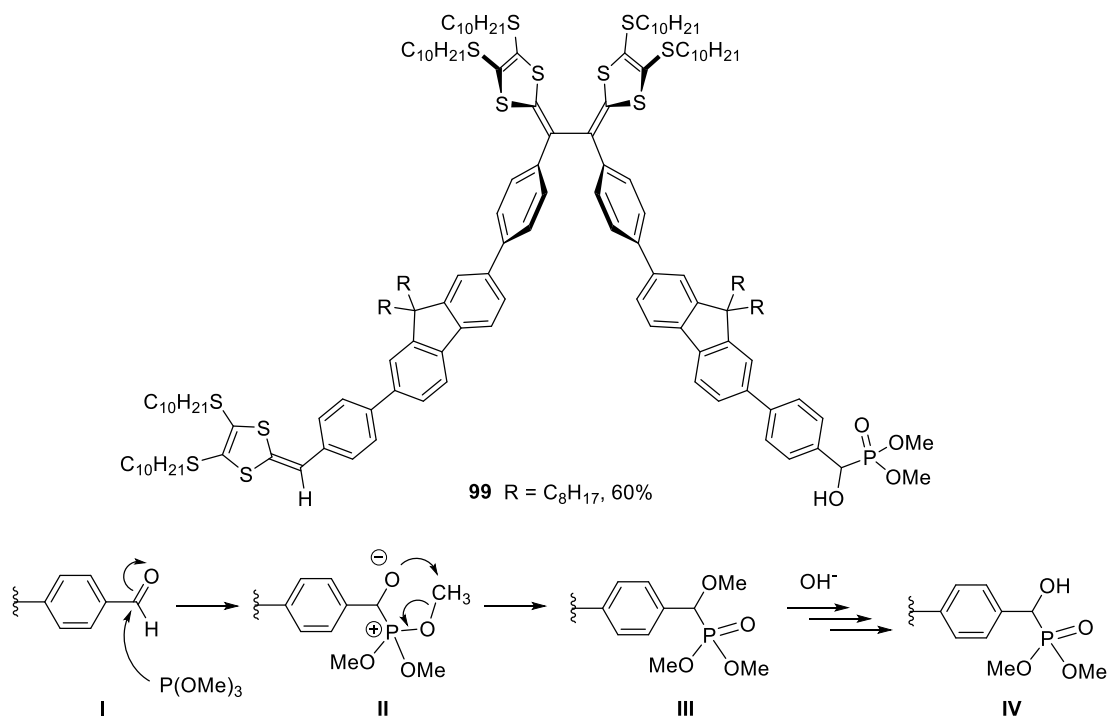
**Table 5.1** Optimization of the olefination reaction of dialdehyde **62b**

Entry	Temp (°C)	Time (h)	Yield (%)
1	100	3	10
2	100	24	10
3	125	8	20
4	145	5	72
5	160	5	40

#### 5.2.4 Effects of Reaction Temperature on Phosphite-Promoted Olefination

The above optimized conditions were successfully applied to the synthesis of different TTFV-fluorene compounds.<sup>7</sup> It was also frequently noted during this PhD thesis work that careful control over the reaction temperature of this type of olefination reactions is critically important. For example, in Chapter 2 the olefination of dialdehyde **67** successfully yielded di-DTF **68** (Scheme 2.4) when the temperature was carefully controlled at 125 °C or slightly higher temperature. If the reaction temperature fluctuated quite significantly, the outcome could be very different. In one particular case, the reaction temperature dropped below 125 °C for some time during the reaction and an unexpected and very polar compound was formed as the major product instead of **68**. This unexpected product was isolated and then characterized by NMR and MS analyses, based on which its molecular structure was identified as **99** (Scheme 5.12). The formation of the  $\alpha$ -hydroxyphosphonate moiety in **99** suggests that the relatively low temperature may divert the reaction pathway to favor a  $\text{P}(\text{OMe})_3$  nucleophilic addition to the aldehyde group in the beginning of the reaction. Mechanistically as demonstrated in Scheme 5.12,

the nucleophilic attack leads to a phosphonium intermediate (**II**) which can quickly undergo a methyl elimination to yield stable phosphonate (**III**), to which an  $\alpha$ -methoxy is attached (known as the Abramov reaction). Hydrolysis at the workup stage then converts it into an  $\alpha$ -hydroxylphosphonate product. The finding here then raises a caution to future practice of this type of olefination reactions; that is, the reaction temperature needs to be optimized based on different aldehyde precursors. Theoretically, high temperature should favour the olefination by averting the formation of by-products such as the  $\alpha$ -hydroxylphosphonate. However, if the temperature is too high, the starting materials and products may decompose significantly to result in low yields. Therefore, from a practical viewpoint, an optimal reaction temperature needs to be found for each particular olefination reaction.



**Scheme 5.12** Structure of compound **99** and proposed mechanism for the formation of the  $\alpha$ -hydroxylphosphonate group in it.

### 5.2.5 Synthesis of TTFV-Phenylene Oligomers

In Chapters 2 and 3, the DTF oxidative dimerization reaction was demonstrated to be able to form TTFV-arene shape-persistent macrocycles. By looking at the two bis(DTF)-arene precursors **68** and **75** (Figure 5.1) that led to the formation of macrocycles, one can easily deduce that the pre-organization of the bis(DTF)-arene can play a critical role in the macrocyclization reactions. The bis(DTF)-pyrene **75** has the ideal pre-organized “wedge-shaped” structure and the resulting macrocycle is defined and high yielding. The bis(DTF)-fluorene **68** has a more flexible backbone and is less pre-organized. Experimentally, the oxidative reaction of **68** resulted in a mixture of macrocycles rather than a major macrocycle product. These results clearly indicate that molecular pre-organization is a key factor for the oxidative DTF macrocyclization reactions. To further verify this conclusion, another bis(DTF)-arene precursor **103** (Figure 5.13) was conceived. The biphenyl segments in **103** make the entire molecule more flexible than **68** and **75**. Therefore, the oxidative reaction of **103** should not favor macrocyclization as much as **68** and **75**.

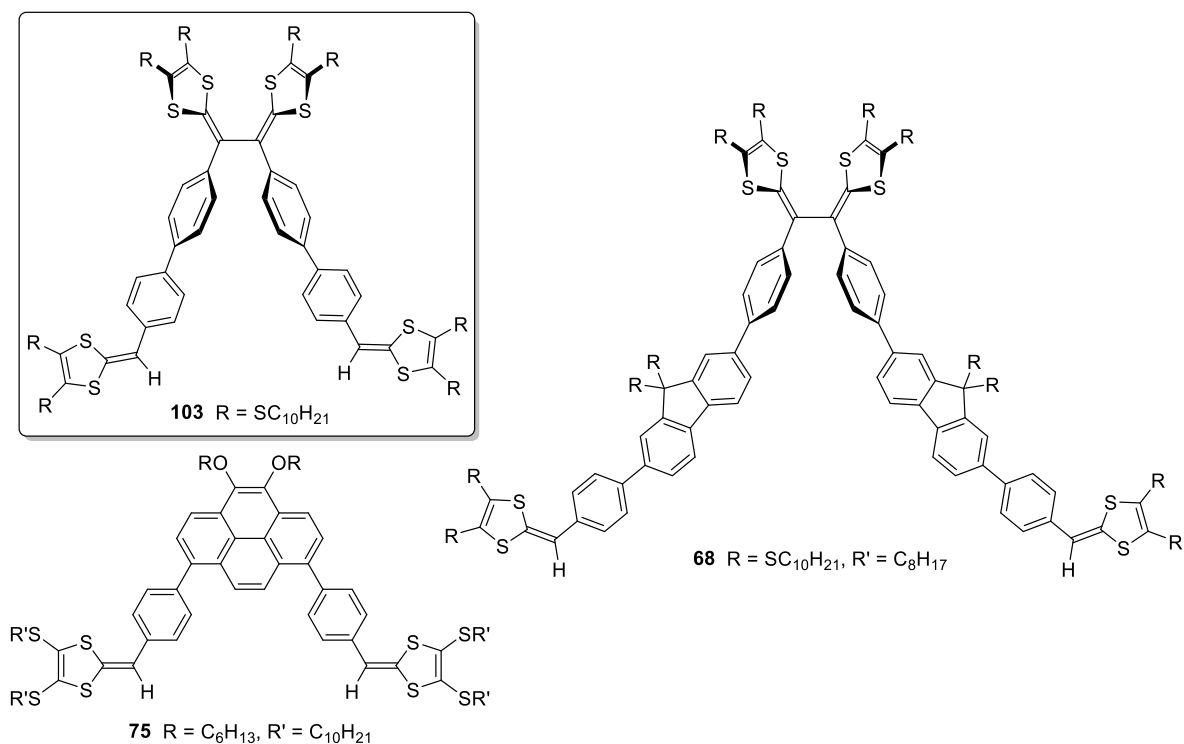
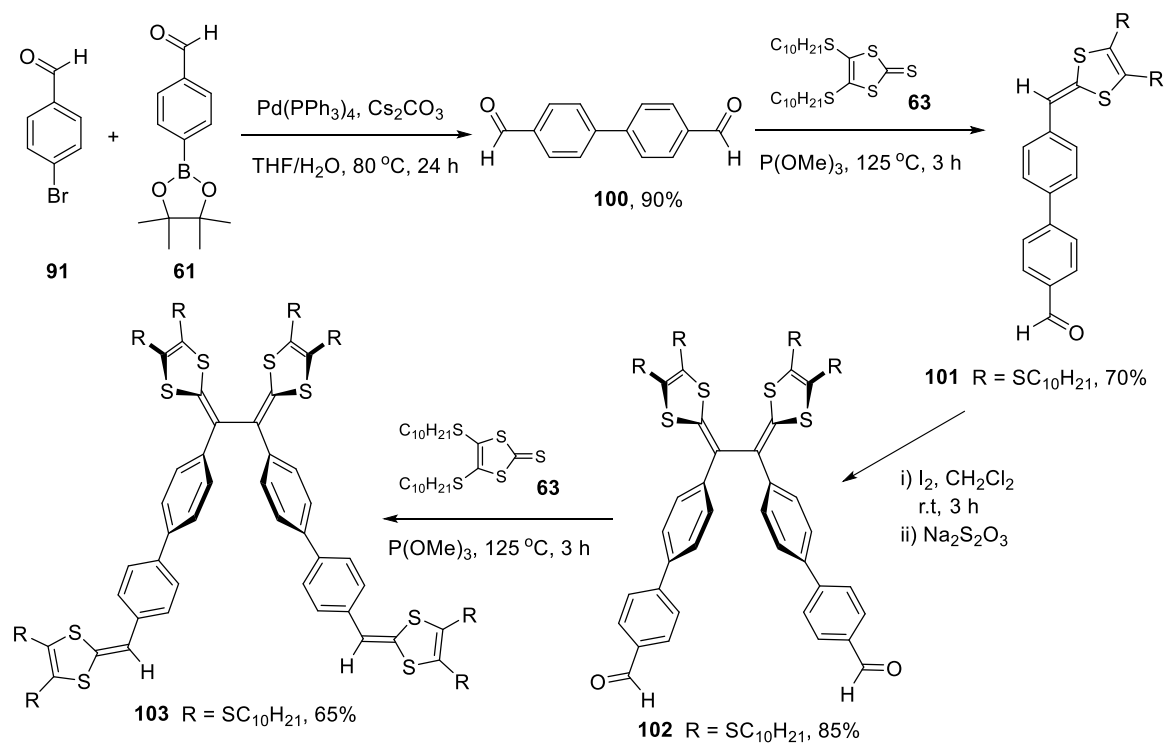


**Figure 5.1** Molecular structures of bis(DTF)-arenes **68**, **75**, and **103**.

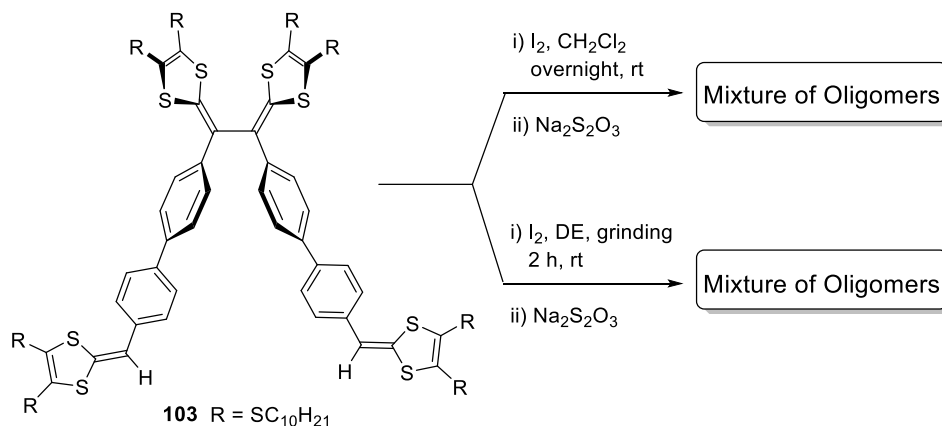
The synthesis of **99** was carried out by a stepwise approach similar to that of **68**. As shown in Scheme 5.13, a Suzuki-Miyaura cross coupling between p-bromobenzaldehyde (**91**) and phenylboronate **61** afforded compound **100** in a good yield. Compound **100** then underwent a mono-olefination reaction with 1,3-dithio-2-thione **63** in the presence of P(OMe)<sub>3</sub> at 125 °C, yielding DTF **101**. Oxidative dimerization of **101** then gave TTFV **102**. Another iteration of P(OMe)<sub>3</sub>-promoted olefination on **102** finally led to the target **103**.



**Scheme 5.13** Synthesis of bis(DTF)-endcapped molecular tweezer **103**.

The oxidative reaction of **103** was then investigated under various conditions. As shown in Scheme 5.14, the solution-phase oxidative DTF coupling of **103** in CH<sub>2</sub>Cl<sub>2</sub> with iodine as oxidant resulted in a mixture of complex oligomeric products. Although the structures of the products have not yet been exactly identified, it is likely that they are a mixture of cyclic and acyclic oligomers. The use of reaction conditions similar to the synthesis of TTFV-pyrene macrocycle **75** also yielded a mixture of oligomer products. No defined macrocyclic products have been successfully separated and identified so far in the oxidative coupling reactions of bis(DTF)-phenylene **103**. Modeling studies show that the formation of macrocyclic products from **103** is not thermodynamically difficult;

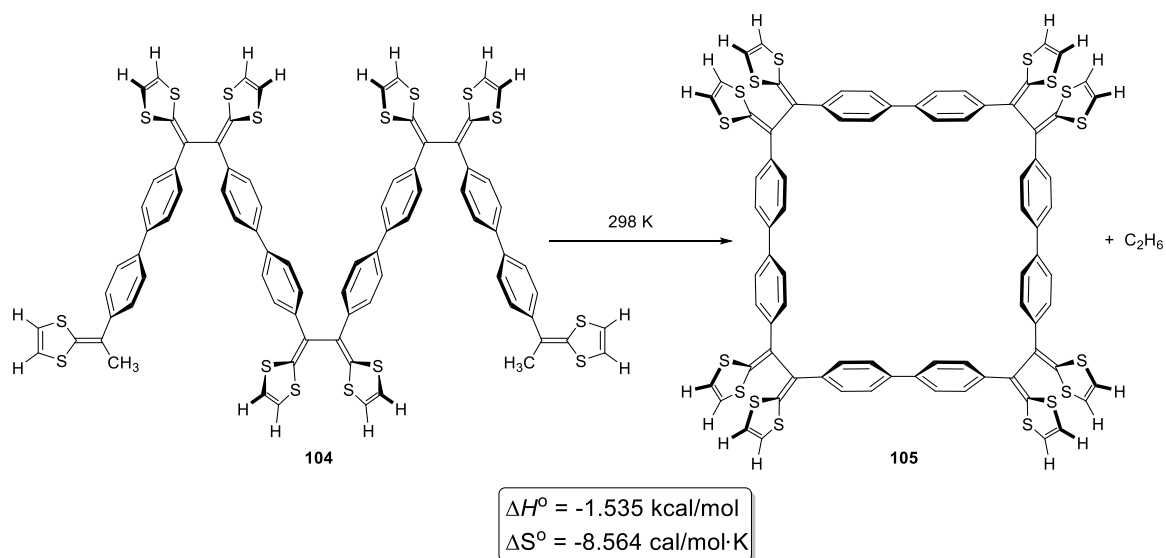
for example, the strain energy of the [1+1] cycloadduct of a model compound of **103** is actually very small (see Scheme 5.15).



**Scheme 5.14** Oxidative coupling of bis(DTF)-phenylene **103**.

To estimate the thermodynamic driving forces for the macrocyclization of **103**, an isodesmic reaction was investigated (Scheme 5.15). An isodesmic reaction is a chemical reaction in which the type of chemical bonds broken in the reactant(s) are the same as the type of bonds formed in the reaction product(s). An isodesmic reaction can be a real reaction or a hypothetical one, and it is often used in the study of thermochemistry. As shown in Scheme 5.15, the transformation from a model compound **104** (with the SC<sub>10</sub>H<sub>21</sub> chains replaced by hydrogen atoms to save computational costs) to macrocycle **105** and ethane is a hypothetical reaction that complies with the requirements of an isodesmic reaction. The calculated standard heat of formation ( $\Delta H_f^\circ$ , 298 K) of this reaction reflects the strain energy incurred in the macrocycle formation. By semi-empirical PM6 calculations, the optimized structures of the reactant and products were

first obtained. Frequency calculations were then conducted to get the thermodynamic data for these compounds. The  $\Delta H_f^\circ$  of the isodesmic reaction (Scheme 5.15) is calculated to be -1.535 kcal/mol, which is insignificant but slightly exothermic. The reason for the value being negative (thermodynamically favoured) is because the hypothetical reactant **104** also contains an extra amount of strain energy due to the steric interactions between the methyl and DTF groups. The  $\Delta S^\circ$  is calculated to be -8.564 cal/mol·K, which is in line with the entropic penalty for the restricted bond rotation in macrocycle **105**. Overall, the theoretical modeling study indicates that macrocyclization of **103** is a possible scenario. On the other hand, it is also easy for **103** to form acyclic oligomers and they are more favored entropically. The lack of pre-organization in **103** makes it difficult to form either macrocycle(s) or acyclic oligomer products with high selectivity through the iodine-promoted oxidative coupling reaction.



**Scheme 5.15** An isodesmic reaction for evaluation of the strain energy of TTFV-phenylene macrocycle **105**.

### 5.2.6 Conclusions

In summary, new classes of DTF and TTFV derivatives were synthetically explored in this work. Although most the synthetic projects reported in this chapter were unsuccessful, the obtained results are still instructive and insightful to our future work in the field of new DTF and TTFV-based organic materials. In particular, some of the compounds made could be used as precursors for the synthesis of other new target compounds. Of them, compound **99** is probably one of the best examples that deserve more investigation. In recent years,  $\alpha$ -hydroxyphosphonate and related phosphonic acid have received considerable attention due to their appealing biological and medicinal applications in enzyme inhibitors, antibacterial, antiviral, and antitumor agents. The accidental formation of an  $\alpha$ -hydroxyphosphonate moiety in **99** can thus be viewed as an opportunity for introducing the redox activity of DTF and TTFV groups to biologically active systems. It is therefore envisioned to open a new avenue to explore the biological and medicinal aspects of DTF and TTFV-based materials, which have not yet been well-documented in the current literature.

## 5.3. Experimental

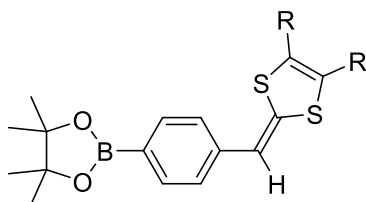
### 5.3.1 General

Chemicals were purchased from commercial suppliers and used directly without purification. All reactions were conducted in standard, dry glassware and under an inert atmosphere of nitrogen or argon unless otherwise noted. Evaporation and concentration were carried out with a rotary evaporator. Flash column chromatography was performed with 240-400 mesh silica gel, and thin-layer chromatography (TLC) was carried out with silica gel F254 covered on plastic sheets and visualized by UV light.  $^1\text{H}$  and  $^{13}\text{C}$  NMR spectra were measured on a Bruker Avance III 300 MHz multinuclear spectrometer. Chemical shifts ( $\delta$ ) are reported in ppm downfield relative to the signals of the internal reference  $\text{SiMe}_4$  or residual solvents ( $\text{CHCl}_3$ :  $\delta_{\text{H}} = 7.24$  ppm,  $\delta_{\text{C}} = 77.2$  ppm;  $\text{CH}_2\text{Cl}_2$ :  $\delta_{\text{H}} = 5.32$  ppm,  $\delta_{\text{C}} = 54.0$  ppm). Coupling constants ( $J$ ) are given in Hz. Infrared spectra (IR) were recorded on a Bruker Alfa spectrometer. MALDI-TOF MS analysis was performed on an Applied Biosystems Voyager instrument using dithranol as the matrix. High resolution APPI-TOF MS analysis was done on a GCT premier Micromass Technologies instrument.

### 5.3.2 Synthesis

Compounds **61**, **90**, **91** was purchased from *Combi-Blocks, Inc.* (San Diego, USA). Compounds **63**<sup>8</sup>, **86**<sup>3</sup>, **94**<sup>9</sup> and **100**<sup>10,11</sup> were prepared according to the literature procedures.

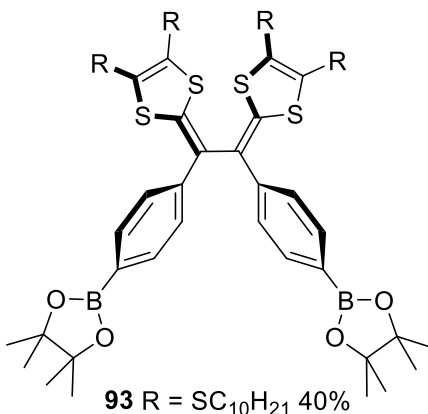
## Compound 92



**92** R = SC<sub>10</sub>H<sub>21</sub> 20%

4-Formylphenylboronic acid, pinacol ester **61** (1.50 g, 6.46 mmol), thione **63** (3.34 g, 7.00 mmol), and P(OMe)<sub>3</sub> (30 mL) were added to a 100 mL round-bottom flask. The mixture was heated to 100 °C and kept at this temperature for 3 h. Then P(OMe)<sub>3</sub> was removed by vacuum distillation, and the crude product was purified through silica column chromatography (hexanes/dichloromethane 1:1) to give **92** (0.83 g, 1.29 mmol, 20%) as a yellow oil. <sup>1</sup>H NMR (300 MHz, CDCl<sub>3</sub>) δ 7.78 (d, *J* = 8.2 Hz, 2H), 7.20 (d, *J* = 8.0 Hz, 2H), 6.47 (s, 1H), 2.84-2.79 (m, 4H), 1.68-0.83 (m, 50H).

## Compound 93

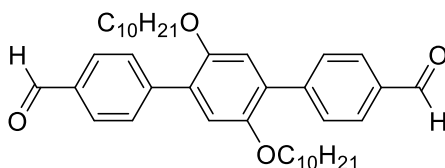


**93** R = SC<sub>10</sub>H<sub>21</sub> 40%

Compound **92** (0.83 g, 1.29 mmol) and iodine (0.98 g, 3.9 mmol) were added in CH<sub>2</sub>Cl<sub>2</sub> (20 mL), and the mixture was stirred at room temperature for 5 h. A saturated

aqueous solution of  $\text{Na}_2\text{S}_2\text{O}_3$  was added, and the resulting mixture was stirred at room temperature for another 1 h. The organic layer was separated, washed with  $\text{H}_2\text{O}$ , dried over  $\text{MgSO}_4$ , and concentrated under vacuum. The crude product obtained was purified through silica column chromatography (hexanes/ethyl acetate, 2:1) to yield compound **93** (0.65 g, 0.51 mmol, 40%) as a yellow oil.  $^1\text{H}$  NMR (300 MHz,  $\text{CDCl}_3$ )  $\delta$  7.72 (d,  $J = 8.4$  Hz, 4H), 7.39 (d,  $J = 8.4$  Hz, 1H), 2.82-2.72 (m, 8H), 1.68-0.88 (m, 88 H).

#### 2,5-Didecyloxy-1,4-bis(4-formylphenyl)benzene (**97**)

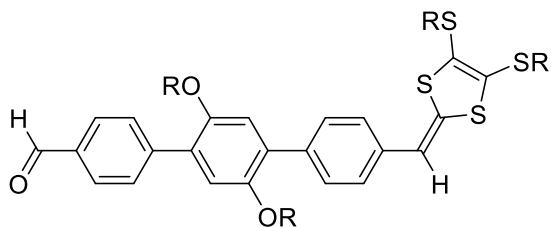


**97** 51%

A mixture of 1,4-didecyloxy-2,5-diiodobenzene (**94**) (1.32 g, 5.0 mmol), 4-formylphenylboronic acid pinacol ester (1.49 g, 10 mmol),  $\text{Pd}(\text{PPh}_3)_4$  (0.29 g, 0.25 mmol), THF (20 mL), and 2 M  $\text{K}_2\text{CO}_3$  solution (20 mL) was heated at 85 °C for 5 h under nitrogen. The reaction mixture was cooled to room temperature. The separated organic layer of filtrate was washed with saturated aqueous  $\text{NH}_4\text{Cl}$  ( $3 \times 100$  mL), then dried over  $\text{MgSO}_4$ . Removal of the solvent by a rotary evaporator and the crude product was purified by column chromatography on silica gel (hexane/ethyl acetate = 5:1) to give the product **97** in a 51% yield (0.89 g) as a pale yellow solid.  $^1\text{H}$  NMR (300 MHz,

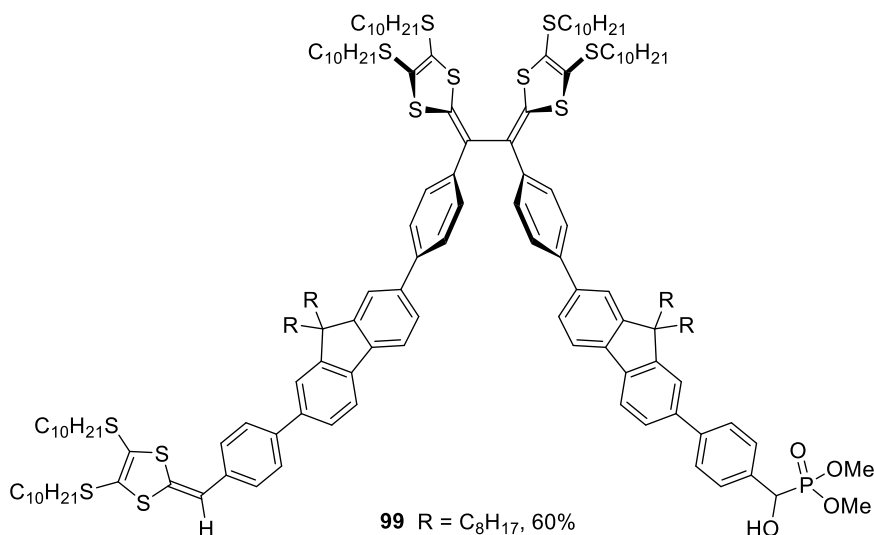
$\text{CDCl}_3$ )  $\delta$  10.07 (s, 2H), 7.94 (d,  $J = 8.4$  Hz, 4H), 7.77 (d,  $J = 8.2$  Hz, 4H), 7.01 (s, 2H), 3.97-3.92 (m, 4H), 1.72-0.85 (m, 38 H).

### DTF **98**



Dibenzaldehyde **97** (1.00 g, 1.67 mmol), thione **63** (0.72 g, 1.50 mmol), and  $\text{P}(\text{OMe})_3$  (30 mL) were added to a 100 mL round-bottom flask. The mixture was heated to 100 °C and kept at this temperature for 3 h. Then  $\text{P}(\text{OMe})_3$  was removed by vacuum distillation, and the crude product was purified through silica column chromatography (hexanes/dichloromethane 3:2) to give **98** (0.85 g, 0.84 mmol, 50%) as a yellow oil:  $^1\text{H}$  NMR (300 MHz,  $\text{CDCl}_3$ )  $\delta$  10.06 (s, 1H), 7.93 (d,  $J = 8.4$  Hz, 4H), 7.78 (d,  $J = 8.2$  Hz, 4H), 7.29 (s, 2H), 7.00 (d,  $J = 5.6$  Hz, 2H), 6.51 (s, 1H), 3.96-3.90 (m, 4H), 2.86-2.81 (m, 4H), 1.72-0.84 (m, 78H).

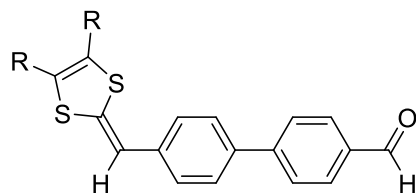
## DTF- $\alpha$ -hydroxyphosphonate **99**



Compound **67** (0.35 g, 0.17 mmol), thione **63** (0.24 g, 0.51 mmol), and P(OMe)<sub>3</sub> (15 mL) were added to a 100 mL round-bottom flask. The mixture was heated to 100 °C and kept at this temperature for 3 h. Then P(OMe)<sub>3</sub> was removed by vacuum distillation, and the crude product was purified through silica column chromatography (hexanes/ethyl acetate 1:1) to give **99** (0.26 g, 0.10 mmol, 60%) as a yellow oil. <sup>1</sup>H NMR (300 MHz, CDCl<sub>3</sub>) δ 7.77 – 7.48 (m, 26H), 7.32 (d, *J* = 8.5 Hz, 2H), 6.52 (s, 1H), 5.14 (d, *J* = 8.3 Hz, 2H), 4.74 (d, *J* = 5.4 Hz, 12H), 3.88 (d, *J* = 10.6 Hz, 36H), 3.77 (d, *J* = 11.1 Hz, 1H), 2.92–2.71 (m, 1H), 1.71 – 0.76 (m, 14H). <sup>13</sup>C NMR (75 MHz, CDCl<sub>3</sub>) δ 151.78, 151.73, 151.6, 142.0, 139.4, 136.7, 136.6, 135.96, 135.92, 135.2, 134.7, 134.6, 132.4, 128.88, 128.82, 128.5, 127.5, 127.4, 127.2, 126.9, 126.0, 125.7, 125.47, 125.45, 125.18, 125.14, 124.8, 124.2, 121.2, 120.0, 55.27, 55.24, 54.7, 54.6, 54.4, 54.3, 42.4, 40.4, 40.2, 36.2, 36.1, 36.0,

36.01, 31.9, 31.7, 30.0, 29.88, 29.80, 29.7, 29.6, 29.4, 29.3, 29.2, 28.6, 28.5, 23.8, 22.7, 22.6, 14.1. HRMS  $[M+H]^+$  calcd for  $C_{157}H_{231}O_4PS_{12}$  2596.4337, found 2596.5911.

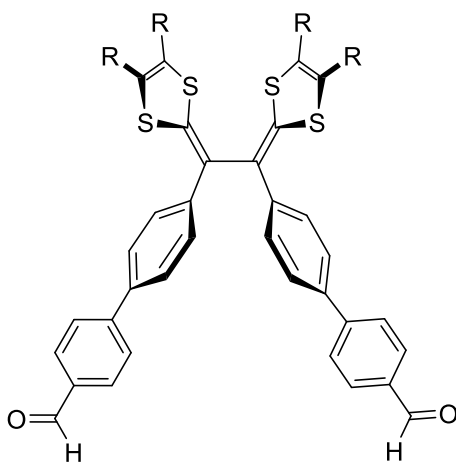
### DTF (101)



**101** R =  $SC_{10}H_{21}$  70%

Dibenzaldehyde **100** (1.00 g, 5.07 mmol), thione **63** (2.39 g, 5.0 mmol), and  $P(OMe)_3$  (30 mL) were added to a 100 mL round-bottom flask. The mixture was heated to 100 °C and kept at this temperature for 3 h. Then  $P(OMe)_3$  was removed by vacuum distillation, and the crude product was purified through silica column chromatography (hexanes/dichloromethane 3:2) to give **101** (2.27 g, 3.55 mmol, 70%) as a yellow oil: IR (neat) 2954, 2916, 2872, 2847, 1700, 1598, 1562, 1194, 1170, 817  $cm^{-1}$ ;  $^1H$  NMR (300 MHz,  $CDCl_3$ )  $\delta$  10.05 (s, 1H), 7.94 (d,  $J = 8.5$  Hz, 2H), 7.76 (d,  $J = 8.2$  Hz, 2H), 7.65 (d,  $J = 8.4$  Hz, 2H), 7.32 (d,  $J = 8.3$  Hz, 2H), 6.51 (s, 1H), 3.76 (d,  $J = 13.5$  Hz, 4H), 2.95–2.77 (m, 4H), 1.65–0.86 (m, 38H).  $^{13}C$  NMR (75 MHz,  $CDCl_3$ )  $\delta$  191.8, 146.5, 136.6, 136.5, 135.0, 134.0, 130.3, 127.9, 127.4, 127.3, 124.8, 113.3, 54.7, 54.6, 36.2, 36.1, 31.9, 31.6, 29.8, 29.7, 29.59, 29.55, 29.3, 29.1, 28.6, 28.5, 22.7, 22.6, 14.1. HRMS  $[M + H]^+$  calcd for  $C_{37}H_{52}OS_4$  641.2979, found 641.2992.

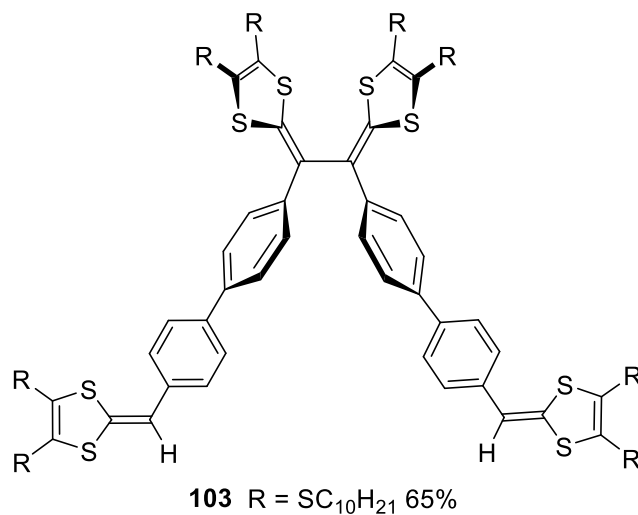
## TTFV (102)



**102** R = SC<sub>10</sub>H<sub>21</sub> 85%

Compound **101** (1.00 g, 1.56 mmol) and iodine (1.14 g, 4.5 mmol) were added in CH<sub>2</sub>Cl<sub>2</sub> (30 mL), and the mixture was stirred at room temperature for 5 h. A saturated aqueous solution of Na<sub>2</sub>S<sub>2</sub>O<sub>3</sub> was added, and the resulting mixture was stirred at room temperature for another 1 h. The organic layer was separated, washed with H<sub>2</sub>O, dried over MgSO<sub>4</sub>, and concentrated under vacuum. The crude product obtained was purified through silica column chromatography (hexanes/CH<sub>2</sub>Cl<sub>2</sub>, 1:1) to yield compound **102** (1.70 g, 1.32 mmol, 85%) as a yellow oil: IR (neat) 2953, 2923, 2852, 1701, 1684, 1602, 1213, 1168, 818 cm<sup>-1</sup>; <sup>1</sup>H NMR (300 MHz, CDCl<sub>3</sub>) δ; 10.04 (s, 1H), 7.93 (d, *J* = 8.4 Hz, 4H), 7.74 (d, *J* = 8.3 Hz, 4H), 7.64-7.54 (m, 8H), 2.87-2.75 (m, 8H), 1.69-0.84 (m, 76H). <sup>13</sup>C NMR (75 MHz, CDCl<sub>3</sub>) δ 191.8, 146.4, 138.2, 137.5, 137.2, 135.1, 130.3, 129.0, 127.5, 127.2, 127.0, 36.2, 36.0, 31.9, 29.7, 29.6, 29.3, 29.2, 28.6, 28.5, 22.7, 14.1. HRMS [M + H]<sup>+</sup> calcd for C<sub>74</sub>H<sub>102</sub>O<sub>2</sub>S<sub>8</sub> 1279.5724, found 1279.5647.

## TTFV (103)



Compound **102** (0.50 g, 0.39 mmol), thione **63** (0.46 g, 0.97 mmol), and P(OMe)<sub>3</sub> (20 mL) The mixture was heated to 125 °C and kept at this temperature for 3 h. Then P(OMe)<sub>3</sub> was removed by vacuum distillation, and the crude product was purified through silica column chromatography (hexanes/dichloromethane 3:1) to give **103** (0.54 g, 0.25 mmol, 65%) as a yellow oil: IR (neat) 2954, 2924, 2853, 1520, 1497, 1457, 1097, 1012, 830, 795 cm<sup>-1</sup>; <sup>1</sup>H NMR (300 MHz, CDCl<sub>3</sub>) δ 7.52-7.42 (m, 12H), 7.20-7.17 (m, 4H), 6.40(s, 2H), 2.79-2.67 (m, 16), 1.58-0.78 (m, 152H) <sup>13</sup>C NMR (75 MHz, CDCl<sub>3</sub>) δ 137.4, 136.6, 136.5, 135.7, 134.9, 134.3, 131.4, 127.8, 126.6, 126.1, 125.9, 125.7, 124.0, 123.7, 123.1, 112.8, 35.1, 35.0, 34.9, 30.9, 30.8, , 28.6, 28.56, 28.50, 28.3, 21.68, 21.66, 13.10. HRMS [M]<sup>+</sup> calcd for C<sub>120</sub>H<sub>186</sub>S<sub>16</sub> 2139.0086, found 2139.0013.

### 5.3.3 NMR Spectra for New Compounds

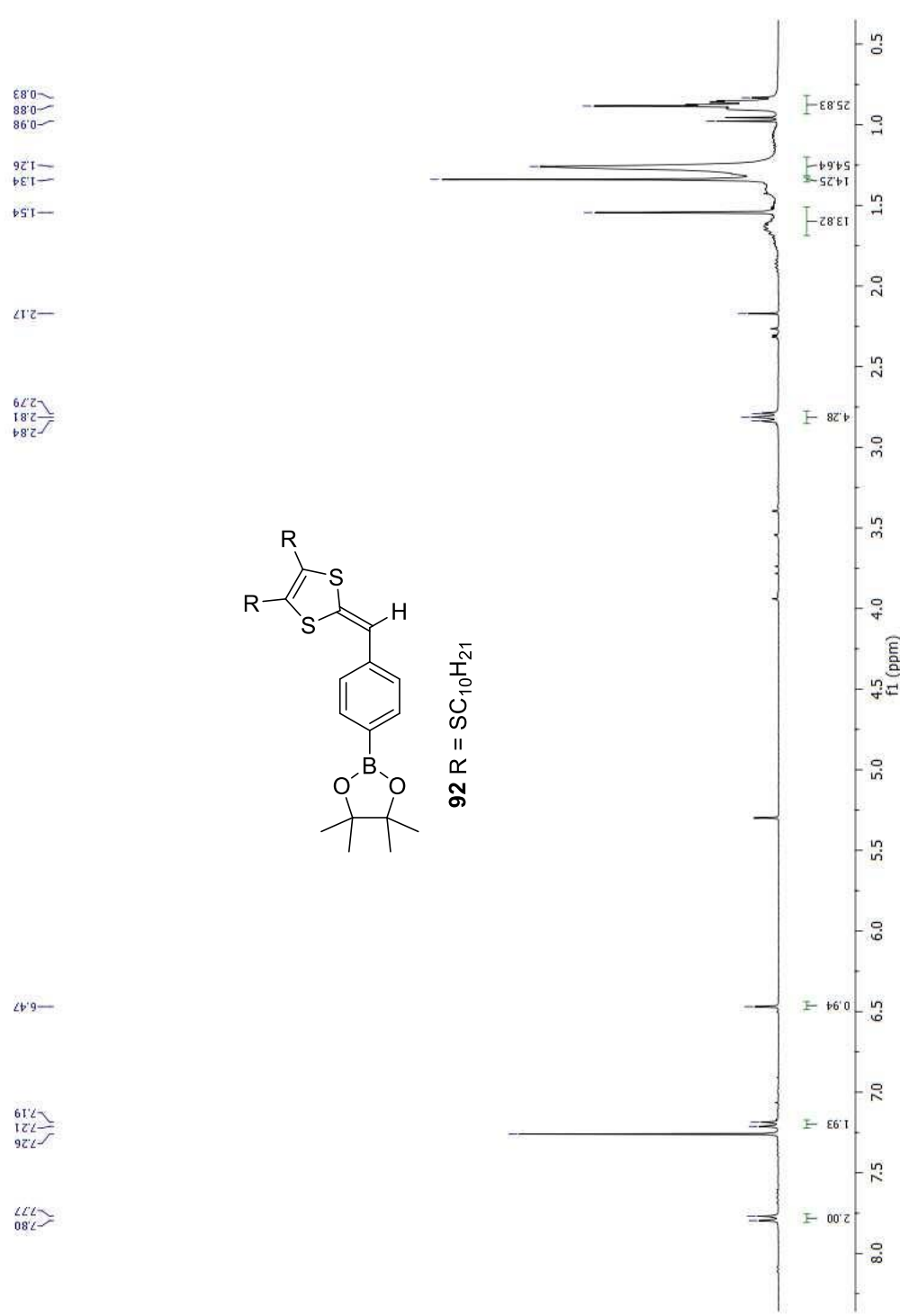


**Fig. 5.2:** <sup>1</sup>H NMR (300 MHz, CDCl<sub>3</sub>) spectrum of compound **92**.

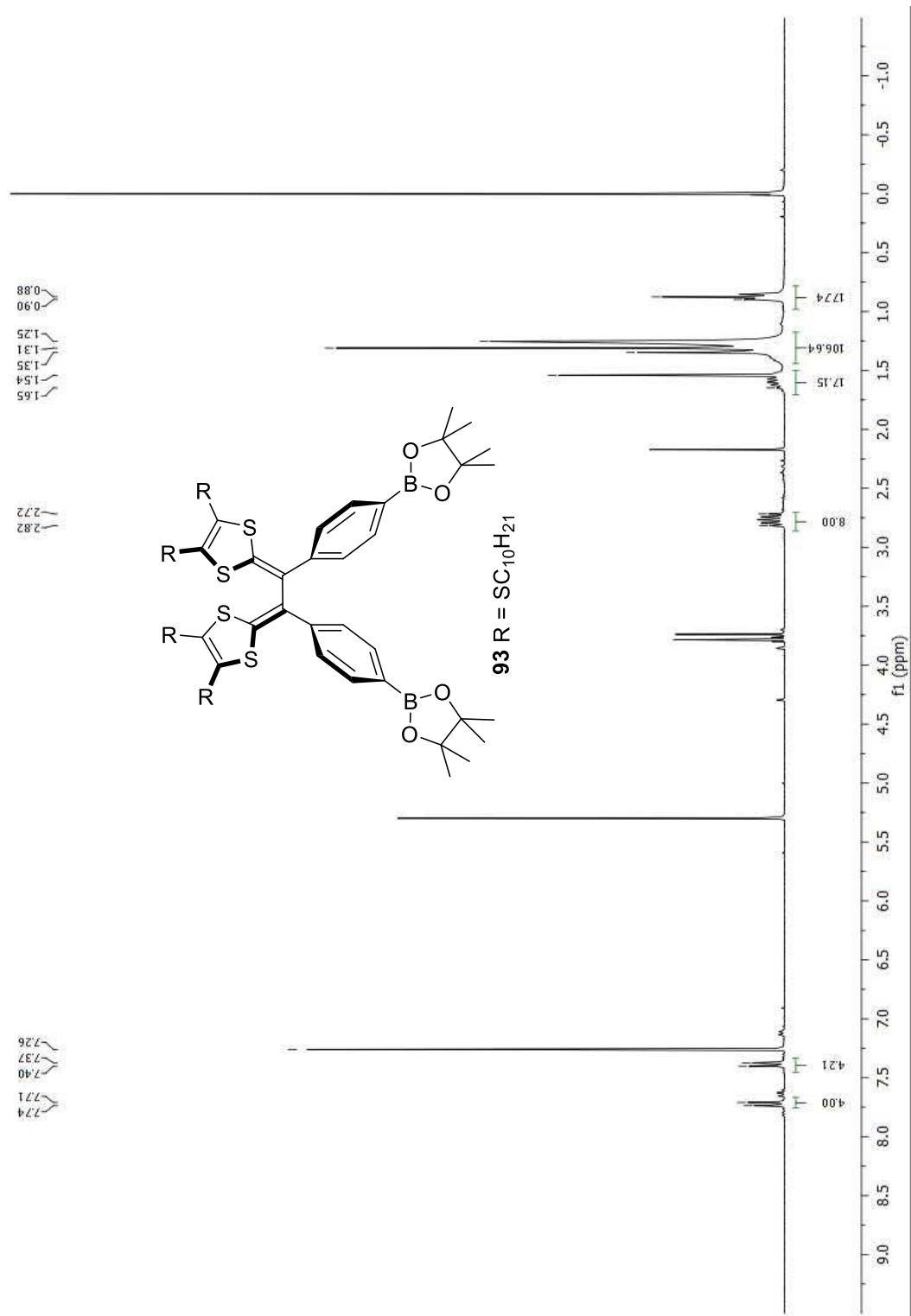


**Fig. 5.3:**  $^1\text{H}$  NMR (300 MHz,  $\text{CDCl}_3$ ) spectrum of compound **93**

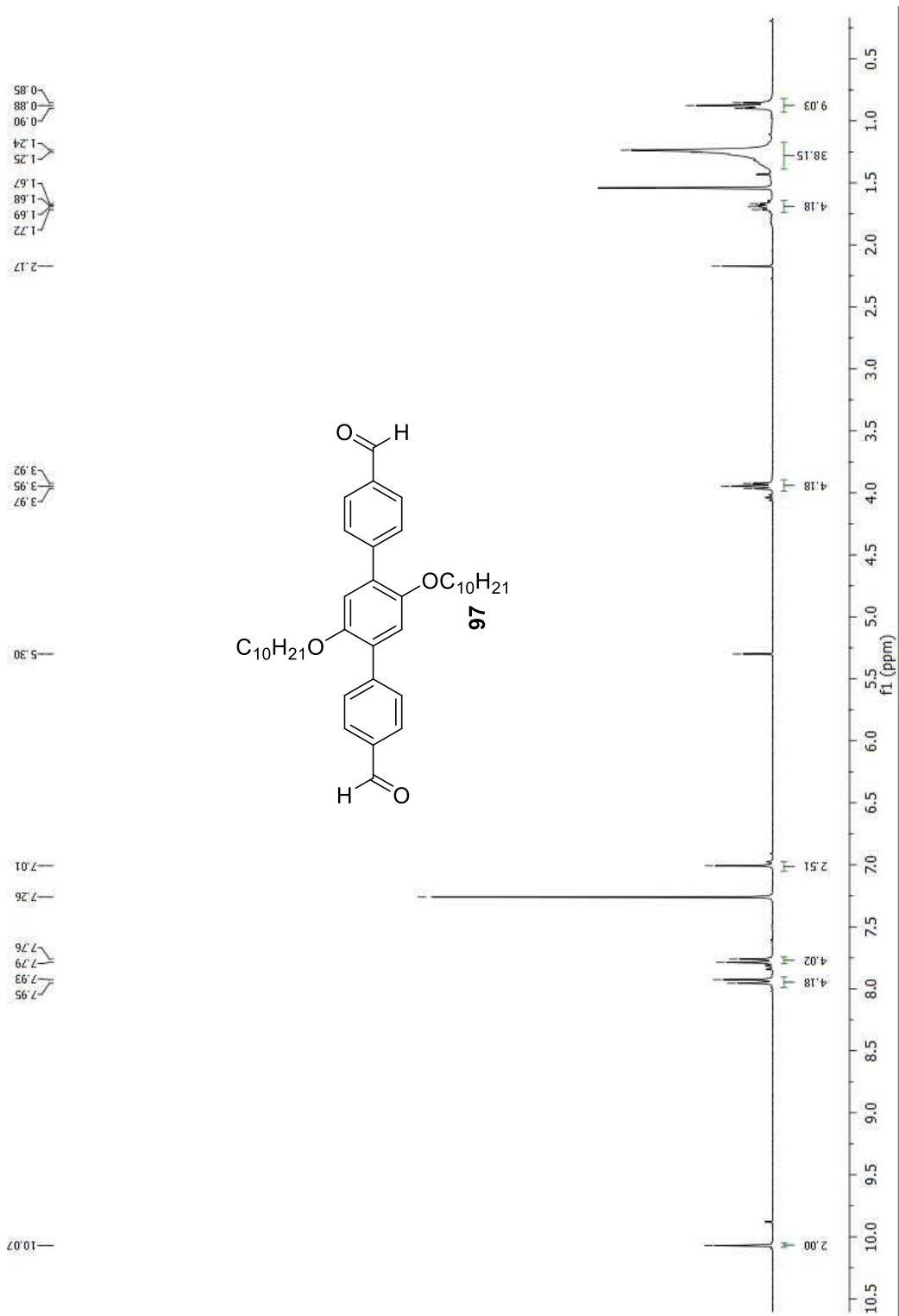


**Fig. 5.4:**  $^1\text{H}$  NMR (300 MHz,  $\text{CDCl}_3$ ) spectrum of compound **97**.

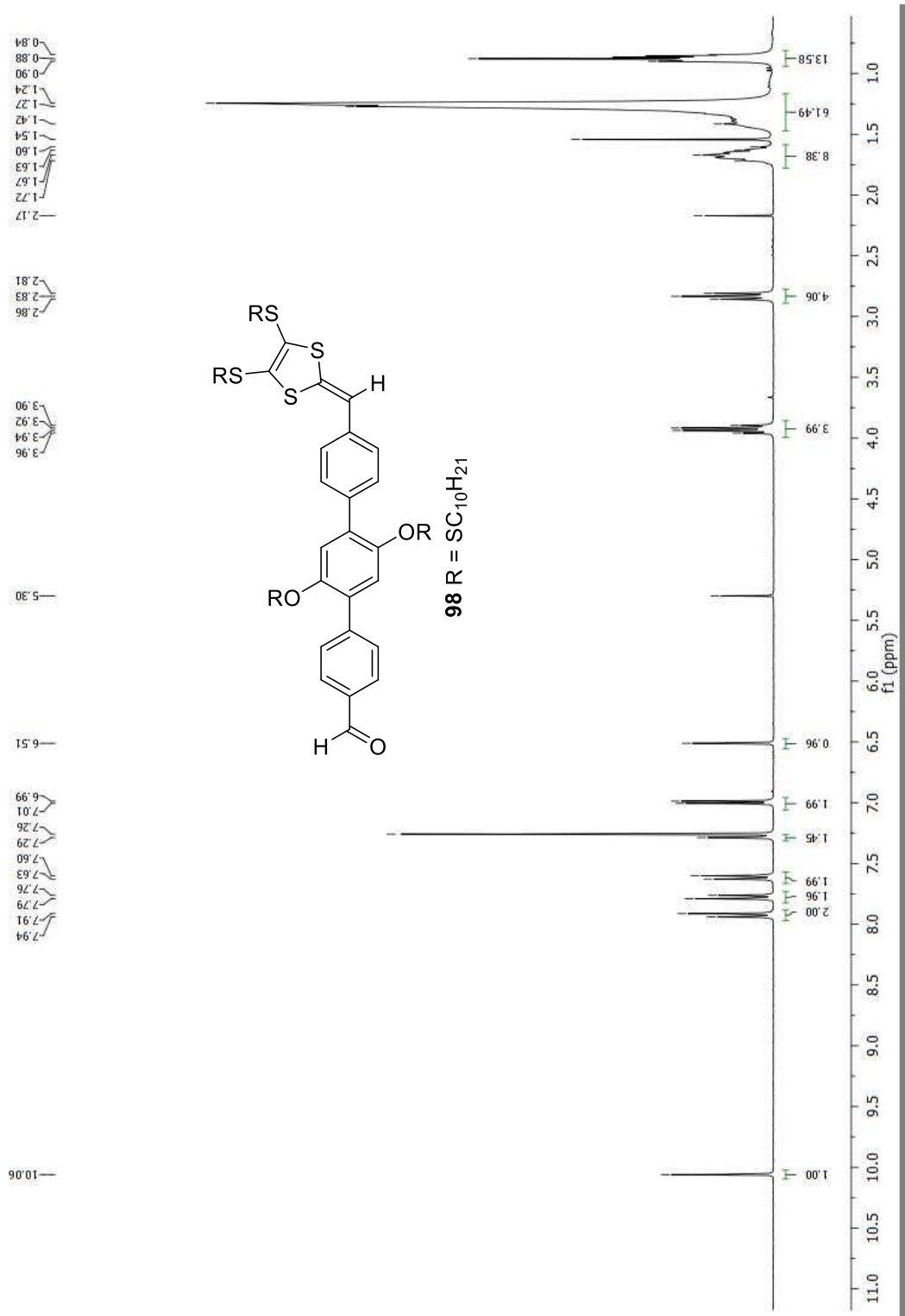


**Fig. 5.5:**  $^1H$  NMR (300 MHz,  $CDCl_3$ ) spectrum of compound **98**.

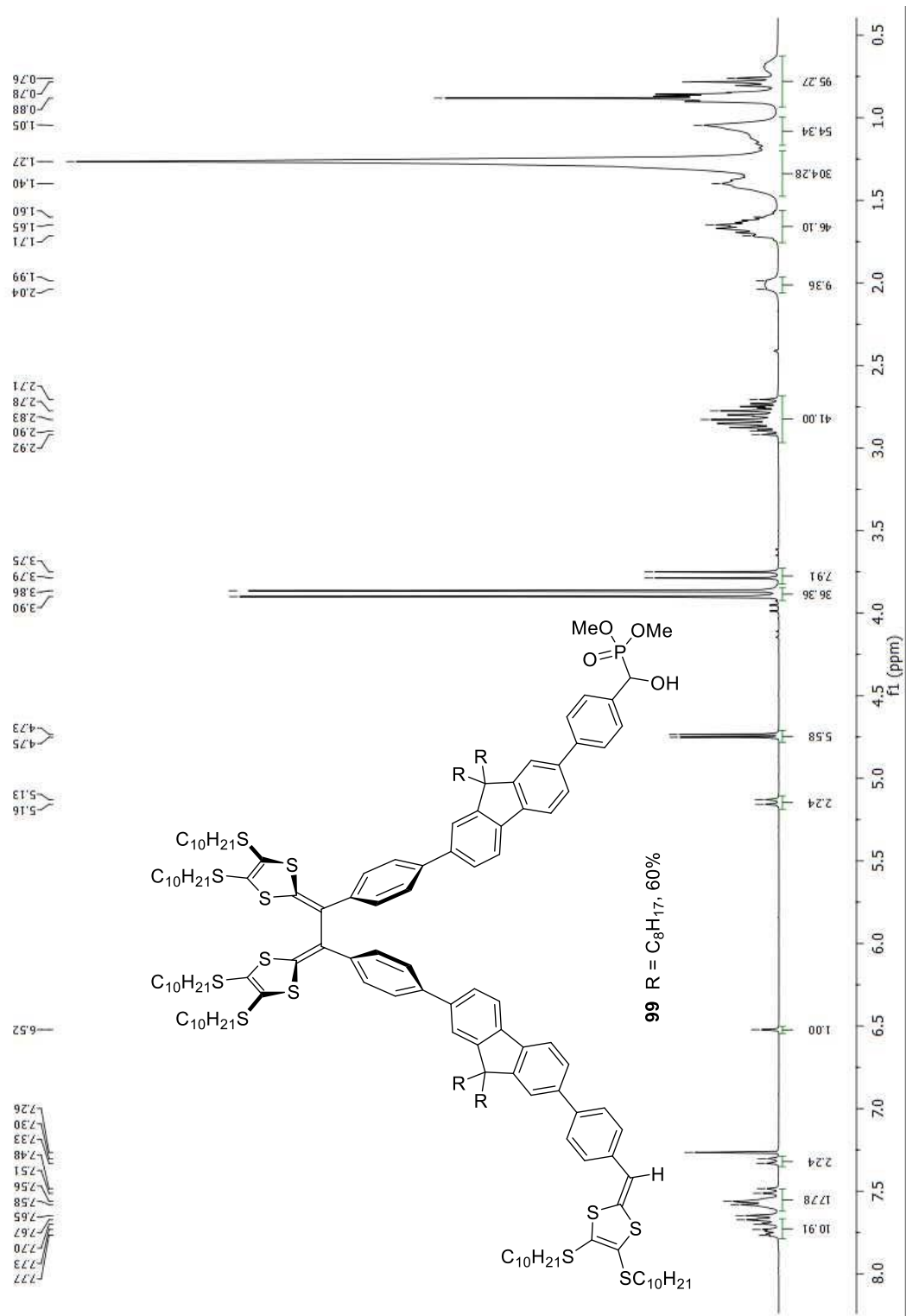


**Fig. 5.6:**  $^1H$  NMR (300 MHz,  $CDCl_3$ ) spectrum of compound **99**.

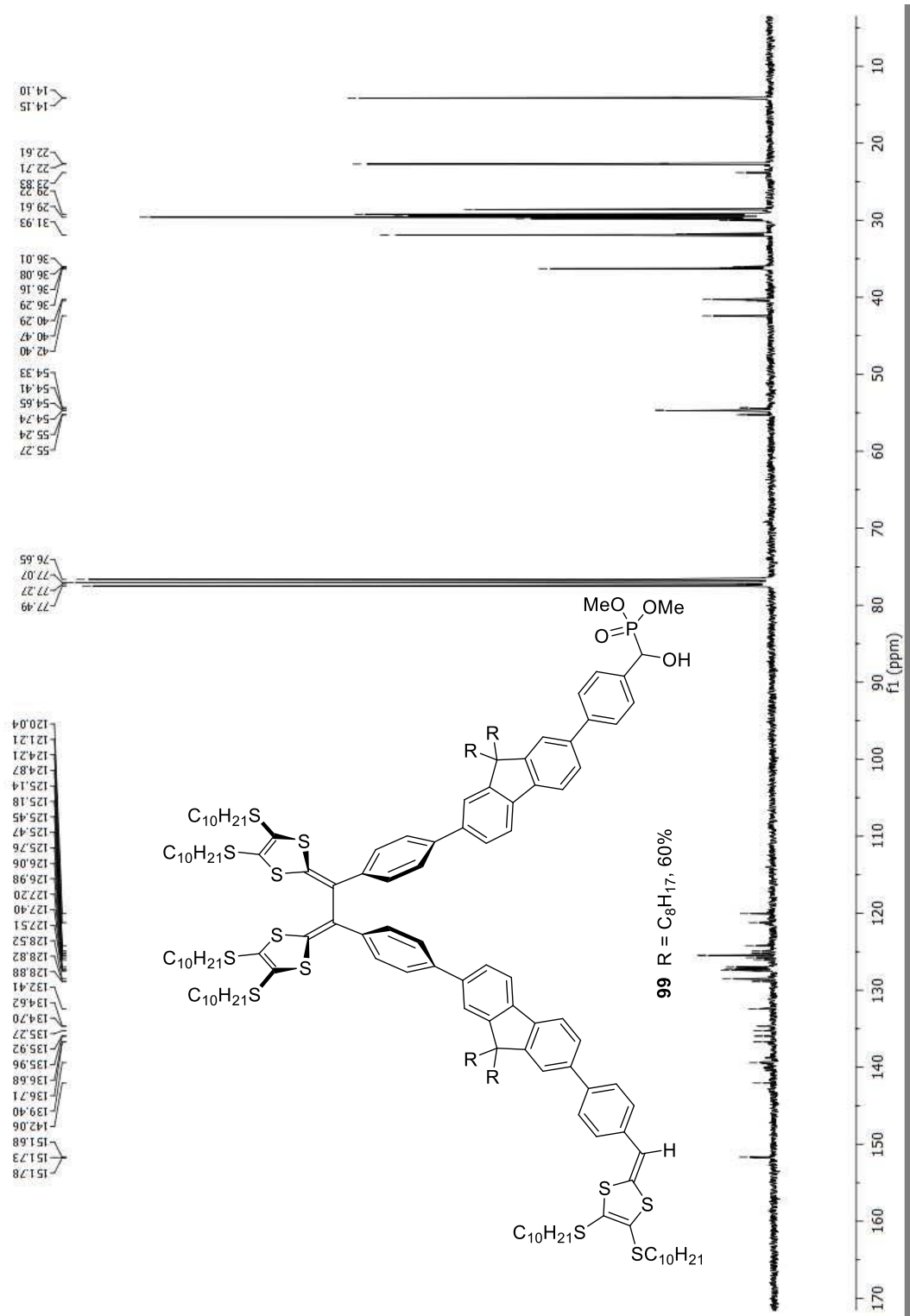


**Fig. 5.7:**  $^{13}C$  NMR (75 MHz,  $CDCl_3$ ) spectrum of compound **99**.

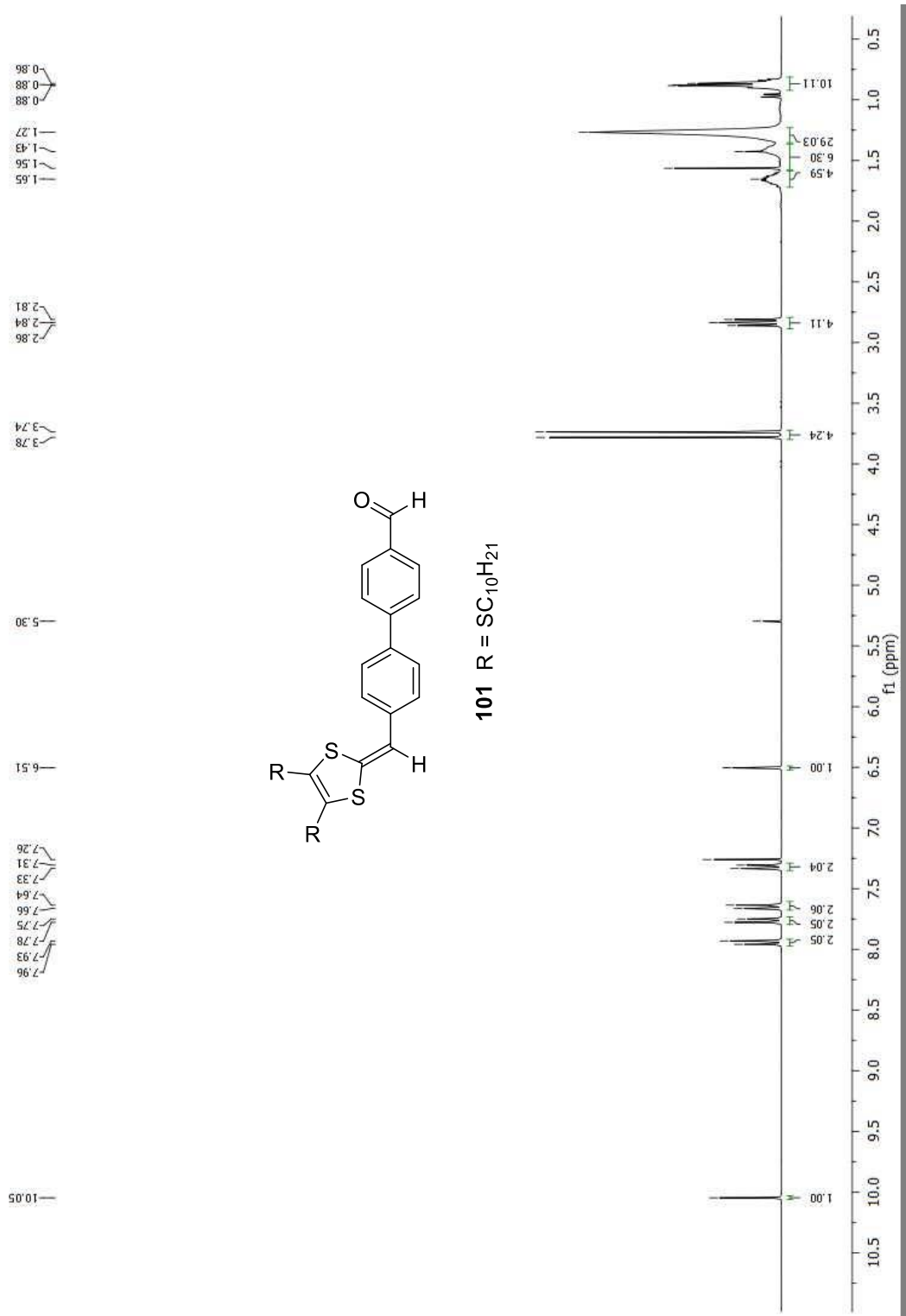


**Fig. 5.8:**  $^1H$  NMR (300 MHz,  $CDCl_3$ ) spectrum of compound **101**.

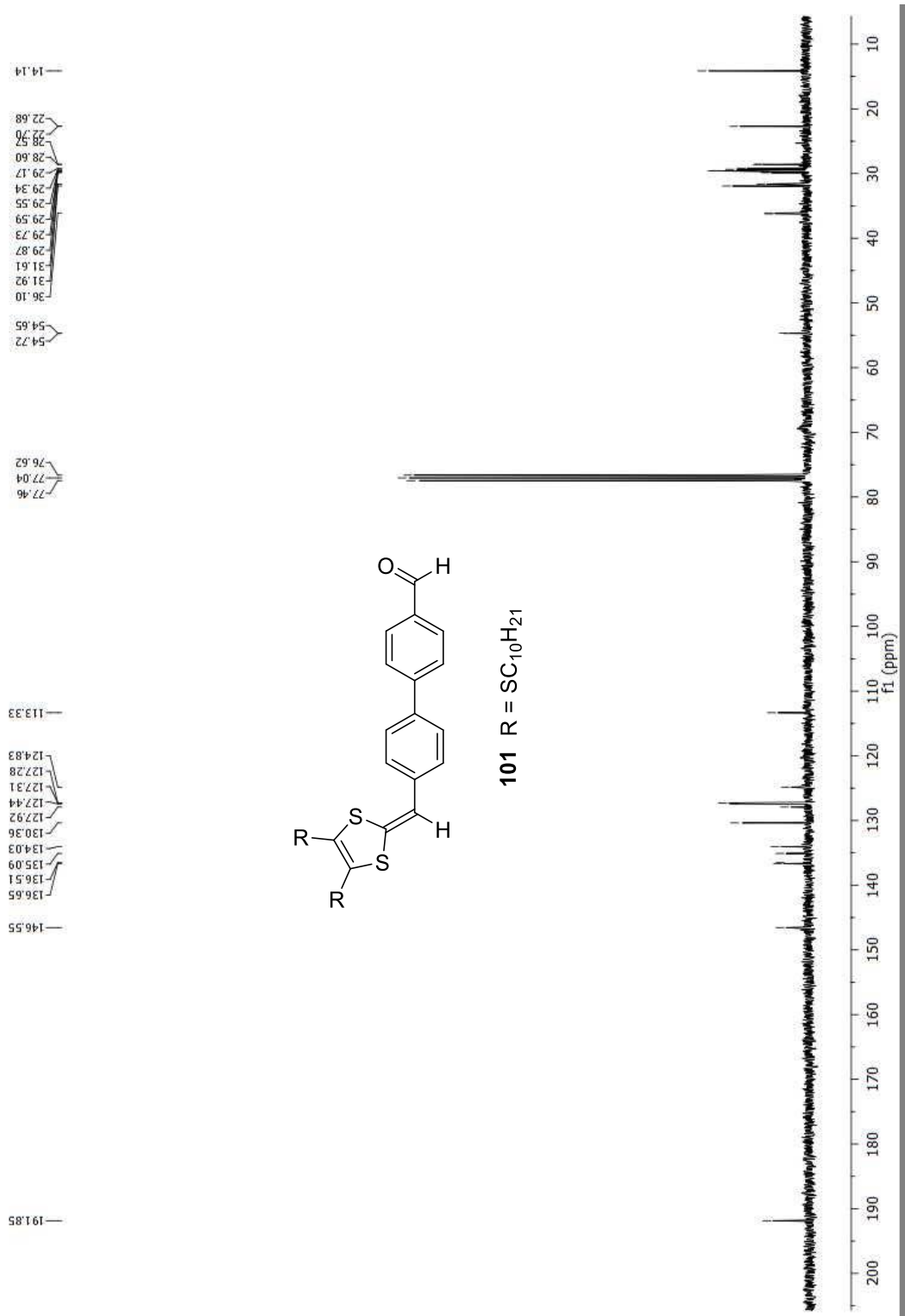


**Fig. 5.9:** <sup>13</sup>C NMR (75 MHz, CDCl<sub>3</sub>) spectrum of compound 101.

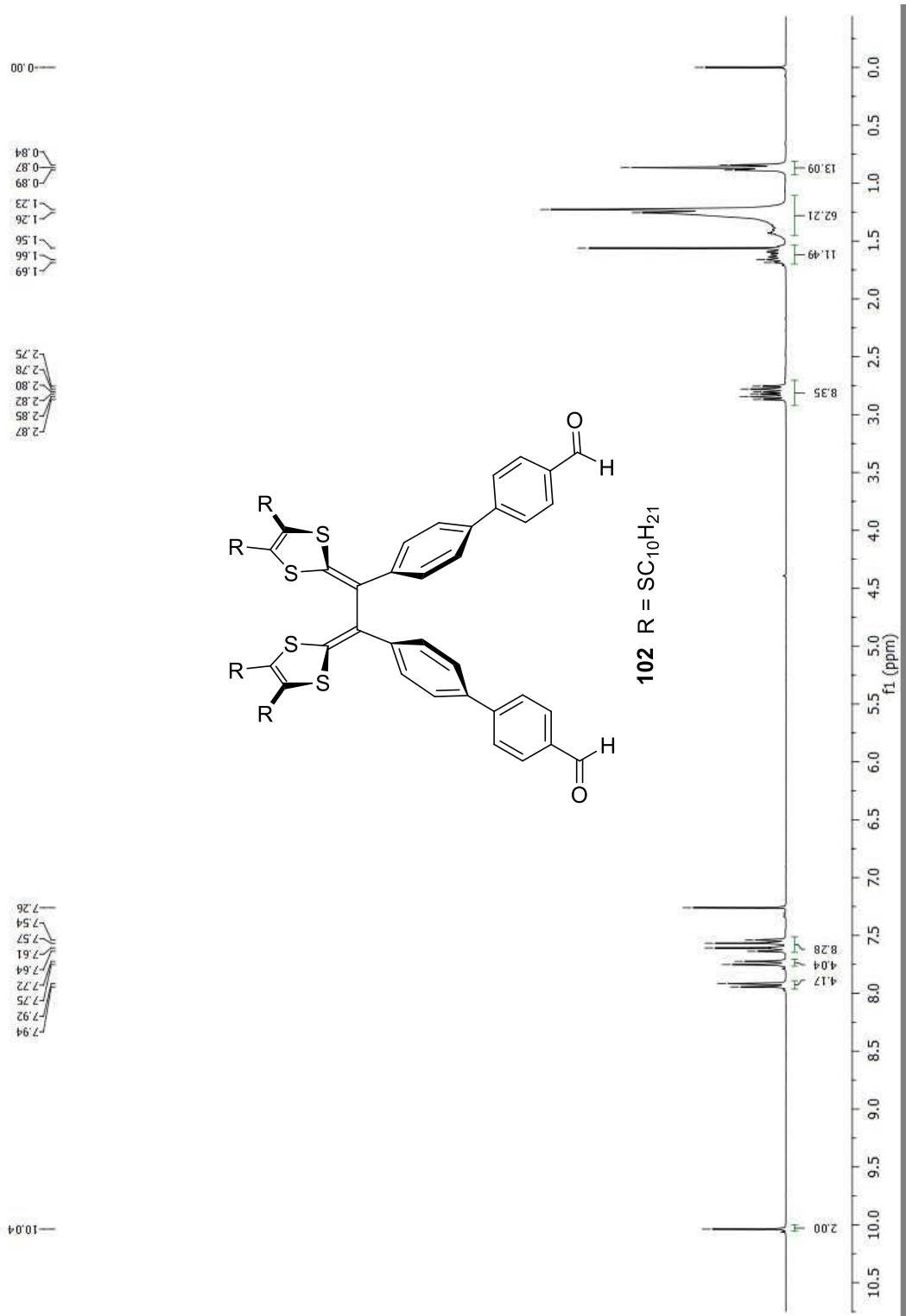


**Fig. 5.10:**  $^1H$  NMR (300 MHz,  $CDCl_3$ ) spectrum of compound **102**.

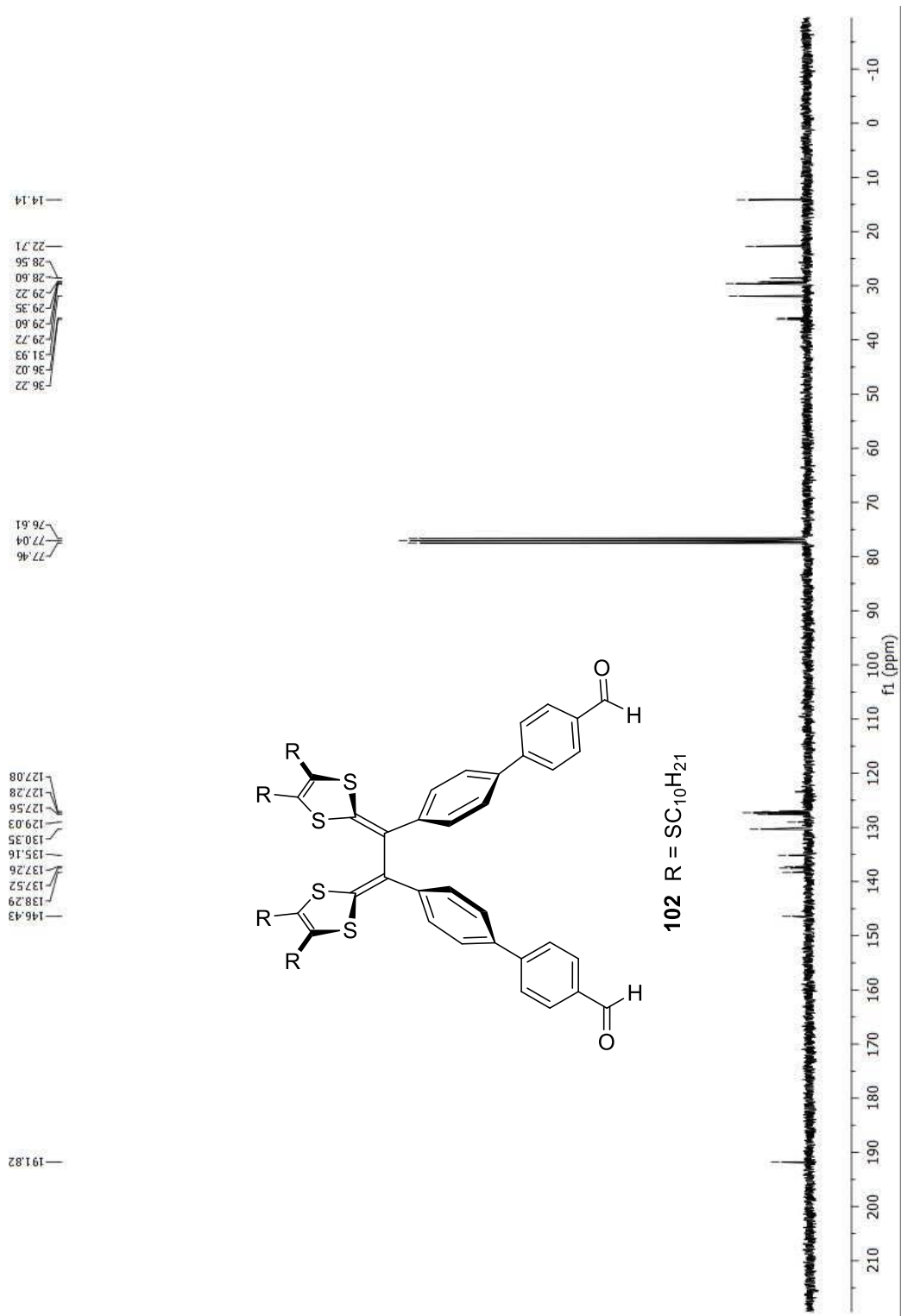


**Fig. 5.11:**  $^{13}C$  NMR (75 MHz,  $CDCl_3$ ) spectrum of compound **102**.

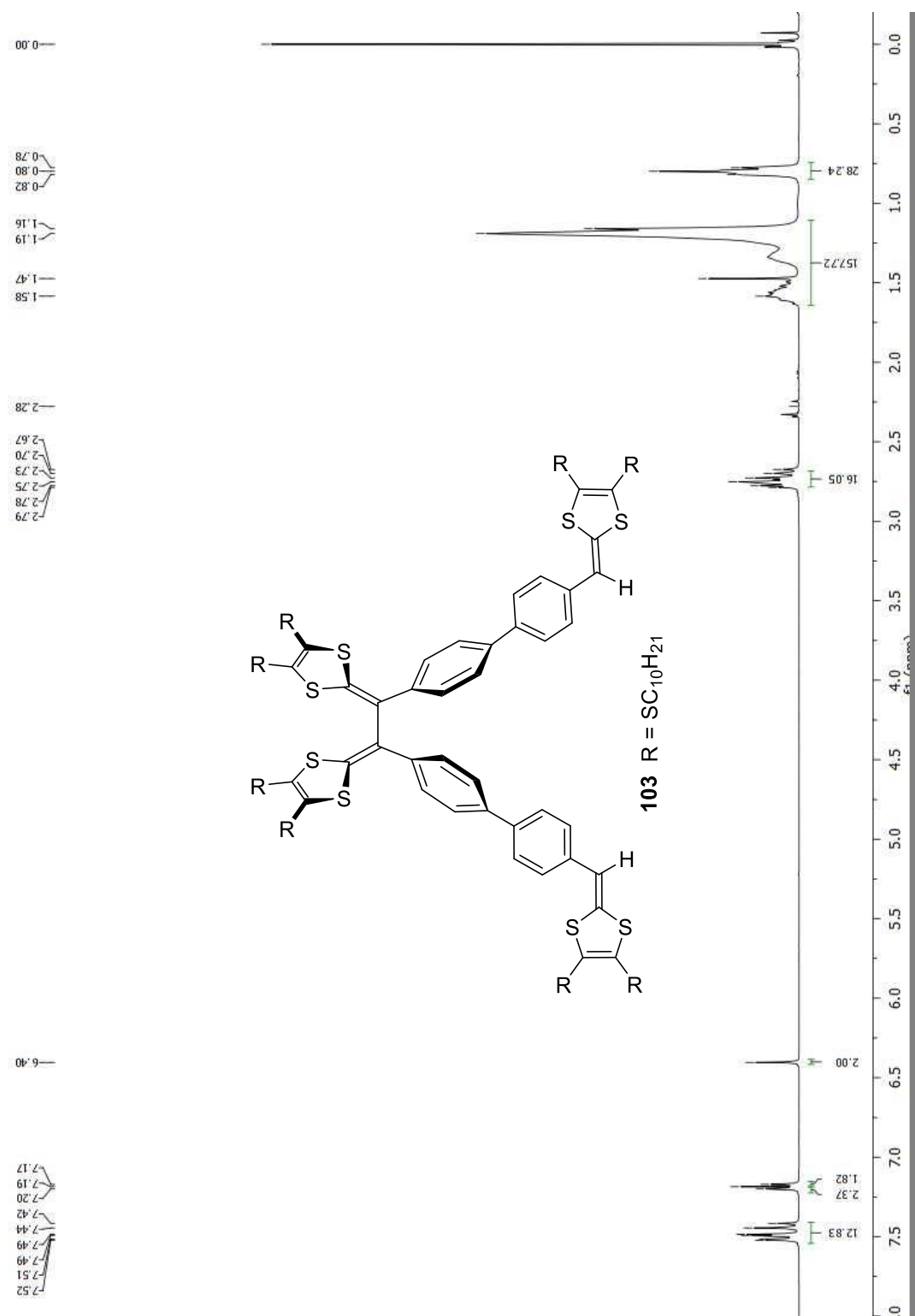


**Fig. 5.12:**  $^1\text{H}$  NMR (300 MHz,  $\text{CDCl}_3$ ) spectrum of compound **103**

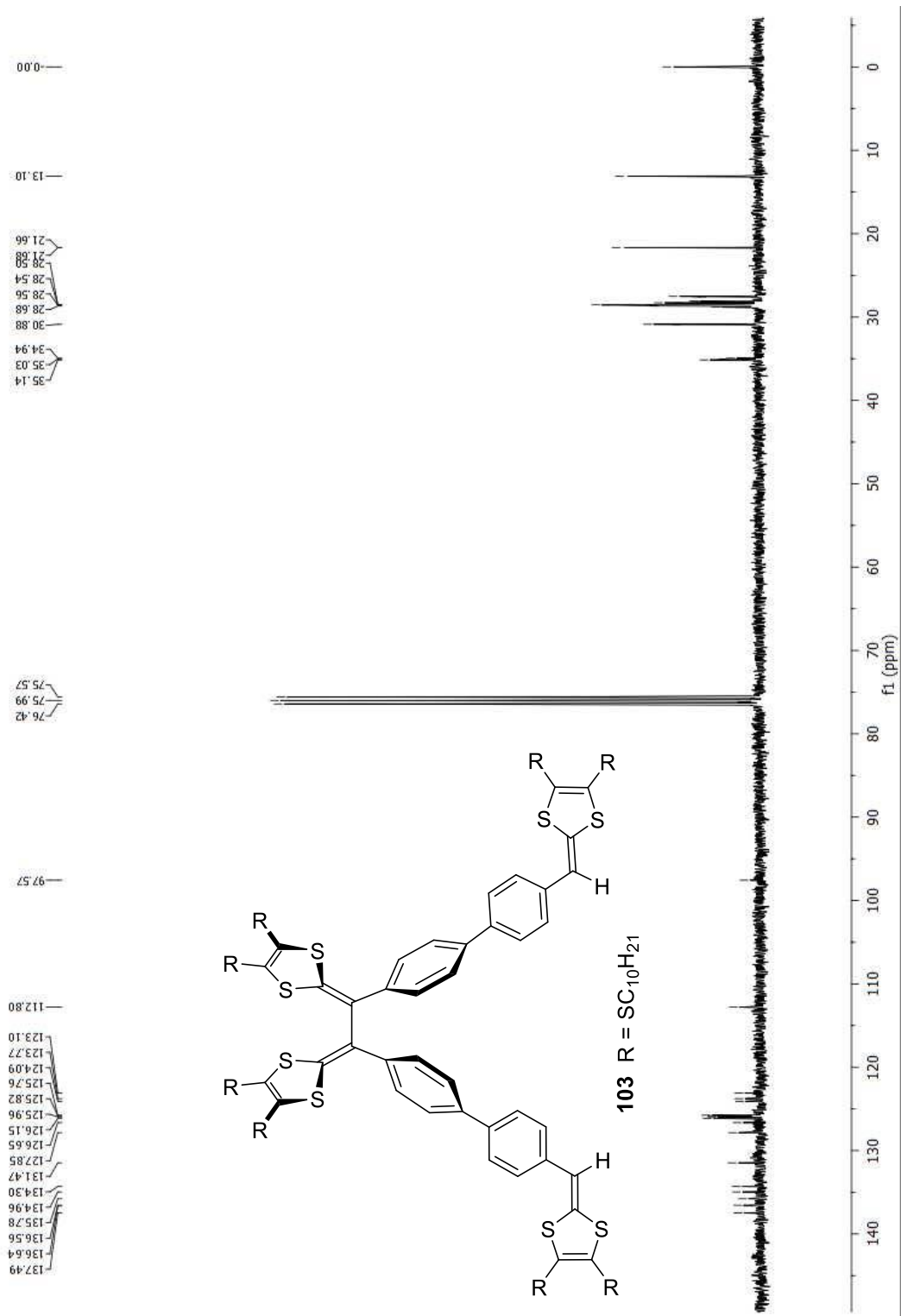


**Fig. 5.13:**  $^{13}C$  NMR (75 MHz,  $CDCl_3$ ) spectrum of compound 103.

## 5.4 References

- (1) Miyaura, N.; Suzuki, A. *Chem. Rev.* **1995**, *95*, 2457.
- (2) Malatesia, L.; Angoletta, M. *J. Chem. Soc.* **1957**, 1186.
- (3) Mulla, K.; Dongare, P.; Thompson, D. W.; Zhao, Y. *Org. Biomol. Chem.* **2012**, *10*, 2542.
- (4) Mulla, K.; Shaik, H.; Thompson, D. W.; Zhao, Y. *Org. Lett.* **2013**, *15*, 4532.
- (5) Molander, G. A.; Trice, S. L.; Dreher, S. D. *J. Am. Chem. Soc.* **2010**, *132*, 17701.
- (6) Hall, D. G. *Boronic acids: preparation, applications in organic synthesis and medicine*; John Wiley & Sons, 2006.
- (7) Khadem, M.; Zhao, Y. *J. Org. Chem.* **2015**, *80*, 7419.
- (8) Moore, A. J.; Bryce, M. R. *Tetrahedron Lett.* **1992**, *33*, 1373.
- (9) Ogi, S.; Sugiyasu, K.; Takeuchi, M. *ACS Macro Lett.* **2012**, *1*, 1199.
- (10) Jayabharathi, J.; Prabhakaran, A.; Thanikachalam, V.; Jeeva, P. *N. J. Chem.* **2016**, *40*, 8768.
- (11) Guo, K.; Yan, K.; Lu, X.; Qiu, Y.; Liu, Z.; Sun, J.; Yan, F.; Guo, W.; Yang, S. *Org. Lett.* **2012**, *14*, 2214.

# Chapter 6

## Conclusions and Future Work

In this PhD thesis, three projects were successfully accomplished, in which novel  $\pi$ -conjugated oligomers and polymers were prepared through advanced organic synthesis and characterized by various spectroscopic techniques and electrochemical analysis. A large portion of the synthetic work utilized the well-known Suzuki coupling reaction as an efficient methodology to prepare functional molecular building blocks, based on which complex polymeric and macromolecular systems were constructed through stepwise synthesis. Another important synthetic tool frequently employed in the synthesis is the DTF chemistry well established by the Zhao group over the past 10 years. Synthetically, functionalization of a DTF to a  $\pi$ -conjugated system can be readily achieved by reacting an aldehyde precursor with a 1,3-dithio-2-thione counterpart in the presence of trialkylphosphite (e.g., P(OMe)<sub>3</sub>, P(OEt)<sub>3</sub>). This olefination reaction has been proven reliably and efficient for most of the synthesis explored in this PhD thesis work; however, cautions are still need to be taken when the target compounds have limited thermal stability, since the reaction has been found to be sensitive to temperature effects. With the DTF group functionalized, a facile oxidative dimerization reaction can be executed to afford redox-active TTFV compounds, the conformational properties of which are controllable by simple redox chemistry. The unique electronic, optical, and structural properties of DTF and TTFV groups have hence allowed various new organic

materials (oligomers, polymers, macrocycles, etc.) to be developed and applied in the fields of chemical sensors, molecular switches, nanoelectronic devices, and so on.

Overall, this PhD thesis work has convincingly demonstrated that DTF and TTFV groups are excellent redox-active building blocks and can be flexibly integrated into a wide range of macromolecular systems to deliver novel optoelectronic functions and redox-activity. The synthesis of DTF and TTFV-based materials can be readily achieved by well-established reactions, for example, transition metal-catalyzed cross coupling and oxidative dimerization reactions. Moreover, the reaction conditions used may have a significant impact on the synthetic outcome. This is especially demonstrated in the work described in Chapter 3, where the combined use of solution-phase and solid-state reaction steps successfully led to a shape-persistent TTFV macrocycle in a good yield. On the other hand, nature of  $\pi$ -conjugated arenes attached to the DTF can also affect the dimerization reactivity. For instance, in the work of Chapter 1, narrowly distributed oligomers rather than polymers were formed in a one-pot reaction using the fluorene-based bis(DTF) precursors. Such structure-dependent reactivity should be taken into serious consideration in our future work of design and synthesis of TTFV-containing conjugated systems, and further mechanistic investigations are warranted to better understand how to predict and control the reactivity. Finally, demonstrated that DTF groups can be integrated into highly twisted poly(arene)s, such as the anthraquinodimethane-cored oligo(phenylene vinylene)s in Chapter 4. Embedded in such sterically hindered environment, the reactivity of DTF towards oxidative dimerization still retains and successfully led to functional polymer thin films through simple electro-

polymerization. This finding points to a great potential in the development of polymer film-based electronic and photonic devices. Along this direction, it is envisioned that a higher generation of multi-DTF functionalized dendrimer deserves synthetic investigation in the future work. The synthesis of a target compound **106** (Fig. 6.1) is currently underway and it is expected to show redox-activity and selective affinity for electron-deficient aromatic compounds, particularly nitrobenzene explosives, through  $\pi$ -stacking and charge-transfer interactions. Electropolymerization of **106** should lead to a redox-active polymer film with high porosity.

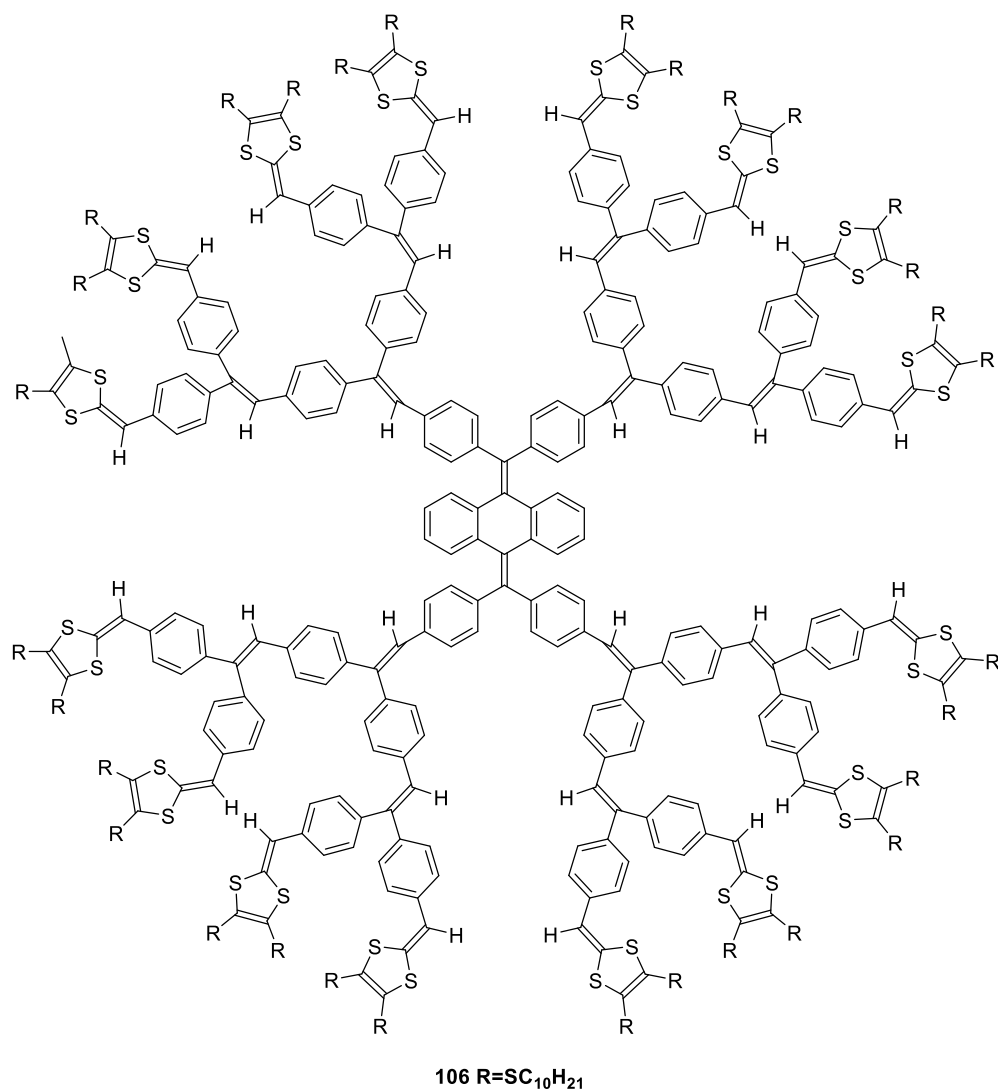


**Fig 6.1** Hexadeca-DTF functionalized  $\pi$ -conjugated dendritic system **106**.

Future studies on this topic are suggested to focus on the following aspects.

- (1) Characterization of the surface area and pore size of the polymer using advanced electronic microscopic (SEM, TEM) and gas adsorption techniques.
- (2) Supramolecular binding analysis of **106** with various nitrobenzene substrates by UV-Vis and fluorescence titration experiments.

- (3) Advanced NMR analysis (e.g., diffusion NMR, VT-NMR) on compound **106** and related derivatives to understand the size effects and aggregation properties.
- (4) Optimization of the polymer thin film fabrication procedures so that better controlled and robust thin films can be easily deposited on various conductive substrates. This study will lead to technological transfer of the DTF and TTFV materials to practical applications in molecular sensors, actuators, and organic photovoltaic devices.